序

我國地大物博，文化早開，四裔皆為未開化民族，自遠古以及兩世紀前，既不需與人貿易以互通有無，除趙武靈王胡服騎射而外，亦不必效人之長，自給自足而成一封閉體系，自秦皇一統而後兩千年來，蚩蚩之氓，除山呼萬歲以頌聖君，力田耕作以仰事俯蓄而外，別無他務，雖然王朝更易，而社會結構毫無變化，有如黃河決堤，搶修之後，在下次決堤之前，仍生活如舊，故不論我國之政治、經濟文化，均呈所謂超穩定狀態，毫無進步，更遑言突破，十四世紀，明太祖為便利其極權統治，厲行興農抑商之政策，更使人民黏著於土地，成祖篡立，遣三保太監出海覓建文帝行蹤，目的非在貿易，然而大帝國之聲威仍遠揚海外，先延平郡王驅荷復台之戰，施琅攻台時澎湖之戰，仍為當年威力強大艦隊之交鋒，為世屬目，然而康熙帝認為台灣乃彈丸之地，得之無所加，不得無所損，殲滅叛逆地方政權之目的已達，即欲棄此島，幸靖海侯力爭而罷，但禁臣民入海如昔也，雍正帝更因教士阻其爭位而逐洋人，東西文化之交流遂斷，而為強弱易位之契機。

反觀歐洲、羅馬大帝國崩潰後，島嶼城邦林立，迄今未能一統於某一王權，各民族競相謀其自利，海運貿易於是興焉，自由經濟與科技應用互相激盪，良性循環，財富蓄積而國力強大，鴉片戰爭一役，海洋商業文明與內陸耕作文明之勝負立現，迄今已逾百五十年矣，雖有原子武器，人造衛星，仍為落後地區，

如不能將黃土色之內陸文明脫胎換骨為蔚藍色海洋文明，終將為人宰割，甚至開除球藉。

鄭王開台，為我民族獲海洋基地，又與日本海島文化揉合五十載，我輩歷代渡海而來之過河卒子，實為開拓蔚藍色華夏文明之先鋒，二千萬眾均應憬悟其繼往開來之重大責任焉。

幼年讀孫文學說，建國方略第一項為東方大港北方大港焉，在日本九州帝國大學農工系就讀時，頗有志於治黃河，乃選修土木系所開"河海工學第一"課目，出生於內陸者，以為先河後海，第一部必為河工也，孰意先師松尾春雄博士(Dr.Matsuo,Haruo)一入教室即言港灣之重要性故第一部全為港工，政治家與學者，均認為築港應先於治河，心竊訝之，至渡台後，見台中民間熱中於台中港之開闢，該港完工典禮時萬人空巷途為之塞之盛況，始知港灣如人之口鼻，無之則窒息，而台灣民眾對海運港灣之體認熱心，尤非大陸人民可比擬，台灣實為我文化轉型復興之基地也。

我國現代港灣技術之發軔，始於台灣，詳見拙著"港灣與海域工程"序文中，而國人自力興建之完整人工大港，由台中港始，該港興建之前，除應用現代海岸工程知識作綿密之調查規劃外，先由台南水工試驗所以模型實驗證實其可行性與校核初步計劃，決定築港之後，再由工程局自建模型試驗室重複進行試驗，所有設備，除略遜於美、日、荷蘭、法國等海岸工程先進國家之大型研究所外，可謂獨步東南亞洲地區，台中港按兩次研究試驗結果施工，已無漂沙淤塞之患，完工而後，省交通處遂將台中港務局模型試驗課等有關研究單位劃出，並增加經費人員，成立港灣技術研究所，迄今已將十載矣。

建港有關知識，至為廣泛，除航運、經貿等有關人文活動者外，海港外廓之規劃設計，主要須利用潮浪漂沙等現象之海岸工程學上之研究成果，而我國現代海岸工程研究工作，三十三年前亦自台中港觀測波浪肇始，經包括台中港建港人員在內之各學術工程機構人員之篳路藍褸奮鬥培育下，成就斐然可觀，為全世界肯定，因而三年前全球有關專家聚集台北參加第二十屆國際海岸工程學會並實地考察我國研究及工程成果，而我國每年亦舉辦海洋工程研討會已達十一屆，青年學人及工程技術專家人才輩出，學術研究與實際工程均在蓬勃發展之中，在海岸港灣工程圈中，我國已為先進國家矣。

此次港灣技術研究所，舉辦有關港灣之數學問題討論會，主講人均為本土培養之青壯學人，更實現民族自信，至盼與會人員及港研所同仁，再堅定其為開創蔚藍色海洋文明先鋒之使命感與信心，在此中華民族五千年來未有之繁榮時代中，勿因享受物慾而迷失，勿沾染行政機關因循敷衍之作風，以與該所以同一漢字為名稱之日本運輸省港灣技術研究所為目標，迎頭趕上，努力超越，實有厚望焉。

己巳小寒前五日亦九十年代開始之日

湯麟武

總　目　錄

流體波動之一些眞實性　■陳陽益、湯麟武　1

摘　要 …… 1

一、前　言 …… 2

二、勢流波動場受黏性與底床作用之影響 …… 4

三、眞實流體波動系統之描述 …… 12

四、眞實流體波動的流場解 …… 19

五、檢核與驗證 …… 27

六、結論與討論 …… 35

堤角渦流之可視化研究　■黃煌煇　43

摘　要 …… 43

一、概　論 …… 43

二、試驗設備、試驗佈置及試驗步驟 …… 45

三、試驗結果與討論 …… 52

四、結　論 …… 66

五、參考資料 …… 66

粗糙紊流渦動滯度與邊界層特性之研究　■歐善惠、許泰文　69

中文摘要 …… 69

一、前　言 …… 70

二、基本方程式 …… 71

三、渦動滯度模式 …… 76

四、渦動滯度模式之檢討 …… 78

五、修正一階閉合模式的探討 …… 85

六、渦動滯度之提議 …… 87

表 2 — 1 試驗造波條件

轉角	斜度	T(sec)	H_i(cm)	d_i(cm)	d_m(cm)	觀測型式
0°	1/15	1.01	4.18	28	10	A,C
	1/15	1.01	2.48	28	10	B
	1/15	1.33	3.21	28	10	B
−30°	1/15	1.01	4.23	28	10	B,C
	1/15	1.01	2.51	28	10	B
	1/15	1.33	3.21	28	10	B
+30°	1/15	1.01	4.08	28	10	B,C
	1/15	1.01	2.17	28	10	B
	1/15	1.33	3.26	28	10	B

符號說明：

T ：週期

H_i ：等水深段波高

d_i ：等水深段水深

d_m ：測點處水深

轉角： 0° ………垂直水槽壁面

+30° ………向遮蔽區轉 30° 角

−30° ………離反射區轉 30° 角

觀測型式：

A ：渦流外觀、內部流場

B ：不同造波條件、模型轉角對照觀測

C ：底部粒子運動現象觀測

3. FINITE ELEMENT FORMULATION ······ 178

4. MODEL APPLICATIONS ······ 187

5. FURTHER EXTENSIONS ······ 193

6. CONCLUSION AND RECOMMENDATION ······ 198

三度空間海洋數值模式　李賢文　221

一、引　　言 ······ 221

二、基本數理方程式 ······ 221

三、多層次模式 ······ 229

四、數值方法 ······ 243

五、討論與結論 ······ 248

颱風湧浪預報數值模式　梁乃匡　251

一、引　　言 ······ 251

二、模式介紹 ······ 252

三、實用電腦程式及實例 ······ 255

四、討論與結論 ······ 257

DHOALING OF A SMALL AMPLITUDE WAVE ON IMPERMEABLE SLOPES　李忠潘 259

1.INTRODUCTION ······ 260

2.THEORETICAL DERIVATION ······ 261

3.ANALYTICAL SOLUTION ILLUSTRATION ······ 268

4.CONCLUSION AMD DISCUSSION ······ 277

5.BIBLIOGRAPHY ······ 278

在時間領域上之波浪與結構物互相作用之有限元素法模擬　李兆芳　281

摘　　要 ······ 281

一、前　　言 ······ 282

二、波浪與結構物互制之有限元素方程式 ······ 285

三、波浪與結構物互制之動力分析 …………………………………… 289
四、計算例 ………………………………………………………………… 297
五、結　論 ………………………………………………………………… 298
六、參考文獻 ……………………………………………………………… 299

第三屆基礎港灣數值（數學）模式研習會論文集　Jan. 17～18，1990　Page 1～41

流體波動之一些眞實性

陳陽益*　湯麟武**

摘　要

對均勻靜穩的大氣下，等深中之自由表面規則前進的眞實流體波動，於 Navier－Stokes equation 之解析下，其流場結構已被本文闡述；且由動量守恒原則得知，在自由表面處的剪力會導引出一額加的壓力量，其脈動相位恰與剪力者成 90° 的差異。由所得之解析中顯現，當波動純在流體黏性因素對其流場內部作用下，波動乃屬勢流（Potential flow）的型式，且於無黏性存在時，則完全變成理想流體的勢流場；至於波動受流體黏性因素與底床邊界效應之雙重作用，所造成的整個流場脈動特性，包括其減衰現象與邊界近處之流速脈動等，亦被涵蓋而予之述說，同時在往昔研究結果的引用比較下，得到理論上的檢核與試驗的印證。

*港灣技術研究所，研究員兼數學模式組組長

**國立成功大學資優教授，現退休兼任

一、前　言

自從Stokes（ 1847 ）以攝動法（ Perturbation method）系統公式化陳述波動理論之後，有關自然界中發生的流體波動現象，於近百多年來有如百花齊放般被廣泛地展開探討。經衆多學者之長期致力研究下，可說成果豐碩非凡。如就波動中之基本成份波而言，卽所謂的自由表面單一規則前進重力波者，水深由深至淺，振幅從微小至近於最高碎波情況，其整體的波動特性已被相當詳盡地描述與瞭解，如見Cokelet（ 1977 ）、Williams（ 1981 ）、Rienecker & Fenton（ 1981 ）、Chen（ 1983 ）與Lin（ 1988 ）等。至於推展到重力駐波、短峰波（ Short crested waves ）與兩波列或三波列之交會組合而成的重複波（ Clapotis ）現象的描述，則有Tadjbakhsh & Keller（ 1960 ）、Phillips（ 1960 ）、Goda & Kakizaki（ 1966 ）、Hsu et al（ 1979 、 1980 ）、Chen（ 1988 、 1989 ）與Chang et al（ 1989 ）等之論述。甚至，延伸對由多波列組合而成的紛紜波動之波譜特性的解說，亦已相繼地被頗爲深入的探究，諸如Tick（ 1959 、 1961 ）、Phillips（ 1961 ）、Hasselmann（ 1961 、 1962 、 1963 、 1973 ）、Pierson & Moskowitz（ 1964 ）、Mitsuyasu（ 1984 ）、Chen（ 1987 ）等之闡論。因此可言，對自然界中會出現的流體波動現象之全盤性地述說，已廓劃出一個頗爲完整性的概論。觀之對這個課題的研究，爲何會被很多學者長期地投入如此大的心力呢？細究其因，這是很顯然地，蓋它經常於自然界中發生而與我們密切相關之故，尤其以廣大海域上之水面波動現象爲最。

雖然自然界中之流體波動現象，已被如此整盤性地闡述；尤其對水波波動有關特性的描述，更是已達到廣泛與詳細。然由這些各有獨特貢獻的流體波動有關文獻的學習與探討中，頗值得吾人關注的是，幾乎所有這些論著皆是以理想流體來解說波動的現象，鮮少以眞實流體爲對象來闡論其波動的眞實性，諸如包括流體黏性（ Viscosity ）與其承受到的邊界效應作用（ Boundary effect ）等。當然，由於眞實流體的黏性，一般而言是頗爲微小，故在巨視的（Macroscopical）觀點下，其對波動眞實性所產生的影響，除對一些特定的目的外，如邊界的剪力或波動的質量傳輸（Mass transport）等需加予考慮外，通常可忽略不計，這更以水波者爲然。是故使然，往昔迄今幾皆以理想流體運動所形成之勢流場（Potential flow）來描述流體波動現象。Hough（1896）與Harrison（1908）雖早直接以控制眞實流體運動的Navier – Stokes 方程式，考慮入黏性因素來處理流體波動現象，然由於他們限定波動的自由表面處無黏性剪力的存在，因而其所獲得的波動流場解，在無黏性之理想流體情況下，無法完全退化成勢流場；亦因如此，純因黏性因素而造成對流體波動的影響，即或言，眞實流體與理想流體波動間的差異，勢難給予比較，蓋因它們兩者間的自由表面邊界條件已不同之故；這尤其對有限水深情況，因黏性而導致底床邊界效應者更然。

經由上述對往昔有關眞實流體波動現象研究的探討，此處吾人似乎可顯然地處在一個立場是：(1)如何在同等的條件下，來比較出眞實流體與理想流體波動間的差異；即說明純因黏性因素而造成對流體波動的影響，且使之在無黏性情況下，能完全退化成勢流場而一致於理想流體波動者。(2)因流體黏性存在而於底床邊界處產生作用效應，導致對波動場的影響。基此兩個目的，本文將以流體波動中之基本成份波者，即所謂的自由表面單一規則前進波型式，來論說眞實流體波動場之脈動特性。

文中第二節，以已存有的勢流波動場開始脈動下，來述說其受黏性因素作用後會衍出的影響，即會產生出減衰（Damping）現象與底床邊界層（Boundary layer）效應者，以爲本文後節解析眞實流體波動結果之檢核與比較印證的有效依據。第三節，則述說所要解析的眞實流體波動流場其運動行爲的性質，包括控制其運動的基本條件式與其會受到的邊界條件，並以公式化列出所有這些必要的控制方程式。第四節，則對第三節所述的波動流場進行解析，並述說其於各種情況下會造致之波動流場的脈動特性。第五節，援引往昔相關的研究結果來對本文解析所得進行必要的理論檢核與試驗印證。第六節，則歸結本文整個論述，給予幾點顯要的結論與一些值得注意的討論。

二、勢流波動場受黏性與底床作用之影響

爲對波動流場受流體黏性因素與底床邊界作用所造成的影響，有初步的瞭解起見，今以一已存有的勢流波動場開始脈動爲例，來說明其在黏性因素與底床邊界效應作用下，會導致的流場特性變化，如波動之減衰與邊界處之脈動等。

設在等深d之流體中，週波率（Angular frequency）爲$\sigma_r = 2\pi / T_o$，T_o 爲週期，或波數（Wave number）爲$k = 2\pi / L$，L爲波長，之一已存在的自由表面前進重力波之勢流波動場開始脈動，則其流場解，於第一階（或線性解）近似下，可被表示爲

$$u_p = a\sigma_r \frac{\cosh k(d+y)}{\sinh kd} \cos(kx - \sigma_r t) \quad \cdots\cdots\cdots (2.1a)$$

$$v_p = a\sigma_r \frac{\sinh k(d+y)}{\sinh kd} \sin(kx - \sigma_r t) \quad \cdots\cdots\cdots (2.1b)$$

$$\eta_p = a\cos(kx - \sigma_r t) \quad \cdots\cdots\cdots (2.1c)$$

$$\sigma_r^2 = gk\tanh kd\ ,\ \sigma_r = ck\ ,\ c = L / T_o \text{爲波速} \quad \cdots\cdots\cdots (2.1d)$$

上式中x軸是沿著波動的傳遞方向取正，且恰位於平均靜止水平線處；而垂直y軸向上取正。u_p與v_p各爲波場中流體質點之水平與垂直速度分量。η_p爲波動水位，$a = a(t)$爲其振幅（Amplitude）是時間t的函數，即因流體黏性等因素而造致的減衰結果。g爲重力加速度（Gravitational acceleration）。

2-1 純在黏性因素作用下造成之減衰

今對一勢流波動場開始脈動後，考量其純因流體黏性因素的作用而造成的影響；即考慮波動無受其邊界因素的作用下，純由流體黏性因素對波動場內部的作功而使之減衰的現象，或謂波動是處在均勻靜穩的大氣壓下與完全光滑的底床上者。如此，可依黏性流體的能量方程式，得每單位面積之波動能量的變率，參見Phillips（1977）之（3.42）式，爲

$$\frac{dE}{dt} = -\frac{\mu}{L}\int_0^L \int_{-d}^{\eta_p} \Phi dy\,dx \qquad \cdots\cdots\cdots (2.2)$$

(2.2) 式中 μ 爲流體的動力黏性 (Dynamic viscosity) 係數；E 爲每單位面積波動的位能 E_p 與動能 E_v 之和的波動總能量；而 $\mu\Phi$ 爲因流體黏性對流場內部作用而產生的消散功率 (Dissipation of energy) 。它們各爲

$$E_p = \frac{1}{2}\frac{\rho g}{L}\int_0^L \eta_p^2\,dx = \frac{1}{4}\rho g a^2 \quad , \qquad \cdots\cdots\cdots (2.3a)$$

$$E_v = \frac{1}{2}\frac{\rho}{L}\int_0^L \int_{-d}^{\eta_p=0} (u_p^2 + v_p^2)\,dy\,dx = \frac{1}{4}\rho g a^2$$

$$E = E_p + E_v = \frac{1}{2}\rho g a^2 \qquad \cdots\cdots\cdots (2.3b)$$

$$\frac{\mu}{L}\int_0^L \int_{-d}^{\eta_p=0} \left[2\left(\frac{\partial u_p}{\partial x}\right)^2 + 2\left(\frac{\partial v_p}{\partial y}\right)^2 + \left(\frac{\partial u_p}{\partial y} + \frac{\partial v_p}{\partial x}\right)^2 \right] dy\,dx$$
$$= 2\mu g k^2 a^2 \qquad \cdots\cdots\cdots (2.3c)$$

ρ 爲流體密度 (Density) ，因此，(2.2) 式可得爲

$$\rho g a \frac{da}{dt} = -2\mu g k^2 a^2 \qquad \cdots\cdots\cdots (2.4)$$

依 (2.4) 式，卽刻可知，在任一均勻等深 d 中，一勢流波動場開始脈動後，純因流體黏性因素對波動場內部的作功而使之減衰的特性，或謂其脈動振幅隨時間的遞減爲

$$a = a(t) = a_o e^{-2\nu k^2 t} \quad , \quad \nu = \mu / \rho \qquad \cdots\cdots\cdots (2.5)$$

此處 ν 爲流體的運動黏性 (Kinematic viscosity) 係數，a_o 爲所考慮的勢流波動場開始脈動時的振幅。因而，在純流體黏性因素對波場內部作用下，所考慮的勢流波動場開始脈動後，其隨時間的減衰爲

$$u_p = \sigma_r a_o e^{-2\nu k^2 t} \frac{\cosh k(d+y)}{\sinh kd} \cos(kx-\sigma_r t) \qquad \cdots\cdots\cdots (2.6a)$$

$$v_p = \sigma_r a_o e^{-2\nu k^2 t} \frac{\sinh k(d+y)}{\sinh kd} \sin(kx-\sigma_r t) \qquad \cdots\cdots\cdots (2.6b)$$

$$\eta_p = a_o e^{-2\nu k^2 t} \cos(kx-\sigma_r t) \qquad \cdots\cdots\cdots (2.6c)$$

$$\sigma_r^2 = gk\tanh kd \quad , \quad \sigma_r = ck \qquad \cdots\cdots\cdots (2.6d)$$

若以波動振幅減衰至原來的 e^{-1} 倍時來評定波動的減衰速率，則對一勢流波動場開始脈動後，純因流體黏性因素於波場內部的作用而生的減衰特性，或所謂的減衰係數（ Modulus of decay ） t_i，為

$$a_o e^{-2\nu k^2 t_1} = a_o e^{-1} \text{ 即 } \quad t_1 = 1/2\nu k^2 = L^2/8\nu\pi^2 \qquad \cdots\cdots\cdots (2.7)$$

因此，明顯可知，在純黏性因素作用下，短波是較長波減衰為快，且以波長的平方為其間的比例，完全與深度無關。

2-2 邊界效應作用之影響

上小節是針對一勢流波動場開始脈動後，波場僅受流體黏性在其內部作用而生之影響，並無慮及受邊界的作用。然由於眞實流體波動中，侷限其脈動的固態底床邊界通常並非完全光滑之理想者，因此，流體波動除純因受黏性作用之外，當會受到底床邊界效應的影響，而需給予考慮之（如同上小節般，仍視自由表面處之大氣對波動無任何作用）。基此，為對流體波動之眞實性描述起見，本小節將對所考慮的勢流波動場開始脈動後，其受底床邊界效應作用的影響進行評量之。

於眞實流體運動中，因流體帶有黏性的因素，故通常視流體質點於其所接觸的固態邊界處是黏住的，即一般以在固體邊界面處的流體質點速度恰等於邊界面本身者為之；當然，若邊界面是靜止時，則此處的流體質點速度等於零（完全光滑的理想邊界如上小節所述者除外）。因此，對本小節所欲處理的一勢流波動場開始脈動後，其受底床邊界效應的影響，亦以 $y=-d$ 之底床處的流

體質點速度為零。基此考量下，則所考慮的波動流場受底床邊界效應的作用後，其流速可被描述，即其水平與垂直速度分量 u 與 v 者，為

$$u = u'_p + u' \qquad \cdots\cdots\cdots (2.8)$$

$$v = v'_p + v' \qquad \cdots\cdots\cdots (2.9)$$

$$\frac{\partial u}{\partial x} + \frac{\partial v}{\partial y} = \frac{\partial u'}{\partial x} + \frac{\partial v'}{\partial y} = 0 \qquad \cdots\cdots\cdots (2.10)$$

$$u = v = 0 \quad , \quad y = -d \quad 或 \quad u' = -u'_p \quad , \quad v' = 0 \ , \ y = -d \qquad \cdots\cdots (2.11)$$

上式中 u'_p 與 v'_p 為上小節所示者，是所考慮的勢流波動場脈動下之流體質點的水平與垂直速度分量；而 u' 與 v' 為此脈動受底床邊界效應作用所引導出的水平與垂直速度分量者，是為待解之量。其中，(2.10) 式表示它們需滿足質量守恒條件，即連續方程式 (Continuity equation)；而 (2.11) 式為它們在底床處的邊界條件。

求解所考慮的波動流場解，即解 u 與 v 或 u' 與 v' 者，可依控制眞實流體運動的Navier − Stokes 方程式為之，於第一階 (或線性階) 次的考量下，有

$$\frac{\partial u}{\partial t} = -\frac{1}{\rho}\frac{\partial p}{\partial x} + \nu\nabla^2 u \qquad \cdots\cdots\cdots (2.12)$$

$$\frac{\partial v}{\partial t} = -g - \frac{1}{\rho}\frac{\partial p}{\partial y} + \nu\nabla^2 v \qquad \cdots\cdots\cdots (2.13)$$

上兩式中 p 為所考慮的波動流場中的壓力，而 $\nabla^2 = \frac{\partial^2}{\partial x^2} + \frac{\partial^2}{\partial y^2}$ 為 Laplacian 運算符號。為解析便利起見，今對(2.12) 式取 $\frac{\partial}{\partial y}$ 之偏微分減去對 (2.13) 式取 $\frac{\partial}{\partial x}$ 之偏微分後，可得

$$\frac{\partial \omega}{\partial t} = \nu\nabla^2 \omega \qquad \cdots\cdots\cdots (2.14)$$

$$\omega=\frac{\partial u}{\partial y}-\frac{\partial v}{\partial x}=\frac{\partial u'}{\partial y}-\frac{\partial v'}{\partial x} \quad , \quad 因 \quad \frac{\partial u'_p}{\partial y}=\frac{\partial v'_p}{\partial x} \qquad \cdots\cdots\cdots (2.15)$$

此處 ω 即所謂的流場漩渦度（ Vorticity ），是因底床邊界效應作用所造成的。由於流體黏性 ν 通常爲微小量，故其使流體質點附着在底床邊界上而導致對流場的影響，其有效作用範圍，一般而言，皆僅侷限在很接近於底床邊界處；就是一般所言的波動的邊界層厚度（The thickness of boundary layer in waves motion ）相較於波長 L 是爲微小者，故使得 $\partial/\partial y \gg \partial/\partial x$ 。因此，（2.14）與（2.15）兩式可簡化爲

$$\frac{\partial \omega}{\partial t}=\nu\frac{\partial^2 \omega}{\partial y^2} \qquad \cdots\cdots\cdots (2.16)$$

$$\omega=\frac{\partial u'}{\partial y}-\frac{\partial v'}{\partial x}\approx\frac{\partial u'}{\partial y} \qquad \cdots\cdots\cdots (2.17)$$

或更可將之合併（對 y 由 $-d$ 至 y 積分之），爲

$$\frac{\partial u'}{\partial t}=\nu\frac{\partial^2 u'}{\partial y^2} \qquad \cdots\cdots\cdots (2.18)$$

整理以上對波動受底床邊界效應作用的論述，即聯合（2.8）至（2.18）式的說明，則對所考慮的一勢流波動場開始脈動後，因流體黏性的存在而致使其受底床邊界效應作用的影響，所導引出的波動特性量 u' 與 v' ，其推求可被述之爲

$$\frac{\partial u'}{\partial t}=\nu\frac{\partial^2 u'}{\partial y^2} \qquad \cdots\cdots\cdots (2.19a)$$

$$\frac{\partial u'}{\partial x}+\frac{\partial v'}{\partial y}=0 \qquad \cdots\cdots\cdots (2.19b)$$

$$u'=-u'_p \ , \ v'=0 \ , \ y=-d \qquad \cdots\cdots\cdots (2.19c)$$

$$u' \rightarrow 0 \;,\; v' \rightarrow 0 \;,\; y + d \rightarrow 大 \qquad \cdots\cdots\cdots (2.19d)$$

(2.19a－d)式之求解，可依最常用的分離變數法(The method of separating variables)爲之，令

$$u' = \mathrm{Re}\ \{X(x)Y(y)Z(t)\} \qquad \cdots\cdots\cdots (2.20)$$

此處Re {·} 代表取其實數部份者。由於(2.19a－d)式爲線性方程式，因此，於求解時方便上，可先直接以 $u' = X(x)Y(y)Z(t)$ 進行求解後，再取其實數部份即可。於配合原先給定的勢流波動場之脈動相位($kx - \sigma_r t$)下，經解析處理後，得滿足(2.19a－d)式之解，爲

$$\begin{aligned} u' &= \mathrm{Re}\ \{-a_o \sigma_r e^{\sigma_i t} \operatorname{csch} kd \cdot e^{-\beta(d+y)} e^{i(kx-\sigma_r t)} e^{i\beta(d+y)}\} \\ &= -a_o \sigma_r e^{\sigma_i t} \operatorname{csch} kd \cdot e^{-\beta(d+y)} \cos[kx - \sigma_r t + \beta(d+y)] \end{aligned} \qquad \cdots\cdots\cdots (2.21a)$$

$$\begin{aligned} v' = \frac{\sqrt{\nu k^2}}{\sqrt{2\sigma_r}} a_o \sigma_r e^{\sigma_i t} \operatorname{csch} kd \cdot (e^{-\beta(d+y)} \{&\cos[kx - \sigma_r t + \beta(d+y)] \\ &+ \sin[kx - \sigma_r t + \beta(d+y)]\} - \cos(kx - \sigma_r t) \\ &- \sin(kx - \sigma_r t)) \end{aligned} \qquad \cdots\cdots\cdots (2.21b)$$

$$\beta = \sqrt{\frac{\sigma_r + i\sigma_i}{2\nu}} \approx \sqrt{\frac{\sigma_r}{2\nu}} \qquad \cdots\cdots\cdots (2.21c)$$

此處 σ_i 爲所考慮的波動場因流體黏性因素與受底床邊界效應之雙重作用下，產生減衰的影響係數，需由能量消散方程式(2.2)式之應用決定之，將被推求於后；且可得 $|\sigma_i| \ll \sigma_r$，此乃因流體黏性通常爲微小之故。$\beta^{-1} = \sqrt{\frac{2\nu}{\sigma_r}}$ 爲一般所言的邊界層厚度。

當波動的減衰不計時，或有外來的做功恰彌補所造成的消散功時，則(2.21a)與(2.21b)兩式所示之 u' 與 v' 可寫成

$$u' = -a_o\sigma_r \operatorname{csch}kd \cdot e^{-\beta(d+y)} \cos[kx - \sigma_r t + \beta(d+y)] \cdots (2.22a)$$

$$v' = \frac{\sqrt{\nu k^2}}{\sqrt{2\sigma_r}} a_o\sigma_r \operatorname{csch}kd \cdot (e^{-\beta(d+y)} \{\cos[kx - \sigma_r t + \beta(d+y)]$$
$$+ \sin[kx - \sigma_r t + \beta(d+y)]\} - \cos(kx - \sigma_r t)$$
$$- \sin(kx - \sigma_r t)) \cdots\cdots\cdots (2.22b)$$

這恰與Phillips（1977）書中第46頁裡所述者一致，亦與Longuet－Higgins（1957）者相當。

為完整地描述所考慮的勢流波動場開始脈動後，其受流體黏性因素與底床邊界效應之雙重作用下之流場脈動的結構特性，即其隨時間的減衰現象，則被導引出的減衰影響係數 σ_i 當需要求解出。這可依（2.2）式之應用，將所解得的 $u = u'_p + u'$ 與 $v = v'_p + v'$ 代入，於忽略高於 νk^2 階次項下，得為

$$\rho g a \frac{da}{dt} = -2\mu g k^2 a^2 - \frac{1}{2}\rho g \sigma_r \sqrt{\frac{2\nu k^2}{\sigma_r}} \operatorname{csch}2kd \cdot a^2 \quad \cdots\cdots (2.23)$$

因此，可得

$$a = a(t) = a_o e^{\sigma_i t} \quad , \quad \sigma_i = -2\nu k^2 - \frac{1}{2}\frac{k}{\beta}\sigma_r \operatorname{csch}2kd \quad \cdots\cdots\cdots (2.24)$$

即所考慮的波動流場之第一階全解為，令 $\chi = kx - \sigma_r t$

$$u = u'_p + u' = \frac{a_o\sigma_r}{\sinh kd} \{\cosh k(d+y) \cdot \cos\chi - e^{-\beta(d+y)}$$
$$\cdot \cos[\chi + \beta(d+y)]\} \cdot e^{\sigma_i t} \quad \cdots\cdots\cdots (2.25a)$$

$$v = v'_p + v' = \frac{a_o\sigma_r}{\sinh kd} \{\sinh k(d+y) \cdot \sin\chi + \frac{1}{2}\frac{k}{\beta}(e^{-\beta(d+y)}$$
$$\cdot \{\cos[\chi + \beta(d+y)] + \sin[\chi + \beta(d+y)]\}$$
$$- \cos\chi - \sin\chi)\} e^{\sigma_i t} \quad \cdots\cdots\cdots (2.25b)$$

波動水位 $\eta = a_o e^{\sigma_i t} \cos\chi$；邊界層厚度 $\beta^{-1} = \sqrt{\dfrac{2\nu}{\sigma_r}}$ ；

減衰係數 $\sigma_i = -2\nu k^2 - \dfrac{k}{2\beta}\sigma_r \operatorname{csch} 2kd$ ········· (2.25c)

$\sigma_r^2 = gk\tanh kd$，$\sigma_r = ck$，c 爲波速 ········· (2.25d)

當深度趨於很大之深海中時，則上式變成

於 $d \to \infty$ 時，

$u = u'_p = a_o \sigma_r e^{-2\nu k^2 t} e^{ky} \cos(kx - \sigma_r t)$，因 $u' = 0$ ········· (2.26a)

$v = v'_p = a_o \sigma_r e^{-2\nu k^2 t} e^{ky} \sin(kx - \sigma_r t)$，因 $v' = 0$ ········· (2.26b)

$\eta = \eta_p = a_o e^{-2\nu k^2 t} \cos(kx - \sigma_r t)$ ········· (2.26c)

$\sigma_r^2 = gk$，$\sigma_r = ck$，c 爲波速；$\sigma_i = -2\nu k^2$ ········· (2.26d)

因此，可得與上小節之純因流體黏性因素下於深海情況者一致之，即與（ 2.6a－d ）式在 $d \to \infty$ 下完全相同，此乃因在深海情況下，開始脈動的勢流波動場，在底部處的流體質點速度爲零，故因底床邊界效應作用所引導出的流速 u' 與 v' 亦爲零之故，即無受底床效應的影響。

最後，歸結本節之論述，由上兩小節所得的結果比較，即（ 2.6a－d ）與（ 2.26a－d ）兩式者，即刻可知，於均勻靜穩的大氣下，等深 d 中之流體以勢流波動場開始脈動後，其受流體黏性因素與底床邊界效應之雙重作用下而造致之減衰，相較於純因流體黏性在其內部作用者，爲快速且以 $e^{\sigma_i t}$ 倍減衰之。如以它們兩者之減衰影響量之比 $|\sigma_i / \nu k^2|$ 來相較時，則它們間的減衰快慢更可明顯地被看出，亦由此可知所考慮的波動隨其深度 d 而受底床邊界效應之影響程度，如下圖㈠所示；得深度愈淺，則底床邊界效應對波動的減衰影響愈強烈顯著。

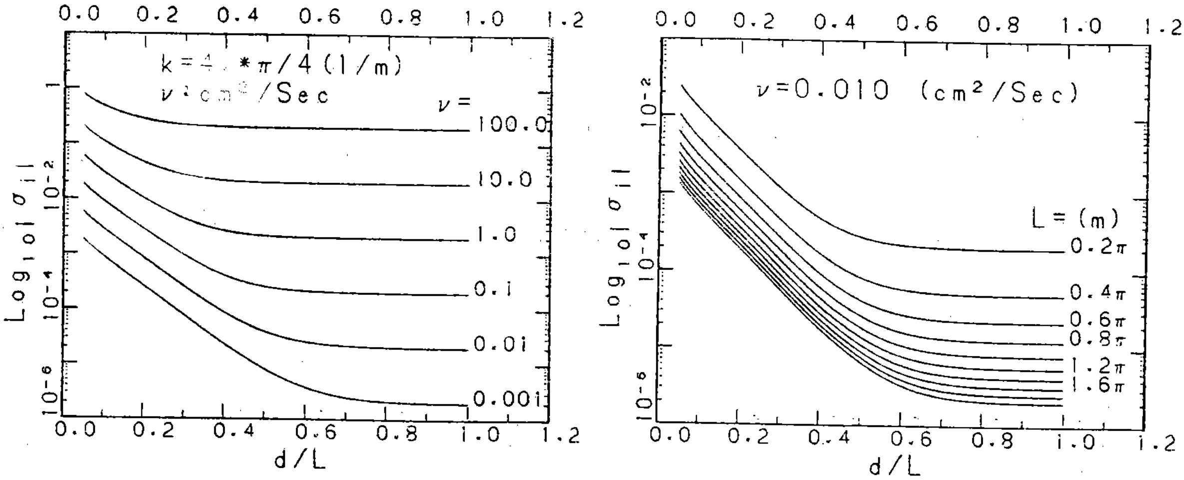

(a)在各種黏性情況　　　　(b)在各種波長情況

圖(一)　波動受底床邊界效應與純因流體黏性因素所造成之減衰率隨深度之變化

三、眞實流體波動系統之描述

由上節之論述，吾人可得知，流體因有黏性的存在而會對其波動流場造成影響的主要概況，然此等闡論是基於勢流波動場已脈動的給定下而展開的；即往昔學者們處理這種問題所常循用的方式者。但由於流體黏性是爲流體具有的本質特性者，因此，於任何的時空情況下，它們會含着在流體上而對其運動產生影響；或更明白地說，只要流體一有運動，則其因黏性因素的影響即刻會呈現，這當然對任一時刻的流體運動皆然，即使因它所造成的影響量甚微。是故，對本文所要描述的眞實流體之波動現象課題，在較逼眞性地述說其具有的特性之目的下，不論最後結果如何，似當得避開以已存有勢流波動場脈動的先給定之限制，而應是一開始就需由黏性流體運動所當要滿足之控制條件式的整體來闡述之，這也就是本文所着重的主旨而謹將於本節中陳述之。爲對所要言的波動系統其脈動流場結構有整體概貌性的認識起見，謹將以圖(二)示之於下。

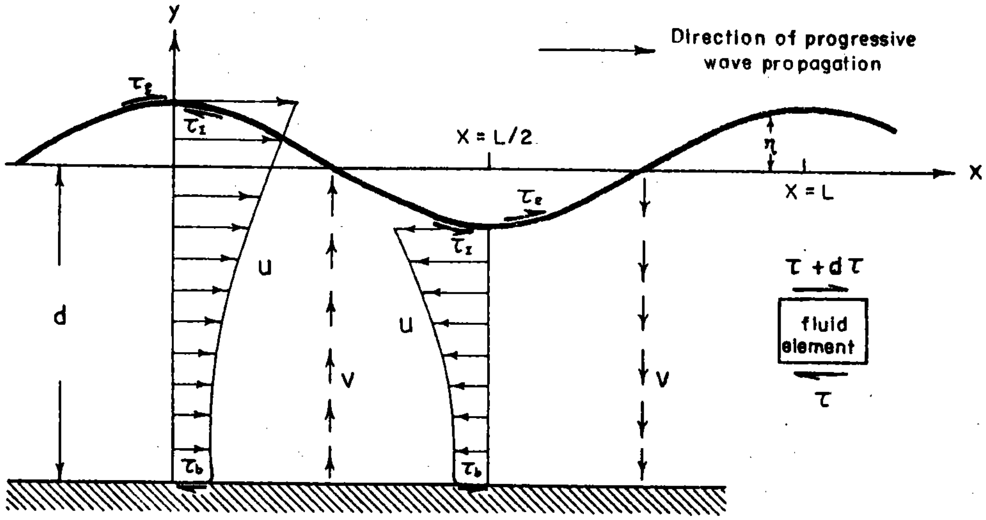

圖(二) 波動系統示意圖

3-1 眞實流體波動內之自由表面處壓力情況

爲能對所考慮的眞實流體之波動現象，給予充足地描述，則波動場內恰位於其自由表面處之流體質點承受的壓力情況應需被考量。

假設波動是處於均勻的大氣壓 p_a 下，除此之外，對波動自由表面處之流體質點上的作用壓力，還有因表面張力與剪力因素所造成者；此乃由於作用在自由表面處之剪力，受波動自由表面之脈動起伏，會間接地導引出對自由表面處之流體質點的作用壓力之故，且其相位的脈動恰與剪力者成 90° 的差異，此可參見 Stewart (1967) 以及 Longuet － Higgins (1969) 之論述。今於此處，爲簡單明瞭起見，將以 Phillips (1977) 之觀點來對本文所要言及者述說之，並延伸至任一等深流體波動中，於下。

設於均勻等深 d 之眞實流體波動中，作用在其自由表面處之總剪應力爲 τ_S，它可被分成兩部份之和：一者是純由外界對波動作用所給予的，如風之吹刮水面所造成的，說是 τ_E；另一者是在外界對波動無給予任何剪力作用下，由

於流體黏性對流體運動而產生的，即會對波動產生本質之減衰者，稱爲τ_I。上述之描述可參見圖(二)中所示。因作用在眞實流體波動之自由表面處的剪應力τ_S，而於該處下整個波動流場內所引導出的動量令爲M_S，因此，於本文所考慮的單一規則前進波動的型式下，有（注意：爲便於述說起見，解析描述將先以複數函數型式表示後，於最後結果中取其實數部份，下文的論述亦如此。）

$$\tau_S = \tau_E - \tau_I = \tau' e^{i(kx-\sigma_r t)} \qquad \cdots\cdots\cdots (3.1)$$

$$M_S = \int_{-d}^{\eta} \rho u_s \, dy \qquad \cdots\cdots\cdots (3.2)$$

上二式中τ'爲τ_S之振幅，u_s爲因τ_S的作用而引導出的流體質點之水平速度分量，其於垂直方向之對應速度分量爲v_s，此將可由下節之解析結果中明確地得知。

依據Phillips（1977）書中第51頁所述，在上述的考量下，則由動量守恒$\tau_S = \tau_E - \tau_I = \dfrac{\partial M_S}{\partial t}$；這是吾人所能深刻理解的，蓋因這恰如外界對流體運動作正功與流體黏性對其本身作負功所致。同時，在質量守恒（即連續方程式者）原則的應用下，即刻得有

$$\frac{\partial \Delta}{\partial t} = v_s \,|_{y=\eta} = \int_{-d}^{\eta} \frac{\partial v_s}{\partial y} dy = -\int_{-d}^{\eta} \frac{\partial u_s}{\partial x} dy \quad \text{（依連續方程式）}$$

$$= \frac{1}{c}\frac{\partial}{\partial t}\int_{-d}^{\eta} u_s dy = \frac{1}{\rho c}\frac{\partial M_S}{\partial t} = \frac{\tau_S}{\rho c}, \quad c \text{ 爲波數；}$$

$$\sigma_r = ck = (gk\tanh kd)^{1/2}$$

或於第一階近似考慮下，得

$$\Delta = i\frac{\tau_S}{\rho c \sigma_r} \qquad \cdots\cdots\cdots (3.3)$$

因此，由作用在所考慮的波動之自由表面處之剪應力 τ_S，而導引出於該處之流體質點上的作用壓力 p' 爲

$$p' = \rho g \Delta = i \tau_S \coth kd \qquad \cdots\cdots\cdots (3.4)$$

當波動處在很深情況中，$d \to \infty$，$\coth kd = 1$，則有 $p' = i\tau_S$，此即爲Stewart (1967)與Longuet－Higgins (1969) 所述者。

由於本文所要描述的眞實流體之波動是處於單純情況者，即波動的自由表面是在均勻靜穩的大氣下，而外界無給予任何的剪力作用。明言之，發生在波動之自由表面處的剪力，除由於流體黏性因素對流體運動而生者外，其他外來者爲零。因此，(3.1)、(3.3)與(3.4)式，於此考慮下，可被寫爲

$$\left.\begin{aligned}
&\text{令} \quad \tau_E = 0 \quad , \quad \text{則} \ \tau_S = -\tau_I \\
&\text{因} \quad \tau_I = \mu \left(\frac{\partial v}{\partial x} + \frac{\partial u}{\partial y} \right)_{y=\eta} , \ \Delta = -i\nu \left(\frac{\partial v}{\partial x} + \frac{\partial u}{\partial y} \right)_{y=\eta} \Big/ (c\sigma_r) \\
&\text{故} \quad p' = -i\rho\nu \left(\frac{\partial v}{\partial x} + \frac{\partial u}{\partial y} \right)_{y=\eta} \coth kd
\end{aligned}\right\} \cdots (3.5)$$

最後，考量入黏性流體之壓力及表面張力 ρT，則所考慮的處於均勻靜穩大氣壓 p_a 下之波動，在其自由表面處之流體質點上的作用壓力 p 可得爲

$$\frac{p}{\rho} = \frac{p_a}{\rho} - T \frac{\partial^2 \eta}{\partial x^2} + 2\nu \frac{\partial v}{\partial y} + \frac{p'}{\rho} = \frac{p_a}{\rho} - T \frac{\partial^2 \eta}{\partial x^2} + 2\nu \frac{\partial v}{\partial y}$$
$$- i\nu \left(\frac{\partial v}{\partial x} + \frac{\partial u}{\partial y} \right) \coth kd \ , \ y = \eta \qquad \cdots\cdots\cdots (3.6)$$

3-2 眞實流體波動之控制式

對眞實流體波動場的描述，即闡述其流場內之流體質點的運動速度 $\vec{V}$，或其水平與垂直速度分量 u 與 v，以及壓力 p 者，此可依Navier － Stokes 方程式行之，於上節所述之座標或如圖(二)所示者之下，爲

$$\frac{du}{dt} = -\frac{1}{\rho}\frac{\partial p}{\partial x} + \nu \nabla^2 u \qquad \cdots\cdots\cdots (3.7)$$

$$\frac{dv}{dt} = -g - \frac{1}{\rho}\frac{\partial p}{\partial y} + \nu \nabla^2 v \qquad \cdots\cdots\cdots (3.8)$$

或以向量形式表示時，則爲

$$\frac{\partial \vec{V}}{\partial t} + \vec{\omega} \times \vec{V} + \nabla \left(\frac{p}{\rho} + gy + \frac{1}{2}\vec{V}^2 \right) = \nu \nabla^2 \vec{V} \qquad \cdots\cdots\cdots (3.9)$$

上式中向量$\vec{\omega}$爲一般所稱的流場渦度量（ Vorticity ），其大小爲$\omega = \left(\frac{\partial u}{\partial y} - \frac{\partial v}{\partial x} \right)$，而其方向垂直於運動所在之$x - y$平面（此可依其定義$\vec{\omega} = \nabla \times \vec{V}$得知）。

基於對上述之波動流場的基本控制方程式便於解析起見，今定義一流函數（ Stream function ）$\Psi = \Psi(x, y, t)$，使得

$$u = \partial\Psi / \partial y \;,\; v = -\partial\Psi / \partial x \qquad \cdots\cdots\cdots (3.10)$$

因（3.7）與（3.8）兩式可由

$$\frac{d}{dt}\left(\frac{\partial u}{\partial y} - \frac{\partial v}{\partial x} \right) = \nu \nabla^2 \left(\frac{\partial u}{\partial y} - \frac{\partial v}{\partial x} \right)$$

而合併成一式爲

$$\frac{d}{dt}\left(\nabla^2 \Psi \right) = \nu \nabla^2 \left(\nabla^2 \Psi \right) \text{ 或 } \frac{d\omega}{dt} = \nu \nabla^2 \omega \qquad \cdots\cdots\cdots (3.11)$$

至於本文所要描述的波動流場，其要滿足的邊界條件，可分自由表面$y = \eta$與底床$y = -d$兩處來說明，如下。

(A)波動自由表面處之邊界條件：

(1)動力邊界條件（Dynamic boundary condition）

由（3.9）式可知，所考慮的波動流場其自由表面處之動力邊界條件為

$$\frac{\partial \vec{V}}{\partial t}+\vec{\omega}\times\vec{V}+\nabla\left(\frac{p}{\rho}+gy+\frac{1}{2}\vec{V}^2\right)=\nu\nabla^2\vec{V}\text{ , }y=\eta \cdots\cdots(3.12)$$

或方便上，將上式分成x與y方向上之分量後，再以（3.10）式之代入且各對x與y積分，就可得其另一型式的表示為

$$\int\frac{\partial^2\Psi}{\partial y\partial t}dx-\int\left(\frac{\partial\Psi}{\partial x}\right)\left(\nabla^2\Psi\right)dx+\frac{p}{\rho}+g\eta+\frac{1}{2}\vec{V}^2$$

$$-\nu\int\nabla^2\left(\frac{\partial\Psi}{\partial y}\right)dx=C_1(t)\text{ , }y=\eta \qquad\cdots\cdots\cdots(3.13)$$

或

$$-\int\frac{\partial^2\Psi}{\partial x\partial t}dy-\int\left(\frac{\partial\Psi}{\partial y}\right)\left(\nabla^2\Psi\right)dy+\frac{p}{\rho}+g\eta+\frac{1}{2}\vec{V}^2$$

$$+\nu\int\nabla^2\left(\frac{\partial\Psi}{\partial x}\right)dy=C_2(t)\text{ , }y=\eta \qquad\cdots\cdots\cdots(3.14)$$

上二式中 $C_1(t)$ 與 $C_2(t)$ 僅為時間 t 之函數且為相等者，通常可被併入在流函數 Ψ 內，如將於下節的解析推導中可得知。

最後，將上小節所得之作用在自由表面處之流體質點上的壓力情況，即（3.6）式的代入，則所考慮的波動流場，其在自由表面處之動力邊界條件之明確表示，可寫為

$$\int\frac{\partial^2\Psi}{\partial y\partial t}dx-\int\left(\frac{\partial\Psi}{\partial x}\right)\left(\nabla^2\Psi\right)dx+\frac{p_a}{\rho}-T\frac{\partial^2\eta}{\partial x^2}-2\nu\frac{\partial^2\Psi}{\partial x\partial y}$$

$$-i\nu\left(\frac{\partial^2\Psi}{\partial y^2}-\frac{\partial^2\Psi}{\partial x^2}\right)\coth kd+g\eta+\frac{1}{2}\left[\left(\frac{\partial\Psi}{\partial x}\right)^2+\left(\frac{\partial\Psi}{\partial y}\right)^2\right]$$

$$-\nu\int\nabla^2\left(\frac{\partial\Psi}{\partial y}\right)dx=C_1(t)\text{ , }y=\eta \qquad\cdots\cdots\cdots(3.15)$$

或 $$-\int\frac{\partial^2\Psi}{\partial x\partial t}dy-\int(\frac{\partial\Psi}{\partial y})(\nabla^2\Psi)dy+\frac{p_a}{\rho}-T\frac{\partial^2\eta}{\partial x^2}-2\nu\frac{\partial^2\Psi}{\partial x\partial y}$$
$$-i\nu(\frac{\partial^2\Psi}{\partial y^2}-\frac{\partial^2\Psi}{\partial x^2})\coth kd+g\eta+\frac{1}{2}[(\frac{\partial\Psi}{\partial x})^2+(\frac{\partial\Psi}{\partial y})^2]$$
$$+\nu\int\nabla^2(\frac{\partial\Psi}{\partial x})dy=C_2(t)\ ,\ y=\eta \qquad \cdots\cdots\cdots(3.16)$$

(2)運動邊界條件(Kinematic boundary condition)

當所考慮的流體是非常的清潔，且其波動自由表面所接觸的空氣亦是很清純地處於均勻靜穩的大氣壓下，而可讓該處的流體質點運動絲毫不生接觸的邊界效應。換言之，在波動的自由表面處並無導引出邊界效應的作用。因此，基此假定下，可給予波動之自由表面處的流體質點其運動爲非旋轉性者(Irrotational)，故可有

$$\frac{\partial u}{\partial y}=\frac{\partial v}{\partial x}\ ,\ y=\eta \quad 或 \quad \nabla^2\Psi=0\ ,\ y=\eta \qquad \cdots\cdots\cdots(3.17)$$

另一自由表面運動邊界條件是吾人所熟知的，爲

$$v=-\frac{\partial\Psi}{\partial x}=\frac{d\eta}{dt}\ ,\ y=\eta \qquad \cdots\cdots\cdots(3.18)$$

(B)底床邊界條件：

依底床材料的性質，茲分完全光滑與否兩者來述說。

(1)完全光滑的底床；因恰在它的上面無流體運動的剪力產生，故有

$$v=-\frac{\partial\Psi}{\partial x}=0\ ,\ y=-d \qquad \cdots\cdots\cdots(3.19)$$

與 $\tau=\mu(\frac{\partial v}{\partial x}+\frac{\partial u}{\partial y})=0\ ,\ y=-d$ 即 $\frac{\partial v}{\partial x}+\frac{\partial u}{\partial y}=0\ ,\ y=-d$

$$\cdots\cdots\cdots(3.20)$$

(2)非完全光滑的底床；通常認定恰在此底床處的眞實流體質點是黏住底床的，故有

$$v=-\frac{\partial\Psi}{\partial x}=0 \text{ ， } y=-d \qquad \cdots\cdots\cdots(3.21)$$

與 $$u=\frac{\partial\Psi}{\partial y}=0 \text{ ， } y=-d \qquad \cdots\cdots\cdots(3.22)$$

四、眞實流體波動的流場解

依據第三節對所考慮的眞實流體之波動流場系統的描述，便於清楚解析起見，將分爲完全光滑與非完全光滑底床兩情況，來逐次對它進行處理之，如后。

4-1 完全光滑底床情況

此情況之波動流場，於第一階次量（或言線性階者）的考慮下，其所有的控制條件式可由（3.11）、（3.15）（或（3.16））與（3.17）至（3.20）式而列出之，且在標準氣壓 $p_a=0$ 下，爲

$$\frac{\partial}{\partial t}(\nabla^2\Psi)=\nu\nabla^2(\nabla^2\Psi)=\nu\nabla^4\Psi \qquad \cdots\cdots\cdots(4.1)$$

$$\int\frac{\partial^2\Psi}{\partial y\partial t}dx-T\frac{\partial^2\eta}{\partial x^2}-2\nu\frac{\partial^2\Psi}{\partial x\partial y}-i2\nu\frac{\partial^2\Psi}{\partial y^2}\coth kd+g\eta$$

$$-\nu\int\nabla^2\left(\frac{\partial\Psi}{\partial y}\right)dx=C_1(t) \text{ ， } y=0 \qquad \cdots\cdots\cdots(4.1a)$$

$$\nabla^2\Psi=\frac{\partial^2\Psi}{\partial x^2}+\frac{\partial^2\Psi}{\partial y^2}=0 \text{ ， } y=0 \qquad \cdots\cdots\cdots(4.1b)$$

$$\frac{\partial\eta}{\partial t}=-\frac{\partial\Psi}{\partial x}\text{ ， } y=0 \qquad \cdots\cdots\cdots(4.1c)$$

$$-\frac{\partial \Psi}{\partial x}=0 \text{ , } y=-d \qquad \cdots\cdots\cdots (4.1d)$$

$$\frac{\partial^2 \Psi}{\partial y^2}-\frac{\partial^2 \Psi}{\partial x^2}=0 \text{ , } y=-d \qquad \cdots\cdots\cdots (4.1e)$$

求解所考慮的波動流場之基本控制方程式（4.1）式，即求其流函數解Ψ者，於單一規則前進波之脈動形式給定下，可依分離變數法來解析之，即可令

$$\Psi=f(y)\,e^{i(kx-\sigma t)} \qquad \cdots\cdots\cdots (4.2a)$$

$$\eta=a_o e^{i(kx-\sigma t)} \qquad \cdots\cdots\cdots (4.2b)$$

$$\sigma=\sigma_r+i\sigma_i \qquad \cdots\cdots\cdots (4.2c)$$

上式中有關符號 k 、σ（包括 σ_r 與 σ_i ）及 a_o 所代表的物理意義，如第二節中所定義者。因此，（4.2a）式代入（4.1）式下，可得

$$\frac{d^4 f}{dy^4}+\left(i\frac{\sigma}{\nu}-2k^2\right)\frac{d^2 f}{dy^2}+\left(k^4-i\frac{\sigma k^2}{\nu}\right)f=0 \qquad \cdots\cdots\cdots (4.3)$$

顯然，解 f(y) 的型式爲

$$f(y)\sim e^{\lambda y} \qquad \cdots\cdots\cdots (4.4)$$

λ 爲待解的常數係數，可由（4.4）式代入（4.3）式來求解，有

$$\lambda^4+\left(i\frac{\sigma}{\nu}-2k^2\right)\lambda^2+\left(k^4-i\frac{\sigma k^2}{\nu}\right)=0 \qquad \cdots\cdots\cdots (4.5)$$

得其四個根 λ_i 分別爲

$$\lambda_1=-\lambda_2=k \text{ , } \lambda_3=-\lambda_4=\sqrt{k^2-i\frac{\sigma}{\nu}}=m \qquad \cdots\cdots\cdots (4.6)$$

因此，得於第一階次量考慮下，所考慮的波動流場之流函數通解其型式爲

$$\Psi = (Ae^{ky} + Be^{-ky} + Ce^{my} + De^{-my})e^{i(kx-\sigma t)} \qquad \cdots\cdots\cdots (4.7)$$

(4.7)式中，A、B、C、D 皆爲待解的常數係數，它們及 k 與 σ 間所關連到的分散關係(Dispersion relation)，則需由所要滿足的邊界條件(4.1a)至(4.1e)式來決定之，謹述之如下。

爲完全求解出在完全光滑底床情況下，所考慮的眞實流體波動流場之第一階解析解，即其所對應的流函數 Ψ 與波形 η 者，則可由(4.7)式代入(4.1a)至(4.1e)式中，得五個必要的方程式所成之聯立方程組來解之，爲(注意：於第一階次下，$C_1(t) = C_2(t) = 0$)

$$\left(-\frac{\sigma}{k} - i2\nu k\right)(kA - kB + mC - mD) + Tk^2a_o - i2\nu k^2(A+B$$

$$+C+D)\coth kd + ga_o + i\frac{\nu}{k}m(m^2-k^2)(C-D) = 0 \qquad \cdots (4.8a)$$

$$(m^2 - k^2)(C + D) = 0 \qquad \cdots\cdots\cdots (4.8b)$$

$$k(A + B + C + D) = \sigma a_o \qquad \cdots\cdots\cdots (4.8c)$$

$$Ae^{-kd} + Be^{kd} + Ce^{-md} + De^{md} = 0 \qquad \cdots\cdots\cdots (4.8d)$$

$$2k^2(Ae^{-kd} + Be^{kd}) + (m^2 + k^2)(Ce^{-md} + De^{md}) = 0 \qquad \cdots\cdots (4.8e)$$

注意：若以(3.16)式取代(3.15)式爲波動之自由表面動力邊界條件表示式時，則所得的解析結果相同，對此之導證謹將陳述於文後的附註中。由(4.8b)式直接可得

$$C = -D \qquad \cdots\cdots\cdots (4.9)$$

由(4.8e)式減去 $2k^2$ 倍的(4.8d)式，再由(4.9)式的應用，可得

$$(m^2 - k^2)C(e^{-md} - e^{md}) = 0，\text{即得 } C = 0 \qquad \cdots\cdots\cdots (4.10)$$

至於求解常數係數A與B，則可由（4.9）與（4.10）兩式代入（4.8c）與（4.8d）（或（4.8e））式中，聯合解得

$$A=\frac{\sigma a_o}{2k}\frac{e^{kd}}{\sinh kd} \qquad \cdots\cdots\cdots(4.11)$$

$$B=-\frac{\sigma a_o}{2k}\frac{e^{-kd}}{\sinh kd} \qquad \cdots\cdots\cdots(4.12)$$

最後，對於此情況下之波動流場的分散關係與其所生成的減衰影響量之推求，可由所解得的常數係數A、B、C、D，即（4.9）至（4.12）式者，代入（4.8a）式中，得有

$$\sigma^2+i4\nu k^2\sigma-(gk+Tk^3)\tanh kd=0 \qquad \cdots\cdots\cdots(4.13)$$

解得

$$\sigma=\sqrt{(gk+Tk^3)\tanh kd-4\nu^2k^4}-i2\nu k^2=\sigma_r+i\sigma_i \qquad \cdots\cdots\cdots(4.14)$$

整理以上解析所得，因此可得，於完全光滑的底床情況下，所考慮的眞實流體之波動流場第一階解爲

$$\Psi=\frac{a_o}{k}(\sigma_r-i2\nu k^2)e^{-2\nu k^2t}\frac{\sinh k(d+y)}{\sinh kd}e^{i(kx-\sigma_rt)} \qquad \cdots(4.15a)$$

$$\eta=a_oe^{-2\nu k^2t}e^{i(kx-\sigma_rt)} \qquad \cdots\cdots\cdots(4.15b)$$

$$\sigma_r=\sqrt{(gk+Tk^3)\tanh kd-4\nu^2k^4}=ck\text{，c 爲波速} \qquad \cdots\cdots\cdots(4.15c)$$

若以具實際物理意義的型式來表示時，則取其實數部份（當然取其所對應的虛數部份亦可），得此情況下之眞實流體的波動流場第一階全解爲

$$\Psi=\frac{a_o}{k}e^{-2\nu k^2t}\frac{\sinh k(d+y)}{\sinh kd}[\sigma_r\cos(kx-\sigma_rt)$$
$$+2\nu k^2\sin(kx-\sigma_rt)] \qquad \cdots\cdots\cdots(4.16a)$$

$$u=\frac{\partial\Psi}{\partial y}=a_o e^{-2\nu k^2 t}\ \frac{\cosh k\,(\,d+y\,)}{\sinh kd}\left[\,\sigma_r\cos\,(\,kx-\sigma_r t\,)\right.$$
$$\left.+2\nu k^2\sin\,(\,kx-\sigma_r t\,)\,\right] \qquad \cdots\cdots\cdots(4.16b)$$

$$v=-\frac{\partial\Psi}{\partial x}=a_o e^{-2\nu k^2 t}\ \frac{\sinh k\,(\,d+y\,)}{\sinh kd}\left[\,\sigma_r\sin\,(\,kx-\sigma_r t\,)\right.$$
$$\left.-\ 2\nu k^2\ \cos\,(\,kx-\sigma_r t\,)\,\right] \qquad \cdots\cdots\cdots(4.16c)$$

$$\eta=a_o e^{-2\nu k^2 t}\cos\,(\,kx-\sigma_r t\,)\,,\ \sigma_r=\sqrt{(\,gk+Tk^3\,)\tanh kd-4\nu^2k^4}$$
$$\cdots\cdots\cdots(4.16d)$$

4-2 非完全光滑底床情況

對於這個情況之眞實流體波動流場，於第一階次量的考慮下，其所有的控制條件式，可由（3.11）、（3.15）（或（3.16））、（3.17）、（3.18）、（3.21）與（3.22）等六式列出，爲

$$\frac{\partial}{\partial t}(\,\nabla^2\Psi\,)=\nu\nabla^2\,(\,\nabla^2\Psi\,)=\nu\nabla^4\Psi \qquad \cdots\cdots\cdots(4.17)$$

$$\int\frac{\partial^2\Psi}{\partial y\partial t}dx-T\frac{\partial^2\eta}{\partial x^2}-2\nu\frac{\partial^2\Psi}{\partial x\partial y}-i2\nu\frac{\partial^2\Psi}{\partial y^2}\coth kd+g\eta$$
$$-\nu\int\nabla^2(\frac{\partial\Psi}{\partial y})\,dx=C_1(t)\ ,\ y=0 \qquad \cdots\cdots\cdots(4.17a)$$

$$\nabla^2\Psi=\frac{\partial^2\Psi}{\partial x^2}+\frac{\partial^2\Psi}{\partial y^2}=0\ ,\ y=0 \qquad \cdots\cdots\cdots(4.17b)$$

$$\frac{\partial\eta}{\partial t}=-\frac{\partial\Psi}{\partial x},\ y=0 \qquad \cdots\cdots\cdots(4.17c)$$

$$-\frac{\partial\Psi}{\partial x}=0\ ,\ y=-d \qquad \cdots\cdots\cdots(4.17d)$$

$$\frac{\partial\Psi}{\partial y}=0\ ,\ y=-d \qquad \cdots\cdots\cdots(4.17e)$$

求解此情況之波動流場的流函數解Ψ，如同於上小節之對完全光滑底床情況者之解析般，得所要滿足的方程式組爲（於第一階次量考慮下）

$$\Psi=(Ae^{ky}+Be^{-ky}+Ce^{my}+De^{-my})e^{i(kx-\sigma t)}\ ,\ m=\sqrt{k^2-i\frac{\sigma}{\nu}} \quad \cdots\cdots\cdots(4.18)$$

與

$$\left(-\frac{\sigma}{k}-i2\nu k\right)(kA-kB+mC-mD)+Tk^2a_o-i2\nu k^2(A+B+C+D)\coth kd+ga_o+i\frac{\nu}{k}m(m^2-k^2)(C-D)=0 \quad \cdots(4.19a)$$

$$(m^2-k^2)(C+D)=0 \quad \cdots\cdots\cdots(4.19b)$$

$$k(A+B+C+D)=\sigma a_o \quad \cdots\cdots\cdots(4.19c)$$

$$Ae^{-kd}+Be^{kd}+Ce^{-md}+De^{md}=0 \quad \cdots\cdots\cdots(4.19d)$$

$$k(Ae^{-kd}-Be^{kd})+m(Ce^{-md}-De^{md})=0 \quad \cdots\cdots\cdots(4.19e)$$

上式解之，得

$$A=\frac{1}{2}\frac{k\tanh md-m}{k\tanh md-m\tanh kd}\frac{e^{kd}}{\cosh kd}\frac{\sigma}{k}a_o \quad \cdots\cdots\cdots(4.20a)$$

$$B=\frac{1}{2}\frac{k\tanh md+m}{k\tanh md-m\tanh kd}\frac{e^{-kd}}{\cosh kd}\frac{\sigma}{k}a_o \quad \cdots\cdots\cdots(4.20b)$$

$$C=\frac{1}{2}\frac{k\,\mathrm{sech}\,kd\cdot\mathrm{sech}\,md}{k\tanh md-m\tanh kd}\frac{\sigma}{k}a_o \quad \cdots\cdots\cdots(4.20c)$$

$$D=-C=-\frac{1}{2}\frac{k\,\mathrm{sech}\,kd\cdot\mathrm{sech}\,md}{k\tanh md-m\tanh kd}\frac{\sigma}{k}a_o \quad \cdots\cdots\cdots(4.20d)$$

$$\sigma=\left[(gk+Tk^3)\left(\tanh kd-\sqrt{\frac{\nu k^2}{2\sigma_r}}\mathrm{sech}^2kd\right)-4\nu^2k^4\right]^{1/2}$$
$$-i\left\{2\nu k^2+\frac{1}{2}\left[(gk+Tk^3)\left(\tanh kd-\sqrt{\frac{\nu k^2}{2\sigma_r}}\mathrm{sech}^2kd\right)-4\nu^2k^4\right]^{1/2}\cdot\sqrt{\frac{2\nu k^2}{\sigma_r}}\mathrm{csch}\,2kd\right\}=\sigma_r+i\sigma_i \quad \cdots\cdots\cdots(4.20e)$$

因此，於非完全光滑底床情況下，所考慮的眞實流體之波動流場其第一階解，爲

$$\Psi=\{\frac{k\tanh md}{k\tanh md-m\tanh kd}\frac{\cosh k(d+y)}{\cosh kd}-\frac{m}{k\tanh md-m\tanh kd}\cdot\frac{\sinh k(d+y)}{\cosh kd}+\frac{k\,\mathrm{sech}\,kd\cdot\mathrm{sech}\,md}{k\tanh md-m\tanh kd}\sinh my\}\frac{\sigma a_o}{k}e^{i(kx-\sigma t)}$$

$$\cdots\cdots\cdots(4.21a)$$

$$u=\frac{\partial\Psi}{\partial y}=\{\frac{k\tanh md}{k\tanh md-m\tanh kd}\frac{\sinh k(d+y)}{\cosh kd}-\frac{m}{k\tanh md-m\tanh kd}\frac{\cosh k(d+y)}{\cosh kd}+\frac{m\,\mathrm{sech}\,kd\cdot\mathrm{sech}\,md}{k\tanh md-m\tanh kd}\cdot\cosh my\}\ \sigma a_o e^{i(kx-\sigma t)}$$

$$\cdots\cdots\cdots(4.21b)$$

$$v=-\frac{\partial\Psi}{\partial x}=-i\ \{\frac{k\tanh md}{k\tanh md-m\tanh kd}\frac{\cosh k(d+y)}{\cosh kd}-\frac{m}{k\tanh md-m\tanh kd}\frac{\sinh k(d+y)}{\cosh kd}+\frac{k\,\mathrm{sech}\,kd\cdot\mathrm{sech}\,md}{k\tanh md-m\tanh kd}\cdot\sinh my\}\ \sigma a_o e^{i(kx-\sigma t)}$$

$$\cdots\cdots\cdots(4.21c)$$

$$\eta=a_o e^{i(kx-\sigma t)}$$

$$\cdots\cdots\cdots(4.21d)$$

$$\sigma=\sigma_r+i\,\sigma_i\ ,\ \sigma_r=[\,(gk+Tk^3)(\tanh kd-\sqrt{\frac{\nu k^2}{2\sigma_r}}\,\mathrm{sech}^2kd)-4\nu^2k^4\,]^{1/2}\ ,\ \sigma_i=-2\nu k^2-\frac{1}{2}\frac{k}{\beta}\sigma_r\,\mathrm{csch}\,2kd\ ,\ \beta=\sqrt{\frac{\sigma_r}{2\nu}}$$

$$\cdots\cdots\cdots(4.21e)$$

當然，若以具實際物理意義的型式來表示時，則取上式之實數部份（或對應的虛數部份亦可），卽爲所考慮的眞實流體於非完全光滑底床上之波動其流場的第一階解。

當深度是很深的流體中，則由（4.20a）至（4.20e）式，有

於 $d \to \infty$， $\tanh kd = 1$， $A = \dfrac{\sigma}{k} a_o$，$B = C = D = 0$ ………（4.22a）

$e^{kd} \to \infty$， $\operatorname{sech} kd = 0$， $\sigma = \sigma_r + i\sigma_i$， $\sigma_r = (gk + Tk^3 - 4\nu^2 k^4)^{1/2}$

， $\sigma_i = -2\nu k^2$ ………（4.22b）

由（4.22a）與（4.22b）兩式代入（4.18）式中，或直接由（4.21a）至（4.21e）式以 $d \to \infty$ 下退化之亦可，則可得所考慮的眞實流體之波動流場，其於深海中之第一階解（取其實數部份），爲

於 $d \to \infty$ 下，

$$\Psi = \frac{a_o}{k} e^{-2\nu k^2 t} e^{ky} \left[\sigma_r \cos(kx - \sigma_r t) + 2\nu k^2 \sin(kx - \sigma_r t) \right] \cdots (4.23a)$$

$$u = \frac{\partial \Psi}{\partial y} = a_o e^{-2\nu k^2 t} e^{ky} \left[\sigma_r \cos(kx - \sigma_r t) + 2\nu k^2 \sin(kx - \sigma_r t) \right]$$

………（4.23b）

$$v = -\frac{\partial \Psi}{\partial x} = a_o e^{-2\nu k^2 t} e^{ky} \left[\sigma_r \sin(kx - \sigma_r t) - 2\nu k^2 \cos(kx - \sigma_r t) \right]$$

………（4.23c）

$$\eta = a_o e^{-2\nu k^2 t} \cos(kx - \sigma_r t)，\sigma_r = (gk + Tk^3 - 4\nu^2 k^4)^{1/2} \quad \cdots (4.23d)$$

上式完全與由（4.16a）至（4.16d）在 $d \to \infty$ 下所得之結果一致。這就是表示，在很深的流體波場中，完全光滑與非完全光滑底床兩情況之眞實流體波動是完全相同的，完全僅受流體黏性因素的影響而與底床完全光滑與否絲毫無關；此乃因波動在很深的底床處之流體質點速度爲零而無底床邊界效應的發生，致使於深度很深的眞實流體中，處於完全與非完全光滑底床上之兩種情況的波動，它們所有必要滿足的控制條件式完全相一致之故。

五、檢核與驗證

基於對上節所解析得的結果，其適足性做個交代起見，於本節中將以往昔之研究結果來對其進行理論檢核與試驗印證之，如下。

5-1 理論檢核

依據第二至第四節所述，茲分無受底床邊界效應影響之純因流體黏性因素於波動場內部作用，與同時再受底床邊界效應影響之兩種情況，即分完全與非完全光滑底床兩者，來對所考慮的眞實流體之波動現象進行理論檢核之。

(A)完全光滑底床情況

由（2.6a）至（2.6d）式與（4.16a）至（4.16d）式之比較可知，在無受邊界效應影響之完全光滑底床情況下，純因流體黏性因素對波動流場內部的作用，所造致的波動仍是屬勢流場的型態是一致的，且都具有相同的減衰特性；在 $\nu=0$ 之無黏性流體下，則完全成爲理想流體的波動勢流場。至於它們間的差異，是在於前者一開始時並無考慮入黏性因素影響在內所造成的；反觀後者則已慮及。亦因如此，這也就說明了因黏性因素的存在，而會導引出表面剪力 τ_s 與因而造致的流速 u_s，導致對波動的自由表面處之流體質點上的作用壓力有一額加的 p'，且與該處之流體剪力成 $90°$ 的相位差異；即以

$$u_s=2\nu k^2 a_o e^{-2\nu k^2 t}\frac{\cosh k(d+y)}{\sinh kd}\sin(kx-\sigma_r t) \quad \cdots\cdots\cdots(5.1)$$

代入（3.2）、（3.5）式與（4.16b）、（4.16c）兩式之應用，得有

$$\frac{1}{\rho c}\frac{\partial M_s}{\partial t}=\frac{1}{\rho c}\frac{\partial}{\partial t}\int_{-d}^{\eta\sim 0}\rho u_s\,dy=-2\nu k^2 a_o e^{-2\nu k^2 t}\cos(kx-\sigma_r t)$$

$$-4\frac{\nu^2 k^4}{\sigma_r}a_o e^{-2\nu k^2 t}\sin(kx-\sigma_r t)=-\frac{1}{\rho c}\mu\left(\frac{\partial v}{\partial x}+\frac{\partial u}{\partial y}\right)_{y=\eta\sim 0}$$

$$=-\frac{\tau_I}{\rho c}=\frac{\tau_S}{\rho c} \qquad \cdots\cdots\cdots(5.2)$$

故滿足動量守恒原則（Conservation of momentum ）而得證之。亦因有此流速的存在，故會與無黏性之理想流體的完全勢流流速者間有相位的小差異 θ_ν，爲

$$\theta_\nu=-\tan^{-1}\frac{2\nu k^2}{\sigma_r}=-\tan^{-1}\frac{k^2}{\beta^2} \qquad \cdots\cdots\cdots(5.3)$$

(B)非完全光滑底床情況

對此情況之檢核，類同上述之對完全光滑底床者般，相較（2.25a）至（2.25d）式與（4.21a）至（4.21e）式可得知，兩者所得之波動流場的減衰結果是一致的。至於進一步地說明起見，對波動流場結構細究之，即其所造致的流速分佈者。於此情況下，波動流場內因受流體黏性因素與底床邊界效應之雙重作用，所導引出的伴隨流速之水平分量說 u_1，此可由其總流速者 u 減去所對應之勢流者 u'_p 而得，故依（4.21a－e）式（於不失正確性下，方便上以複數函數型式來運算）有（當然它是純因流體黏性因素所生者 u_s與底床邊界效應造致者u_b之和）。

$$u_1=u_s+u_b=\frac{\partial\Psi}{\partial y}-a_o\sigma_r\frac{\cosh k(d+y)}{\sinh kd}e^{i(kx-\sigma t)}$$

$$=\{\sigma\Big[\frac{k\tanh md}{k\tanh md-m\tanh kd}\frac{\sinh k(d+y)}{\cosh kd}$$

$$-\frac{k\tanh md}{k\tanh md-m\tanh kd}\frac{\cosh k(d+y)}{\sinh kd}+\frac{m\,\text{sech}\,kd\cdot\text{sech}\,md}{k\tanh md-m\tanh kd}$$

$$\cdot\cosh my\Big]+i\sigma_i\frac{\cosh k(d+y)}{\sinh kd}\}\,a_o e^{i(kx-\sigma t)} \qquad \cdots\cdots\cdots(5.4)$$

由此 u_1 而於波動流場中所導引出的對應動量M_1，當然，它是由純因流體黏性因素所造成者M_s 與由底床邊界效應所導致者M_b 之和，即由 u_s 與 u_b所導引出

來者之和，為

$$M_1=\int_{-d}^{\eta\approx 0}\rho u_1\,dy=\int_{-d}^{\eta\sim 0}\rho u_s\,dy+\int_{-d}^{\eta\approx 0}\rho u_b\,dy=i\,\rho\frac{a_o}{k}\sigma_i\,e^{i(kx-\sigma t)}$$
$$=M_s+M_b \qquad\cdots\cdots\cdots(5.5)$$

依(4.21e)式及對應於上小節所述之純因流體黏性因素所導致者，則上式顯然可有

$$M_s=-i\,2\mu ka_o e^{i(kx-\sigma t)}\quad,\quad M_b=-i\frac{1}{2}\rho\frac{a_o}{\beta}\sigma_r\,\mathrm{csch}\,2kd\cdot e^{i(kx-\sigma t)}$$
$$\cdots\cdots\cdots(5.6)$$

而於此情況下，作用在波動之自由表面處之流體質點上的剪應力 τ_S，依(4.21b)與(4.21c)兩式為

$$\tau_S=-\tau_I=-\mu\left(\frac{\partial v}{\partial x}+\frac{\partial u}{\partial y}\right)_{y=\eta\sim 0}=-\mu\left(\frac{2k^2\tanh md-2mk\tanh kd}{k\tanh md-m\tanh kd}\right)$$
$$\cdot a_o\sigma e^{i(kx-\sigma t)}=-2\mu ka_o\sigma e^{i(kx-\sigma t)} \qquad\cdots\cdots\cdots(5.7)$$

由(5.6)與(5.7)兩式即刻可知 $\tau_S=\dfrac{\partial M_s}{\partial t}$，故滿足動量守恒原則，因此，3－1節所述者得證，即其於有底床邊界效應作用下亦成立之。另外，在此需做一特別說明的是，於此情況下，由於波動中恰位於底床處的流體質點其速度為零，因此，發生在底床處的剪力對波動流場並無任何作功，即其並無導致波動流場之動量的變化。由此之故，M_b 的意義是明顯的，它是純因眞實流體波動於非完全光滑的底床上之本質的邊界條件，所導致的波動本質的減衰特性者。

接著，確切地與2－2節所述之往昔結果進行比較，於此，可對(4.21a－e)式做些適足的簡化，如下。由於一般流體其黏性都為小量，故有

$$\nu\rightarrow\text{小},\ |\sigma_r/\nu|\gg k,\ |\sigma_r/\nu|\gg|\sigma_i/\nu|,$$

$$|m|=\left|\sqrt{k^2-i\frac{\sigma}{\nu}}\right|\rightarrow\left|(1-i)\sqrt{\frac{\sigma_r}{2\nu}}\right|\rightarrow\text{大} \qquad\cdots\cdots\cdots(5.8)$$

與 $\tanh md \to 1$，$|m \tanh kd| \gg |k \tanh md|$ ⋯⋯⋯(5.9)

因此，受純流體黏性因素與底床邊界效應之雙重作用下的所考慮的波動，其流場解(4.21a)至(4.21c)式可被簡化成

$$\Psi = \left\{-\frac{k}{m}\tanh md\,\frac{\cosh k(d+y)}{\sinh kd} + \frac{\sinh k(d+y)}{\sinh kd} - \frac{k}{m}\operatorname{csch} kd\,\frac{\sinh my}{\cosh md}\right\}\frac{a_o\sigma}{k}\,e^{i(kx-\sigma t)} \quad \cdots\cdots\cdots(5.10a)$$

$$u = \frac{\partial\Psi}{\partial y} = \left\{-\frac{k}{m}\tanh md\,\frac{\sinh k(d+y)}{\sinh kd} + \frac{\cosh k(d+y)}{\sinh kd} - \operatorname{csch} kd\,\frac{\cosh my}{\cosh md}\right\} a_o\sigma e^{i(kx-\sigma t)} \quad \cdots\cdots\cdots(5.10b)$$

$$v = -\frac{\partial\Psi}{\partial x} = -i\left\{-\frac{k}{m}\tanh md\,\frac{\cosh k(d+y)}{\sinh kd} + \frac{\sinh k(d+y)}{\sinh kd} - \frac{k}{m}\operatorname{csch} kd\,\frac{\sinh my}{\cosh md}\right\} a_o\sigma e^{i(kx-\sigma t)} \quad \cdots\cdots\cdots(5.10c)$$

又由(5.8)式之m及$\sqrt{\dfrac{\sigma_r}{2\nu}} \to$大與$0 \leq y+d \leq d+\eta$等條件，故可有

$$\frac{\sinh my}{\cosh md} \to -e^{-m(d+y)} \quad \text{與} \quad \frac{\cosh my}{\cosh md} \to e^{-m(d+y)} \quad \cdots\cdots\cdots(5.11)$$

因此，(4.21a)至(4.21c)式經(5.10a)至(5.10c)式與(5.11)式之應用可再被簡化爲

$$\Psi = \left\{-\frac{k}{m}\frac{\cosh k(d+y)}{\sinh kd} + \frac{\sinh k(d+y)}{\sinh kd} + \frac{k}{m}\frac{e^{-m(d+y)}}{\sinh kd}\right\}\frac{a_o\sigma}{k}e^{i(kx-\sigma t)} \quad \cdots\cdots\cdots(5.12a)$$

$$u=\frac{\partial\Psi}{\partial y}=\left\{-\frac{k}{m}\frac{\sinh k(d+y)}{\sinh kd}+\frac{\cosh k(d+y)}{\sinh kd}\right.$$
$$\left.-\frac{e^{-m(d+y)}}{\sinh kd}\right\}a_o\sigma e^{i(kx-\sigma t)} \qquad \cdots\cdots\cdots(5.12b)$$

$$v=-\frac{\partial\Psi}{\partial x}=-i\left\{-\frac{k}{m}\frac{\cosh k(d+y)}{\sinh kd}+\frac{\sinh k(d+y)}{\sinh kd}\right.$$
$$\left.+\frac{k}{m}\frac{e^{-m(d+y)}}{\sinh kd}\right\}a_o\sigma e^{i(kx-\sigma t)} \qquad \cdots\cdots\cdots(5.12c)$$

若還原至以其具有實際物理意義之型式表示時，則取其實數部份，因此，所考慮的波動流場解（4.21a）至（4.21e）式爲

$$m=(1-i)\sqrt{\frac{\sigma_r}{2\nu}}=(1-i)\beta\ ,\ \beta=\sqrt{\frac{\sigma_r}{2\nu}}\ ;\ \chi=(kx-\sigma_r t)\ ;$$

$$\sigma=\sigma_r+i\sigma_i=|\sigma|\,e^{i\theta_\sigma}$$

$$\Psi=\frac{a_o|\sigma|e^{\sigma_i t}}{k\sinh kd}\left\{\sinh k(d+y)\cdot\cos(\chi+\theta_\sigma)+\frac{k}{2\beta}\left(e^{-\beta(d+y)}\right.\right.$$
$$\cdot\{\cos[\chi+\theta_\sigma+\beta(d+y)]-\sin[\chi+\theta_\sigma+\beta(d+y)]\}$$
$$\left.\left.-\cosh k(d+y)[\cos(\chi+\theta_\sigma)-\sin(\chi+\theta_\sigma)]\right)\right\} \qquad \cdots\cdots(5.13a)$$

$$u=\frac{\partial\Psi}{\partial y}=\frac{a_o|\sigma|e^{\sigma_i t}}{\sinh kd}\left\{\cosh k(d+y)\cdot\cos(\chi+\theta_\sigma)-\frac{k}{2\beta}\sinh k(d+y)\right.$$
$$\cdot[\cos(\chi+\theta_\sigma)-\sin(\chi+\theta_\sigma)]-e^{-\beta(d+y)}$$
$$\left.\cdot\cos[\chi+\theta_\sigma+\beta(d+y)]\right\} \qquad \cdots\cdots\cdots(5.13b)$$

$$v=-\frac{\partial\Psi}{\partial x}=\frac{a_o|\sigma|e^{\sigma_i t}}{\sinh kd}\left\{\sinh k(d+y)\cdot\sin(\chi+\theta_\sigma)\right.$$
$$+\frac{k}{2\beta}\left(e^{-\beta(d+y)}\{\cos[\chi+\theta_\sigma+\beta(d+y)+\sin[\chi+\theta_\sigma\right.$$
$$\left.\left.+\beta(d+y)]\}-\cosh k(d+y)[\cos(\chi+\theta_\sigma)+\sin(\chi+\theta_\sigma)]\right)\right\}$$
$$\cdots\cdots\cdots(5.13c)$$

$$\eta = a_0 e^{\sigma_i t} \cos(kx - \sigma_r t) \quad \cdots\cdots\cdots (5.13d)$$

$$\sigma_r = \left[(gk + Tk^3)(\tanh kd - \frac{k}{2\beta} \mathrm{sech}^2 kd) - \nu^2 k^4 \right]^{1/2} ,$$

$$\sigma_i = -2\nu k^2 - \frac{k}{2\beta} \sigma_r \mathrm{csch}\, 2kd \quad \cdots\cdots\cdots (5.13e)$$

$$|\sigma| = (\sigma_r^2 + \sigma_i^2)^{1/2} = \left[1 + (\frac{k^2}{\beta^2} + \frac{k}{2\beta} \mathrm{csch}\, 2kd)^2 \right]^{1/2} \sigma_r ,$$

$$\theta_\sigma = \tan^{-1} \frac{\sigma_i}{\sigma_r} = -\tan^{-1} \left[\frac{k}{\beta} (\frac{k}{\beta} + \frac{1}{2} \mathrm{csch}\, 2kd) \right] \quad \cdots\cdots\cdots (15.13d)$$

若如2－2節所述之往昔學者，如Longuet－Higgins（1957）與Phillips（1977）等，對此種問題研究解析之考慮般，取近於底床處之微小邊界層厚度 β^{-1} 內時，則上式可由

$$\nu \to 小，T \to 小；\beta \to 大，|\sigma| \to \sigma_r ，\theta_\sigma \to 0 ；$$

$$d + y \leq \beta^{-1} ，\cosh k(d+y) \to 1 ，\sinh k(d+y) \to 小 \cdots (5.14)$$

代入之得（5.13b）至（5.13e）式恰可被簡化成（2.25a）至（2.25d）式，即與Phillips（1977）者完全一致。

5-2 試驗印證

為對本文所推導得的眞實流體之波動流場解做更具體地檢核，今引Horikawa（1968）之對水波受底床邊界效應作用下所量測得的近底床處之水平流速分佈結果，來進行實際的印證。由於清潔水的黏性甚為微小，因此，可由（5.13b）式所示之流體質點的水平速度分量u，來與Horikawa（1968）之試驗測定值比較之；清楚說明起見，該式之u被寫為

$$u = \hat{u} \cos(kx - \sigma_r t + \theta_\sigma - \theta) \quad \cdots\cdots\cdots (5.15)$$

此處 $\hat{u}$ 為u之振幅，$\varepsilon = \theta - \theta_\sigma$ 為u與所對應的脈動水位 η 間的相位差異角度；其

中 θ_σ 爲受流體黏性因素與底床邊界效應之雙重作用下而造成波動減衰，所衍生出的脈動相位角如(5.13f)式所示者。則 $\hat{u}$ 與 θ 有

$$\hat{u}=\{[\cosh k(d+y)-e^{-\beta(d+y)}\cos\beta(d+y)-\frac{k}{2\beta}\sinh k(d+y)]^2$$
$$+[e^{-\beta(d+y)}\sin\beta(d+y)+\frac{k}{2\beta}\sinh k(d+y)]^2\}^{1/2}\cdot\frac{a_o|\sigma|e^{\sigma_i t}}{\sinh kd}\qquad\cdots\cdots\cdots(5.16)$$

$$\theta=\tan^{-1}\{[e^{-\beta(d+y)}\sin\beta(d+y)+\frac{k}{2\beta}\sinh k(d+y)]$$
$$/[\cosh k(d+y)-e^{-\beta(d+y)}\cos\beta(d+y)-\frac{k}{2\beta}\sinh k(d+y)]\}\qquad\cdots\cdots\cdots(5.17)$$

如同Horikawa(1968)之試驗情況，當能量繼續補足因流體黏性因素與受底床邊界效應之雙重作用下而生之波能消散時，即在所考慮的流體波動無減衰而如最初 $t=0$ 時的脈動情況下，則在Horikawa(1968)所定義之水平速度分量的振幅的無因次形式下，有

$$t=0,\ \frac{\hat{u}}{\hat{U}}=\{[\cosh k(d+y)-e^{-\beta(d+y)}\cos\beta(d+y)$$
$$-\frac{k}{2\beta}\sinh k(d+y)]^2+[e^{-\beta(d+y)}\sin\beta(d+y)$$
$$+\frac{k}{2\beta}\sinh k(d+y)]^2\}^{1/2}\cdot\{1+(\frac{k^2}{\beta^2}+\frac{k}{2\beta}\operatorname{csch}2kd)^2\}^{1/2}\qquad\cdots\cdots\cdots(5.18)$$

式中 $\hat{U}$ 爲Horikawa(1968)所引用的水平流速分量的振幅參數，於本文的符號下，爲

$$\hat{U}=\frac{a_o\sigma_r}{\sinh kd}=\frac{\pi H_o}{T_o\sinh kd},\ \sigma_r=\frac{2\pi}{T_o},\ H_o=2a_o,\qquad\cdots\cdots\cdots(5.19)$$

T_o 爲波動之週期，H_o 爲其起始之波高。

以(5.17)至(5.19)式所示之本文對水波情況的理論解析結果與Horikawa(1968)之試驗值比較，如圖㈢與圖㈣所示。

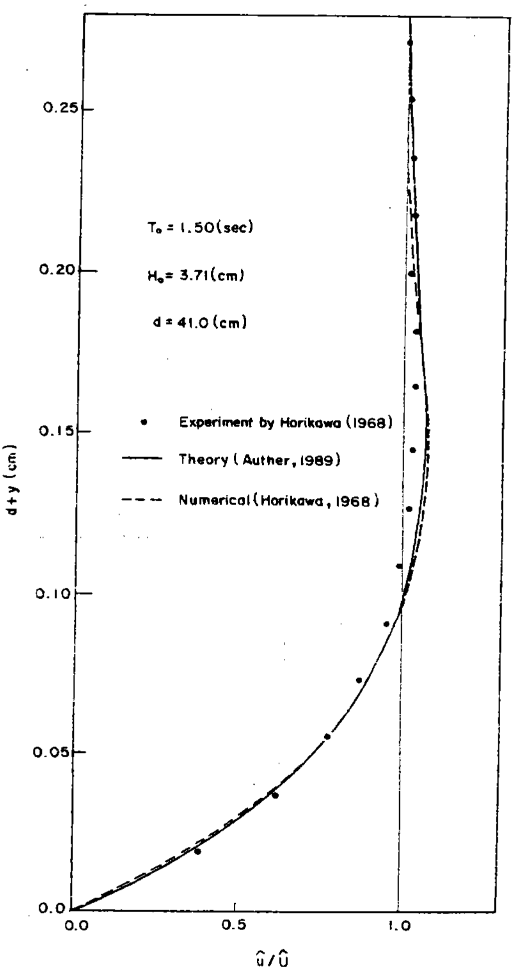

圖㈢　水平速度分量之振幅比 $\hat{u}/\hat{U}$

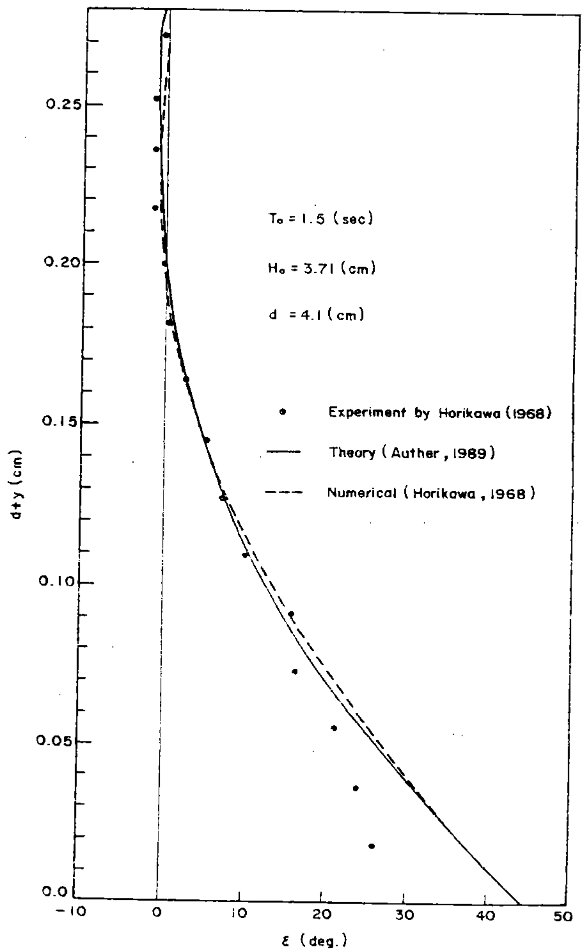

圖㈣　水平速度分量與水位脈動間之相位差

由上二圖的顯示，即刻可知本文的理論結果與試驗者頗相一致，因而得到適切的驗證。

依據本節上述的闡論，這當是明顯可被確知的，本文對均勻靜穩大氣下等深中之自由表面規則前進的眞實流體波動，所解析推導得的結果，其適足性已獲得當有的理論檢核與試驗印證。

六、結論與討論

綜合本文以上之整個論述，在此可對所考慮的均勻靜穩大氣下，等深中之自由表面規則前進的眞實流體波動，其流場機構特性給予幾點較明確顯然的結語，有

(一)波動自由表面處因流體黏性因素而生剪力的存在，會導引出對該處的流體質點有一額加的作用壓力，且其脈動相位與剪力者恰成 90° 的差異。

(二)在純受流體黏性因素之作用下，眞實流體之波動流場仍屬勢流場的型態，且其與理想流體者間的差異受流體黏性因素的左右，當流體無黏性時，則波動流場完全退化成理想流體者。

(三)波動受底床邊界效應的作用所造成的影響，由深海時的無影響隨深度的變淺而急遽地加烈之，成深度的超越函數（ Transcendental function ）之反比。

(四)由於一般的流體其黏性爲小，故大觀而言，除受邊界效應作用下之近於邊界處的流體薄層內，如本文所述者之非完全光滑底床情況除很近於底床處，波動場可視爲勢流的形式。亦因如此，除對一些很特定的課題外，如風吹刮流體表面生波或波對底床質的推移等之考慮外，否則眞實流體的波動可依理想流體者處理之，即不計流體黏性，其他工程上的目的亦可不考量之。

雖然於本文所考慮的情況下，眞實流體波動之主要現象已被概要地描述，然對其會涉及到的一些實際現象，於此似乎可稍做些討論：如當底床是粗糙者，則波動會在近於底床處產生紊亂流動的現象當需被注意，參見 Kajiura（ 1968）、Horikawa（ 1968 ）與 Hsu & Ou（ 1989 ）等；另，當底床質是鬆的，如沙者，則流體質點於上面之可滑動性與滲透性亦得慮及；至於自由表面處之外來

剪力與不均勻氣壓的作用，對眞實流體波動會造成相當的影響亦該探究；對波動更細節特性的考量，如其質量傳輸（Mass transport），則當推求至較高階的解析中。

附　註

於第四節之波動流場解的解析中所言，以（3.15）式或（3.16）式做爲所要解的波動流場之自由表面的動力邊界條件式，不論於完全或非完全光滑底床情況，是一致的，茲將導證之於下。

以波動流函數 Ψ 之通解式（4.7）或（4.18）式代入（3.15）與（3.16）兩式中，於第一階下，得

$$\left(-\frac{\sigma}{k}-i2\nu k\right)(kA-kB+mC-mD)+Tk^2a_o-i2\nu k^2(A+B+C+D)$$
$$\cdot\coth kd+ga_o+i\frac{\nu}{k}m(m^2-k^2)(C-D)=C_1(t) \qquad \cdots\cdots\cdots (A.1)$$

與
$$-k\sigma\left(\frac{A}{k}-\frac{B}{k}+\frac{C}{m}-\frac{D}{m}\right)-i2\nu k(kA-kB+mC-mD)+Tk^2a_o$$
$$-i2\nu k^2(A+B+C+D)\coth kd+ga_o+i\nu k\left[(m^2-k^2)\right.$$
$$\left.\cdot\left(\frac{C}{m}-\frac{D}{m}\right)\right]=C_2(t) \qquad \cdots\cdots\cdots (A.2)$$

由（A.1）式減（A.2）式，得

$$\left(-\frac{\sigma m}{k}+\frac{\sigma k}{m}\right)(C-D)+i\nu\left(\frac{m}{k}-\frac{k}{m}\right)(m^2-k^2)(C-D)$$
$$=\left[\sigma-i\nu(m^2-k^2)\right]\left(\frac{k}{m}-\frac{m}{k}\right)(C-D)=C_1(t)-C_2(t)=0$$
$$\cdots\cdots\cdots (A.3)$$

此乃因 $m^2=k^2-i\dfrac{\sigma}{\nu}$ 故，故得證。

參考文獻

Chen,Y.Y.1988 Investigation on the finite-amplitude standing gravity waves in water of any uniform depth. Research Paper of Basic Theory , The Institute of Harbour & Marine Technology, Wuchi, Taiwan, T.O.C.

Cokelet,E.D.1977 Steep gravity waves in water of arbitrary uniform depth. Phil. Trans.R.Soc.A.286,183-230.

Goda,Y.and Kakizaki,S.1966 Study on finite amplitude standing waves and their pressure on a vertical wall(in Japanese). Rep. Port Harbour Res. Inst. Japan, Vol.5,No.10.

Harrison,W.J.1908 The influence of viscosity and capillarity on waves of finite amplitude. Proc. Lond. Math. Soc. Ser.2, Vol.7,107-121.

Hasselmann,K.1961 On the nonlinear energy transfer in a wave spectrum. In Ocean Wave Spectra. Englewood Cliffs, N.J.: Prentice-Hall, Inc.pp.191-197.

Hasselmann,K.1962 On the non-linear energy transfer in a gravity wave spectrum. Part 1, General theory, J. Fluid Mech, 12,481-500.

Hasselmann, K. 1963 On the non-linear energy transfer in a gravity wave spectrum. Part 2, Conservation theorems ; wave Particle analogy; irreversibility. J.Fluid Mech. 15,273-281.

Hasselmann,K.1963 On the non-linear energy transfer in a gravity wave spectrum. Part 3, Evaluation of the energy flux and swell sea interaction for a Neumann spectrum. J.Fluid Mech. 15,385-

398.

Hasselmann,K.et XV al. 1973 Measurements of wind wave growth and swell decay during the Joint North Sea Wave Project(JONSWAP). Herausgegeben vom Deutsh. Hydrograph. Institut., Reihe A,No.12.

Horikawa,K.and Watanabe, A.1968 Laboratory study on Oscillatory boundary layer flow.Coastal Engineering in japan, Vol.11,13-28.

Hough,S.S.1896 On the influence of viscosity on waves and currents. Proc. Lond. Math. Soc. Ser.1.28,264-288.

Hsu,J.R.C., Tsuchiya,T.& Silvest3r, R.1979 Third-order approximation to short-crested waves. J.Fluid Mech. 90,179-196.

Hsu,J.R.C.,Silvester,R.& Tsuchiya,Y.1980 Boundary-layer velocities and mass transport in short-crested waves, J.Fluid Mech.99 ,321- 342.

Hsu,T.W. and Ou,S.H.1989 Turbulent boundary layer of water waves near a smooth bottom. J.C.I.E. Vol.12,No.5,545-555.

Kajiura,K.1968 A model of the bottom boundary layer in water waves. Bull. Earthquake Res Inst., Univ, of Tokyo, Vol.46.

Longuet-Higgins, M.S.1957 The mechanics of the boundary layer near the bottom in a progressive wave. Proc. 6th Conf. on Coastal Eng. 184-193.

Longuet-Higgins,M.S. 1969 Action of a variable stress at the surface of water waves. Phys. Fluids, 12,737-740.

Mitsuyasu, H.1984 Recent studies on ocean wave spectra. 18th Internatioal Cong. of Theo. and Appl. Mech., Denmark,1-13.

Phillips, O.M.1960 On the dynamics of unsteady gravity waves of finite amplitude. Part 1, The elementary interactions. J.Fluid Mech. 9,193-217.

Phillips, O.M.1961 The dynamics of random finite amplitude gravity waves. In Ocean Wave Spectra. Englewood Cliffs, N.J.: Prentice-Hall, Inc.pp.171-178.

Phillips, O.M. 1977 The dynamics of the upper ocean. Cambridge University Press, London. 2-ed.

Pierson, W.J., Jr., and Moskowitz. L. 1964 A proposed spectral form for fully developped wind seas based on the similarity theory of S.A. Kitaigorodskii. J.Geophys. Res. 69,5181-5190.

Rienecker,M.M.and Fenton,J.D.1981 A Fourier approximation method for steep water waves. J.Fluid Mech. 104,119-137.

Stewart. R.W. 1967 Mechanics of the air-sea interface. Phys. Fluids, Suppl.10,S47-54.

Stokes,G.G.1847 On the theory of oscillatory waves. Trans. Camb. Phil. Soc.8,441-455.(Also in Mathematical and Physical papers, Vol.I.London: Cambridge University Press,1880.pp.197-229.)

Tadjbakhsh, I. and Keller, J.B.1960 Standing surface waves of finite amplitude. J.Fluid Mech.8,442-451.

Tick,L.J.1959 A non-linear random model of gravity waves I.J.Math. & Mech.8,643-652.

Tick,L.J. 1961 Nonlinear probability models of ocean waves. In Ocean Wave Spectra. Englewood Cliffs, N.J.: Prentice-Hall, Inc.pp.163-169.

Williams,J.M.1981 Limiting gravity waves in water of finite

depth. Phil. Trans.R.Soc.Lond.A.302,139-188.
林西川 1988 非線性重力波之數值解析，國立成功大學土木工程研究所博士論文。
陳陽益 1983 波浪通用模式與最大波之解析，國立成功大學土木工程研究所博士論文。
陳陽益、湯麟武 1987 波譜之力學基礎，第九屆海洋工程研討會論文集，271 — 287 。
陳陽益、許榮中 1988 檢視兩前進重力波列之交會，第十屆海洋工程研討會論文集，79 — 113 。
陳陽益、莊文傑 1988 深海中兩規則前進重力波列交會之流場特性，第十二屆全國力學會議，19 — 31 。
陳陽益 1988 重力駐波，港灣技術第三期，71 — 107 。
陳陽益 1989 兩波交會之系統化與流場機構，港灣技術第四期，27 — 60 。
陳陽益 1989 直立堤面上重複波之解析，港灣技術研究所 78 — 研㈨報告。
陳陽益、邱永芳、莊文傑 1989 前進重力波與鮮波之關連，第十一屆海洋工程研討會論文集，273 — 298 。
陳陽益 1989 等深水中兩規則前進重力波列交會之解析，港灣技術第五期，1 — 45 。
陳陽益、邱永芳 1989 短峰波——兩規則前進波列交會之一例，港灣技術第五期，125 — 162 。
張憲國、陳陽益、歐善惠 1989 深海中三重力波列之交互作用㈠——三階攝動近似解，港灣技術第五期。

Some Realities for Waves Motion in Fluid

Chen Yang-Yih

Senior Researcher & Chief of Mathematical Model Division
Institute of Harbour & Marine Technology, Taiwan, R.O.C.

Frederick Tang, L.W.

The Emeritus Professor of Cheng Kung University, R.O.C.

ABSTRACT

In stationary atmosphere, the progressive waves motion in a real fluid of uniform depth is analysed by using Navier-Stokes equation, and describe its mechanism in first-order approximation. Based on the principle of momentum conservation, it is shown that the tangential stress existed at the free surface of the waves motion will dynamically induce a normal pressure at there, and having difference $\pi/2$ in phase with the tangential stress. From the obtained solution,it finds that the waves motion in real fluid is still belonging to the potential flow type under the influence of its viscosity purely, and being degenerated to that of ideal fluid as the viscosity without existence; for the case in which the bottom effect is acting, the mechanics of the waves motion in whole flow field, including the structure in the boundary layer near the bottom, is demonstrated. The analytical results derived in this paper are compared to those obtained by the preceding investigators both theoretically and experimentally for near the bottom,the good agreements between them reveal that the present analytical formulation to the waves motion of real fluid is fairly appropriate.

第三屆基礎港灣數值（數學）模式研習會論文集　　Jan. 17～18，1990 Page 43～68

堤角渦流之可視化研究

黃煌煇

國立成功大學水利及海洋工程研究所教授
台南水工試驗所所長

摘　要

為瞭解海岸人工結構物受波浪作用後之流場特性及其影響地形變化之力學機構，本研究乃以流場可視化法（Flow Visualization）並輔以特殊雷射光切面技術，藉此則可對受波浪作用而衍生之渦流結構作一定性之研究。以探討堤體附近底床粒子之傳輸特性。根據實驗之結果可獲至以下之結論：當波浪入射角小時，堤體底床附近粒子將因渦流之擾動而產生侵蝕現象，反之則堤體內側產生淤積。此外，堤體之渦流結構及其尺度之大小與水深條件或入射波高均有顯著關係，而週期亦為一重要影響因素；例如長週期之渦流外形較為明顯完整，其質傳捲動力亦強。由以上結果可知，受波浪作用之堤體渦流結構應是決定堤體附近是否淤積或侵蝕之重要因素。

一、概　論

沙質底床之海岸有時為防止波浪侵襲或阻截沿岸漂沙活動等等目的而構築海岸結構物，然在結構物設置下，波浪能量引起沿海岸方向之漂沙運動受到遮攔，因此在結物前端附近時常產生局部性之淤積或侵蝕，引起海岸地形發生嚴重變化，此等變化為一工程師從事港灣規劃設計不可或缺之重大參考資料。

海岸結構物之設置沿海底床沉積物之傳輸、堆積、侵蝕，皆受海洋波浪及流況之影響。尤其在海岸結構物附近之水流運動現象及機構更為複雜而難以預

知，因此，須先藉流場可視化(Flow Visualization)法進行一定性上之研究，掌握其運動現象，始能進一步深入探究其中之各種力學機構。

本文之主要目的，亦即利用流場可視化法探討防波堤堤脚受波浪作用所產生之渦流(Vortex)流況。在前人的研究中，關於防波堤附近流況有謝、郭、楊[1]等提出防波堤與海岸交角附近，水流受到反射波之擾動而產生許多正逆向迴流，迴流流況與堤之距離有密切關係。Gourlay[2](1974)提出離岸堤之沿岸流流況在遮蔽區內，受堤體阻擋爲一封閉圓形式。而磨[3]之數值模擬分析則顯示堤角渦度(Vorticity)在波浪斜向入射時，上游堤端變化較下游劇烈，此外亦可藉分析影響區域範圍及流速變化，對侵淤現象加以預估。在底床粒子運動方面，歐、張[4]指出在流速、波高較大情況下，堤體附近沙粒不易沉降，此乃由於強勁之離岸流帶走部放份漂沙。

鑑於波浪由深海傳至防波堤時，由於波浪水流衝擊堤岸，因而堤岸之二側(向岸側，離岸側)將產生渦流(Vortex)及一連串混亂之流況。而此類流況與堤角附近地形穩定性間之關係，乃爲結構物安定性及工程維護上之一重要影響因素，是以本文以流場之可視化法，利用雷射光切面及聚苯乙烯顆粒對渦流之內部流場，底床流場，渦流外觀做一定性可視化研究，以期能瞭解渦流場及內部，底床之運動現象。同時比較不同波浪條件及波浪入射角度下底床顆粒之動向。

根據實驗瞭解，渦流之大小與堤岸處的水深有密切關係。一般言之，堤岸水深較淺處產生的渦流較大；同一造波條件下，波浪的入射角度差異對於堤岸附近產生渦流的位置有十分密切的關係，波浪入射角愈小時粒子帶往深海者較多。在此情況下，堤岸本身將會有侵蝕現象發生，反之入射角愈大粒子帶往淺海者多，因此可能導致堤岸內側有淤積之行爲；深海波高較大作用下，堤岸附近之渦流明顯，鑽深程度與底床顆粒運動加劇。而長週期之波浪其挾帶之能量較大，渦流外形完整，渦動力量大，捲動粒子多且拋射較遠。其次，渦流影響區域僅侷限於堤角附近之一鐘形區域，其區域範圍大小受波高因素影響較劇。

二、試驗設備、試驗佈置及試驗步驟

2－1 試驗設備

2－1－1 造波水槽

本試驗係在台南水工所之雷射試驗室進行，試驗水槽長 9.5 公尺、寬0.3 公尺、高 0.7 公尺，兩側以強化透明玻璃敷設，以便利於觀察。底床爲可活動式，分成兩部份，前半段爲固定式水平底床長爲 3.8 公尺，後半段底床之設計爲活動式斜坡底床，可調整所需之底床坡度，長爲 5.7 公尺。整個試驗水槽之設置如圖 2 － 1 所示。

水槽之造波機爲平推活塞式（Piston Type）造波機，其造波週期可由 0.3 秒至 1.5 秒任意調整，而波高最大可達 15 公分，斜坡活動底床可由支撐桿調整至1/10 以下之坡度。

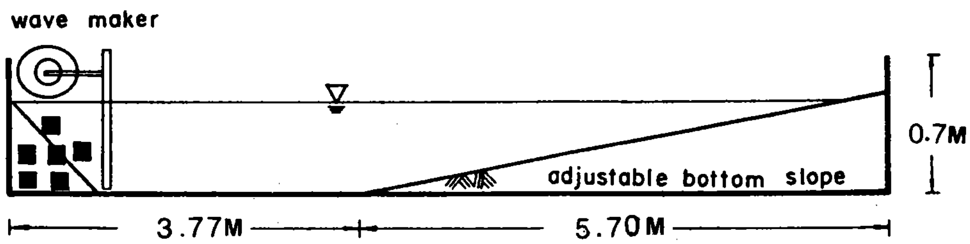

圖 2 － 1　試驗水槽設置圖

2－1－2 光源、影像分析及攝影設備

本試驗旨以流場可視化法（ Flow Visualization ）觀測堤角渦流（ vortex ）之運動現象，並以追蹤顆粒觀測外觀，內部流場和底床顆粒運動現象。因此必須借助各種不同攝影器材，並輔以適當之照相光源，以高速拍攝其運動軌跡及流場變化。

至於試驗中使用之攝影器材及影像分析設備簡述如下：

(1)高級專業用單眼相機：爲日本Kyoreca 公司製造之Contex單眼相機，配合自動捲片機，捲片時間可達 0.3 秒，曝光時間可至 1/2000 秒。可依觀測流場之運動狀況，調整曝光時間，凍結流場運動，得到適當的流況記錄。

(2)錄影攝影機：爲日本 Sony 公司製造之攝影機，可同時由監視器觀測並錄下分析所需的畫面。

(3)錄放影機及監視器：爲日本 Sony 公司製造，可錄下影像，依正常放映速度或五分之一、十分之一及三十分之一的速度放映。

配合攝影的輔助光源有：

(1)攝影燈：爲西德 Bohme 公司所製造，其輸出功率可達 2000 w，主要用於渦流外觀結構之觀測。

(2) 2 W Argon Ion 雷射：雷射光束經光學圓柱晶棒，可折射爲片狀光面，其厚度約 1 mm 至 3.3 mm ；以利於內部流場及底床顆粒運動之觀測，追蹤顆粒在此薄片光面下之運動變化。

2－2 追蹤顆粒

本試驗採用之追蹤顆粒係有二種：一爲半透明之聚苯乙烯顆粒（polystyrene bead），其比重約 1.032 ，顆粒直徑約 0.3 mm 至 1.2 mm之間。另一爲聚苯乙烯顆粒表面以凡立水（Vanish）作粘著劑，均勻包襯微量之螢光劑，形成有色顆粒。而本試驗所使用之螢光劑和追蹤顆粒之製作均和許．[5] (1987) 相同。

2－3 試驗佈置

2－3－1 試驗模型佈置

本試驗採用之模擬堤體，乃爲一透明壓克立平板置於水槽內。平板寬4.0 公分、厚 1.0 公分、高 45.0 公分，上方連結另一塊壓克立平板以固定之。模型緊貼水槽玻璃壁，下方並粘上厚約 5 mm 之軟塑膠，以利於水槽上方施以重

壓時，模型下方可以和斜坡底床完全密和。另外爲了模擬不同之波浪入射角度，特將模型製成可向岸或離岸旋轉 30° 角。其模型略圖如圖 2 － 2 所示。

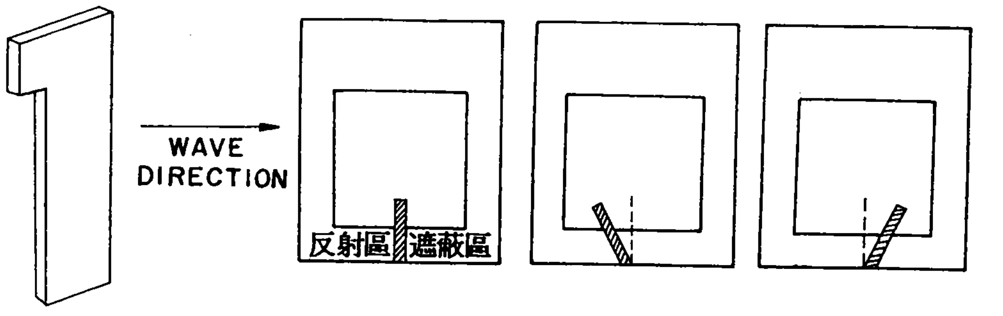

圖 2 － 2　試驗模型圖

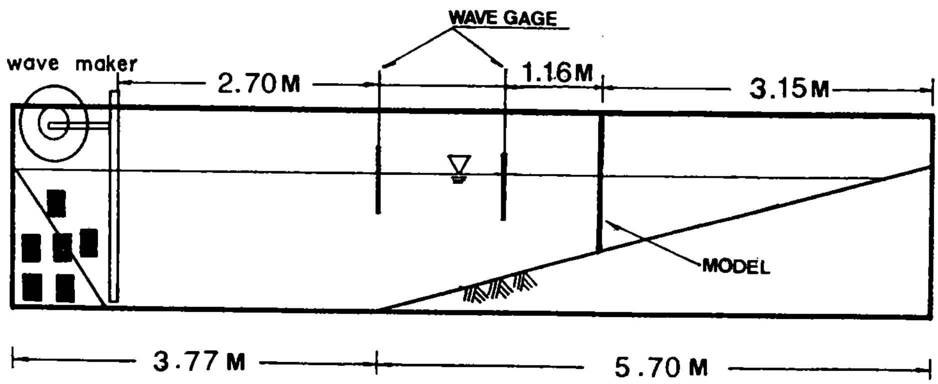

圖 2 － 3　試驗佈置圖

爲了拍攝清晰明亮的畫面，以利定性分析，故除了觀測區域外，均以黑色壁報紙阻絕一切可能強烈反射之光源，並關閉所有燈光，以免影響光源效果。另爲瞭解入射波浪之特性，因此乃在等水深段佈置一波高計，而測區之相位變化則經事先測試後，以另一支波高計置於與測區有同時相位變化的位置，如此可得測區之相位變化。整個試驗模型與波高計佈置圖如圖 2 － 3 所示。

2－3－2　攝影器材佈置

觀測渦流之外觀結構時，水面變化及渦流捲入氣柱乃爲主要研究對象，故試驗中以2000 瓦特之攝影燈，置於水槽上方照射，繼以相機拍攝之。爲免水面波動強烈散射光源，影響畫面效果，故以俯角拍攝一系列之渦流外觀結構，以作爲渦流形成與消散之定性變化上之觀測。其試驗佈置如圖 2 － 4 所示。

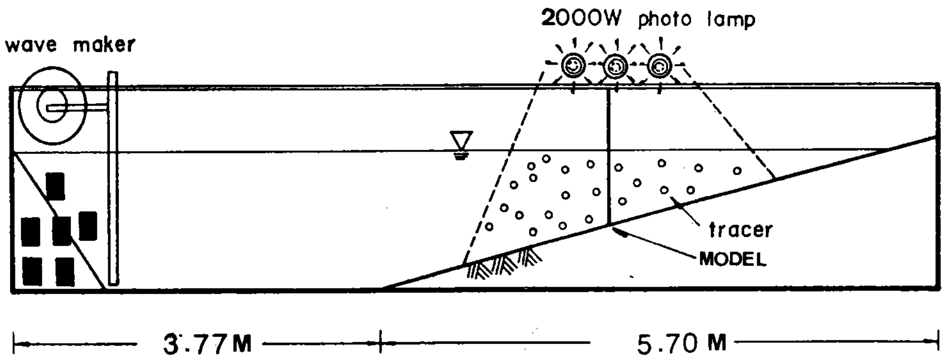

圖 2 － 4　2000 瓦特光源照相佈置圖

再者，爲瞭解渦流內部流場之整個流場結構，乃藉重 2 W Argon Ion 雷射作爲入射光源。鑑於渦流附近水面波動極爲混亂，易將雷射入射光源散射，影響可視化效果。爲解決此一問題必需將雷射光束由底部往上切光，因此乃將光學圓柱晶棒與一平面反射鏡置於碎波點附近底床，在水中將雷射光束折射爲薄片扇狀光面，使光面不受水面波動影響，且平面反射鏡與晶棒均極小並遠離測區，故可減少其對波動流場之影響。其佈置圖如圖 2 － 5 所示。

由於渦流流場爲一個典型的三維運動，欲觀測垂直渦流之流場結構及底床

顆粒運動情形運動情形，特將Argon Ion 雷射置於水槽側方，調整光學圓柱晶棒折射角度使扇狀光面平貼底床，激發底床之追蹤顆粒，使底床運動現象可視化。圖２－６爲其佈置示意圖。

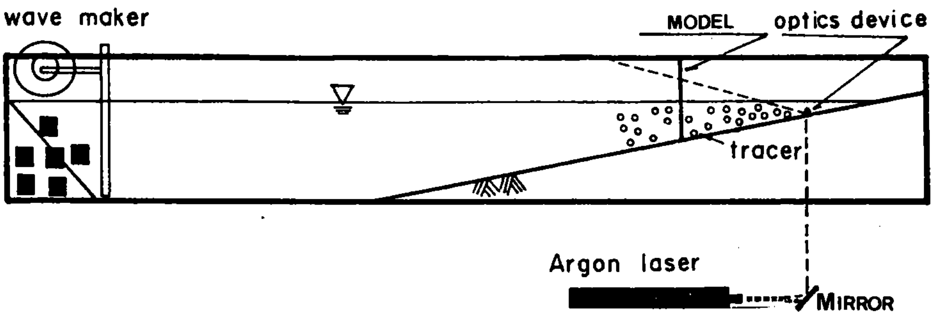

圖２－５　雷射光切面水底佈置圖

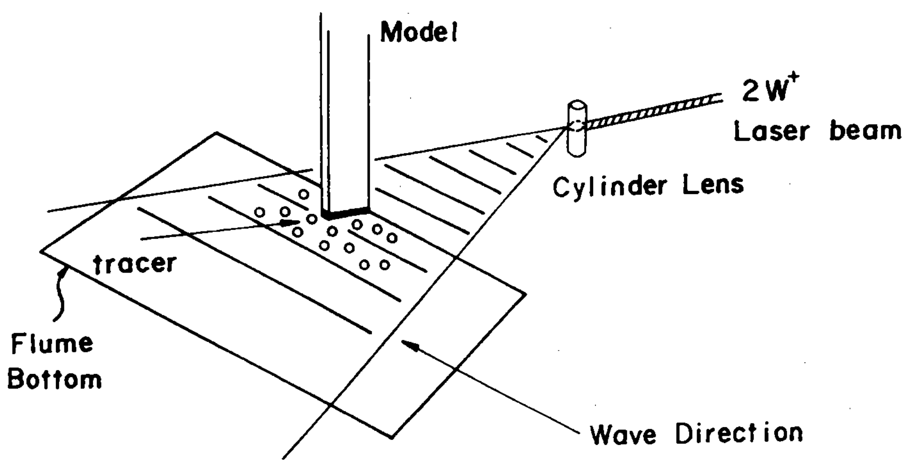

圖２－６　雷射光面平貼底床示意圖

2－4　試驗條件與試驗步驟

2－4－1　試驗條件

本試驗旨在觀測渦流外觀，內部流場及底床顆粒運動之特徵。為使渦流現象能清晰顯像，因此必需愼選其造波條件，由於模型結構物影響水槽波浪之反射率，致使波高發生擾動，是以選定之標準有二：一為不使內部流場速度過大，以利凍結流況，得到較佳的效果；一為等水深段的造波條件不因結構物影響而變化太大，選定等水深段擾動前後的波高誤差在百分之五以下。再者，為明瞭波浪入射角度的影響，因此改變模型角度，如圖２－２所示。除此之外，另選定兩種造波條件，作為對照觀測；期能瞭解不同之波高，週期而造成底床質傳之定性差異。整個試驗之造波條件詳見表２－１。

2－4－2　試驗步驟

首先，為便於觀測與分析，在從事可視化試驗前，先於靜水狀態下利用鋼尺，置於觀測區內，測定焦距。

本可視化試驗計有下列三項，其步驟分述如下：

(1)渦流外觀及內部場：如圖２－４、圖２－５所示，放入追蹤粒子，懸浮水體中，由於受到渦流擾動顯像流場運動後再予以攝取整體畫面。

(2)底床粒子運動現象：光源切面如圖２－６所示。造波前先在底床放置追蹤粒子，相機以一適當的俯角拍攝畫面。相機快門線與波高計同時連結於類比數位信號轉換器（Analog/Digital Converter）經由電腦取樣並分析，如此便可精確地得知每張相片相對之相位記錄。以上兩種均在同一造波條件下進行。

(3)第三種則是在不同模型轉角，不同造波條件下，分別在造波前、後拍攝底床粒子分佈狀況。全部過程均經由電視錄影攝影機拍攝之。

表 2 — 1　試驗造波條件

轉角	斜度	T (sec)	H_i (cm)	d_i (cm)	d_m (cm)	觀測型式
0°	1/15	1.01	4.18	28	10	A , C
	1/15	1.01	2.48	28	10	B
	1/15	1.33	3.21	28	10	B
− 30°	1/15	1.01	4.23	28	10	B , C
	1/15	1.01	2.51	28	10	B
	1/15	1.33	3.21	28	10	B
+ 30°	1/15	1.01	4.08	28	10	B , C
	1/15	1.01	2.17	28	10	B
	1/15	1.33	3.26	28	10	B

符號說明：

T ：週期

H_i ：等水深段波高

d_i ：等水深段水深

d_m ：測點處水深

轉角：　0° ………垂直水槽壁面

+ 30° ………向遮蔽區轉 30° 角

− 30° ………離反射區轉 30° 角

觀測型式：

A ：渦流外觀、內部流場

B ：不同造波條件、模型轉角對照觀測

C ：底部粒子運動現象觀測

三、試驗結果與討論

3－1 渦流的外觀現場

波浪由深海傳播至淺海的過程中，當波峰面到達堤岸，靠堤側之波浪面將沖擊堤岸而產生反射，此區稱之爲反射區，遠離堤岸側之波浪將繼續通過堤岸，此區稱之爲進行區，而在堤岸後側之水面稱之爲遮蔽區。如圖３－１所示。

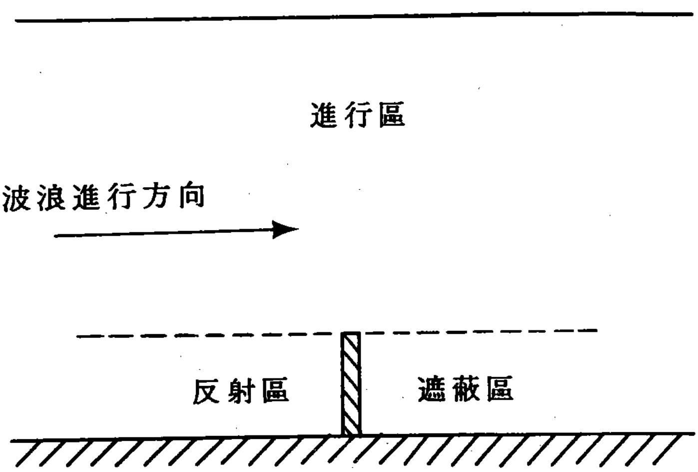

圖３－１　波浪到達堤前之分區圖

本實驗進行時，當波峰傳播至堤岸時，反射區內之波浪將由於結構物之阻擋而產生反射，同時亦將在堤前產生水面湧昇之現象，而使反射區內的水位比遮蔽區之水位爲高，即在二區間產生一明顯的速度差，而在遮蔽區內產生一順時針渦流ｖ１，（如相片３－１－１），渦流ｖ１隨著波峰的前進，向岸流速度的增大，氣柱將漸漸地增大鑽深，（如相片３－１－２），隨後當渦流完全成熟後，渦流ｖ１最下方之氣柱將因上層速度大於下層速度產生扭曲現象（相片３－１－３），而將氣柱內之氣泡捲入水中，水面下之氣泡隨波浪前進，直到向岸流逐漸被離岸流取代，渦流ｖ１也因此消滅變小，最後只剩下些許氣泡

反射區　　遮蔽區

相片 3 － 1 － 1 堤岸前後水位差

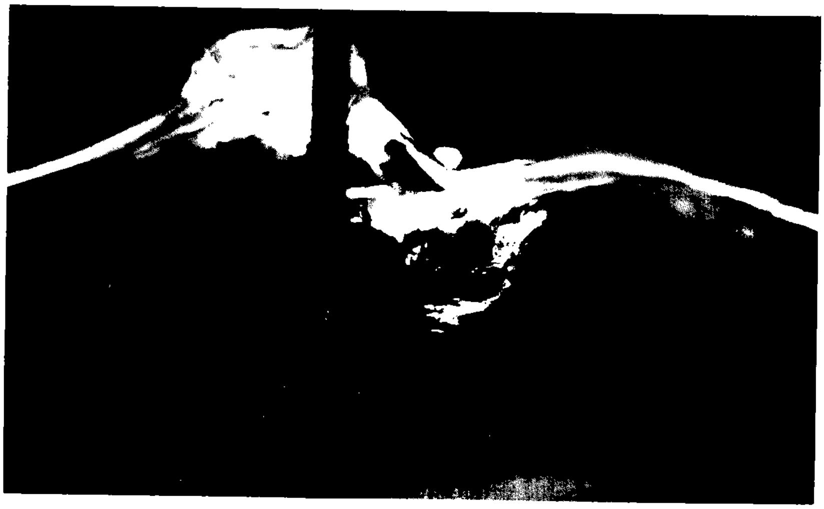

反射區　　遮蔽區

相片 3 － 1 － 2 遮蔽區之渦流氣柱鑽深

反射區　　遮蔽區

相片 3 － 1 － 3 遮蔽區之渦流到達最大鑽深深度後向上浮升過程

漂浮在水中。（如相片３－１－４）。

然當遮蔽區之渦流消失時，反射區之波浪已在波谷之相位，因此遮蔽區之水位反而高於反射區，此時很明顯地可見到亦產生一渦流ｖ２，但其方向則爲反時針方向（如相片３－１－５）。而此渦流ｖ２發生之相位經實驗觀察結果發現在波谷到達時形成並向深海方向擴張（如相片３－１－６所示）。然當深海之波浪在往前傳遞而與渦流ｖ２相遇後，渦流即停止繼續往深海移動，而隨波峰撞擊堤面而消失。往後波浪及渦流流場將如前所述重覆發生。

由實驗所測得之波形資料知，波浪行經斜坡堤岸，將發生水平非對稱，零上切點以上波峰面約爲波谷面之１／２，因此渦流ｖ２從產生到消失之時間約爲渦流ｖ１的２倍，但由於反射區之水位差較小，因此渦流ｖ２的大小反比渦流ｖ１小。

由於波浪碰及堤岸結構時，會產生嚴重的擾動現象，光線到達水面後將有嚴重的漫射現象，所以難以使用相機攝取渦流的水平位置圖，僅能由試驗中觀察知之其梗概。現將觀測結果說明如下：

波浪之波峰面產生之渦流ｖ１，由水槽上方觀察得悉順時針渦流ｖ１於遮蔽區之堤頭產生後隨波浪之前進，渦流ｖ１增大且鑽深，同時整個渦流亦以反時針方向向淺岸移動。然當波谷相位到達堤岸後，於反射區之堤頭將產生反時針之渦流ｖ２，渦流ｖ２亦隨波谷相位之延續而以順時針方向往向海面移動，直到下一個波峰面與之接觸後，旋即再往向岸面移動。（如圖３－２）。

3－2 渦流的底床狀況

由於海床底質受到渦流運動之變化無法應用一般觀測方法得悉，因此必需應用雷射光切割運動面後由其激發底床處之懸浮顆粒之光點攝取運動畫面以瞭解其運動軌跡。基此，首先以雷射光平切於水槽底床，以Ａ／Ｄ同時搜取相機快門時間以及波形之相位，得如相片３－２－１至相片３－２－９，九個不同相位的底床粒子運動現象。而相位之決定以波形之零上切點至下一個零上切點爲一週期。

相片３－２－１之可視化結果係波浪相位在堤面處爲ｔ／Ｔ＝0.03之渦流

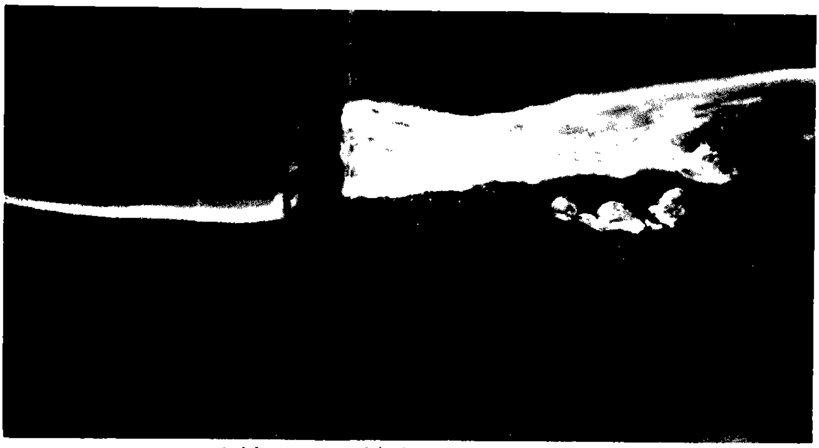

反射區　　遮蔽區

相片3－1－4 遮蔽區之渦流消失氣泡浮至水面

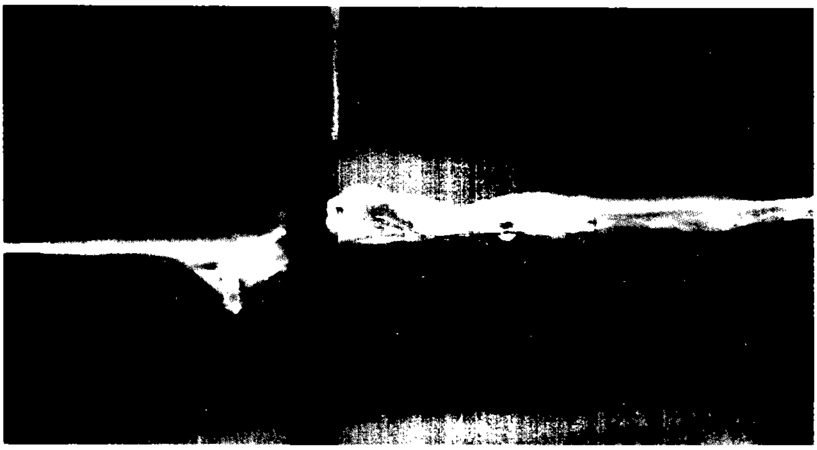

反射區　　遮蔽區

相片3－1－5 遮蔽區水位大於反射區而產生渦流

反射區　　遮蔽區

相片3－1－6 波谷到達後反射區形成渦流氣柱向下鑽深

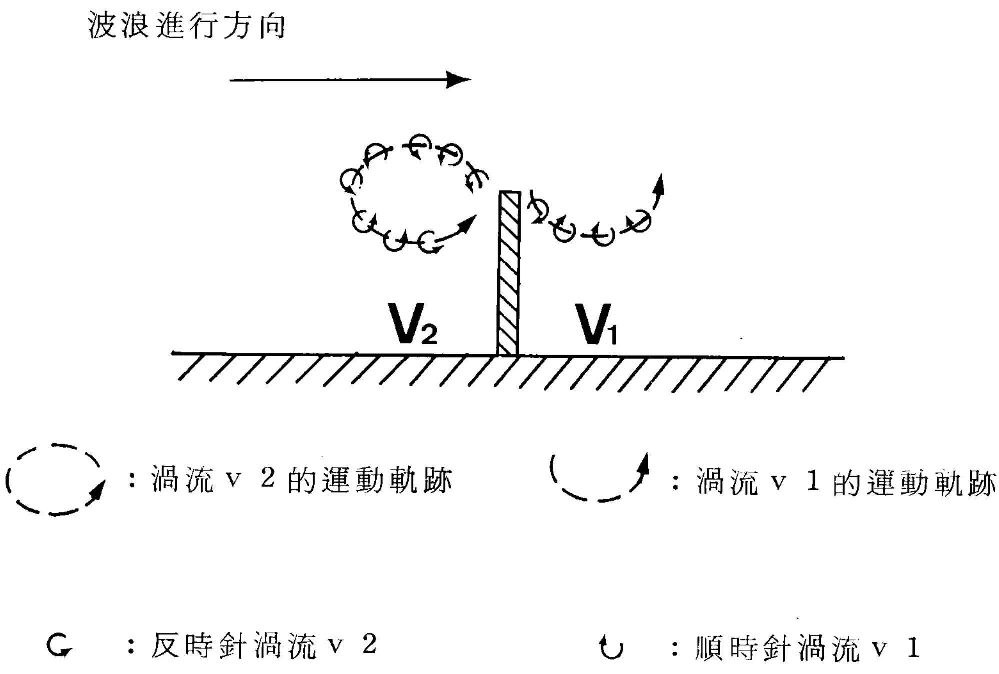

圖３－２　波浪在堤岸附近形成之上視示意圖

流況，吾人可清楚看出堤岸右側遮蔽區由於波浪受到堤岸結構之影響，因此逐漸產生渦流（此可由相片中右側之不規則化光點視之）。相片３－２－２則爲波浪ｔ／Ｔ＝0.07之流況，在右側靠近堤岸結構處有明顯較小尺度之渦流形成。及至波浪相位ｔ／Ｔ＝0.17時（相片３－２－３）除較小尺度之渦流已逐漸擴展且由於此時波浪相位已在波峰之附近，因此吾人可明顯看到堤岸右側已存有大形之渦流運動。再者，波峰相位通過後，此渦流運動乃隨波浪向岸側擴展，因此由相片３－２－４（ｔ／Ｔ＝0.22）可看出其渦流尺度大而強度漸減。然後，波浪相位逐漸接近靜水位時，波浪水平速度亦逐漸變小，因此渦流運動逐漸消失。接著，波浪相位逐漸入波谷之時段，因此遮蔽區外之渦流則消失殆盡而堤岸左側之反射區亦將形成小尺度之渦流，此可由相片３－２－６及３－２－７示之。而相片３－２－８則爲波浪相位ｔ／Ｔ＝0.87時之流況，由於此

相片 3 － 2 － 1 波浪相位 t ／ T＝ 0.03 之渦流流況

相片 3 － 2 － 2 波浪相位 t ／ T＝ 0.07 之渦流流況

相片 3 － 2 － 3 波浪相位 t ／ T＝ 0.17 之渦流流況

相片 3 － 2 － 4 波浪相位 t ／ T＝ 0.22 之渦流流況

相片 3 － 2 － 5 波浪相位 t ／ T＝ 0.40 之渦流流況

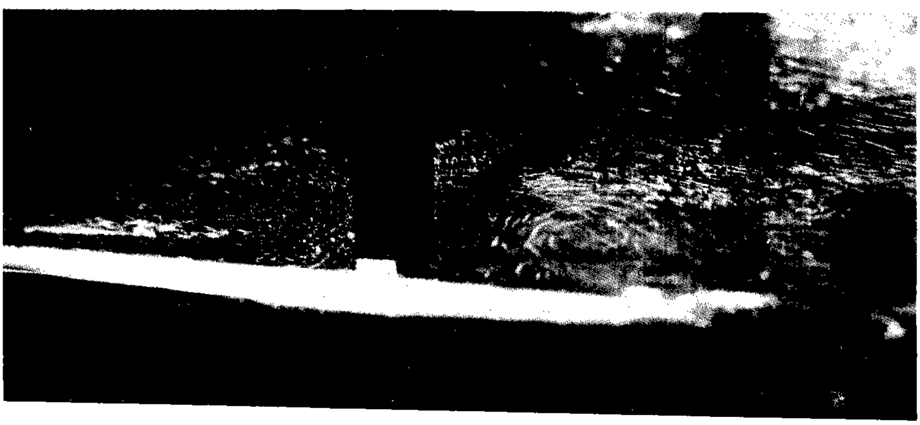

相片 3 － 2 － 6 波浪相位 t ／ T＝ 0.63 之渦流流況

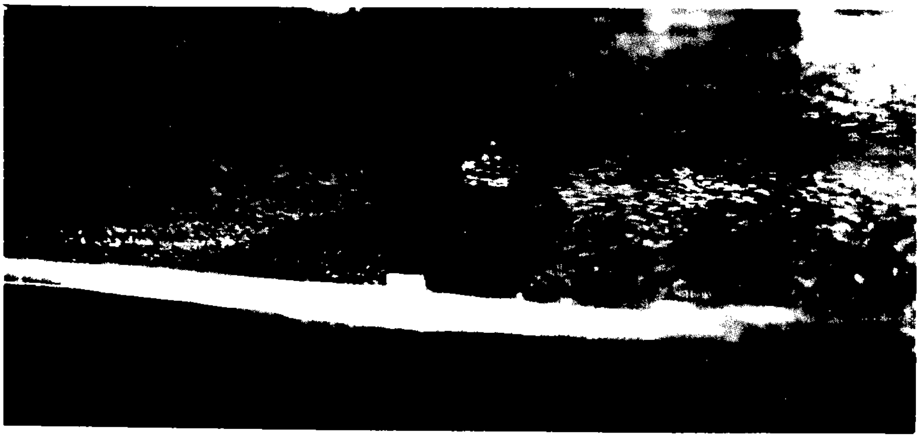

相片 3 － 2 － 7 波浪相位 t ／ T＝ 0.71 之渦流流況

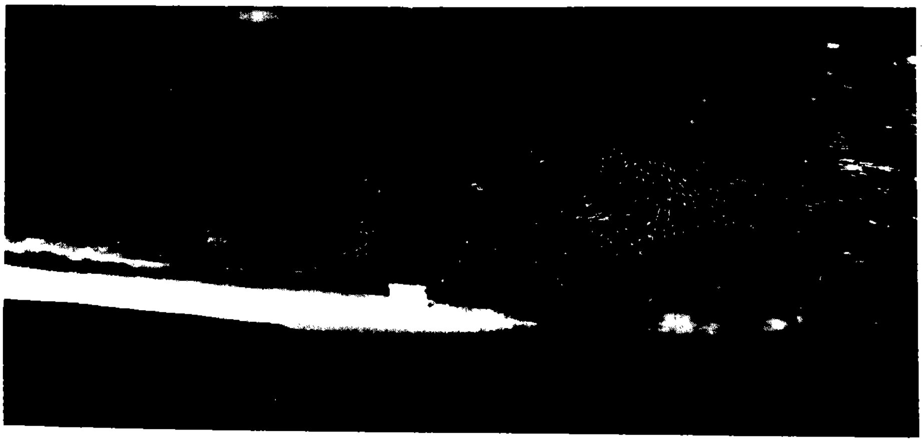

相片 3 － 2 － 8 波浪相位 t ／ T＝ 0.87 之渦流流況

相片 3 － 2 － 9 波浪相位 t ／ T＝ 0.90 之渦流流況

相位係在波谷附近，因此波浪向海側之流速最大，而在堤岸左側附近有明顯之渦流存在，然根據上節中吾人觀察到堤岸左、右側之水位變化在波谷相位時，反射區與遮蔽區之水位差較小，致使其形成之渦流之尺度與強度自然較小。最後，相片3－2－9爲波浪又將回後靜水位狀態，因此其水中運動之流場逐漸減弱，依上述之波浪運動相位，在堤岸附近之渦流型態即循序出現。

3－3 底床粒子的傳輸現象

在波浪作用中之流場，一般以勢能流（Potential Flow）爲主要型式。懸浮水體中之粒子運動近似一橢圓軌跡，根據黃等（1989）之研究，底床粒子係隨邊界層流場之運動而向岸傳輸。然而波浪行經堤岸時，遮蔽區產生順時針渦流v1，反射區產生反時針渦流v2，都對底床粒子之傳輸產生重大之影響，此渦流機構對底床粒子及水體中粒子之傳輸，爲本節探討之主要對象。

在試驗過程中，未造波前先以聚苯乙烯螢光粒子置於堤岸遮蔽區之一側，利用相機捕捉波浪作用下底床螢光粒子運動及傳輸現象。當第一個波浪到達，水面渦流v1尚未捲入空氣，但流場中之渦流已產生並延伸至底床將置放之螢光粒子以螺旋狀軌跡往上捲起，如相片3－3－1所示；隨波谷相位之來臨，渦流v1漸消失，而反射區內渦流v2漸形成，螢光粒子將不斷地向上捲起，且因渦流v2之運動作用下拋向深海，如相片3－3－2。此被拋出之螢光粒子團有部份存在反射區，而另一部份則由下一次渦流v1之形成帶向遮蔽區，如相片3－3－3。而藉由相片3－3－4更可看出，經過一波浪週期後在渦流v1、v2各自作用下，可知堤岸附近底床粒子傳輸有著以下之循環步驟：

渦流v1之作用力將粒子捲起向上，隨渦流v1消失，v2之形成而螢光粒子團會被拋向深海，一部份因慣性力脫離反射區之渦流作用範圍；另一部份存留在作用區內之粒子則伴隨著底床傳送上之其它粒子再度被捲起帶向遮蔽區；同理一部份粒子亦脫離遮蔽區渦流範圍向前傳送，另一部份則等待下一次之渦流v2形成而又被捲起，如此循環不已。經由本實驗觀察結果發現在堤體結構與堤線成90度交角時，雖有部份螢光粒子在反射區會被拋向外海，但因螢光粒子較海水爲重而逐漸沉澱至底床，復因邊界層流場之運動再向淺岸傳輸，因

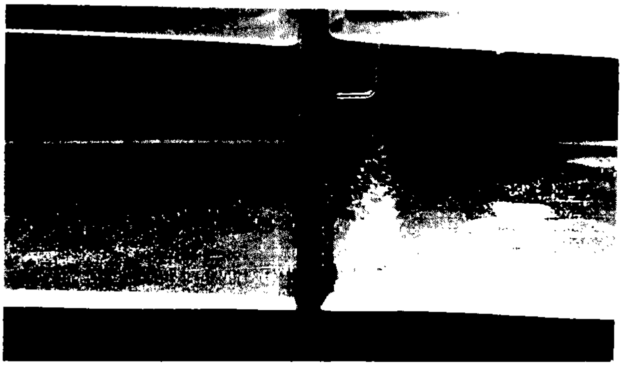

相片 3 － 3 － 1
底床粒子以螺旋狀
向上捲起

相片 3 － 3 － 2
遮蔽區渦流Ｖ 1 消失而
反射區渦流Ｖ 2 漸形成

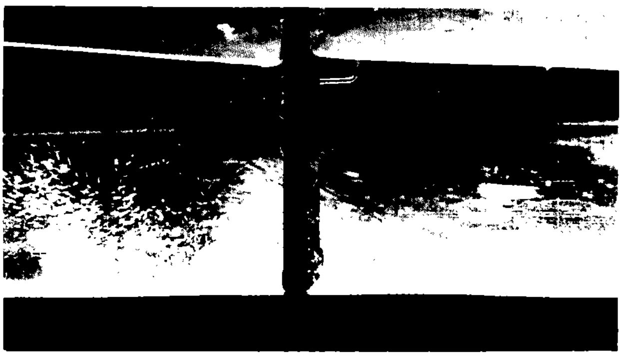

相片 3 － 3 － 3
螢光粒子部份存留在反射區，部
份則又渦流Ｖ1作用再帶回遮閉區

相片 3 － 3 － 4
經波浪一週期Ｖ1、Ｖ2 運動
作用後之螢光粒子分佈狀況

此最後螢光粒子均被帶往遮蔽區內。

3－4 波浪入射方向、週期、波高對渦流之影響

本試驗藉由不同模型轉角來模擬不同之波浪入射角度，瞭解不同波浪條件下之底床粒子之運動特性。其過程均以電視攝影機攝取各種條件下之渦流外觀及內部流場結構，再以相機拍攝定性之底床粒子去向；然後利用錄放影機以每張三十分之一或十分之一放映速率，逐步觀察其間變化情形，即可知波浪入射方向、週期、波高對渦流流況之影響。

3－4－1 波浪入射方向

由觀察得知，波浪入射方向對於渦流之形成位置與堤岸兩側渦流之大小有較大影響。在相同造波條件下，對於反射區之渦流ｖ２而言：由於堤岸阻擋波浪前進之影響，可以發現堤岸結構轉向反射區時，渦流ｖ２旋轉氣柱鑽深較深，且氣柱之圓徑較大；至於渦流ｖ２氣柱中心距離堤頭之位置，當堤岸結構轉向遮蔽區時乃較堤岸結構轉向反射區時爲遠。而遮蔽區之渦流ｖ１亦當堤岸結構轉向遮蔽區時鑽深較深，結構較完整，至於渦流ｖ１、ｖ２與堤體轉角之關係如圖３－３所示。

其次，波浪入射角之不同對渦流內部流場及底床顆粒運動亦有不同之結果。由相片３－４－１、３－４－２、３－４－３可知同一造波條件下（波浪週期 $T = 1.01$ sec．波高 $H = 2.48$ cm．波浪作用 45－50 sec．)堤體轉向遮蔽區

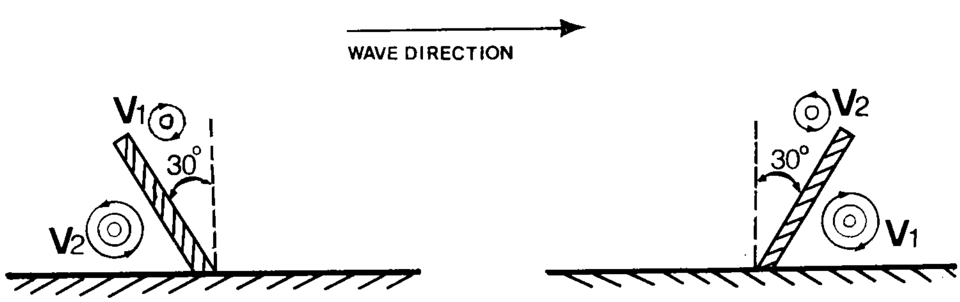

圖３－３　渦流ｖ１、ｖ２形成位置與堤體轉角之示意圖

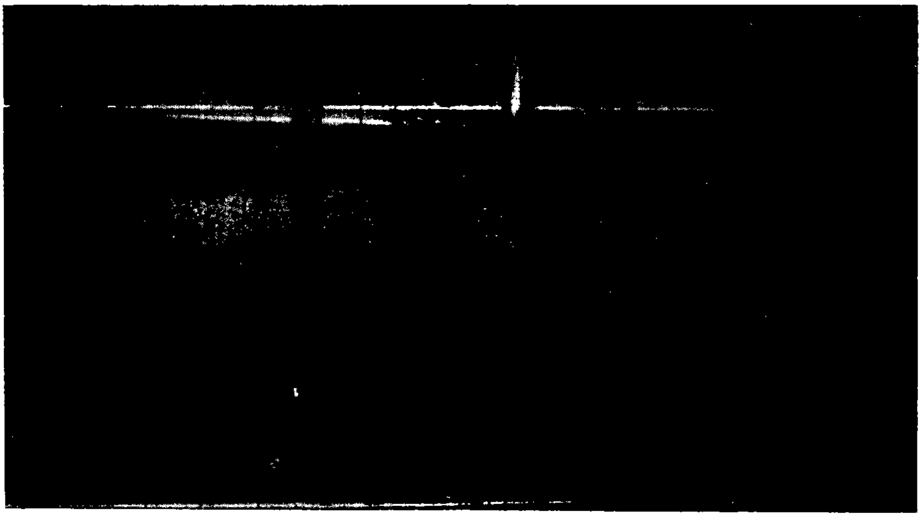

相片 3 － 4 － 1
堤體垂直岸線
週期T＝ 1.01 sec
波高H＝ 2.48 cm
波浪作用 45 － 50 sec

相片 3 － 4 － 2
堤體轉向遮蔽區 30° 角
週期T＝ 1.01 sec
波高H＝ 2.48 cm
波浪作用 45 － 50 sec

相片 3 － 4 － 3
堤體轉向反射區 30° 角
週期 T＝ 1.01 sec
波高 H＝ 2.48 cm
波浪作用 45 － 50 sec

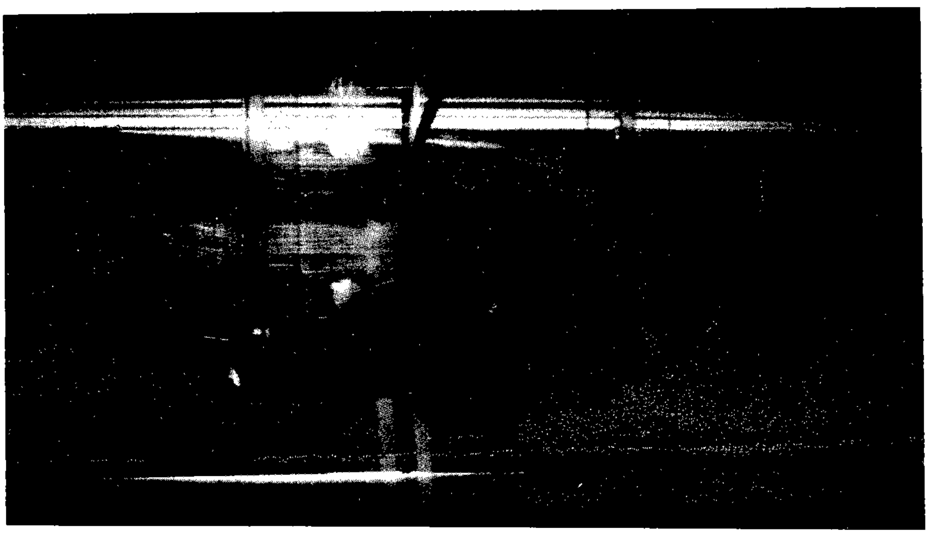

相片 3 － 4 － 4
堤體垂直岸線
週期 T＝ 1.01 sec
波高 H＝ 2.48 cm
波浪作用 45 － 50 sec

30° 時，由於渦流ｖ 2 距堤頭較遠，底床粒子被帶往反射區者較多；而當堤體轉向反射區 30° 則因渦流ｖ 1 靠近堤頭而渦流ｖ 2 靠近岸壁，因此底床粒子迅速被帶往遮蔽區內。

3－4－2　波高對渦流運動之影響觀測

深海入射波浪之波高直接影響流場中水粒子流速，因此對於堤岸兩側渦流大小有密切關係。相同週期不同波高之條件下觀測，可以明顯看出：深海波高較大者其兩側渦流亦較明顯易見；且波浪行至淺水中波峰出現時流速較波谷出現時流速爲大，時間短促而加速度增大。因此大波高作用下，遮蔽區處渦流v1捲動現象加劇較反射區處渦流ｖ 2 明顯清晰。由於波高大者粒子流速亦大，渦流轉動速度快，鑽深程度較深，對底床顆粒捲動力量亦較小波高者爲強。在渦流捲動範圍方面，大波高乃較小波高者寬廣，而底床粒子運動現象激烈、混亂。

3－4－3　波浪週期對渦流運動之影響觀測

一般而言，週期對於遮蔽區渦流ｖ 1 之影響較反射區渦流ｖ 2 爲大。由於長週期之能量較強，渦流ｖ 1 形成時間長且完整，捲動力量強，是以長週期波浪作用下，堤趾處粒子被捲起帶走之距離亦較短週期爲遠。底床粒子經由渦流運動作用下，帶向渦流運動範圍外者亦較多。此可由相片 3 － 4 － 4 顯示出。

3－4－4　影響區域之討論

由相片 3 － 4 － 1 至相片 3 － 4 － 4 可知不同波浪入射方向及入射週期、波高對於底床粒子有著不同程度之捲帶力量，因此可就造波後螢光粒子之運動判斷其影響區域之變化。另外，堤體附近區域之流速、水位深受外海入射波浪條件因素之影響。由觀察得知，水深愈淺、渦流愈明顯、影響範圍亦較巨大。本試驗僅由定性瞭解波浪作用下堤岸附近之流況：由實驗中發現渦流之捲動乃局部現象，堤體附近水位、流速之影響僅侷限於堤體附近之渦流氣柱類似鐘形之區域內。除此，其它區域仍屬波浪之勢能流作用範圍。在不同堤體轉角及波浪作用下，堤角之影響區域自有些許差異：其主要差異僅在此鐘形區域內之兩側渦流ｖ 1 、ｖ 2 大小及捲動速度上之差異。至於波高之影響則較其他因素強烈，波高大者其鐘形影響區域範圍較波高小者爲大，粒子捲動之範圍亦較寬廣。

四、結　論

由於堤防之設置形成部份反射波及堤體附近之渦流運動，於堤趾附近發生沖刷；堤身發生淘空現象，堤頂之安全堪慮。是以本實驗藉由流場可視化法觀測堤角附近渦流流況，自其生成消散乃至底床粒子運動現象均列入觀察及定性分析。且經由流場可視化方法中之懸浮顆粒追蹤觀測渦流內部流場之運動狀況。

經由本實驗觀測結果可歸納如下：

(1)波浪行經堤岸時，受堤體阻擋之影響，遂在堤角兩側產生正逆向之渦流流場，因此渦流之內部流場形成後乃由表面捲入空氣形成氣柱，但對底床粒子之捲動力量仍相當巨大，隨著水深加深而有減弱之趨勢。

(2)深海波高大之波浪作用下，渦流捲動現象加劇，影響範圍類似鐘形區域亦較寬廣。由於波峰流速加大，故遮蔽區之渦流ｖ１捲動較劇，氣柱鑽深亦深。渦流捲動底床粒子之過程爲自底床向上捲動顆粒，懸浮水體中，再經渦流捲動之作用及波浪向前傳動遂將顆粒拋出影響區。

(3)長週期波浪對遮蔽區渦流ｖ１之形成影響較劇，其形成完整，捲動力量強，底床粒子捲起並拋射範圍較短週期爲遠。

(4)堤趾處底床粒子之運動，視不同之波浪條件及堤體轉角而定。大體上，在渦流影響區域內底床粒子均被捲起帶走；堤體轉向遮蔽區時，粒子被帶往反射區者多，而堤體轉向反射區時則粒子被帶往遮蔽區範圍內，波高及長長期波浪作用下，粒子被拋射至渦流運動範圍外較迅速。

(5)由於堤體兩側渦流之捲動作用，故堤趾處底床粒子在此兩渦流作用下將逐漸被淘空，而影響堤身本身之安全，因此對於海岸結構物設計時不可不愼重保護之。

五、參考資料

1. 謝金勳，郭金棟，楊春生：斜防波堤附近流場之研究，第八屆海洋工程研討會論文集，p.209 － p.242，民國七十四年。

2. Gourlay, M. R. : Wave Set-up and Wave Generated Currents in the Lee of a Breakwater or Headland, Proc. 14th Int. Conf. Coastal Eng., pp.1976-1995, 1974.

3. 磨年生：離岸堤背後之流場研究，國立成功大學水利及海洋研究所碩士論文，民國七十六年。

4. 歐善惠，張介忠：離岸堤堤後堆沙效果之試驗研究，第八屆海洋工程研討會論文集，p.381 － p.396，民國七十四年。

5. 許明雄：應用可視化法探討碎波之流場，國立成功大學水利及海洋研究所碩士論文，民國七十六年。

6. 黃煌輝，林呈：碎波帶內亂流流場及渦流結構之研究，國科會研究報告，民國七十六年。

7. 林呈：應用流場可視化法及ＬＤＶ探討斜坡上波動內部流場及底部邊界層之特性，國立成功大學水利及海洋研究所博士論文，民國七十八年。

8. F. FRUNGEL, C. KOCH : Fast Measurement of Fiouorescent Tracers in Fiow and Their Turbdity, Flow visualization II proceedings of the Second International Sysmposium of flow visualization, September 9-12, 1980, Bochum West Germany.

9. TAKEO NAKAGAWA : On characteristics of the water-particle velocity in aplunging Breaker, J. Fluid Mech., vol.126 pp.251-268,1983.

10. T. S. Hedges, M. S. Kirkgoz : An Experiment Study of the Transformation zone of plunging breaker, Coastal Engineering, pp.319-333, 1981.

11. P. BONMARIN : Laboratory Observation of Gravity Wave Breaking on DeepWater, Flow visualization II, proceedings of the second Internation Symposium of flow Visualization, Sep. 9-12, 1980, Bochum, West Germany.

13. 黃煌輝，林呈，黃國書：斜坡上波浪運動質量傳輸速度分佈之特性，第十一屆海洋工程研討會論文集， p.61 － p.79, 民國七十八年。

第三屆基礎港灣數值(數學)模式研習會論文集　Jan. 17～18, 1990 Page 69～111

粗糙紊流渦動滯度與邊界層特性之研究

歐善惠*　許泰文**

中文摘要

本文由理論探討粗糙紊流(rough turbulent flow)邊界層相關物理現象。文中先根據修正一階閉合模式所獲之渦動滯度，經由離散富立葉轉換(Discrete Fourier Transform)分析結果，提出一個與時間無關的單層渦動滯度分佈函數，此一分佈型式之合理性亦經試驗數據進一步驗證。再將此一渦動滯度代入控制方程式中，求得一階解之速度剖面分佈，以解析邊界層內相關物理量。此一單層模式為一連續函數，可改進多層模式繁瑣之計算過程，節省計算時間。數值計算結果發現，一階解所獲之邊界層特性符合大部份的試驗數據。流速剖面超射現象之模擬優於目前外層未減衰之單層或多層渦動滯度模式。當相對糙度(relative roughness)小於30時，本文理論模式模擬效果較差。

* 國立成功大學水利及海洋工程研究所教授

** 國立成功大學水利及海洋工程研究所博士班研究生

一、前　言

當波浪傳遞至較淺海域時，海灘底部的流況多屬粗糙紊流，流體流經邊界由於剪力的作用而形成紊流邊界層。對於設計近海的海岸結構物時，波高減衰和漂沙移動爲兩項重要考慮因素，前者爲決定設計波高、碎波水深之要素，後者與海岸的侵淤特性有關，而紊流邊界層之運動機構則影響波浪能量消散和漂沙移動之變化特性。

波浪作用下，流體爲一往復運動之現象，其流經之邊界依物理性質可分爲定床面（fixed bed）及動床面（movable bed）。定床面包含粗糙面與光滑面，粗糙面與光滑面的界定一般由參數 k_s/D_l 所決定，其中 k_s 爲底床粗糙度；D_l 爲滯性層厚度（thickness of viscous layer）。據Kajiura（1968）之研究，由平滑面至粗糙面的過渡區（transition）爲

$$0.4 \leqq k_s/D_l \leqq 5 \qquad \cdots\cdots(1)$$

當界面性質超越了過渡區，則粗糙度對紊流邊界層特性的影響變爲重要，此時的流況爲粗糙紊流。粗糙紊流流體運動滯度（kinematic viscosity）對流速、滯性剪力的影響可以忽略。粗糙紊流的範圍，Jonsson（1966）定義如下：

$$R_E \geqq 10^4 \quad , \quad 當\ 1 \leqq A_b/k_s \leqq 10 \qquad \cdots\cdots(2)$$

或

$$R_E \geqq 10^3 A_b/k_s \quad , \quad 當\ 10 \leqq A_b/k_s \leqq 1000 \qquad \cdots\cdots(3)$$

式中　$R_E = \hat{U}A_b/\nu$ = 雷諾數

$\hat{U}$ = 邊界層外流速振幅

$A_b = H/2\sinh(kh)$ = 邊界層外水粒子運動振幅

H = 波高

零階閉合模式的解析方式又分為與時間相關及與時間無關的渦動滯度空間分佈。通常空間分佈又依邊界層特性分成幾個層次，各層依其性質而有不同的分佈函數，如Kajiura（1968）將渦動滯度分為三層，第一層為定值，第二層則為線性增加，第三層則又為定值，各層解析完後再行連接，成為一連續之速度剖面。

一階閉合模式主要以一條紊流動能傳播方程式配合動量方程式求解，二階閉合模式則有二條傳播方程式，這兩條傳播方程式有兩種不同的描述方法，第一種為包含紊流動能與混調尺度的（ k‧ϵ model ），又稱為微擾模式。第二種則考慮紊流動能與渦度（vorticity），此為Saffman（1970）所提出的模式。

本文由理論分析探討粗糙紊流、平滑紊流及薄層流之邊界層特性。目前的理論模式在渦動滯度（eddy viscosity）的假設上大多使用多層模式（multiple layers）求解海灘底部之邊界層特性，層與層的連接點在數學上屬於不可析，在處理上較為繁瑣。本文先使用修正一階閉合模式（modified one-equation closure model）探討渦動滯度的分佈型式，再經由離散傅立葉轉換（Discrete Fourier Transform）分析渦動滯度隨底部高程之變化，據此提出一個簡單實用的波浪邊界層模式，以解析粗糙紊流、平滑紊流及薄層流邊界層特性、質量傳輸現象及輸沙濃度等物理現象。期能從理論探討上，進一步瞭解波浪作用下，海灘底部紊流邊界層之力學機構，提供今後海岸工程規劃、設計之參考。

二、基本方程式

在解析有關波浪作用下，底床所衍生之亂流邊界層時，經級數大小比較後，所採用的水平近似運動方程式為：

$$\frac{\partial u}{\partial t}+u\frac{\partial u}{\partial x}+w\frac{\partial u}{\partial z}=-\frac{1}{\rho}\frac{\partial p}{\partial x}+\frac{\partial}{\partial z}\left(\frac{\tau}{\rho}\right) \qquad \cdots\cdots(4)$$

其中　t：時間

x：波浪前進方向（向前爲正）

z：垂直底床座標（向上爲正）

ρ：流體密度

p（x，t）：流體壓力

τ（x，z，t）：流體之剪力

u（x，z，t）：水平平均流速

w（x，z，t）：垂直平均流速

上式之邊界條件爲

$$u = w = 0 \qquad 當 \quad z = z_o \qquad \cdots\cdots(5)$$

$$u \rightarrow U \qquad 當 \quad z \rightarrow \infty \qquad \cdots\cdots(6)$$

其中U（x，t）爲邊界層外流速，z_o爲理論計算高程，粗糙紊流 $z_o = k_s/30$。

在(4)式中，邊界層外緣之水平流速及壓力在垂直方向的梯度爲零，因此，在邊界層內的水平壓力梯度可以邊界層外流速表示：

$$-\frac{1}{\rho}\frac{\partial p}{\partial x} = \frac{\partial U}{\partial t} + U\frac{\partial U}{\partial x} \qquad \cdots\cdots(7)$$

紊流邊界層內，Boussinesq（1847）建議剪力的計算式爲

$$\frac{\tau}{\rho} = k_z \frac{\partial u}{\partial z} \qquad \cdots\cdots(8)$$

式中 k_z 代表有效滯度（effective vissosity），爲渦動滯度 ν_t 與運動滯度 ν 之和，粗糙紊流時 $\nu_t \gg \nu$，故

$$k_z = \nu_t + \nu \approx \nu_t \qquad \cdots\cdots(9)$$

紊流邊界層內必須滿足質量守恒

k ＝周波數

h ＝水深

波浪作用下所產生紊流邊界層架構，包括流速剖面、流速位相差、剪力剖面、剪力位相差、摩擦係數、邊界層厚度及渦動滯度分佈等相關物理量。波浪紊流邊界層的研究依試驗或理論兩方面進行，分述如下：

試驗方面，Jonsson（1966），Jonsson and Carlsen（1976）曾在U型槽（water tunnel）佈置人工沙漣，使用微流速儀量測邊界流速剖面，據此求出剪力分佈及摩擦係數，並由試驗數據歸納摩擦係數與邊界層厚度的經驗式。van Doorn and Godefroy（1978），van Doorn（1981），Sumer et al.（1987）及Sleath（1987）則在斷面水槽（wave flume）中以雷射杜普勒流速儀（Laser-Doppler Velocimeter，簡稱LDV），量測粗糙紊流的流速剖面，進而分析剪力分佈。底床剪力除由速度剖面計算外，亦可由儀器直接量測。Riedel et al.（1972）及Kamphuis（1975）使用自製剪力計，經由不同的波浪條件及底床型態，直接施測底床剪力，進而推求摩擦係數與影響因素的經驗式。

至於理論方面，因海灘底部紊流的況極為複雜，其力學機構目前尚不明瞭，且缺乏足夠的觀測數據參考應用，一般先經由一些基本假設而達到解析目的。Boussinesq（1877）渦動滯度的觀念建立了雷諾剪應力與平均速度梯度的關係，對於紊流邊界層架構提供方便的途徑。對於渦動滯度的處理方式，目前使用的模式有三種，為零階閉合模式（zero-equation closure model）；一階閉合模式（one-equation closure model）及二階閉合模式（two-equation closure model）。零階閉合模式係直接由動量方程式求解流速剖面，較具代表性的有混調尺度（mixing length）模式及渦動滯度分佈函數兩種。一階閉合模式除動量方程式外，再結合描述紊流動能（turbulent energy）的傳播方程式（transport equation）求解。二階閉合模式由動量方程式及二條描述紊流動能與混合長度的傳播方程式解析。一般而言，零階閉合模式計算簡單，但較不適合複雜的流況；而一階或二階閉合模式則計算繁瑣，需花費較大的計算時間，實用上費力費時，然對複雜流況則具較佳的預測能力。

$$\frac{\partial u}{\partial x}+\frac{\partial w}{\partial z}=0 \qquad \cdots\cdots(10)$$

由於本文所探討邊界層流場爲一非線性之運動現象，而此種現象由邊界層外非線性流體所引發，因此，邊界層外之流體不可僅以線性流場處理，須以非線性流場進行探討。邊界層外之流速可經由參數 ε（$\varepsilon=kA_b$）展開如下：

$$U=U_1+U_2+U_3+\cdots\cdots\cdots \qquad \cdots\cdots(11)$$

其中 $U_{n+1}/U_n=0(\varepsilon)$，$n=1,2,3\cdots\cdots$。其中 U_1 及 U_2 的解本文由 Stokes 波以複數表示爲

$$U_1=A_b\,\omega\,e^{i\theta}=\hat{U}_1\,e^{i\theta} \qquad \cdots\cdots(12)$$

$$U_2=\overline{U}_2+\frac{3\,kA_b}{4\,\sinh^2 kh}A_b\,\omega\,e^{i2\theta} \qquad \cdots\cdots(13)$$

式中 $\hat{U}_1$ 爲 U_1 之振幅，$\overline{U}_2$ 爲邊界層外緣之定常流（steady streaming），係由邊界層特性所決定。θ 爲波浪位相角；$\theta=\omega t-kx$；$i=\sqrt{-1}$。

如同邊界層外流速的展開，邊界層內各物理量亦以攝動法展開如下：

$$u=u_1+u_2+u_3+\cdots\cdots\cdots \qquad \cdots\cdots(14)$$

$$w=w_1+w_2+w_3+\cdots\cdots\cdots \qquad \cdots\cdots(15)$$

$$\tau=\tau_1+\tau_2+\tau_3+\cdots\cdots\cdots \qquad \cdots\cdots(16)$$

其中前後階物理量的比爲 $u_{n+1}/u_n=0(\varepsilon)$。由(8)、(14)及(16)式比較，得剪力一階的表示式分別爲

$$\frac{\tau_1}{\rho}=k_z\frac{\partial u_1}{\partial z} \qquad \cdots\cdots(17)$$

將(14)－(17)式代入(4)式，得第一階的控制方程式爲：

$$\frac{\partial u_1}{\partial t}=\frac{\partial U_1}{\partial t}+\frac{\partial}{\partial z}\left(k_z\frac{\partial u_1}{\partial z}\right) \qquad \cdots\cdots(18)$$

$$\frac{\partial u_1}{\partial x}+\frac{\partial w_1}{\partial z}=0 \qquad \cdots\cdots(19)$$

其邊界條件爲

$$u_1=w_1=0 \quad 在 \quad z=z_o \qquad \cdots\cdots(20)$$

$$u_1=U_1 \quad 當 \quad z\to\infty \qquad \cdots\cdots(21)$$

從 (12) 式觀察，邊界層外緣一階之底床流速在時間領域而言具以下之函數特性：

$$U_1(x,t)=-U_1\left(x,t\pm\frac{\pi}{\omega}\right) \qquad \cdots\cdots(22)$$

同理，邊界層內一階之水平平均流速應具有相同之性質：

$$u_1(x,z,t)=-u_1\left(x,z,t\pm\frac{\pi}{\omega}\right) \qquad \cdots\cdots(23)$$

根據 (23) 式可知一階解中流速與剪力均爲以基頻 ω 爲基礎之奇調和函數 (odd harmonics)，故一階解之流場可由下列式子表示：

$$u_1=\sum_{n=0}^{+\infty} u_1^{(2n+1)}(z)\, e^{i(2n+1)\theta} \qquad \cdots\cdots(24)$$

$$w_1=\sum_{n=0}^{+\infty} w_1^{(2n+1)}(z)\, e^{i(2n+1)\theta} \qquad \cdots\cdots(25)$$

$$\tau_1=\sum_{n=0}^{+\infty} \tau_1^{(2n+1)}(z)\, e^{i(2n+1)\theta} \qquad \cdots\cdots(26)$$

三、渦動滯度模式

於 (9) 式中，渦動滯度係隨流況（紊流強度及渦粒尺度（eddy scale））而變，其機構目前尚未明瞭，通常予以模式化，代入控制方程式中求解邊界層內各相關物理量，目前使用的模式說明如下：

㈠零階閉合模式

零階閉合模式即直接假設渦動滯度，而無其他傳播方程式。此一模式通常有兩種處理方式，一爲 Prandtl（1925）的混合長度假說，其假設擾動量 u'，w' 正比於混合長度 ℓ 與速度梯度乘積，而由類比法則得知渦動滯度表示爲：

$$\nu_t = \ell \left| \frac{\partial u}{\partial z} \right| \qquad \cdots\cdots (27)$$

Prandtl 建議 ℓ 隨底部高程呈線性增加

$$\ell = k(z + z_0) \qquad \cdots\cdots (28)$$

其中 k 爲 von Karman 常數。另外，類似於單向流之處理方式，渦動滯度可以用局部長度尺度（local length scale）及速度尺度（velocity scale）之函數關係予以描述，前者表示渦粒的大小，後者則表紊流之強度，其表示式爲：

$$\nu_t = f(z)\, \hat{u}_b^* \qquad \cdots\cdots (29)$$

式中 u_b^* 表示摩擦速度之振幅。有關文獻對長度尺度 $f(z)$ 的假設方式將於下文詳述之。

㈡一階閉合模式

一階閉合模式以係一偏微分之傳播方程式描述紊流動能（Reynolds，1976）

$$\nu_t = C_2 q \ell \qquad \cdots\cdots (30)$$

式中C_2為一常數，q為紊流動能之均方根：

$$q = \sqrt{\overline{u'^2} + \overline{w'^2}} \qquad \cdots\cdots (31)$$

u′，w′分別為水平及垂直擾動速度分量（fluctuation velocity component）。紊流動能的傳播方程式為（Townsend，1976）

$$\frac{\partial}{\partial t}\left(\frac{q^2}{2}\right) + u\frac{\partial}{\partial x}\left(\frac{q^2}{2}\right) + w\frac{\partial}{\partial z}\left(\frac{q^2}{2}\right) = \frac{\tau}{\rho}\frac{\partial u}{\partial z} + \frac{\partial D}{\partial z} - E \qquad \cdots\cdots (32)$$

式中$q^2/2$為平均紊流動能，右邊第一項表示紊流能量的衍生（production），D表紊流之能量擴散（diffusion），E則為紊流之能量消散（dissipation）。D與E分別以下二式予以模式化：

$$D = C_3\ \nu_t \frac{\partial}{\partial z}\left(\frac{q^2}{2}\right) \qquad \cdots\cdots (33)$$

$$E = C_1 \frac{q^3}{\ell} \qquad \cdots\cdots (34)$$

其中C_1、C_3為一常數。當紊流能量之衍生被能量之消散所平衡時，則可得零階閉合模式之(27)式。

㈢二階閉合模式

二階閉合模式係分別以二個偏微分方程式描述紊流動能及長度尺度，渦動滯度依Kolmogorov（1962）之建議為

$$\nu_t = \sqrt{k_t}\ \ell \qquad \cdots\cdots (35)$$

式中$k_t = q^2/2$，為紊流動能。長度尺度ℓ係由紊流能量之消散E（(34)式）所決定；Rodi（1980）提議有關紊流動能k_t及能量消散E的傳播方程式為

$$\frac{\partial k_t}{\partial t} + u\frac{\partial k_t}{\partial x} + w\frac{\partial k_t}{\partial z} = \frac{\partial}{\partial z}\left(\frac{\nu_t}{\sigma_k}\frac{\partial k_t}{\partial z}\right) + \nu_t\left(\frac{\partial u}{\partial z}\right)^2 - C_{k1}E \qquad \cdots\cdots (36)$$

$$\frac{\partial E}{\partial t}+u\frac{\partial E}{\partial x}+w\frac{\partial E}{\partial z}=\frac{\partial}{\partial z}\left(\frac{\nu_t}{\sigma_d}\frac{\partial E}{\partial z}\right)+C_{e1}\frac{E}{k_t}\left(\frac{\partial u}{\partial z}\right)^2-C_{k1}C_{e2}\frac{E_2}{k_t} \qquad \cdots\cdots(37)$$

式中σ_k、C_{k1}、σ_d、C_{e1}及C_{e2}爲常數，上式已普遍應用於明渠中穩定流紊流邊界層之解析。

四、渦動滯度模式之檢討

使用與時間無關之渦動滯度來處理邊界層有關的各種物理量，目前仍然相當普遍，其優點在於它能節省計算時間，在實際應用上簡單便利。然而渦動滯度的假說，迄今尚找不到一種理論，能夠完整地詮釋它，依照 Jonsson and Carlsen（1976）實驗結果分析得知，渦動滯度是一個與時間和高程相關的函數。Trowbridge and Madson（1984a）曾以一個時間相關的渦動滯度模式解析波浪作用下粗糙紊流邊界層特性，解析結果顯示，與時間有關渦動滯度對一階解相關物理量之影響不大，和時間無關之渦動滯度所獲結果類似，但二階解則於較淺水深發現有反向之定常流（steady streaming）。

事實上，由 Jonsson and Carlsen（1976）實測數據分析結果顯示，渦動滯度隨時間的變化趨勢相當零亂，欲以一個合理的時間函數予以描述則屬困難。

由以上的分析可知，與時間無關渦動滯度假說，對於處理邊界層有關的各種物理量，迄至目前仍然相當重要。渦動滯度之空間分佈通常以多層模式描述，各種模式特性則整理於表一，以供分析比較。

對於表一中渦動滯度的假說，各相關文獻從經驗上的分析比較或學理上的探討，發現有數點不完整之處：

(1)與實際物理現象較不一致：渦動滯度在外層區假設爲定值或線性增加時，此與實際的物理現象比較並不相符。Vonguisessomjai（1984）由實測數據迴歸速度剖面的經驗式，再由速度剖面推求渦動滯度分佈，所獲結果示於圖一。Lundgren（1972）由實測剪力及流速剖面分析，所得渦動滯度的分佈型式如圖二所示。圖一及圖二顯示，在內層區，渦動滯度會隨底床高度成長，而於

表一　與時間無關渦動滯度之分佈型式

渦動滯度分佈 模式種類	渦動滯度分佈型態	分　佈　型　式
單層模式 Grant and Madsen (1979)	呈線性成長	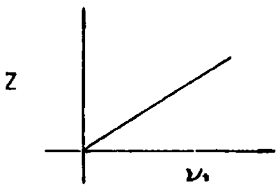
雙層模式 Brevik (1981)	內層：線性成長 外層：定値	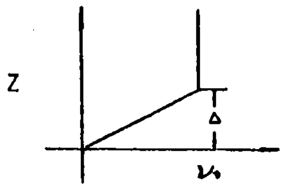
雙層模式 Myrhaug (1982)	內層：拋物線成長 外層：定値	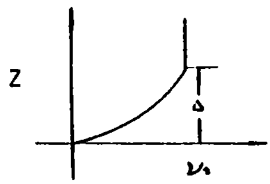
叁層模式 Kajiura (1968)	內層：定値 重覆層：線性成長 外層：定値	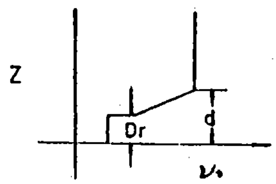
叁層模式 Aukrust and Brevik (1985)	內層：線性成長 外層：線性減衰 外層：定値	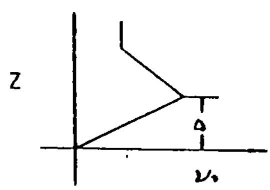

註：D_r：底床粗糙度之半

　　d：重覆層參考高度

　　△：邊界層參考高度

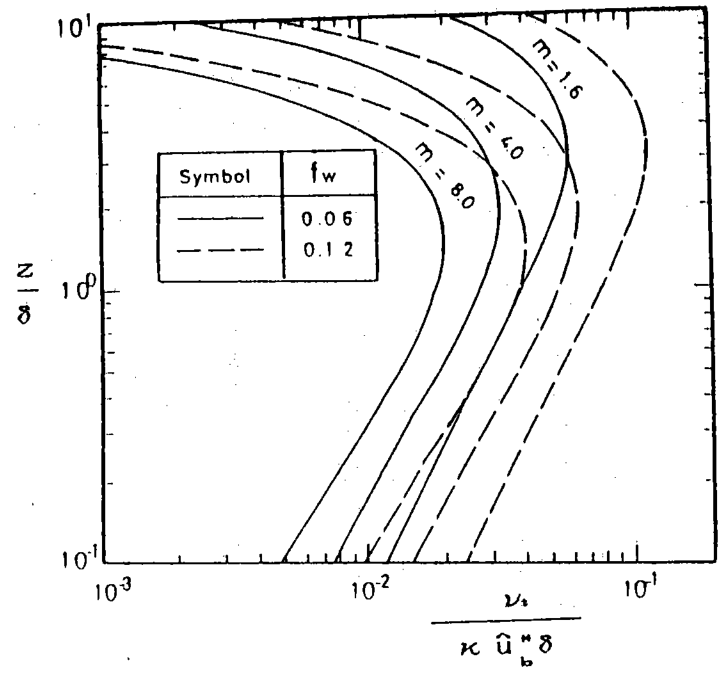

圖一　渦動滯度分佈型式（與時間無關）
（Vonguisessomjai, 1984）

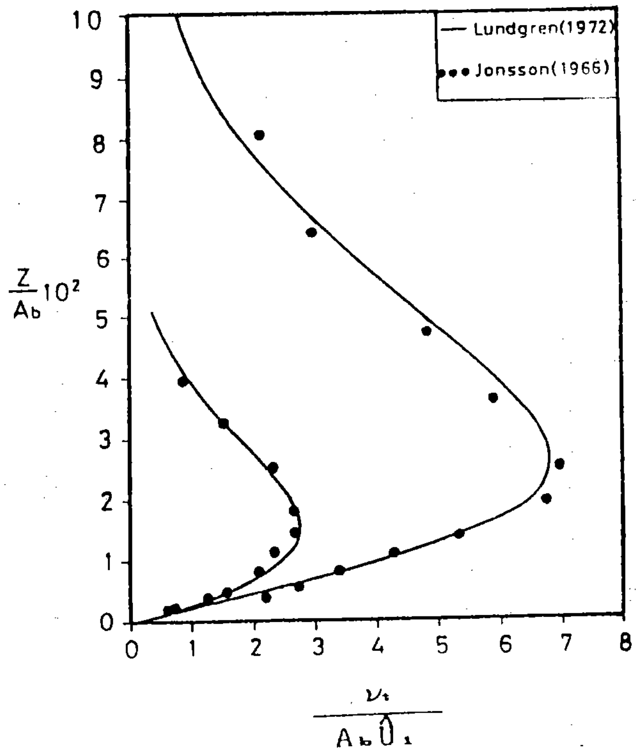

圖二　渦動滯度分佈型式（與時間無關）
（Lundgren, 1972）

某一高度達到最大值，此後由於衍生的小渦粒和較大渦粒之間藉著能量交互作用及摩擦的影響，因此產生離散效應，由離散效應導致渦動滯度開始減衰，於離開邊界層較遠位置則漸趨爲零（Hinze,1975）。

(2)線性假設適用範圍有限：Nielsen（1985）的研究認爲線性假設之渦動滯度難以描述波浪邊界層的主要特徵。根據線性渦動滯度分佈假設可得流速剖面爲對數律（Nielsen, 1985）：

$$\frac{u}{u_b^*} = \frac{1}{k} \ln \frac{z}{z_0} \qquad \cdots\cdots (38)$$

然Vonguisessomjai（1984）由 Jonsson and Carlsen（1976）所測的流速剖面分析，結果如圖三所示，由圖中觀察，對數律僅適用於較靠近邊界層之位置，離開底部較遠之高程則有高估的現象。此現象說明線性渦動滯度比較適合於底部位置，離底部愈遠，則其適用性隨之降低。其原因乃邊界層內部形成之渦粒相互干擾，導致渦動滯度呈非線性變化。Vonguisessomjai（1984）的分析結果認爲在離底部較遠位置 ν_t 呈 $\eta^{\frac{2}{3}} \exp(m\eta^{\frac{2}{3}})$ 之非線性增加，此處m爲流速剖面之參數，$\eta = z/\delta$，δ 爲邊界厚度。

(3)渦動滯度的不連續與不可析：目前多層模式所假設的渦動滯度不連續，或層與層間有轉析點存在，這種假設將造成雷諾剪力在層與層間的不連續（參考(8)式、(9)式）或不可析，從數學觀點視之，將產生奇異點之不合理現象。

(4)實際應用頗爲不便：多層模式層與層間的連接點爲不可析，處理上較爲繁瑣，且所獲理論解之型式亦極複雜，需花費較多計算時間，在實際應用上頗爲不便。

(5)外層呈定值或線性增加對超射現象（overshoot）模擬不佳：Aukrust and Brevik（1985）處理粗糙紊流邊界層時，設水平流速之缺損爲

$$u_d = u_1 - U_1 \qquad \cdots\cdots (39)$$

如將 ν_t 在外層視爲定值，則上式代入(8)式得 u_d 解的型式爲

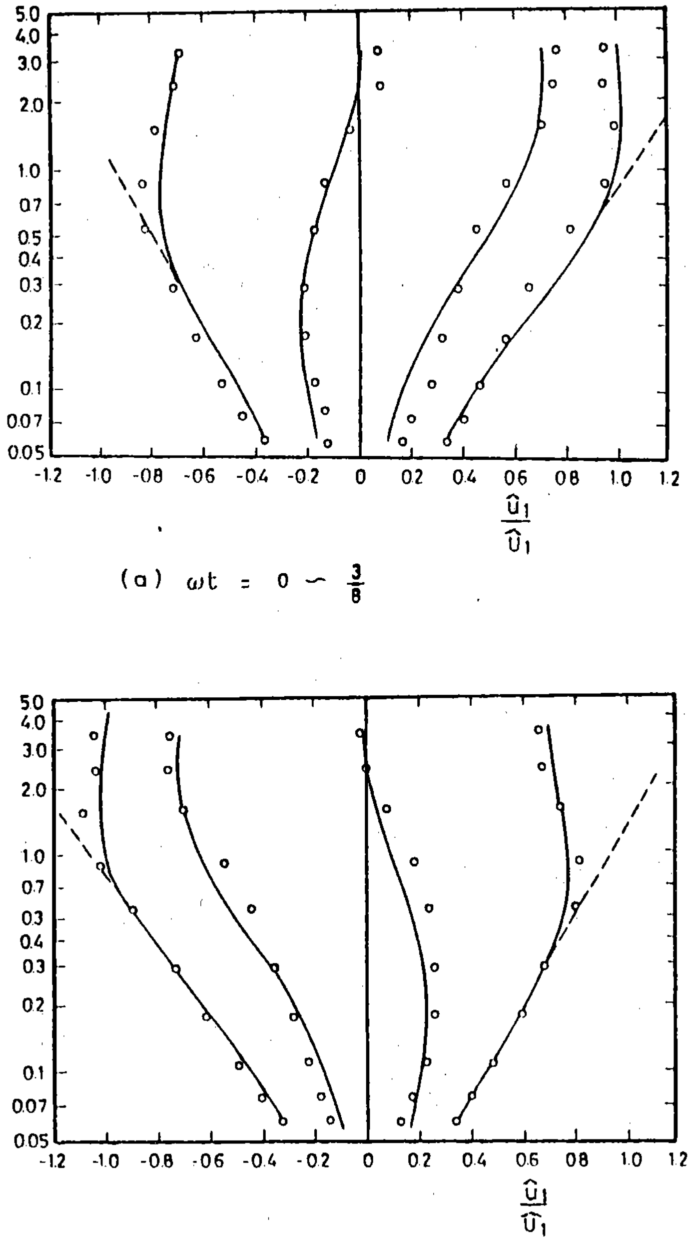

圖三　對數分佈與實測流速剖面之比較

(Vonguisessomjai , 1984)

$$u_d \sim \exp\left[-(1+i)\left(\frac{\omega}{2\nu_t}\right)^{\frac{1}{2}} z\right] \qquad \cdots\cdots(40)$$

當 ν_t 很大時，$u_d \neq 0$，即 $u_1 \neq U_1$，超射現象的範圍相當大，然 ν_t 很小時，$u_d = 0$ 且 $u_1 = U_1$，超射現象在較短距離即行收斂。圖四爲兩種不同的渦動滯度模式，圖中實線在外層有減衰，虛線則呈定值，所解析之流速剖面及其位相如圖五及圖六所示，由圖比較得知，外層區減衰的渦動滯度模式所獲結果接近實測數據。

由以上之分析得知，目前在與時間無關渦動滯度的假設上仍有不完善之虛，如何根據紊流特性，尋求渦動滯度的合理分佈，進而建立波浪邊界層理論模式，以解析波浪作用下，底部邊界層特性爲一值得深入探討的問題。

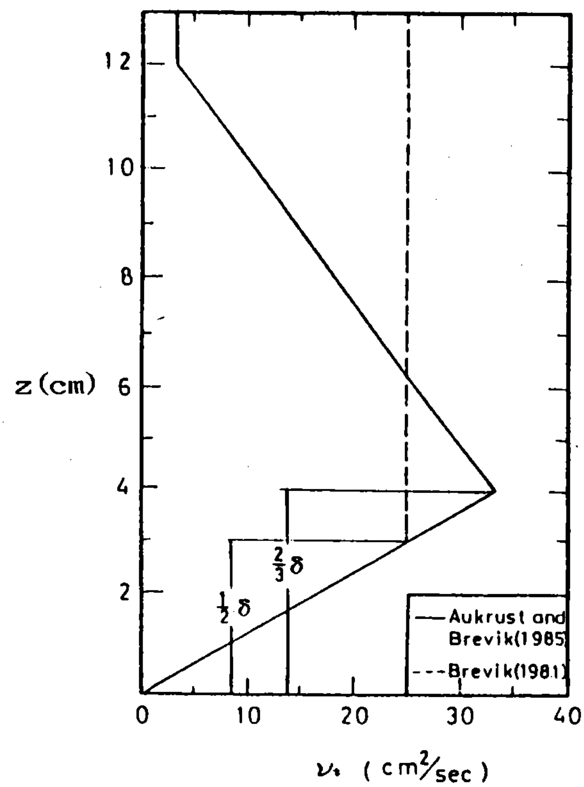

圖四　兩種不同的渦動滯度分佈模式（與時間無關）
（Aukrust and Brevik, 1985）

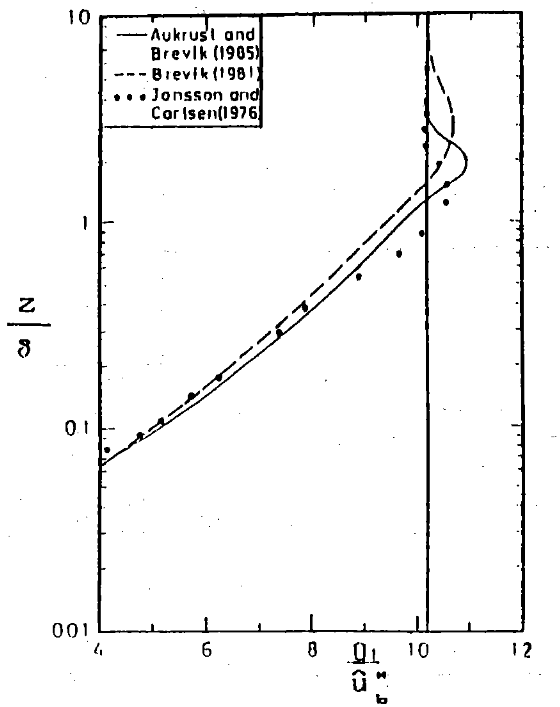

圖五　兩種不同的渦動滯度模式解析之水平流速剖面與實測數據比較（Aukrust and Brevik, 1985）

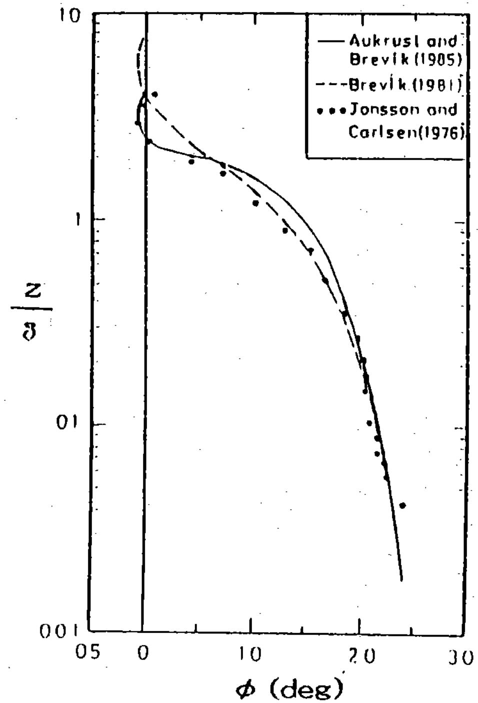

圖六　兩種不同的渦動滯度模式解析之水平流速位相差與實測數據比較（Aukrust and Brevik, 1985）

五、修正一階閉合模式的探討

Trowbridge et al.（1986）在各種不同的數值試驗中，發現使用一階閉合模式模擬粗糙紊流邊界層特性時，長度尺度的假設對於流速剖面的模擬具有重要之關係。他們建議將（28）式 Prandtl 的混合長度尺度修正爲與底部高程呈指數函數之減衰

$$\ell(z) = k(z+z_0)\exp(-z/\Delta) \qquad \cdots\cdots (41)$$

式中△爲一邊界層之參考厚度，其表示式爲（Grant，1977）

$$\frac{\Delta}{k_s} = k\sqrt{\frac{f_w}{2}\,\frac{A_b}{k_s}} \qquad \cdots\cdots (42)$$

f_w 爲紊流的摩擦係數。

圖七爲利用修正一階閉合模式所得之流速剖面，與未經修正一階閉合模式之計算結果比較，圖中 $\eta = z/z_0$，從圖中明顯看出，修正一階閉合模式具較佳預測之能力，特別是在超射現象的模擬方面。圖八爲兩種不同模式，流速位相差 ϕ 的比較，圖中的結果亦顯示修正一階閉合模式的預測結果較佳。

修正一階閉合模式中長度尺度的修正，可由二階閉合模式中之平均長度尺度進一步說明。圖九中實線爲 Justensen（1988）以 k・ϵ 模式所得長度尺度隨底部高程之變化，計算所選擇之相對糙度（relative roughness）A_b/k_s 爲 1000。圖中虛線爲（28）式之混合長度表示式，點線則爲修正一階閉合模式的長度尺度。從圖中明顯看出，混合長度的適用範圍在非常靠近底床的位置，其高度約在 0.125 倍邊界層參考厚度位置，而超過這個高度則有明顯的高估現象，此乃表示混合長度在離底部較遠的高度已不能適用。值得注意的是，圖中的結果顯示，k・ϵ 模式之長度尺度在某一個底部高程，以後則呈急速減衰。Trowbridge et al.（1986）所提議修正長度尺度，其最大值位置比 k・ϵ 模式略低，但整個長度尺度分佈述勢則與 k・ϵ 模式接近。

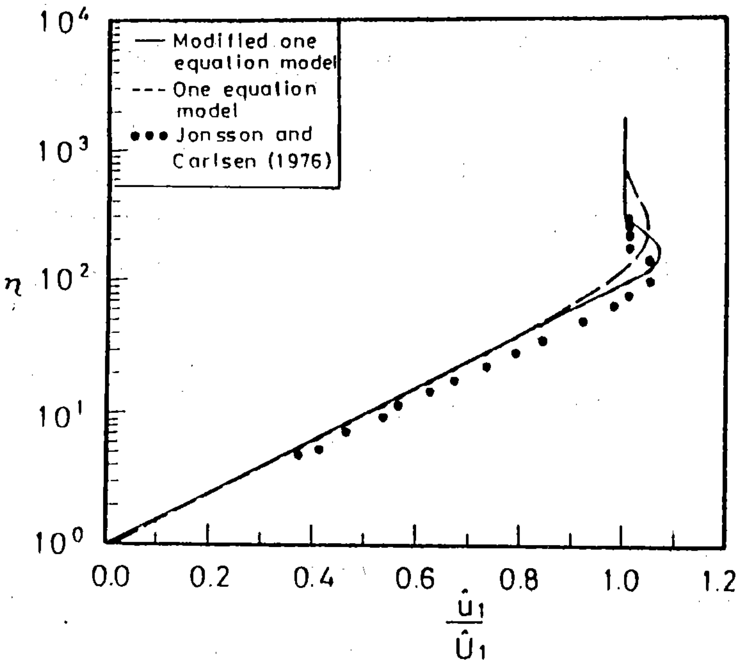

圖七 修正一階閉合模式與一階閉合模式之水平流速剖面比較

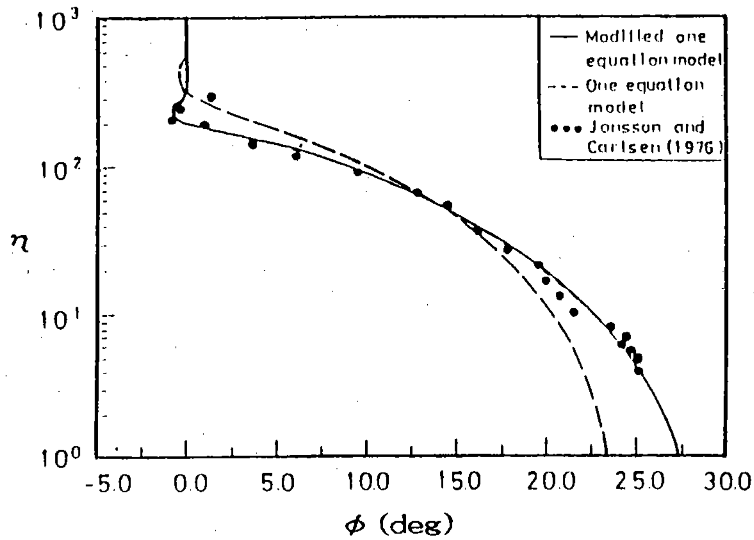

圖八 修正一階閉合模式與一階閉合模式之水平流速位相差比較

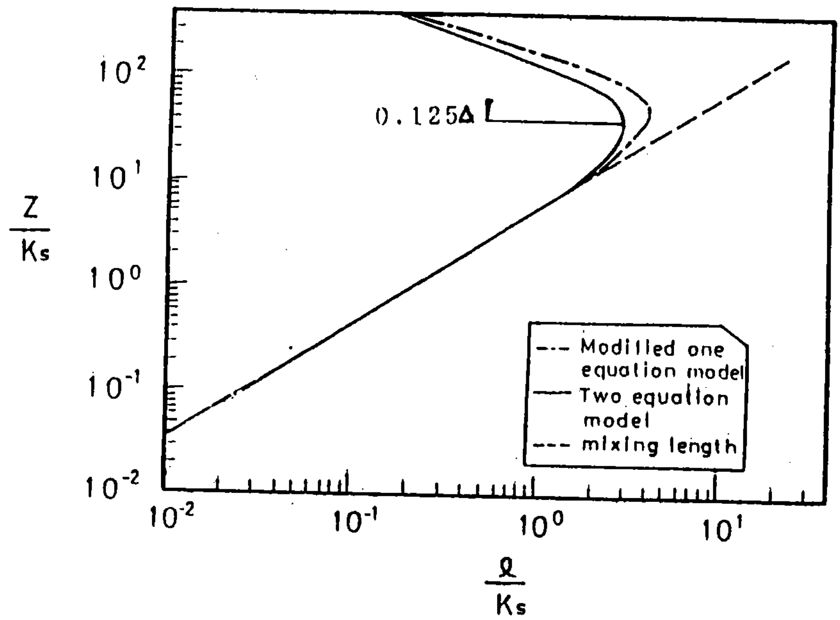

圖九　平均長度尺度隨底部高程之變化

從以上之分析得知，修正一階閉合模式具較佳之預測能力，其長度尺度與 k·ε 模式之結果較爲接近，與實際現象較爲一致，在計算上，比 k·ε 模式簡單，並可節省時間。本節之目的，即進一步應用修正一階閉合模式推求合理渦動滯度之空間分佈，使紊流邊界層的模擬更爲簡單便利。

六、渦動滯度之提議

如前所述，以修正一階閉合模式求解紊流邊界層特性，雖具有相當的預測能力，然因重覆疊代時間步驟，而耗費龐大的計算時間。本節之目的，即將修正一階閉合模式所獲之渦動滯度經由離散富立葉進一步分析，據此求出一與時間無關之渦動滯度模式，而由零階閉合模式求解紊流邊界層，以節省計算時間。

$q_1(z, t)$ 經修正一階閉合模式解出後，則由（30）式可求得無因次渦動滯度爲

$$\nu_t = C_2 \; q_1(z, t) \; \ell(z) \qquad \cdots\cdots (43)$$

式中 u_1 及 τ_1 均為奇函數，故由 (8) 式知 ν_t 為偶函數：

$$\nu_t(z, t) = \sum_{n=0}^{+\infty} \nu_t^{(2n)} e^{i2n\theta} \qquad \cdots\cdots (44)$$

上式對時間取平均，得與時間無關之渦動滯度分佈：

$$\nu_t(z) = \overline{\nu_t} = C_2 \; \overline{q_1(z, t)} \; \ell(z) \qquad \cdots\cdots (45)$$

利用 $z_o = k_s/30$ 及 $\hat{u}_b^* = \sqrt{f_w/2} A_b \omega$，則 (45) 式再經無因次化得

$$K(\eta) = \frac{\nu_t}{k \hat{u}_b^* z_o} = \nu_t(\eta) \frac{30\sqrt{2}}{k\sqrt{f_w}} \frac{A_b}{K_s} \qquad \cdots\cdots (46)$$

圖十及圖十一之虛線為修正一階閉合模渦動滯度之計算結果，其相對糙度 A_b/k_s 分別為 28.4 及 123.9。從圖中可以看出，靠近底部時，渦動滯度呈線性增加，遠離底部時，非線性效應增強，在某一高度時達到最大，以後則為急速減衰，此一現象與前人的分析結果 (Vonguisessomjai , 1984 ; Lundgren, 1972) 一致。為便於比較，將 Lundgren (1972) 由 Jonsson and Carlsen (1976) 試驗數據所分析結果，再經新參數 $k \hat{u}_b^* z_o$ 的無因次化，所得結果分別點繪圖中，發現修正一階閉合模式之渦動滯度與 Lundgren 分析結果相近，其合理性可獲進一步證實。

至於不同相對糙度，其渦動滯度最大值的發生位置，經本文計算結果示圖十二，圖中顯示，不同的情況，其最大值之相對高程 $\triangle^*_{max}$，介於 $0.42\triangle^*$ 及 $0.48\triangle^*$ 之間，平均值為 $0.45\triangle^*$。$\triangle^*$ 係以 z_o 為分母的無因次邊界層厚度參數：

$$\triangle^* = \frac{\triangle}{z_o} = 30\frac{\triangle}{k_s} \qquad \cdots\cdots (47)$$

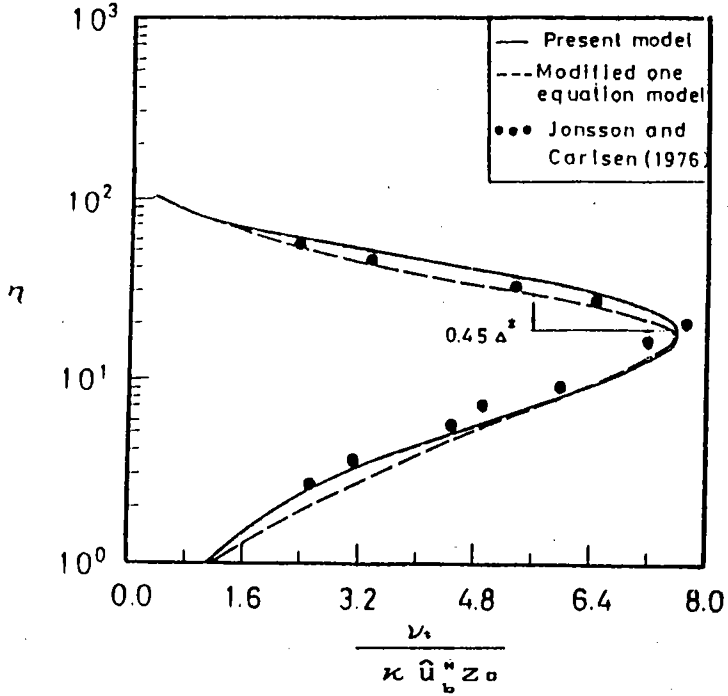

圖十　渦動滯度隨底部高程之變化

$(A_b / k_s = 28.4)$

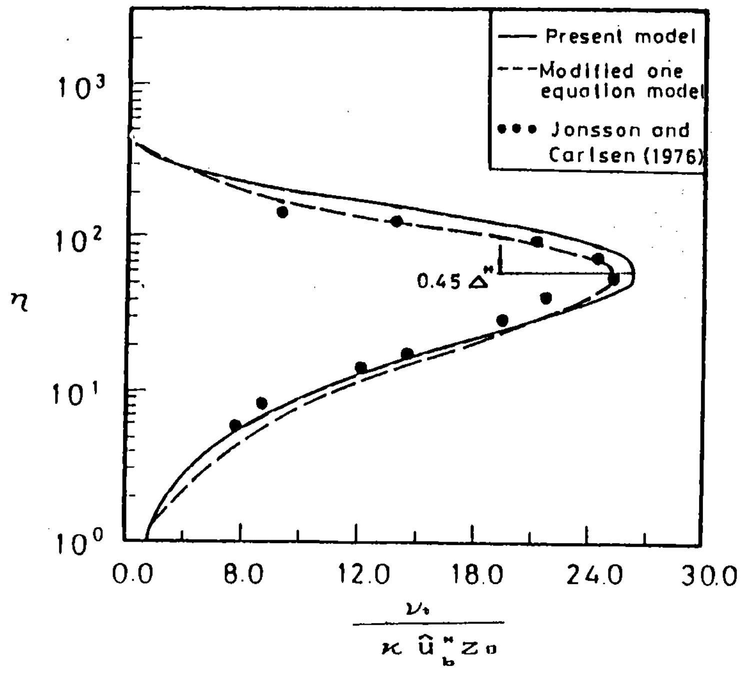

圖十一　渦動滯度隨底部高程之變化

$(A_b / k_s = 123.9)$

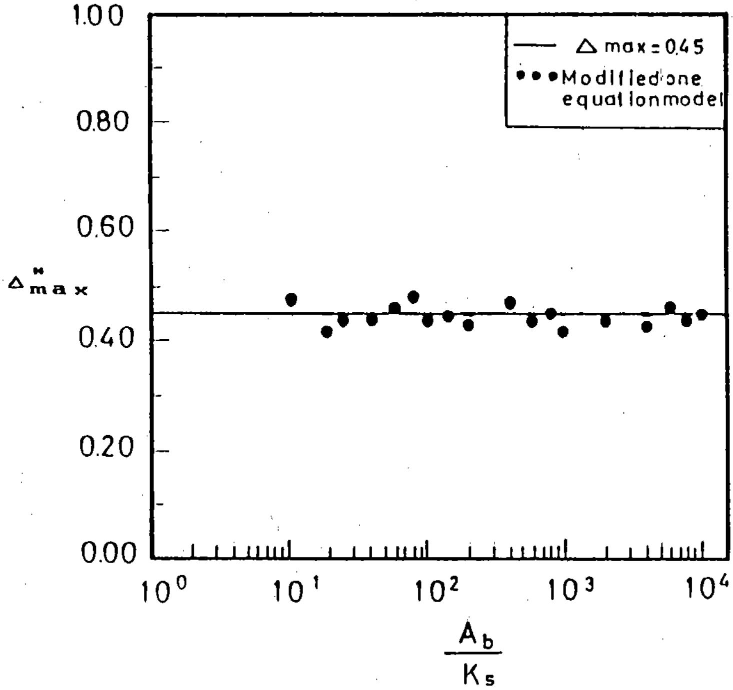

圖十二　不同相對糙度渦動滯度最大值發生位置

經以上之分析，渦動滯度隨底部高程之變化已可合理解釋，而其分佈函數類似指數減衰函數，可表示爲

$$\frac{\nu_t}{k\,\hat{u}_b^*\,z_o} = \eta\, e^{-\alpha\eta} \qquad \cdots\cdots (48)$$

上式中 α 爲一係數，可由 ν_t 之極值求出，上式對 η 微分爲零，得

$$\alpha = 1/\eta \qquad \cdots\cdots (49)$$

根據 (42) 式及利用 (47) 式，可得極值之 η 爲

$$\begin{aligned} \eta &= 0.45\,\Delta^* \\ &= 5.4\sqrt{f_w/2}\ A_b/K_s \end{aligned} \qquad \cdots\cdots (50)$$

將上式代入 (49) 式得 α 爲

$$\alpha = 0.2619\,(\sqrt{f_w}\,A_b/K_s)^{-1} \qquad \cdots\cdots (51)$$

在（48）式中，當 $\eta \to \eta_o$ 時，$e^{-\alpha\eta} \to 1$，即非常靠近底部位置，其渦動滯度 ν_t 爲線性分佈：

$$\nu_t = k\,\hat{u}_b^* z \qquad \cdots\cdots (52)$$

當離邊界甚遠時，函數 $e^{-\alpha\eta}$ 的值變小，其渦動滯度有減衰現象，符合前人的研究結果。

（48）式的分佈函數繪於圖十及圖十一的實線，與修正一階閉合模式的分佈型式甚爲接近，且此種分佈爲一連續性函數，不必分層求解。本文將根據這個渦動滯度模式，由控制方程式以零階閉合模式直接求解紊流之邊界層特性。

七、粗糙紊流海灘底部邊界層特性研究

本節之目的，即由第五節修正一階閉合模式所推求與時間無關之渦動滯度，據此將其代入控制方程式中解求粗糙紊流海灘底部邊界層特性。爲便於分析，首先將 $\eta = z/z_o$ 之無因次高度代入（18）式中，得粗糙紊流（$k_z = \nu_t$）一階控制方程式爲

$$\frac{\partial}{\partial t}(u_1 - U_1) = \frac{1}{z_o}\frac{\partial}{\partial \eta}\left(\frac{\tau_1}{\rho}\right) \qquad \cdots\cdots (53)$$

其中

$$\frac{\tau_1}{\rho} = \frac{1}{z_o}\left(\nu_t \frac{\partial u_1}{\partial \eta}\right) \qquad \cdots\cdots (54)$$

連續方程式經無因次轉換，垂直流速分量表示爲

$$w_1 = -z_o \int_{\eta_o}^{\eta} \frac{\partial u_1}{\partial x}\, d\eta \qquad \cdots\cdots (55)$$

爲解析方便，在此引用速度缺損律（ velocity defect law）以求解速度剖面：

$$u_1 = U_1 \left[1 - F(\eta) \right] \\ = A_b\,\omega \left[1 - F(\eta) \right] e^{i} \qquad \cdots\cdots (56)$$

由（46）、（53）、（54）及（56）式，得常微分方程式如下：

$$\frac{d}{d\eta}\left(K \frac{dF}{d\eta} \right) = aF \qquad \cdots\cdots (57)$$

式中

$$a = \frac{i\,\omega\,z_o}{k\,\hat{u}_b^*} \qquad \cdots\cdots (58)$$

其邊界條件爲

$$\eta = \eta_o \quad ; \quad F(\eta_o) = 1 \qquad \cdots\cdots (59)$$

$$\eta \rightarrow \infty \quad ; \quad F(\eta) = 0 \qquad \cdots\cdots (60)$$

今以控制體積法（ Trowbridge et al., 1986 ）求解（57）式可得

$$aF(I)\,\triangle\eta = K(\eta_2)\,F_\eta(\eta_2) - K(\eta_1)\,F_\eta(\eta_1) \qquad \cdots\cdots (61)$$

在高程 η_1 之剪力可由以下二式求之：

$$\tau(\eta_1) = k\,\hat{u}_b^*\,z_o K(I) \frac{F(I) - F(\eta_1)}{\eta(I) - \eta_1} \qquad \cdots\cdots (62)$$

$$\tau(\eta_1) = k\,\hat{u}_b^*\,z_o K(I-1) \frac{F(\eta_1) - F(I-1)}{\eta_1 - \eta(I-1)} \qquad \cdots\cdots (63)$$

由以上二式得

$$F(\eta_1)=\frac{K(I)F(I)+K(I-1)F(I-1)}{K(I)+K(I-1)} \qquad \cdots\cdots (64)$$

同理，$F(\eta_2)$ 爲

$$F(\eta_2)=\frac{K(I+1)F(I+1)+K(I)F(I)}{K(I+1)+K(I)} \qquad \cdots\cdots (65)$$

再利用下二式關係

$$K(\eta_1)F_\eta(\eta_1)=K(I)\frac{F(I)-F(\eta_1)}{\eta(I)-\eta_1} \qquad \cdots\cdots (66a)$$

$$F_\eta(\eta_1)=\frac{F(I)-F(I-1)}{\eta(I)-\eta(I-1)} \qquad \cdots\cdots (66b)$$

再根據（64）、（66a）及（66b）三式求得$K(\eta_1)$爲

$$K(\eta_1)=\frac{2K(I)K(I-1)}{K(I)+K(I-1)} \qquad \cdots\cdots (67)$$

同理，$K(\eta_2)$ 爲

$$K(\eta_2)=\frac{2K(I+1)K(I)}{K(I+1)+K(I)} \qquad \cdots\cdots (68)$$

將（64）－（68）式代入（61）式，則（61）式之標準化爲

$$b(I)F(I+1)+c(I)F(I-1)=a(I)F(I) \qquad \cdots\cdots (69)$$

其中

$$b(I)=\frac{2K(I+1)K(I)}{[K(I+1)+K(I)][\eta(I+1)-\eta(I)]} \qquad \cdots\cdots (70)$$

$$c(I)=\frac{2K(I)\;K(I-1)}{[K(I)+K(I-1)][\eta(I)-\eta(I-1)]} \quad \cdots\cdots (71)$$

$$a(I)=[\,b(I)+c(I)+a\triangle\eta\,] \quad \cdots\cdots (72)$$

(69) 式為一標準化之矩陣解，其中包含一未知數 u_b^* 在方程式中，因此海灘底部邊界層相關物理量解析尚無法完成。對 (53) 式積分並配合 (56) 式，可得剪力分佈為

$$\frac{\tau_1}{\rho}=i\,\omega^2 A_b z_o\left[\int_{\eta}^{\infty} F d\eta\right] e^{i\theta} \quad \cdots\cdots (73)$$

根據上式，底床剪力為

$$\frac{\tau_{1b}}{\rho}=i\,\omega^2 A_b z_o\left[\int_{\eta_o}^{\infty} F d\eta\right] e^{i\theta}$$

$$=\frac{\hat{\tau}_{1b}}{\rho}\,e^{i(\theta+\psi)} \quad \cdots\cdots (74)$$

再由 (74) 式，剪力的振幅 $\hat{\tau}_{1b}$ 與位相差 ψ 為

$$\frac{\hat{\tau}_{1b}}{\rho}=\omega^2 A_b z_o\left[\left(i\int_{\eta_o}^{\infty} F d\eta\right)\left(i\int_{\eta_o}^{\infty} F d\eta\right)^*\right]^{\frac{1}{2}} \quad \cdots\cdots (75a)$$

$$\psi=\tan^{-1}\frac{\mathrm{Im}\left[i\int_{\eta_o}^{\infty} F d\eta\right]}{\mathrm{Re}\left[i\int_{\eta_o}^{\infty} F d\eta\right]} \quad \cdots\cdots (75b)$$

利用 $\tau_{1b}=\rho\,\hat{u}_b^{*2}$ 之關係，則由 (75a) 式可得摩擦速度之振幅為：

$$\hat{u}_b^*=\omega\,(A_b z_o)^{\frac{1}{2}}\left[\left(i\int_{\eta_o}^{\infty} F d\eta\right)\left(i\int_{\eta_o}^{\infty} F d\eta\right)^*\right]^{\frac{1}{4}} \quad \cdots\cdots (76)$$

在 (76) 式中，右邊 F 爲 $\hat{u}_b^*$ 之函數，如已知相對糙度，邊界層外流速及波浪週期，則 $\hat{u}^*$ 可由疊代法求解，其精度本文取 10^{-5} 。

F 的解求出後，水平流速與邊界層外的流速位相 ϕ 爲

$$u_1 = \hat{u}_1 \, e^{i(\theta-\phi)} \qquad \cdots\cdots (77)$$

根據 Jonsson (1966) 對底床剪力之定義爲

$$\tau_{1b} = \frac{\rho}{2} C_f \, | \cos(\theta+\psi) | \cos(\theta+\psi) \, \hat{U}_1^2 \qquad \cdots\cdots (78)$$

上式經富立葉函數展開並取第一分量得：

$$\tau_{1b} = \frac{4}{3\pi} C_f \cos(\theta+\psi) \, \hat{U}_1^2 \qquad \cdots\cdots (79)$$

由 (75a) 、(78) 及 (79) 式得摩擦係數 C_f 爲

$$C_f = \frac{\pi}{40} \left(\frac{K_s}{A_b}\right) \left[\left(i\int_{\eta_0}^{\infty} F d\eta \right) \left(i\int_{\eta_0}^{\infty} F d\eta \right)^* \right]^{\frac{1}{2}} \qquad \cdots\cdots (80)$$

從 (80) 式看出，摩擦係數 C_f 爲相對糙度 A_b/k_s 之函數。 最大剪力摩擦係數 f_w 之定義爲：

$$\hat{\tau}_{1b} = \frac{\rho}{2} f_w \hat{U}_1^2 \qquad \cdots\cdots (81)$$

由 (79) 及 (81) 式之 f_w 及 C_f 之關係如下：

$$f_w = \frac{8}{3\pi} C_f \qquad \cdots\cdots (82)$$

八、計算結果與討論

本文有關紊流邊界層的計算結果，將與往昔學者之試驗數據加以比較。試驗數據之試驗條件列於表二。由 (1) 式可知，表中各試驗條件參數 k_s / D_l 值符合粗糙底床之條件，再由振幅雷諾數R及相對糙度 A_b / k_s 根據 (2) 及 (3)式判斷，各試驗均符合粗糙紊流之條件。

圖十三及圖十四分別爲 Jonsson and Carlsen(1976) 試驗中之水平流速振幅及位相角。圖中之實線爲本文提議渦動滯度之預測結果，虛線則爲線性增加渦動滯度 (Grant and Madsen, 1979) 的計算結果。由圖中看出，在靠近底床位置，不論實測或理論值，均顯示流速呈對數分佈，但理論值偏高。由於試驗中舖設之糙度爲人工沙漣，故接近底部之流況受個別糙度的影響愈爲明顯，此時紊流已不具均一性，但目前粗糙紊流模式均使用均一性之理論底床模擬，此一現象爲造成理論與實測偏差之原因。又圖中之結果說明本文減衰之渦動滯度在超射現的模擬較線性增加之渦動滯度爲佳，其原因已於前面詳述。

圖十五與圖十六爲試驗二之比較。圖中實線、虛線及點線分別代表本文、修正一階閉合模式及Myrhaug (1982) 雙層模式之計算結果。經比較後發現，本文與修正一階閉合模式之結果甚爲接近，然雙層模式在超射現象之預測較差。本文及Myrhang 在速度位相之預測在靠近底部位置均有高估的現象，而離開底部較遠時雙層模式則與實測數據偏離。Trowbridge and Madsen(1984a) 使用與時間相關之渦動滯度所預測的速度位相，在非常接近底部時也有明顯的高估現象。

圖十七至圖二十分別爲 Sumer et al. (1987) 及 Sleath(1987) 不同位相之實測水平流速剖面，其底床均爲天然沙粒，因此，對數分佈區的模擬已有明顯改善，且所用儀器爲 LDV，對於流況的干擾較小。大體而言，預測值與實測值呈良好的一致性。

表二 粗糙紊流流速剖面試驗條件

試驗條件 試驗者及儀器	水粒子振幅 A_b(m)	底床流速振幅 $\hat{U}$(m/s)	頻率 ω rad/s	粗糙度 k_s(m)	相對糙度 A_b/k_s	振幅雷諾數 R	滯性層厚度 D_l(m)	$\frac{k_s}{D_l}$
Jonsson and Carlsen(1976) (Test No.1) 微流速儀	2.85	2.13	0.749	0.023	123.9	6×10^{6}	4.1×10^{-5}	565.1
Jonsson and Carlsen (1976) (Test No.2) 微流速儀	1.79	1.56	0.873	0.063	28.4	2.74×10^{6}	5.1×10^{-5}	1229.9
Sumer et al. (1987) LDV	2.71	2.10	0.774	0.0038	720	5×10^{6}	6.1×10^{-5}	62.8
Sleath (1987) LDV	0.49	0.686	1.384	0.0032	151	2.8×10^{5}	1.7×10^{-5}	18.9
Sleath (1987) LDV	0.45	0.617	1.372	0.0032	138	2.3×10^{5}	1.8×10^{-5}	17.8
van Doorn (1981) LDV	0.085	0.267	3.142	0.021	4.05	2.3×10^{4}	2.5×10^{-5}	83.0

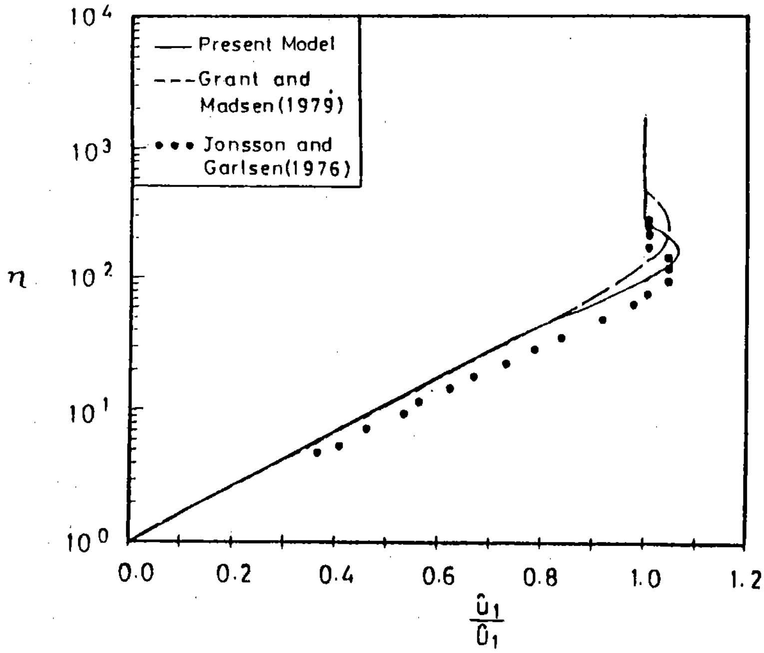

圖十三　粗糙紊流水平流速振幅預測值與實測值比較
（ $\hat{U}_1 = 213$ cm/ sec , $A_b = 285$ cm , h= 30 cm , T= 8.39 sec
$k_s = 2.3$ cm , $A_b/k_s = 123.9$ ）

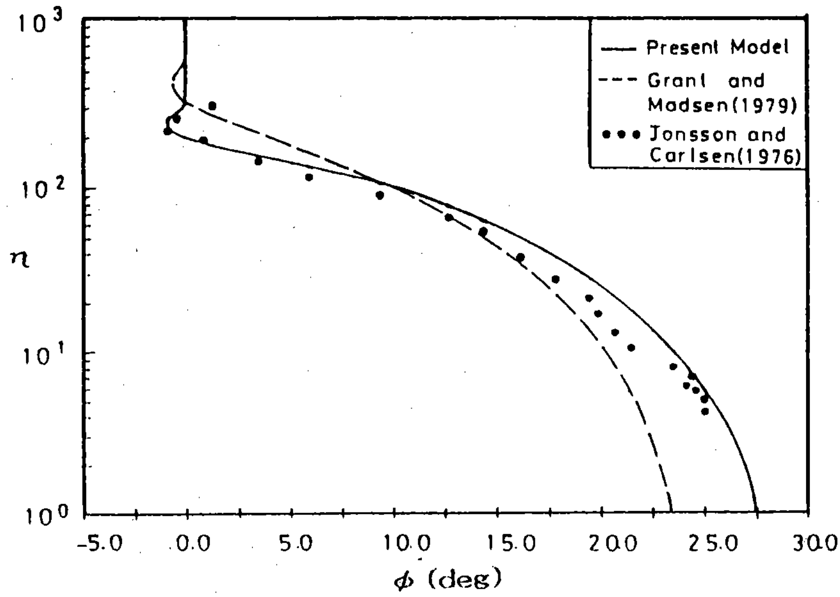

圖十四　粗糙紊流水平流速振幅預測值與實測值比較
（ $\hat{U}_1 = 213$ cm/ sec , $A_b = 285$ cm , h= 30 cm , T= 8.39 sec
$k_s = 2.3$ cm , $A_b/k_s = 123.9$ ）

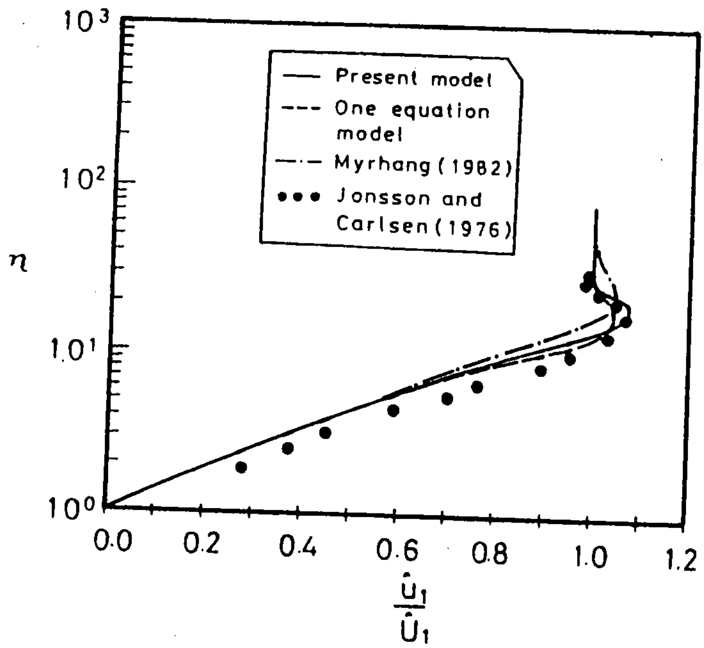

圖十五　粗糙紊流水平流速振幅預測值與實測值比較
($\hat{U}_1 = 156$ cm/ sec , $A_b = 179$ cm , h=30 cm , T= 7.20sec
$k_s = 6.3$ cm , $A_b / k_s = 28.4$)

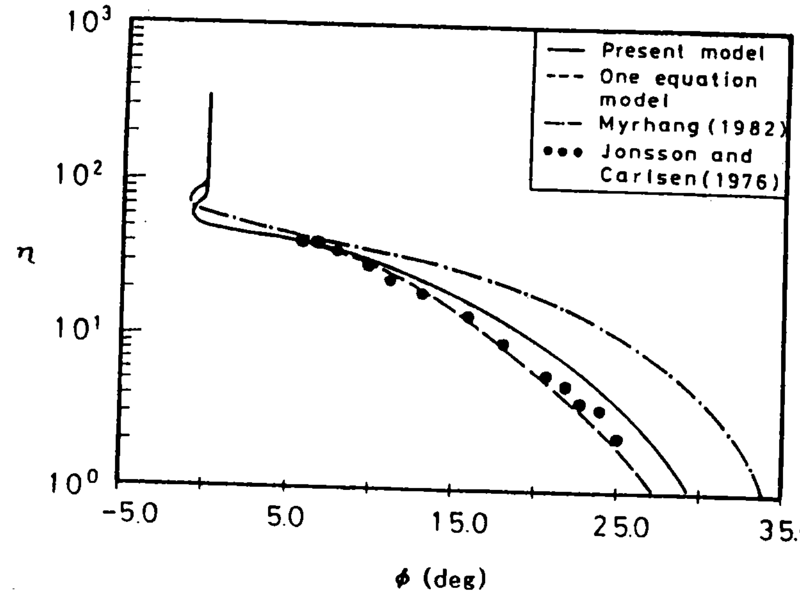

圖十六　粗糙紊流水平流速位相差預測值與實測值比較
($\hat{U}_1 = 156$ cm/sec , $A_b = 179$ cm , h=30 cm , T= 7.20 sec
$k_s = 6.3$ cm , $A_b/k_s = 28.4$)

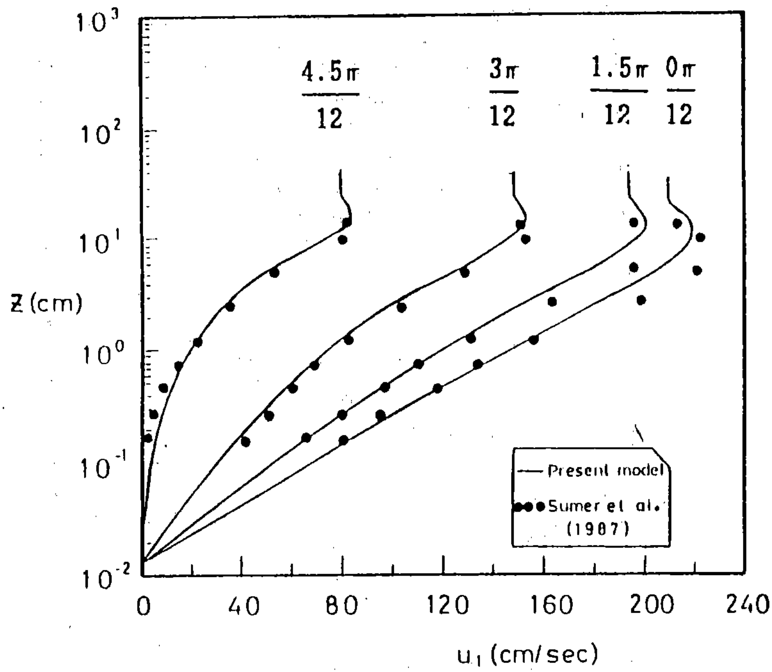

圖十七　粗糙紊流水平流速預測值與實測值比較

（加速度位相；$\hat{U}_1 = 210$ cm/sec，$A_b = 27$ cm，$h = 30$ cm

$T = 8.12$ sec，$k_s = 0.38$ cm，$A_b / k_s = 270$）

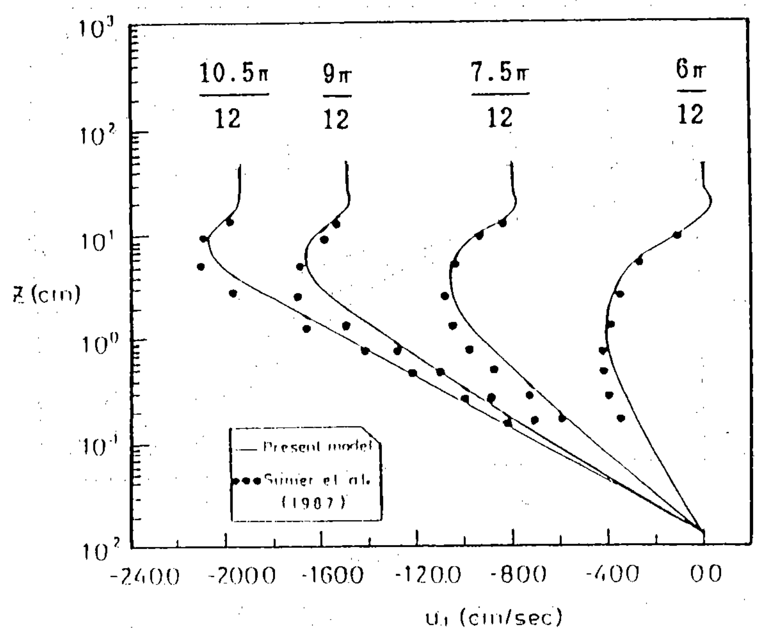

圖十八　粗糙紊流水平流速預測值與實測值比較

（加速度位相；$\hat{U}_1 = 210$ cm/sec，$A_b = 27$ cm，$h = 30$ cm

$T = 8.12$ sec，$k_s = 0.38$ cm，$A_b / k_s = 720$）

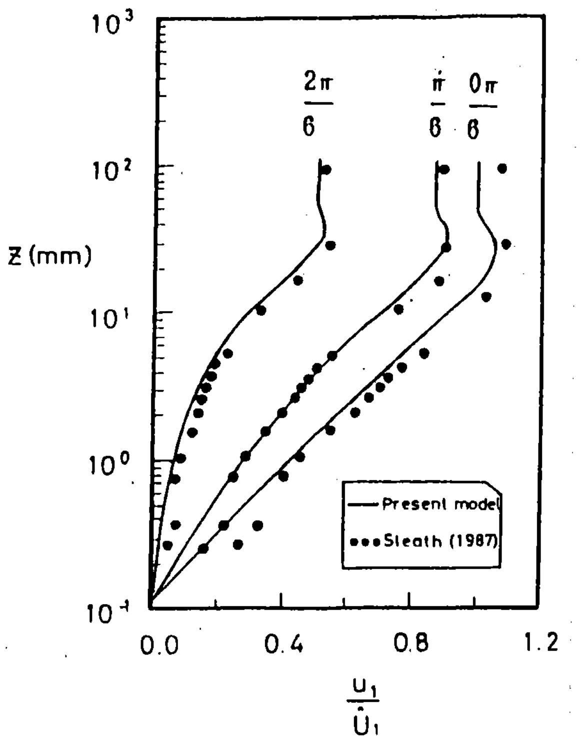

圖十九　粗糙紊流水平流速預測值與實測值比較

（加速度位相；$\hat{U}_1 = 68.6$ cm/sec, $A_b = 49$ cm, h=45 cm

T=8.12 sec, $k_s = 0.32$ cm, $A_b/k_s = 151$）

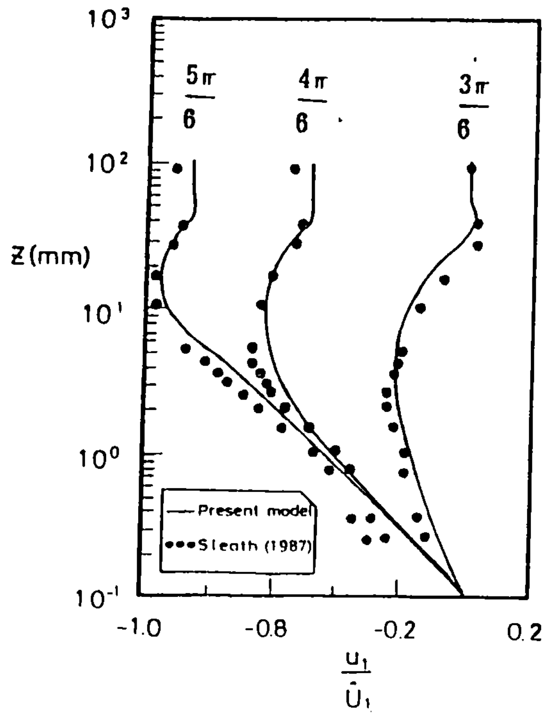

圖二十　粗糙紊流水平流速預測值與實測值比較

（加速度位相；$\hat{U}_1 = 68.6$ cm/sec, $A_b = 49$ cm, h = 45 cm

T = 8.12 sec, $k_s = 0.32$ cm, $A_b/k_s = 151$）

在較小相對糙度之情況，van Doorn(1981)以LVD 在人工沙漣底面量測沙漣波峰與波谷的水平流速及定常流。圖二十一及圖二十二分別爲理論值與實測值之比較。在圖二十一中，實線與虛線分別代表本文及Trowbridge and Madsen(1984a)之預測值，而黑點則爲沙漣波峰與波谷水平流速的平均值。圖中結果顯示，兩種理論的解析均不很理想，原因乃相對糙度太小，底部流速受個別糙度影響很大而不具均一性，至於圖二十二中位相的預測尚稱滿意。

在不同位相水平流速的等值線(iso-valued curves)較具物理意義，它表示在不同高程、不同流速的連線，可以解釋水平流速在時間領域上空間分佈的特性。相對糙度 $A_b/k_s=123.9$ 半個週期的水平流速等值線示於圖二十三，圖中不對稱現象乃位相差所造成。

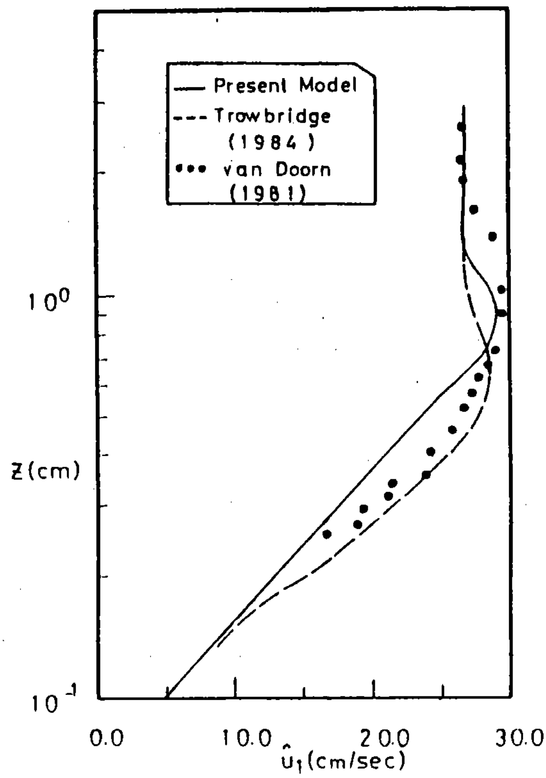

圖二十一　粗糙紊流水平流速振幅預測值與實測值比較
($\hat{U}_1=26.7$ cm/sec, $A_b=8.5$ cm, h=30 cm, T=2.0 sec
$k_s=2$ cm, $A_b/k_s=4.05$)

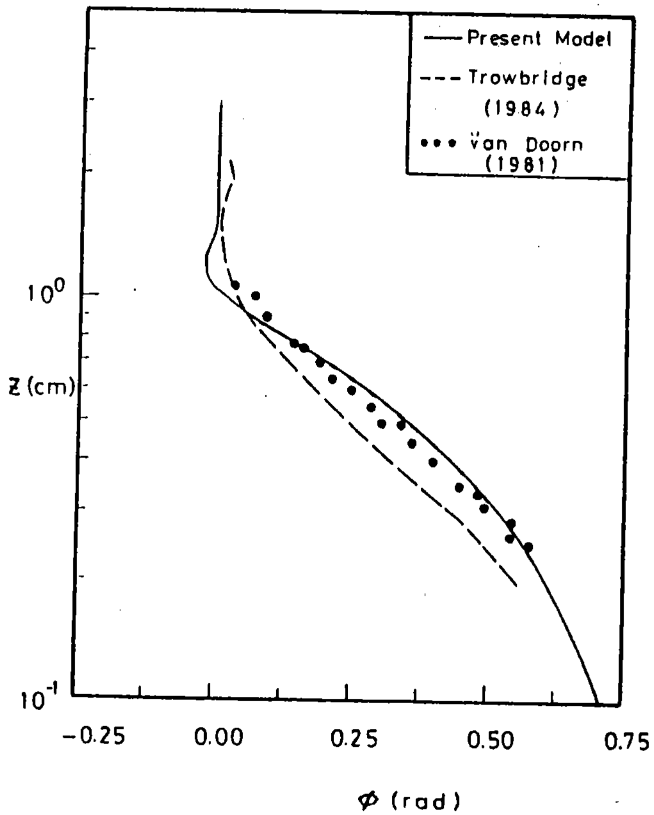

圖二十二　粗糙紊流水平流速位相差預測值與實測值比較

($\hat{U}_1 = 26.7$ cm/sec, $A_b = 8.5$ cm, h=30 cm, T= 2.0 sec

$k_s = 2$ cm, $A_b/k_s = 4.05$)

粗糙紊流的剪力分佈由 (73) 式計算 。圖二十四顯示從計算中所得到的剪力振幅分佈，黑點為 Jonsson and Carlsen (1976) 試驗 ——由對數分佈所得結果，經比較發現除底床剪力較不符合外，其餘則十分良好，原因為個別糙度附近的流況不能以理論完整地描述所致。

圖二十五為摩擦係數比較圖，本文理論係由 (80) 及 (81) 式所求得，為使於比較 Jonsson and Carlsen (1976) 半經驗公式，修正一階閉合模式及二階閉合模式之結果以及相關試驗值亦點繪於圖中。從圖中發現，摩擦係數隨相對糙度 A_b/k_s 之增加而減小。當 A_b/k_s 小於 30 時，本文理論值有明顯低估現象

，此現象說明當相對糙度小時，理論模式已不能適用，此時沙漣個別糙度已顯重要。另者，當$A_b/k_s>30$時，本文理論曲線與修正一階閉合模式之結果相當類似，與實測數據比較亦屬合理，但 Jonsson and Carlsen (1976) 的數據則有高估現象。從以上之比較得知本文模式之適用範圍爲A_b/k_s大於30之情況。

摩擦係數位相差隨相對糙度之變化示於圖二十六。圖中實線爲本文理論值，而虛線則爲Kajiura (1968) 理論所計算的結果。圖中顯示，位相角亦隨相對糙度的增加而減小，而本文理論較Kajiura (1968) 爲小。在A_b/k_s較小情況，此時流況接近於層流，Lamb (1942) 由理論推導底床剪力的位相差爲$\pi/4$。本文理論值低於$\pi/4$。約有4.5%的誤差，其原因乃本文數值計算時用梯形積分，所產生的誤差所致。

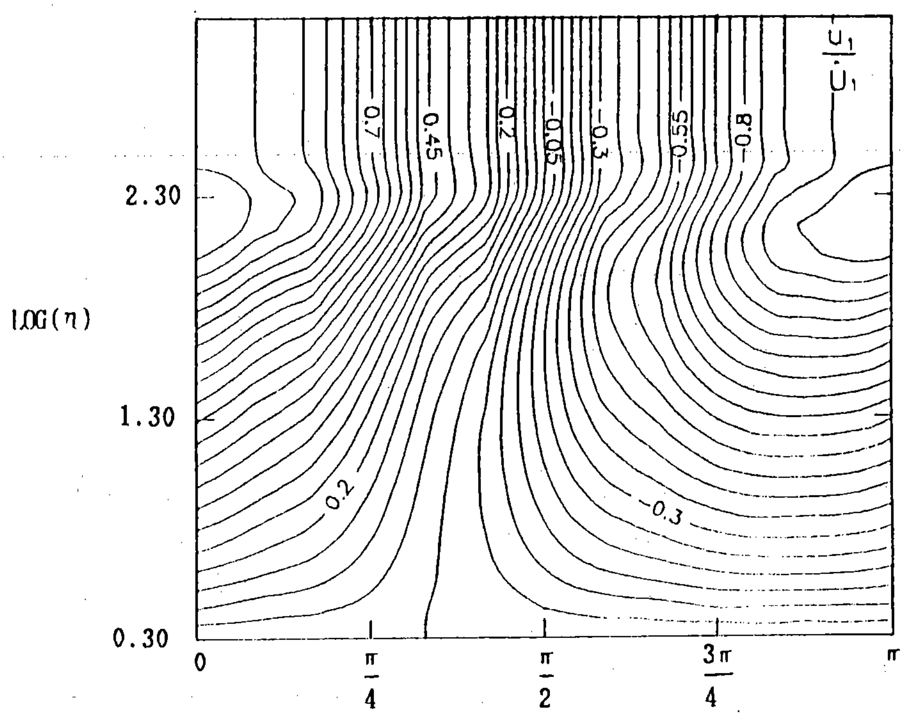

圖二十三　粗糙紊流水平流速在時間領域之等值線

($A_b/k_s=123.9$)

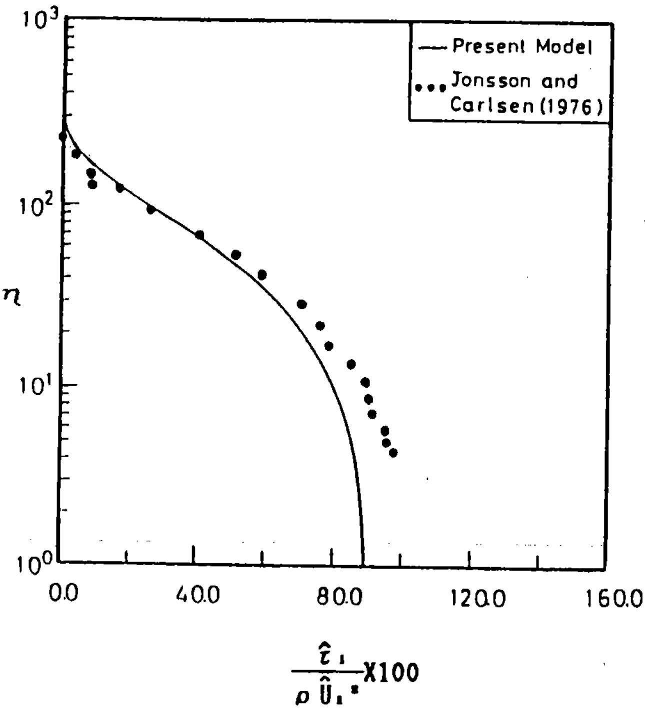

圖二十四　粗糙紊流剪力振幅預測值與實測值比較

($\hat{U}_1 = 213$ cm/ sec , $A_b = 285$ cm , h=30 cm , T=8.39 sec
$k_s = 2.3$ cm, $A_b / k_s = 123.9$)

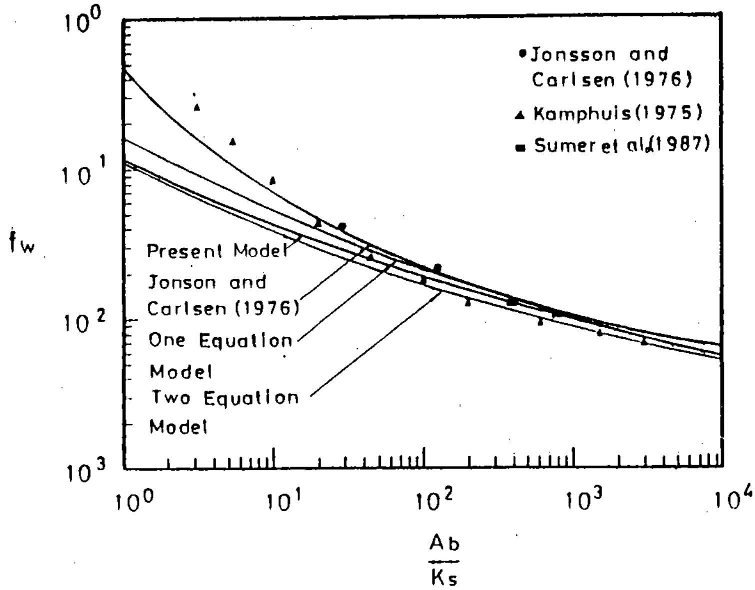

圖二十五　粗糙紊流摩擦係數預測值與實測值比較

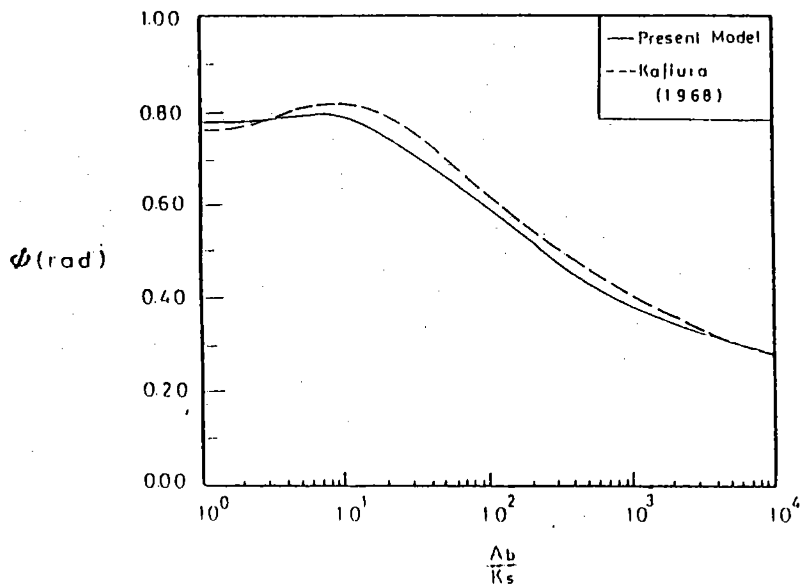

圖二十六　粗糙紊流摩擦係數位相差與相對糙度之關係

九、結　論

1. 修正一階閉合模式的分析結果顯示，靠近底部時，渦動滯度呈線性增加，遠離底部時，非線性效應增強，在 $0.45\Delta^*$ 之高度達最大時，其中 Δ^* 爲邊界層參考厚度，以後則急速減衰。
2. 根據修正一階閉合模式所獲之渦動滯度，經由離散富立葉轉換分析，本文提議一個單層渦動滯度分佈函數，此一分佈與前人經由試驗數據的分析結果相近，其合理性可獲進一步證實。
3. 利用本文之渦動滯度模式，解析海灘底部粗糙紊流邊界層特性，發現流速剖面及位相差能符合大部份的試驗結果，特別在超射現象的模擬，優於外層未減衰之渦動滯度函數。此一單層模式爲一連續函數，可改進多層模式繁瑣之計算過程，節省計算時間。
4. 粗糙紊流摩擦係數及摩擦係數位相差，均隨相對糙度之增加而減小。當相對糙度小於 30 時，本文理論值明顯低估，理論模式已不能適用。

参考文獻

1. Aukrust,T. and I. Brevik: Turbulent viscosity in rough oscillatory flow,J. Waterway,Port and Ocean Eng. Div,ASCE,Vol.111, WW3,525-541,1985.
2. Brevik,I: Oscillatory rough turbulent boundary layers, J. Waterway, Port and Ocean Eng. Div.,ASCE,Vol.107,WW3,175-188,1981.
3. Boussinesq,J.: Essai sur la theorie des eaux courantes, Mem. Pres. Acad. Sci,XXIII,46,Paris,1877.
4. Grant,W.D.: Bottom friction under waves in the presence of a weak current: Its relationship to coastal sediment transport, Sc.D. the-sis,Massachusetts Institute of Technology,1977.
5. Grant,W.D. and O.S. Madsen: Combined wave and current interaction with a rough bottom,J. Geophys. Res.,Vol.84,No.C4,1797-1808,1979.
6. Hinze,J.O.: Turbulence,2nd ed.,McGraw-Hill,New York,1975.
7. Horikawa,K. and A. Watanabe: Laboratory study on oscillatory boundary layer flow,Proc. llth International Conf. on Coastal Eng.,London.467-486,1968.
8. Jonsson,I.G.: Wave boundary layers and friction factor,Proc. 10th International Conf. on Coastal Eng.,Tokyo,127-148,1966.
9. Jonsson,I.G. and N.A. Carlsen: Experimental and theoretical investegations in an oscillatory turbulent boundary layer,J.Hydraul.Res.,Vol.14,45-60,1976.
10. Justesen,P.: Prediction of turbulence oscillatory flow over rough beds,Coastal Engineering,257-284,1988.
11. Kajiura,K.: A model of the bottom boundary layer in water waves, Bull. Earthq.Res.Inst.,Univ. of Tokyo,Vol.46,75-123,1968.
12. Kamphuis,J.W.: Friction factor under oscillatory waves,J. Waterways, Harbor and Coastal Eng. Div.,ASCE,Vol.101,WW2,135-144,1975.

13. Kolmogorov,A.N.: A Refinement of previous hypothesis concerning the local structure of a turbulence in a viscous incompressible fluid at high Reynolds number,J.Fluid Mech.,Vol.13,82-85,1962.

14. Lamb,H.: Hydrodynamics,Dover,New York,1945.

15. Lundrgren,H.: Turbulent currents in the presence of waves,Proc. 13th International Conf. on Castal Eng.,Vancouner,623-634,1972.

16. Myrhaug,D.: On a theoretical model of rough turbulent wave boundary layers, Ocean Engineering, Vol.9,547-565,1982.

17. Nielsen,P.: On the structure of oscillatory boundary layers, Coastal Engineering,Vol.9,261-276,1985.

18. Prandtl,L.: Essentials of fluid dynamics, Hafner Publishing Co., Inc., New York, Article IIb, 1952.

19. Reynolds,W.C.: Computation of turbulence flows, Annual Review of Fluid Mechanics,Vol.8,183-208,1976.

20. Riedel,H.P., J.W.Kamphuis and A.Brebner::Measurement of bed shear stress under waves, Proc.13th International Conf. on Coastal Eng., Vanconver,587-603,1972.

21. Rodi,W.: Turbulence models and their application in hydraulics, IAHR,Delft, The Netherlands, 104pp., 1980.

22. Saffman,P.G.: A model for inhomogeneous turbulence flow,Proc. Roy.i Soc., London,Series A,Vol.317,417-433,1970.

23. Sheng,Y.P.: Modeling turbulent bottom boundary layer dynamics,Proc.20th International Conf. on Coastal Engineering, Taipei, 1496-1508,1986.

24. Sleath,J.F.A.: Turbulent oscillatory flow over rough beds, J. Fluid Mech.,Vol. 182,369-409,1987.

25. Sumer,B.M., B.L.Jensen and J. Fredsoe: Turbulence in oscillatory boundary layers, Advances in Turbulence, Springer Verlag, Berlin, 556-567,1987.

26. Trowbridge, J. and O.S. Madsen(a) : Turbulnt wave boundary layer 1 : model formulation and first-order solution, J. Geophys. Res., Vol.89,No.C5,7987-7997,1984.

27. Trowbridge, J.,C.N. Kanetkar and N. T-Wu: Numerical simulation of turbulent boundary layers,Proc. 20th International Conf. on Coastal Engineering, Taipei, 1623-1637, 1986.

28. van Doorn, Th. and H.W.H.E. Godefory: Experimental investigation of the bottom boundary layer under progressive water waves, Report No. M1362, Delft Hydraulics Laboratory,1978.

29. van Doorn, Th.: Experimental investigation of near-bottom velocities in water waves with and without a current Report No.M1423, Delft Hydraulics laboratory, 1981.

30. Vonguisessomjai, S.: Oscillatory boundary layer and eddy viscosity, J.Hydraul. Eng., Vol.110, No.4, 387-403, 1984.

EDDY VISCOSITY MODEL AND TURBULENT BOUNDARY LAYER NEAR ROUGH BOTTOM IN WATER WAVES

Shan-Hwei Ou* and Tai-Wen Hsu**

英文摘要

A theoretical study on the wave-induced fully turbulent boundary layer over rough bed is presented. A one layer time-invariant eddy viscosity model which is more realistic under natural conditions is proposed to describe the flow field inside the boundary layer. The eddy viscosity distribution is obtained from the numerical results of the one-equation closure model by the Discrete Fourier Transform(DFT) method. Computations based on this eddy viscosity model compare favorably with the published data. The first-order solution for the case of Stokes waves are invesigated. These results include the velocity profile, shear stress, friction factor. The present study simplifies much complexity in many of the existing models. The first order solution shows good agreement with the experimental data.

---

*Professor, Ph.D, Dept.of Hydraulics & Ocean Engineering National Cheng Kung University, Taiwan, Taiwan 70101,R.O.C.

**Graduate Student,ditto.

第三屆基礎港灣數值(數學)模式研習會論文集 Jan. 17～18, 1990 Page 113～124

海洋風浪之波譜模式

郭一羽

國立交通大學土木系教授

一、前 言

海洋或海岸工程結構物之設計，主要在於如何克服波浪之影響與作用，因此對波浪本身之力學機構的瞭解，是海洋或海岸工程上最主要的課題。目前爲止我們對於單一周期的規則性波浪，甚至已具有某種程度的非線性的單一周期波浪而言，在理論與應用上目前已有很大的成就和進展。然而實際上海洋波是一種具有極端不規則性的波浪，以線形近似的觀點，海洋波可看成是一種具有無限多之不同波高、周期、方向與位相的成分波的組合。欲描述此不規則波動現象，利用頻譜來表示乃不失爲一個好的方法。

對海洋波之頻譜的構造的瞭解，在物理上、工程上都是個有趣而重要的問題，最早從Neumaun (1952 年) 與 Pierson (1952 年) 的研究，三十多年以來已有豐碩的成果出現。尤其是最近10年來，電子計算機的普及，大大簡化了頻譜分析的繁雜過程，因此在工程應用上爲提高工程設計的水準，海洋波譜的應用也日趨廣泛。本文基於欲對海洋波浪力學有進一步的瞭解，謹對目前爲止的各種研究成果所提出的波譜構造或模式做一簡單的介紹。

二、風浪的成長及波譜的相似性

風吹在水面上，水面開始形成風波，隨時間的經過及吹送距離的增加風浪逐漸變大。當吹送距離較短時風浪大小達到飽和的時間較短，吹送距離較長時達到飽和所需的時間則較長。當然風速愈大則飽和時的風浪的規模也愈大。總之風浪的發生與大小隨著風速、吹送時間和吹送距離而變。這樣的發達過程對風

浪的頻譜的構造而言，又是如何呢？

圖㈠是在一定的風速，且吹送距離達到飽和的情況，各種不同吹送距離的風浪頻譜的實驗結果，圖㈡則是在固定的吹送距離下，風速不同時的各風浪頻譜的實驗結果，從上面兩圖可發現：

㈠風速變化與吹送距離變化所產生的風浪成長極爲相似。

㈡各發展階段的波譜形狀相當類似。

㈢主頻率往低頻的方向移動。

㈣高頻成分的能量有逐漸減衰的現象。

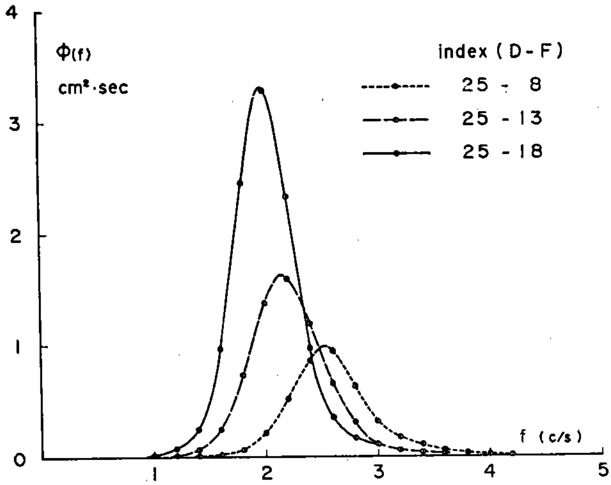

圖㈠　風浪頻譜隨吹送距離改變而發生的變化

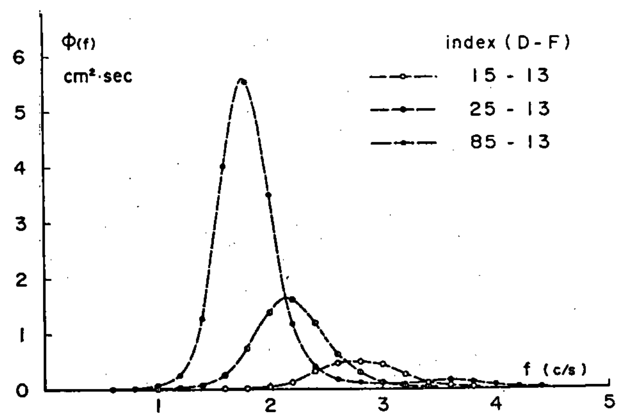

圖㈡　風浪頻譜隨風速改變而發生的變化

進一步若對風浪頻譜的主頻率 f_m，波譜的總能量 $E\ (=\int_0^\infty \phi(f)\,df)$，風的摩擦速度 u_*（海面上 10m 的風速 $U_{10} = 25u_*$）以及吹送距離 F 加以討論，可以得到如下相當單純的關係式。

$$\frac{g\sqrt{E}}{u_*^2} = 1.31 \times 10^{-2} \left(\frac{gF}{u_*^2}\right)^{0.504} \qquad \cdots\cdots\cdots(1)$$

$$\frac{u_* f_m}{g} = 1.0 \left(\frac{gF}{u_*^2}\right)^{-0.33} \qquad \cdots\cdots\cdots(2)$$

上面兩式的適用範圍約在 $F\ (=\frac{gF}{u_*^2}) = 10^2 \sim 10^6$。由此可知在相當廣泛的範圍內頻譜的一些代表量與發生條件有一定的關係存在。今若是波譜的形狀也有一定的規則可循，則風浪發生之各階段的波譜即可容易的被表示出來。

事實上若在實驗室中，將各種不同吹送距離與風速的波譜以如下的方式規格化重疊畫出，

$$\frac{\phi(f)\,f_m}{E} = F\left(\frac{f}{f_m}\right) \qquad \cdots\cdots\cdots(3)$$

則如圖㈢所示呈現出一個相當一致的形狀。今若再以不同的條件或環境所產生

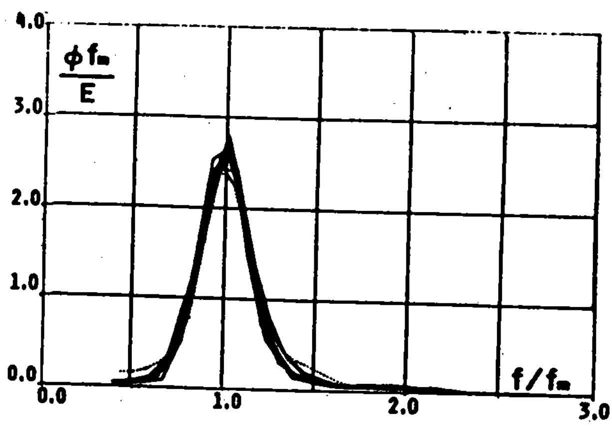

圖㈢　實驗水槽風浪正規化頻譜之一致性

的風浪的正規化波譜來比較，結果如圖(四)所示。圖(四)中(A)是表示上述的 3m × 1.5m × 20m的風洞水槽的風浪（ $F = 10^2 \sim 10^3$ ）。(B)是表示一大型開放式送

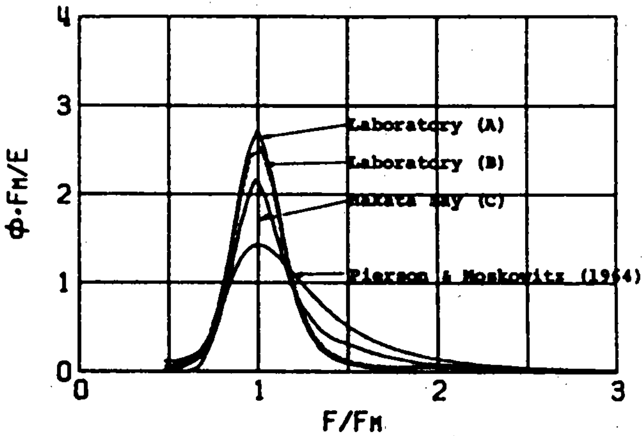

圖(四) 各種風浪之正規化頻譜

風水槽（ 3m × 8m × 70m ）中的風浪。(C)是表示在一海灣內（ $F = 10^5$ ）測到的風浪。另有 Pierson － Moskowitz 波譜是外洋波浪之典型代表例（ $F = 10^7$ ）。從圖(四)中的比較，可以發現F愈大的風浪其波譜形狀愈趨於平緩（能量趨於分散），實際上依照Mitsuyasn（ 1975年）的研究，發現外洋上的風浪波譜形狀大抵均介於實驗室波譜與P－M型波譜之間。故P－M型波譜可能是一種時間尚未達到飽和（因吹送距離太長）或是已離開風域呈減衰狀態的風浪。

三、標準波譜形態

㈠一次元波譜：

由以上所述已知風浪之一次元波譜大致上有固定的形狀存在。關於此一次元波譜至今已有不少的研究，利用一些觀測數據提出海洋波譜的標準模式。以下舉出目前使用較爲普遍的兩種模式。

一爲上述的 Pierson － Moskowitz 波譜，此爲北太平洋上具無限吹送距離下獲得的風浪波譜模式。

$$\phi(f) = k_1 f^{-5} \exp\left[-k_2 f^{-4}\right] \qquad \cdots\cdots\cdots (4)$$

$$k_1 = 8.10 \times 10^{-3} (2\pi)^{-4} g^2 \text{ , } k_2 = 0.74 (g/2\pi U)^4$$

將上式以(3)式的形狀正規化，則成為

$$\frac{\phi(f) f_m}{E} = 5 \left(\frac{f}{f_m}\right)^{-5} \exp\left[-\frac{5}{4}\left(\frac{f}{f_m}\right)^{-4}\right] \qquad \cdots\cdots\cdots (5)$$

我們亦可將(1)式與(2)式的關係代入上式來使用，則可由已知風速及吹送距離求得波譜。

另一種為以北海有限吹送距離下獲得的風浪資料整理出來的JONSWAP波譜。

$$\phi(f) = \alpha g^2 (2\pi)^{-4} f^{-5} \exp\left[-\frac{5}{4}\left(\frac{f}{f_m}\right)^{-4}\right] \cdot \gamma^{\exp-\left\{\frac{(f-f_m)^2}{2\sigma^2 f_m^2}\right\}}$$

$$\cdots\cdots\cdots (6)$$

$$\begin{cases} \alpha = 0.076 \tilde{F}^{-0.22} \\ \dfrac{f_m U_{10}}{g} = 3.5 \tilde{F}^{-0.33} \\ \gamma = 3.3 \\ \sigma = \begin{cases} 0.07 & f \leq f_m \\ 0.09 & f > f_m \end{cases} \end{cases}$$

其中的係數α及γ經Mitsuyasu (1980年)的研究，認為其與無次元吹送距離$\tilde{F}$有關。

$$\alpha = 8.17 \times 10^{-2} \tilde{F}^{-\frac{2}{7}} \qquad (7)$$

$$\gamma = 7.0 \times \tilde{F}^{-\frac{1}{7}} \qquad (8)$$

當 $\widetilde{F}\left(=\dfrac{gF}{U_{10}^{2}}\right)=2\times10^{2}$ 時 $\gamma=3.3$ ，此爲上述的 JONSWAP 波譜。當 $\widetilde{F}=10^{6}$ 時 $\gamma=1.0$ ，此爲 Pierson －Moskowitz 波譜。若改變(6)式成爲如(3)式的規格化形態即爲

$$\frac{\phi(f)f_m}{E}=Z\,f^{-5}\ \exp\left[-\frac{5}{4}\widetilde{f}^{-4}\right]\cdot\left\{\gamma^{\exp\left[-\frac{(\widetilde{f}-1)^2}{2\sigma^2}\right]}\right\}\quad\cdots(9)$$

$$(\widetilde{f}=f/f_m)$$

此爲一般化的波譜形態，式中 Z 爲能夠滿足 $\int_o^\infty \dfrac{\phi(f)f_m}{E}\,d\widetilde{f}=1$ 的正規化係數。任意改變式中參數 γ 的值，即可得到任何形狀的波譜。

此外另一種一般化的波譜形態是爲

$$\frac{\phi(f)f_m}{E}=\frac{n}{\Gamma\left(\frac{m-1}{n}\right)}\left(\frac{m}{n}\right)^{\frac{m-1}{n}}\widetilde{f}^{-m}\exp\left[-\frac{m}{n}\widetilde{f}^{-n}\right]\quad\cdots\cdots\cdots(10)$$

改變式中的參數m及 n 亦可得到各種不同形狀的波譜。

若有充分的現地波浪資料，對其實際波譜形狀加以分析，將其正規化、重疊，求出一代表性的形狀，再套用(9)式或(10)式的模式，找出適當的參數m 、n 或 γ 即可得適用於當地的標準波譜模式。例如圖(五)即是鼻頭角東北季風期之風浪波譜資料。

其中的粗實線即爲(10)式（ n ＝ 4 ， m＝ 9.5 ）的標準波譜形態。

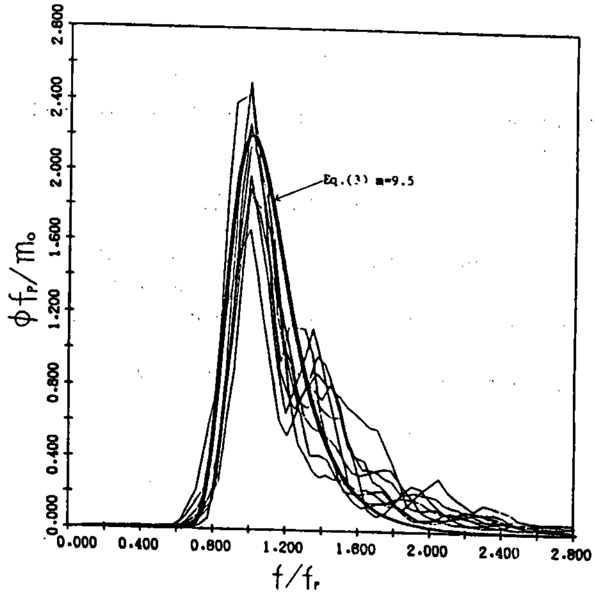

圖(五)　鼻頭角沿海風浪之正規化波譜

(二)二次元波譜：

比起一次元波譜，至目前爲止對二次元波譜的研究和成果均甚爲稀少，主要原因是測定不易花費龐大而缺乏實地觀測數據。以較簡便的方式，我們可把二次元波譜 $\psi(f, \theta)$ 寫成

$$\psi(f, \theta)=\phi(f)G(f, \theta) \quad \cdots\cdots\cdots (11)$$

$G(f, \theta)$ 稱爲方向分布函數，而 $\int_{o}^{2\pi} G(f, \theta)\, d\theta = 1$

圖(六)爲一在風洞水槽中測得的方向分布函數。由圖中可看出即使在水槽中甚爲均一的風速下，波浪各頻率成分的方向分布仍有甚大的差異。海洋上實測到的方向波譜較著名的有 SWOP（ 1957 年 ），其在北大西洋利用航空觀測所得數據整理出來的方向分布函數如下：

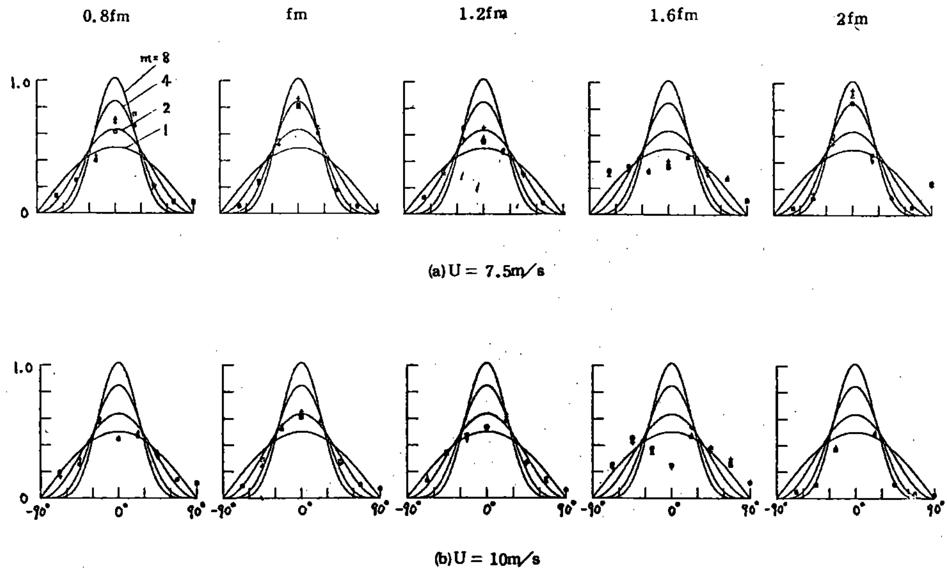

圖㈥　實驗水槽風浪之各頻率成份的方向分布。(縱座標：能量比例；橫座標：波向角度；實線爲 $\cos^m\theta$ 之理論分布)

$$G(\tilde{\tilde{f}},\theta)=\begin{cases}\dfrac{1}{\pi}\left[1+a\cos 2\theta+b\cos 4\theta\right], & |\theta|\le\dfrac{\pi}{2}\\[2ex] 0 & |\theta|>\dfrac{\pi}{2}\end{cases}\qquad\cdots\cdots\cdots(12)$$

$$\left(\tilde{\tilde{f}}=\frac{2\pi f_m U_{10}}{g}\right)$$

$$\begin{cases}a=0.5+0.82\exp\left[-\dfrac{1}{2}\tilde{\tilde{f}}^4\right]\\[2ex] b=0.32\exp\left[-\dfrac{1}{2}\tilde{\tilde{f}}^4\right]\end{cases}$$

另有Mitsuyasu（1975 年）利用Longuet－Higginns(1963 年）的數式加以改善提出的方向分布函數。

$$G(f,\theta)=G_1(s)\left[\cos\frac{(\theta-\bar{\theta})}{2}\right]^{\frac{s}{2}} \qquad \cdots\cdots\cdots (13)$$

$$G_1(s)=\frac{1}{\pi}2^{2s-1}\frac{\Gamma^2(s+1)}{\Gamma(2s+1)}$$

式中$\bar{\theta}$爲成分波之主方向。Mitsuyasu 利用廣泛的觀測數據發現參數S爲頻率及無因次吹送距離$\widetilde{F}$的函數。

$$S/S_m=\begin{cases}(f/f_m)^{-2.5} & f/f_m\geq 1\\ (f/f_m)^{5} & f/f_m\leq 1\end{cases} \qquad \cdots\cdots\cdots (14)$$

$$S_m=7.5\times 10^{-3}\,\widetilde{F}^{-0.825} \qquad \cdots\cdots\cdots (15)$$

由上式可以知道海洋波浪的方向分散，隨著無次元吹送距離的增加而減少。而且在能量集中的主頻率附近分散較小，離開主頻率的高頻或低頻部份分散較大。台灣沿海目前爲止尚未有完整的方向波譜的實測資料。

四、淺海波譜及非線形性的問題

風浪之波譜表示方法，乃是視波浪爲無限多的線形波的線性重疊的結果。依照波浪理論所得的觀念知道，當波浪尖銳度變大或水深變淺，則波浪的非線形性變大。當非線形効應不可忽視時波譜模式的使用便會產生很多困難。圖(七)爲水槽風浪的波速頻譜的實驗結果。由圖中可看出波速頻譜與線形理論之間存有明顯的差異。然而若是進一步觀察，亦可發現在波譜能量集中的頻譜區間內線形理論大致上仍能適用。至於海洋風浪，雖其能量分布的頻率區間較廣，但即使是對湧浪而言，在深水域的風浪非線形効應一般是相當微弱而可以忽略。但對淺水波浪而言，非線形效應有可能大到不可忽視，此時波譜的應用需要特別加以小心。利用二階波譜（ Bispectrum ）之計算去探討其非線形量大小是

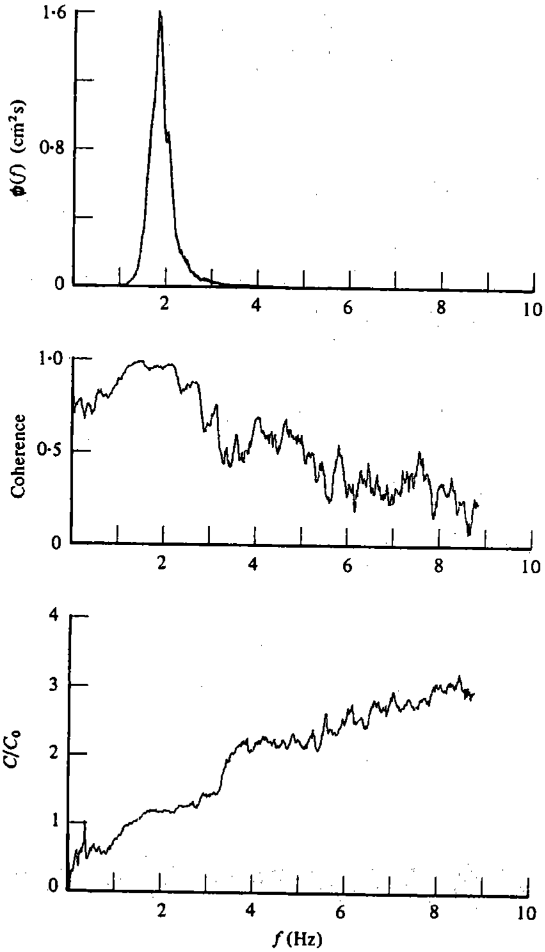

圖(七)　實驗水槽風浪之能譜、相關函數、波速頻譜（ C ：實測波速， Co ：線性理論波速 ）

一有效可行的辦法。

一般而言，波浪進入淺水其波譜形狀變緩（能量分布較廣），Kitaigordskii 等（ 1975 年 ）曾提出 f^{-3} 形態的淺水波譜模式如下：

$$\phi(f, h) = \alpha g h f^{-3} / (2(2\pi)^2) \qquad \cdots\cdots\cdots (16)$$

但根據理論或實驗觀測結果，關於淺水波譜之形態有各種不同的提案。其中Sawaragi（1980年）經由因次分析結果得到中度淺水波浪的波譜斜率爲－3，極淺水深波浪爲－1。另據現場資料分析，Goda（1974年）認爲淺水波譜斜率爲－4，Ou（1977年）則認爲波譜斜率是－3。最近本文著者曾利用風洞水槽中之風浪，研究水深變化時波譜斜率的變化，發現波譜斜率係一漸變值，隨著水深、風速之變化而做連續性的改變。故淺水波之波譜似乎不像深水波一樣有明確的標準形態存在。

另依據Huang（1981年）之研究，認爲淺水波譜之高頻部份的能量是由主頻成份經非線形相互作用傳遞而來。因此提出了如下的Wallop型波譜。

$$\phi(f)=\frac{\beta g^2}{f^m f_m^{5-m}}\exp\left[-\frac{m}{4}\left(\frac{f}{f_m}\right)^{-4}\right] \quad \cdots\cdots\cdots(17)$$

式中β及m是爲以指示波定義的波浪尖銳度的函數。Wallop型波譜的優點是：①利用波高、周期卽可簡單得到所要的波譜。②波譜斜率可直接表示能量集中部份之波譜形狀。③波譜斜率並無固定的值存在，較符合實際現況。但缺點是：①使用規則波理論，不合波譜存在之本意。②對此型波譜之適用性未做明確的討論和合理的說明。著者曾以不規則波理論修改其模式並對適用性加以討論，求出計算⑽式中之m值（令n＝4）的公式如下：

$$m=-17.48-6.64\log\delta+163\tilde{h}-628\tilde{h}^2+1110\tilde{h}^3-741\tilde{h}^4 \quad \cdots(18)$$

式中之$\tilde{h}$及δ爲依指示波定義的相對水深及波浪尖銳度。圖㈤中所示之m＝9.5，卽爲以上式計算所得的波譜。但上式祇能適用於中度淺水，對於極淺水深之波譜模式仍有待繼續進一步的研究。

五、結　論

以上簡單對一般海洋波浪的波譜形態做一概要的敍述。前人利用廣泛的實

測數據，經分析、整理，提出各種類型的波譜模式供後人參考使用。對於無法以實際觀測數據做爲根據的工程設計而言，因此可得到很大的方便。有關波譜在工程設計上之應用，本文並未敍及。但値得注意的是波譜之應用，由於強烈非線性的存在，淺水波浪波譜之功用受到很大的限制，目前大部份仍以傳統的統計方法結果做爲設計的根據。

第三屆基礎港灣數值（數學）模式研習會論文集　　Jan. 17～18 , 1990 Page 125～172

近岸流力學

MECHANICS OF NEARSHORE CURRENTS

林銘崇

台灣大學造船工程系教授

1. INTRODUCTION

Fig.1-1 ～ 1-4

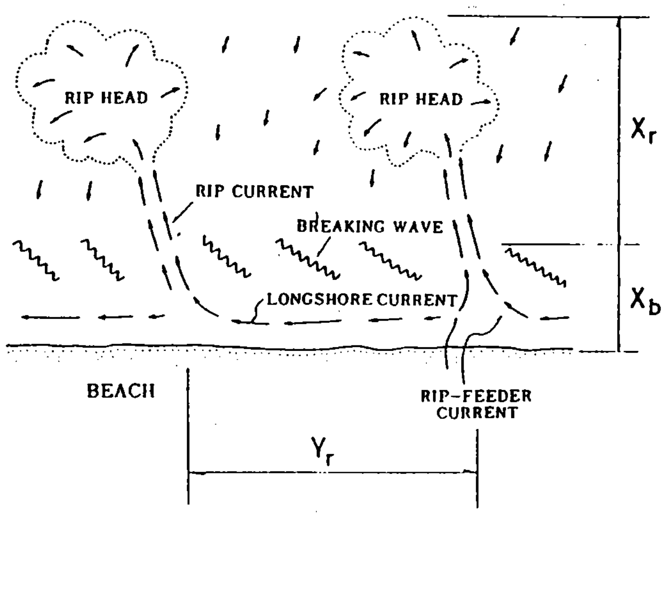

圖 1-1　海浜循環流系（Shepard . Inman, 1950 ）

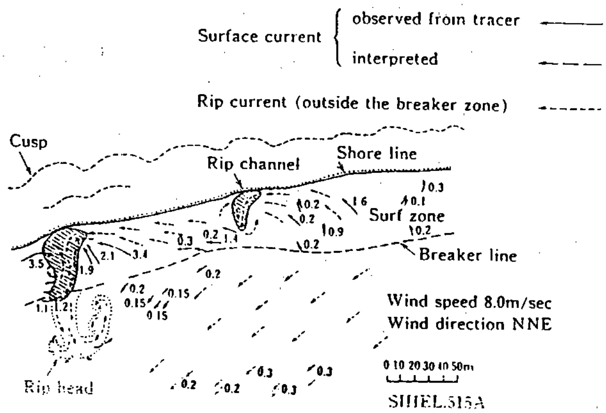

Fgoire 1.2 Nearshore currenl Pattern on the Shouan const. Kanafawa Prefecture. Japan(Horikawa and Sasaki,1972).

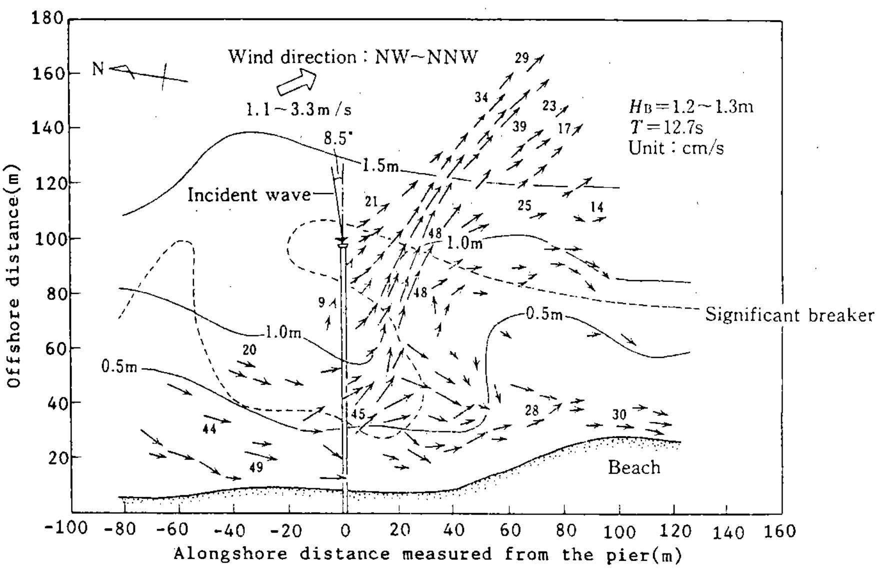

Figure 1.3 Measured nearshore current velocity field(rip current)(Sasali and Horikawa,1975).

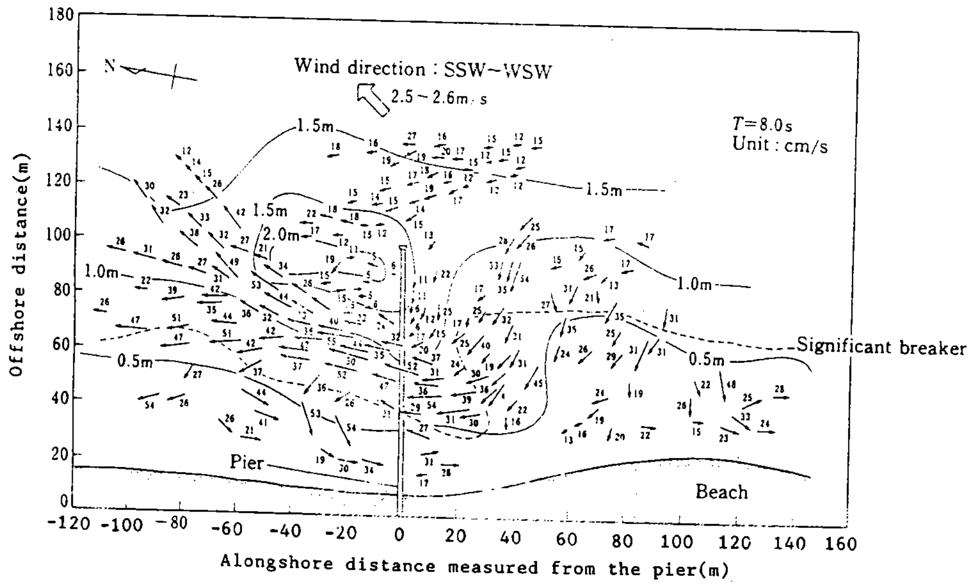

Figure 1.4 Measured nearshore current velocity field.(meandering currents)(Sasaki and Horikawa,1975).

2. GOVERNING EQUATIONS FOR NEARSHORE CURRENTS

包括摩擦項R_α時，動量守恒方程式則爲

$$\frac{\partial \widetilde{M}_\alpha}{\partial t} + \frac{\partial}{\partial x_\beta}\{ \widetilde{U}_\alpha \widetilde{M}_\beta + S_{\alpha\beta} \} = T_\alpha + R_\alpha \quad , \alpha , \beta = 1 , 2$$

$S_{\alpha\beta}$: Radiation stress components

$$R_\alpha = \overline{\int_{-h}^{\eta} \frac{\partial \tau_{\beta\alpha}}{\partial x_\beta} dz} + \overline{\tau}_{\eta\alpha} - \overline{\tau}_{h\alpha}$$

$\tau_{\beta\alpha}$ = stress (components) including the wave-current interaction

$\overline{\tau}_{\eta\alpha}$ = mear stress at the free surface

$\overline{\tau}_{h\alpha}$ = mear stress at the sea bottom

$$T_\alpha = -\rho g\,(h+\overline{\eta})\,\frac{\partial \overline{\eta}}{\partial x_\alpha}$$

現在假設運動呈穩定狀態（令 $D = h+\overline{\eta}$）

連續式 $$\cancel{\frac{\partial(\rho D)}{\partial t}} + \frac{\partial \widetilde{M}_\alpha}{\partial x_\alpha} = 0$$

動量式 $$\cancel{\frac{\partial \widetilde{M}_\alpha}{\partial t}} + \underbrace{\frac{\partial}{\partial x_\beta}(\widetilde{U}_\alpha \widetilde{M}_\beta)}_{\widetilde{U}_\alpha \cancel{\frac{\partial \widetilde{M}_\beta}{\partial x_\beta}} + \widetilde{M}_\beta \frac{\partial \widetilde{U}_\alpha}{\partial x_\beta}} + \frac{\partial S_{\alpha\beta}}{\partial x_\beta} = T_\alpha + R_\alpha$$

令 $\widetilde{U}_\alpha = u_\alpha$（周期水深平均後之量）， $u_\alpha = (u\,,\,v)$
$\widetilde{M}_\alpha = \rho D u_\alpha$

則 $$\begin{cases} \dfrac{\partial}{\partial x_\alpha}(\rho D u_\alpha) = 0 \\[2ex] \rho D u_\beta \dfrac{\partial u_\alpha}{\partial x_\beta} + \dfrac{\partial S_{\alpha\beta}}{\partial x_\beta} = T_\alpha + R_\alpha \end{cases}$$

i.e.

$$\begin{cases} \dfrac{\partial}{\partial x}(Du) + \dfrac{\partial}{\partial y}(Dv) = 0 \\[2ex] u\dfrac{\partial u}{\partial x} + v\dfrac{\partial u}{\partial y} = \underbrace{\dfrac{1}{\rho D}T_x}_{-g\,\partial\eta/\partial x} + \dfrac{1}{\rho D}R_x - \dfrac{1}{\rho D}\left(\dfrac{\partial S_{xx}}{\partial x} + \dfrac{\partial S_{xy}}{\partial y}\right) \end{cases}$$

$$u\frac{\partial v}{\partial x}+v\frac{\partial v}{\partial y}=\underbrace{\frac{1}{\rho D}T_y}_{-g\partial\eta/\partial y}+\frac{1}{\rho D}R_y-\frac{1}{\rho D}\left(\frac{\partial S_{xy}}{\partial x}+\frac{\partial S_{yy}}{\partial y}\right)$$

Introduce transport stream function ψ :

$$uD=-\frac{\partial\psi}{\partial y}$$

$$vD=\frac{\partial\psi}{\partial x}$$

且令 $$\xi=\frac{\partial v}{\partial x}-\frac{\partial u}{\partial y}$$

$$=\frac{1}{D}\left(\frac{\partial^2\psi}{\partial x^2}+\frac{\partial^2\psi}{\partial y^2}\right)-\frac{1}{D^2}\left(\frac{\partial\psi}{\partial y}\frac{\partial D}{\partial y}+\frac{\partial\psi}{\partial x}\frac{\partial D}{\partial x}\right)$$

則 $$\underbrace{\frac{\partial\psi}{\partial y}\frac{\partial}{\partial x}\left(\frac{\xi}{D}\right)-\frac{\partial\psi}{\partial x}\frac{\partial}{\partial y}\left(\frac{\xi}{D}\right)}_{\text{nonlinear term}}=\underbrace{\frac{\partial}{\partial y}\left(\frac{R_x}{\rho D}\right)-\frac{\partial}{\partial x}\left(\frac{R_y}{\rho D}\right)}_{\text{frictional term}}$$

$$\underbrace{-\frac{\partial}{\partial y}\left\{\frac{1}{\rho D}\left(\frac{\partial S_{xx}}{\partial x}+\frac{\partial S_{xy}}{\partial y}\right)\right\}+\frac{\partial}{\partial x}\left\{\frac{1}{\rho D}\left(\frac{\partial S_{xy}}{\partial x}+\frac{\partial S_{yy}}{\partial y}\right)\right\}}_{\text{forcing term}}$$

3. RADIATION STRESS

$$S_{ij}=E\frac{C_g}{c}\frac{k_ik_j}{k}+E\left(\frac{c_g}{c}-\frac{1}{2}\right)\delta_{ij}\ ,\quad i\,j=1\ ,\ 2$$

$k_1 = k\cos\theta$, $k_2 = k\sin\theta$

θ = angle of wave incidence measured comterclockwise from x-axis

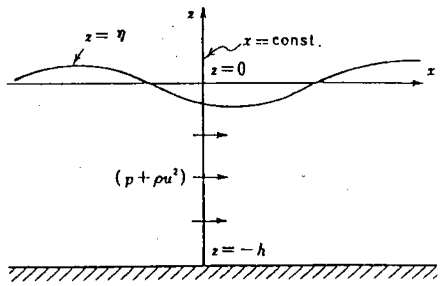

Figure 3.1 Definition sketch for instaneous momentum flux across a vertical plane(Longuet-Higgins and Stewart,1964).

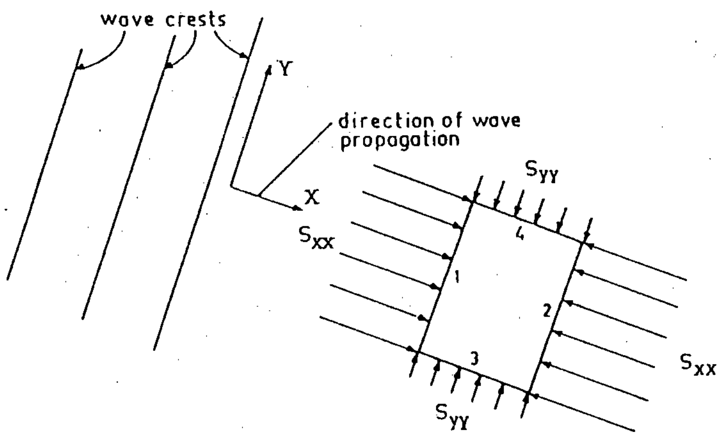

Figure 3-2 PLAN SHOWING PRINCIPAL STRESSES

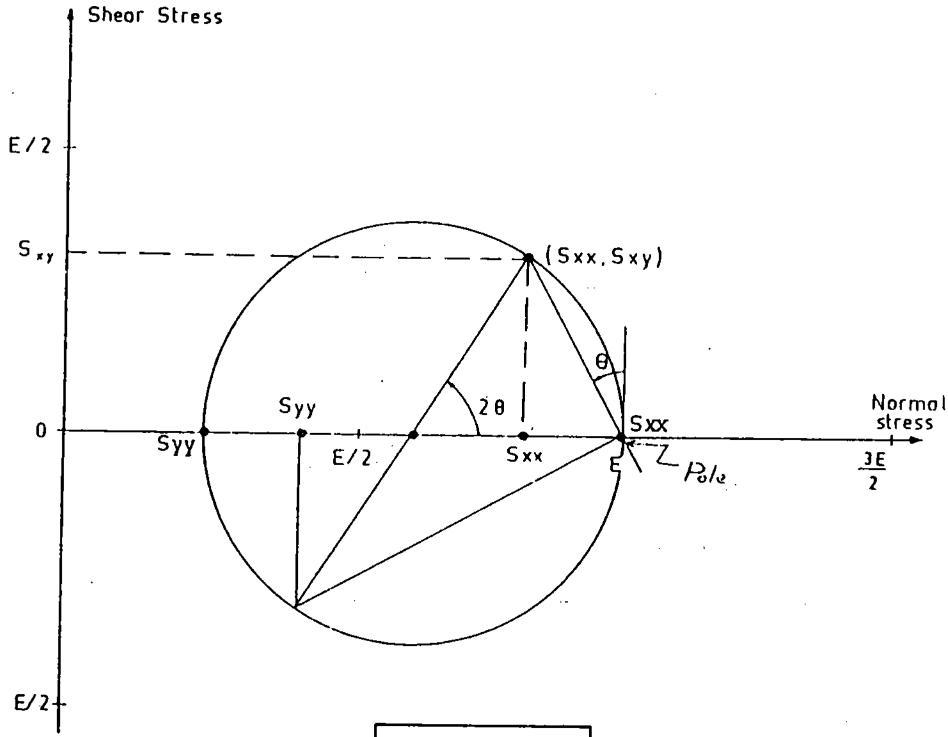

a. MOHR'S CIRCLE

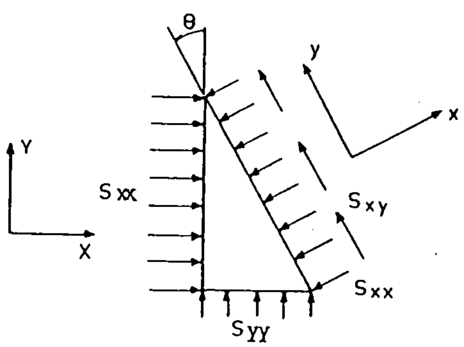

b. STRESS ELEMENT

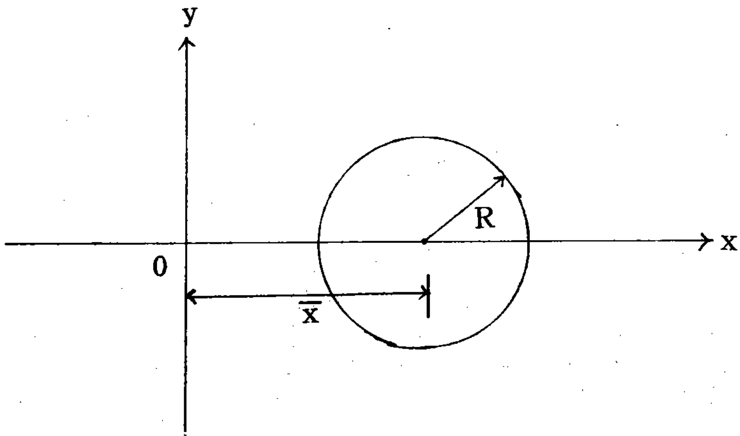

Figure 3-3 MOHR'S CIRCLE ANALYSIS

$$(x+\overline{x})^2+y^2=R^2$$

$$\overline{x}=\frac{1}{2}(S_{XX}+S_{YY})$$

$$R=\left[\left(\frac{S_{XX}-S_{YY}}{2}\right)^2+\underbrace{S_{XY}^2}_{\substack{\| \\ 0\ ,\ \mathrm{mow}}}\right]^{1/2}$$

4. *WAVE SET-DOWN AND SET-UP*

x-momentum eqn. ($D = h + \overline{\eta}$)

$$\frac{\partial \widetilde{M}_x}{\partial t}+\frac{\partial}{\partial x}(\widetilde{U}_x\widetilde{M}_x+S_{xx})+\frac{\partial}{\partial y}(\widetilde{U}_x\widetilde{M}_y+S_{xy})=-\rho g D\frac{\partial\overline{\eta}}{\partial x}$$

若 steady，$\frac{\partial}{\partial y} \equiv 0$，$\widetilde{U}_x = 0$，則

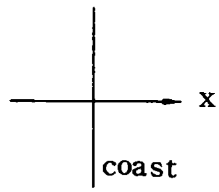

$$\frac{\partial S_{xx}}{\partial x} = -\rho g D \frac{\partial \overline{\eta}}{\partial x} \underset{\substack{\uparrow \\ \overline{\eta} \ll h}}{\approx} -\rho g h \frac{\partial \overline{\eta}}{\partial x} \quad \cdots\cdots(1)$$

又 $S_{xx} = E\left(\frac{2c_g}{c} - \frac{1}{2}\right)$，$\frac{c_g}{c} = \begin{cases} 1/2 & \text{深海} \\ 1 & \text{淺海} \end{cases}$

$\frac{\partial S_{xx}}{\partial x} > 0$ （∵ S_{xx} 隨水深之減少而增加）

$\therefore \quad \frac{\partial \overline{\eta}}{\partial x} < 0 \Rightarrow$ wave set-down

但 $$S_{xx} = E\left(\frac{2c_g}{c} - \frac{1}{2}\right) = \underbrace{Ec_g}_{F\text{ (energy flux)}}\left(\frac{2}{c} - \frac{1}{2c_g}\right)$$

$$= F\left\{\frac{2k}{\sigma} - \frac{1}{2}\,\frac{1}{(\partial \sigma / \partial k)}\right\}$$

$$= F\sigma\left\{\frac{2k}{\sigma^2} - \frac{1}{(\partial \sigma^2 / \partial k)}\right\}$$

$$= F\sigma\left\{\frac{2k}{\sigma^2} - \left(\frac{\partial k}{\partial \sigma^2}\right)\right\}$$

令 $\xi = kh$，$\zeta = k_0 h = \frac{\sigma^2 h}{g}$ $\qquad$ k_0：深海波波數

$$\therefore \quad \frac{\partial k}{\partial \sigma^2} = \frac{\partial(\xi / h)}{\partial(g\zeta / h)} = \frac{1}{g}\frac{d\xi}{d\zeta} \quad \cdots\cdots(2)$$

ξ、ζ：x 之函數

$$\therefore \quad S_{xx} = F\sigma\left(\frac{2\,\xi/h}{\zeta\, g/h} - \frac{1}{g}\frac{d\xi}{d\zeta}\right) = \frac{F\sigma}{g}\left(\frac{2\xi}{\zeta} - \frac{d\xi}{d\zeta}\right)$$

$$\therefore \quad \text{式(1)} \Rightarrow \quad d\overline{\eta} = -\frac{1}{\rho g h}\, d S_{xx} = \frac{F\sigma}{\rho g^2 h}\, d\left(\frac{d\xi}{d\zeta} - \frac{2\xi}{\zeta}\right)$$

$$= \frac{F\sigma^3}{\rho g^3} \cdot \underbrace{\underbrace{\frac{1}{\sigma^2 h/g}}_{\frac{1}{\zeta}} d\left(\frac{d\xi}{d\zeta} - \frac{2\xi}{\zeta}\right)}_{d\left\{\frac{d}{d\zeta}\left(\frac{\xi}{\zeta}\right)\right\}}$$

假設無任何能量損失，F ＝一定

$$\therefore \quad \overline{\eta} = \frac{F\sigma^3}{\rho g^3}\frac{d}{d\zeta}\left(\frac{\xi}{\zeta}\right) + \text{const}$$

（∵深海處，$\eta = 0$，$\xi \to \zeta$，$\frac{d}{d\zeta}(\xi/\zeta) = 0$ ）

又∵ $\sigma^2 = gk \tanh kh \rightarrow \frac{\sigma^2 h}{g} = kh \tanh kh$

i.e. $\zeta = \xi \tanh \xi$

$\therefore \quad \frac{\xi}{\zeta} = \coth \xi$，〔$\rightarrow 1$，當 $\xi \gg 1$ 時（深海）〕

$$\therefore \quad \overline{\eta} = \frac{F\sigma^3}{\rho g^3}\frac{d}{d\zeta}(\coth \xi) \qquad \cdots\cdots\cdots\cdots(3)$$

假設無碎波或海底摩擦等引起之能量損失

$$F = E_o c_{go} = E c_g = E\left(\frac{\partial \sigma}{\partial k}\right) = \frac{E}{2\sigma}\left(\frac{\partial \sigma^2}{\partial k}\right) \underset{\uparrow}{=} \frac{Eg}{2\sigma}\frac{d\zeta}{d\xi}$$

(2)

$$\therefore \quad 式(3) \Rightarrow \overline{\eta} = \frac{\sigma^2 E}{2\rho g^2}\frac{d}{d\xi}(\coth\xi)$$

$$\underset{\uparrow}{=} \frac{1}{4} a^2 k \tanh\xi \cdot \left(-\frac{1}{\sinh^2\xi}\right)$$

$$\sigma^2 = gk\tanh\xi$$

&

$$E = \frac{1}{2}\rho g a^2$$

$$= -\frac{1}{4} a^2 k \frac{1}{\sinh\xi\cosh\xi}$$

故 $\overline{\eta} = -\frac{1}{2}\frac{a^2 k}{\sinh 2\xi}$

or $\overline{\eta} = -\frac{1}{8}\frac{\eta^2 k}{\sinh 2kh}$ (wave set-down) ...... (5)

至于碎波帶內，

$\because \quad c_g = c \qquad \therefore \quad S_{xx} = \frac{3}{2}E$

設 $H = \gamma(h + \overline{\eta})$

則 $S_{xx} = \frac{3}{16}\rho g \gamma^2 (h + \overline{\eta})^2$

$$\therefore \quad 式(1) \Rightarrow \frac{d\overline{\eta}}{dx} = -\frac{1}{\rho g(h+\eta)}\frac{d}{dx}\left\{\frac{3}{16}\rho g \gamma^2 (h+\overline{\eta})^2\right\}$$

$$= -\frac{\frac{3}{16}\gamma^2 \cdot 2(h+\overline{\eta})}{(h+\overline{\eta})} = \frac{d}{dx}(h+\overline{\eta})$$

$$= -\frac{3}{8}\gamma^2 \left(\frac{dh}{dx} + \frac{d\overline{\eta}}{dx}\right)$$

$$\therefore \quad \left(1 + \frac{8}{3\gamma^2}\right)\frac{d\overline{\eta}}{dx} = -\frac{dh}{dx}$$

$$令 \quad K = \left(1 + \frac{8}{3\gamma^2}\right)^{-1}$$

$$\frac{d\eta}{dx} = -K\frac{dh}{dx}$$

$$\therefore \quad \overline{\eta} = K\,(h_b - h) + \overline{\eta}_b \qquad (\text{wave set-up}) \qquad \cdots\cdots (6)$$

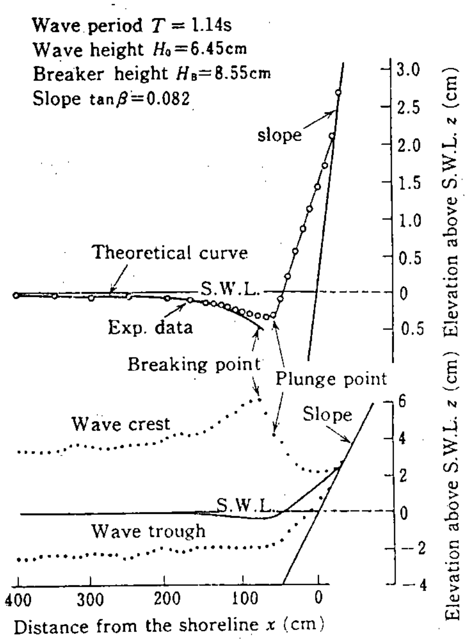

Figure 4.1 Experimental results on wave setup and setdown(Bowen,Inman,and Simons,1968).

5. GENERAL CONSIDERATION OF (NEARSHORE) CIRCULATION CELL FORMULATION

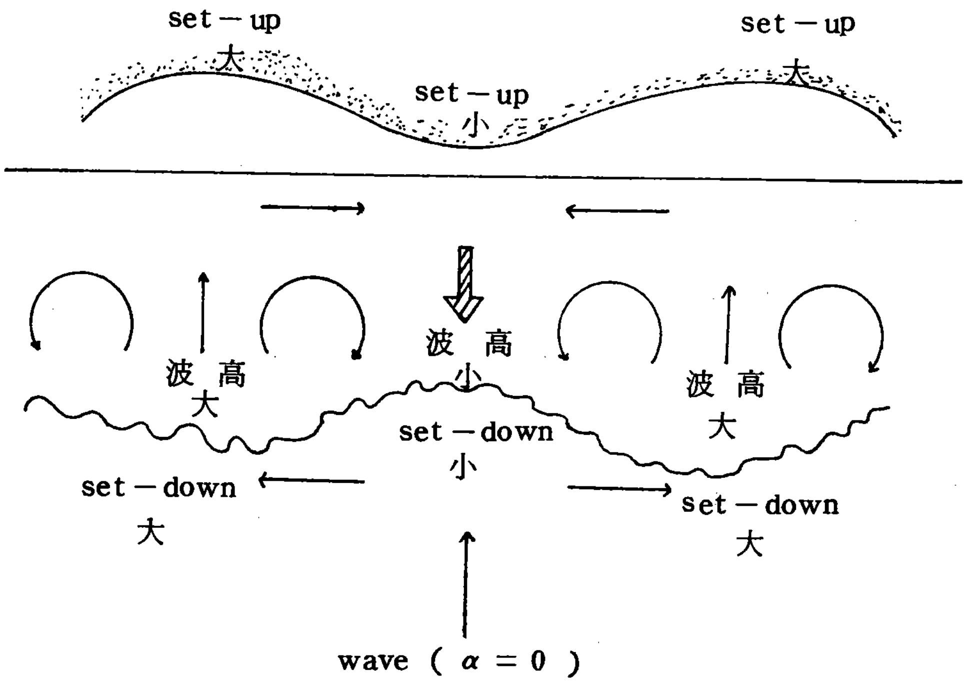

wave set-down $\overline{\eta} = -\frac{1}{8}\frac{H^2 k}{\sinh 2kh}$

H大→ set-down 大

wave set-up $\overline{\eta} = K (h_b - h) + \overline{\eta}_b$

H大→ set-up 大

6. GENERAL REVIEW OF MODELS FOR RIP CURRENT

$$\underbrace{u\frac{\partial u}{\partial x}+v\frac{\partial u}{\partial y}}=-g\frac{\partial \overline{\eta}}{\partial x}+\frac{R_x}{\rho(h+\overline{\eta})}-\frac{1}{\rho(h+\overline{\eta})}\left(\frac{\partial S_{xx}}{\partial x}+\frac{\partial S_{xy}}{\partial y}\right)$$

$$\underbrace{u\frac{\partial v}{\partial x}+v\frac{\partial v}{\partial y}}=-g\frac{\partial \overline{\eta}}{\partial y}+\frac{R_y}{\rho(h+\overline{\eta})}-\frac{1}{\rho(h+\overline{\eta})}\left(\frac{\partial S_{xy}}{\partial x}+\frac{\partial S_{yy}}{\partial y}\right)$$

non-linear term
(usually neglected)

let $R_x, R_y \to fu, fv$, f : friction factor

momentum egn.

$$\left.\begin{aligned}\frac{\partial S_{xx}}{\partial x}+\frac{\partial S_{xy}}{\partial y}+\rho g(h+\eta)\frac{\partial \overline{\eta}}{\partial x}+fu=0\\ \frac{\partial S_{xy}}{\partial x}+\frac{\partial S_{yy}}{\partial y}+\rho g(h+\eta)\frac{\partial \overline{\eta}}{\partial y}+fv=0\end{aligned}\right\}\qquad(1)$$

Continuity egn.

$$\frac{\partial}{\partial x}[u(h+\eta)]+\frac{\partial}{\partial y}[v(h+\overline{\eta})]=0\qquad(2)$$

式(1), (2) : unknown —— S, η, u, v, 4 個

但方程式只有 3 個

1. free type rip current system —— to add one more egn.

   Hino (1974) etc : $H=\gamma(h+\overline{\eta})$

   or

   LeBlond.Tang (1974) etc : energy egn.

$$\frac{\partial}{\partial x}[E(u-c_g)]+\frac{\partial}{\partial y}[Ev]+S_{xx}\frac{\partial u}{\partial x}+S_{yy}\frac{\partial v}{\partial y}=\underbrace{-f_D}_{\text{dissipation}}$$

⇒ eigen value problem

2. forced type rip current system

— give a wave height distribution (or a radiation stress distribution) by something come from the outside of the equation system.

The forced type

edge-waves (or infra-gravity wave)	Bowen (1967 or 1969) Harris (1967) Bowan • Inman (1969) Sasaki (1974 or 1975)
cross waves	Dalrymple (1975) Marayama • Horikawa (1977)
(bottom) topography	Bowen (1969) Sonu(1972) Noda (1974) Sasaki (1975) , Mei 、Liu(1977) Lin 、Liou (1986) , Lin 、Hwang(1988)

wave diffraction (→ cross wave) — Liu. Mei (1974 or 1975)

<u>The free type</u>

hydrodynamic instability
- Hino (1974)
- Miller - Barcilon (1978)

eigenvalue problem
- LeBlond・Tang (1974)
- Iwata (1976)
- Mizuguchi (1976)
- Dalrymple・Lazano (1978)

7. LONGSHORE CURRENTS

7-1 Basin equations

mass
$$\frac{\partial}{\partial t}\left[\cancel{\rho\,(h+\overline{\eta})}\right]+\frac{\partial}{\partial x_\alpha}(\widetilde{M}_\alpha)=0$$

momentum
$$\frac{\partial}{\partial t}(\cancel{\widetilde{M}_\alpha})+\frac{\partial}{\partial x_\beta}(\widetilde{U}_\alpha\widetilde{M}_\beta+S_{\alpha\beta})=T_\alpha+R_\alpha$$

$$T_\alpha=-\rho g(h+\overline{\eta})\frac{\partial\overline{\eta}}{\partial x_\alpha},\quad R_\alpha=\text{frictional term}$$

Steady

$$\frac{\partial}{\partial y}=0\ ,$$

x — offshore direction

y — alongshore direction

$$\frac{\partial \widetilde{M}_x}{\partial x} + \cancel{\frac{\partial \widetilde{M}_y}{\partial y}} = 0$$

$$\widetilde{M}_x = \text{const.} = 0$$

而 momentum eqn. 則爲

$$x — ,\quad \frac{\partial}{\partial x}\left(\cancel{\widetilde{U}_x \widetilde{M}_x} + S_{xx} \right) + \cancel{\frac{\partial}{\partial y}\left(\widetilde{U}_x \widetilde{M}_y + S_{xy} \right)} = T_x + R_x \quad \cdots\cdots(1)$$

$$y — ,\quad \frac{\partial}{\partial x}\left(\cancel{\widetilde{U}_y \widetilde{M}_x} + S_{xy} \right) + \cancel{\frac{\partial}{\partial y}\left(\widetilde{U}_y \widetilde{M}_y + S_{yy} \right)} = \cancel{T_y} + R_y \quad \cdots\cdots(2)$$

$$(1) \Rightarrow \quad \frac{\partial S_{xx}}{\partial x} = T_x + R_x$$

$$(2) \Rightarrow \quad \boxed{\frac{\partial S_{xy}}{\partial x} = R_y} \qquad \cdots\cdots(3)$$

$$(\text{ driving force }) + \underbrace{(\text{ frictional force })}_{} = 0 \qquad (\text{ steady state })$$

$$\left\{ \begin{array}{l} \text{bottom friction} \\ \text{lateral friction (diffusion)} \end{array} \right.$$

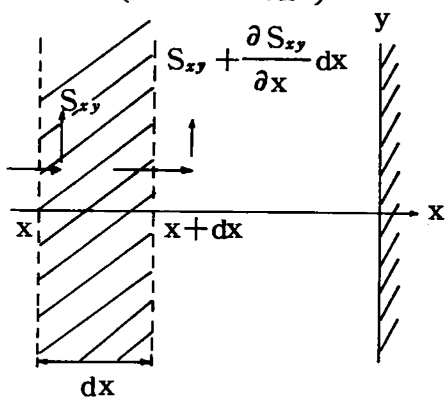

另外，Bakker (1971)
Komar (1975)
$\Big\}$: steady ,

$$\tilde{u} = (0, v(x)), \quad \frac{\partial}{\partial y} \neq 0$$

$$\left(\text{i.e. } \frac{\partial}{\partial y} \left(\begin{matrix} \text{wave} \\ \text{height} \end{matrix} \right) \neq 0 \right)$$

則　式(2)⇒

$$\frac{\partial S_{xy}}{\partial x} + \frac{\partial S_{yy}}{\partial y} = T_y + R_y$$

or

$$\underbrace{\frac{\partial S_{xy}}{\partial x} + \frac{\partial S_{yy}}{\partial y} - T_y}_{\text{driving force}} = R_y \qquad \cdots\cdots(4)$$

$$T_y = -\rho \underbrace{(h+\bar{\eta})}_{D} \frac{\partial \bar{\eta}}{\partial y}$$

7－2　The Longuet-Higgins model

$$\frac{d S_{xy}}{d x} = R_y$$

$$= \frac{d T_{xy}}{d x} - \tau_y$$

$$\frac{d S_{xy}}{d x} = \frac{\sin\theta}{c} \frac{d}{d x} \left(E c_g \cos\theta \right)$$

$$= \frac{5}{16} \rho g^{\frac{3}{2}} \gamma^2 (h+\overline{\eta})^{\frac{3}{2}} \tan\beta' \frac{\sin\theta_b}{\sqrt{(h+\overline{\eta})_b}}$$

$$\tan\beta' = \frac{d}{dx}(h+\overline{\eta})$$

$$\frac{d}{dx}(T_{xy}) = \frac{d}{dx}\{ N p g^{\frac{1}{2}} x (h+\eta)^{\frac{3}{2}} \frac{dv}{dx} \}$$

$$\tau_y = \frac{1}{\pi} \rho c_f \gamma \sqrt{g(h+\overline{\eta})}\, v$$

$$\Rightarrow N\rho g^{\frac{1}{2}} (\tan\beta')^{\frac{3}{2}} \frac{d}{dx}(x^{\frac{5}{2}} \frac{dv}{dx}) - \frac{1}{\pi}\rho c_f \gamma g^{\frac{1}{2}} (\tan\beta')^{\frac{1}{2}} x^{\frac{1}{2}} v$$

$$\begin{cases} = -\frac{5}{16} \rho g^{\frac{3}{2}} \gamma^2 (\tan\beta')^{\frac{5}{2}} \frac{\sin\theta_b}{\sqrt{(h+\overline{\eta})_b}} x^{\frac{3}{2}} \quad , \quad 0 < x < x_b \\ = 0 \ , \ x_b < x < \infty \end{cases}$$

Neglecting lateral diffusion

$$v = \begin{cases} \frac{5\pi}{16} \frac{\gamma}{c_f} g \tan\beta' \frac{\sin\theta_b}{\sqrt{g(h+\overline{\eta})_b}} (h+\overline{\eta}) \quad , \quad 0 < x < x_b \\ 0 \qquad\qquad x_b < x < \infty \end{cases}$$

at $x = x_b$, $v = v_b$

$$v_b = \frac{5\pi}{16} \frac{\gamma}{c_f} \sqrt{g(h+\overline{\eta})_b} \tan\beta' \sin\theta_b$$

$$V = \frac{v}{v_b} \qquad X = \frac{x}{x_b} \qquad \Rightarrow$$

$$P \frac{d}{dX}(X^{\frac{5}{2}} \frac{dV}{dX}) - X^{\frac{1}{2}} V = \begin{cases} -X^{\frac{3}{2}} & , \quad 0 < X < 1 \\ 0 & \quad\ \ 1 < X < \infty \end{cases}$$

in which $\quad P = \dfrac{\pi N \tan \beta'}{\gamma c_f}$

(i) $P \neq 2/5$

$$V = \begin{cases} \beta_1 X^{p1} + AX & 0 < X < 1 \\ \beta_2 X^{p2} & , \quad 1 < X < \infty \end{cases}$$

$$p_1 = -\frac{3}{4} + \left(\frac{9}{16} + \frac{1}{P}\right)^{\frac{1}{2}}$$

$$p_2 = -\frac{3}{4} - \left(\frac{9}{16} + \frac{1}{P}\right)^{\frac{1}{2}} \quad ,$$

$$A = \left(1 - \frac{5}{2} P\right)^{-1} \quad ,$$

$$B_1 = \{ P(1 - p_1)(p_1 - p_2) \}^{-1}$$

$$B_2 = \{ P(1 - p_1)(p_1 - p_2) \}^{-1}$$

(ii) $P = 2/5$

$$V = \begin{cases} \dfrac{10}{49} X - \dfrac{5}{7} X \log X & 0 < X < 1 \\ & , \\ \dfrac{10}{49} X^{-\frac{5}{2}} & 1 < X < \infty \end{cases}$$

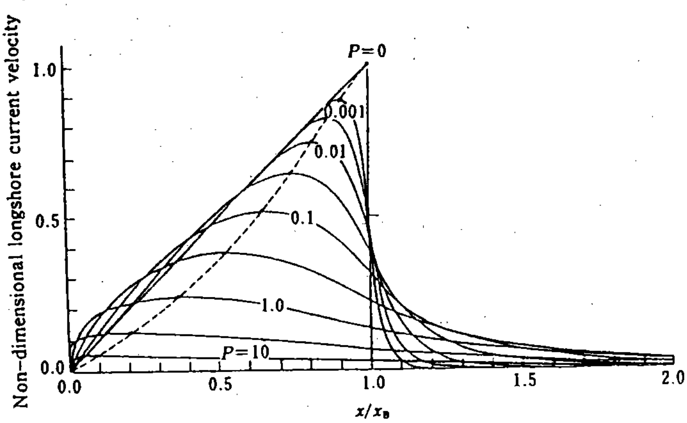

Fogire 7.1 Calculatee distributions of the longshore current velocity(Longuet-Higgins,1970).

7 − 3 *The Kraus、Sasaki model*

Kraus, N. C. and T. O. Sasaki (1979) : " Influence of wave angle and lateral mixing on the longshore current " , Marine Science Communication, Vol.5, No.2, pp.91 ~ 126.

$$(\text{driving force}) + \underbrace{(\text{lateral friction}) - (\text{bottom friction})}_{R_y} = 0 \quad (1)$$

i.e. $\partial S_{xy}/\partial x = R_y$

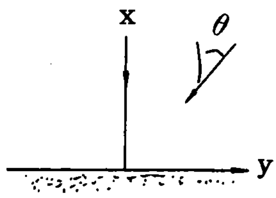

driving force (D_y)

$$D_y = -\frac{\partial S_{xy}}{\partial x}$$

$$= -\frac{\partial}{\partial x}\{ E c_g \cos\theta \underbrace{\frac{\sin\theta}{c}}_{\substack{\parallel \\ \text{const.(Snell's law)}}} \}$$

$$= -\frac{\partial (E c_g \cos\theta)}{\partial x}\left(\frac{\sin\theta}{c}\right)$$

$$H = \gamma h \ , \ E = \frac{1}{8}\rho g H^2 = \frac{\gamma^2}{8}\rho g h^2$$

Snell's law $\dfrac{\sin\theta}{c} = \dfrac{\sin\theta_b}{c_b}$

$$\therefore \quad \sin\theta = \frac{c \sin\theta_b}{c_b} \underset{\substack{\uparrow \\ c = \sqrt{gh}}}{=} \frac{h^{\frac{1}{2}} \sin\theta_b}{h_b^{\frac{1}{2}}} = \sin\theta_b \left(\frac{h}{h_b}\right)^{\frac{1}{2}}$$

$$\therefore \quad \sin^2\theta = \sin^2\theta_b \left(\frac{h}{h_b}\right) \qquad \cdots\cdots (2)$$

$$\frac{\partial(E\, c_g \cos\theta)}{\partial x} \underset{\substack{\uparrow \\ 長波\ c_g = c = \sqrt{gh}}}{=} \frac{\partial}{\partial x}\left\{\frac{1}{8}\gamma^2 \rho\, g^{\frac{3}{2}} h^{\frac{5}{2}} \cos\theta\right\}$$

$$= \frac{1}{8}\gamma^2\rho\, g^{\frac{3}{2}}\left\{ \cos\theta \cdot \frac{5}{2}\, h^{\frac{3}{2}} \underbrace{\frac{\partial h}{\partial x}}_{\underbrace{-\tan\beta^*,}_{\tan\beta/(1+\frac{3\gamma^2}{8}),}} + h^{\frac{5}{2}} \underbrace{\frac{\partial(\cos\theta)}{\partial x}}_{\frac{\partial[(1-\sin^2\theta)^{\frac{1}{2}}]}{\partial x}} \right\}$$

$$= \frac{1}{8}\gamma^2\rho\, g^{\frac{3}{2}}\left\{-\frac{5}{2}h^{\frac{3}{2}}(1-\sin^2\theta)^{\frac{1}{2}}\tan\beta^* - h^{\frac{5}{2}}\frac{1}{2(1-\sin^2\theta)^{\frac{1}{2}}}\frac{\partial(\sin^2\theta)}{\partial x}\right\}$$

$$= \frac{5}{16}\gamma^2\rho\, g^{\frac{3}{2}} h^{\frac{3}{2}}\left\{-\tan\beta^*(1-\sin^2\theta)^{\frac{1}{2}} - \frac{h}{5}(1-\sin^2\theta)^{-\frac{1}{2}} \underbrace{\frac{\partial(\sin^2\theta)}{\partial x}}_{\underbrace{\frac{\partial}{\partial x}\left[\sin^2\theta_b\left(\frac{h}{h_b}\right)\right]}_{\frac{\sin^2\theta_b}{h_b}\frac{\partial h}{\partial x} = -\frac{\sin^2\theta_b}{h_b}\tan\beta^*}}\right\}$$

$$= -\frac{5}{16}\gamma^2\rho\, g^{\frac{3}{2}} h^{\frac{3}{2}}\tan\beta^*\left\{\left(1-\sin^2\theta_b\frac{h}{h_b}\right)^{\frac{1}{2}} - \frac{\sin^2\theta_b}{5}\frac{h}{h_b}\left(1-\sin^2\theta_b\frac{h}{h_b}\right)^{-\frac{1}{2}}\right\}$$

又 $\dfrac{\sin\theta}{c} = \sin\theta_b \left(\dfrac{h}{h_b}\right)^{\frac{1}{2}} (gh)^{-\frac{1}{2}} = \sin\theta_b\, g^{-\frac{1}{2}} h_b^{-\frac{1}{2}}$

故

$$D_y = \begin{cases} \dfrac{5}{16}\rho g \gamma^2 \tan\beta^* \sin\theta_b \left(\dfrac{h^3}{h_b}\right)^{\frac{1}{2}} \left\{ \left(1-\sin^2\theta_b \dfrac{h}{h_b}\right)^{\frac{1}{2}} \right. \\ \qquad \left. - \dfrac{\sin^2\theta_b}{5}\dfrac{h}{h_b}\left(1-\sin^2\theta_b \dfrac{h}{h_b}\right)^{-\frac{1}{2}} \right\}，\text{碎波帶內} \\ 0 \ ，\text{碎波帶外} \end{cases} \qquad \cdots\cdots(3)$$

• lateral stress (τ_L)

$$\tau_L = \frac{\partial}{\partial x}\left(\rho\, \varepsilon_L h \frac{\partial v}{\partial x}\right)$$

Madsen et al.(1978)： ……(4)

$$\varepsilon_L = \Gamma x u_{max} = \frac{\Gamma}{2} x \sqrt{gh} \begin{cases} \gamma & \text{碎波帶內} \\ H/h & \text{碎波帶外} \end{cases}$$

由長波理論：$H = \left(\dfrac{\cos\theta}{\cos\theta_b}\right)^{\frac{1}{2}} \left(\dfrac{h_b}{h}\right)^{\frac{1}{4}} H_b \doteqdot \left(\dfrac{h_b}{h}\right)^{\frac{1}{4}} H_b$

(note：Green's law $\dfrac{H_1}{H_0} = \left(\dfrac{h_0}{h_1}\right)^{\frac{1}{4}} \left(\dfrac{b_0}{b_1}\right)^{\frac{1}{2}}$)，折射 $\dfrac{b_0}{b_1} = \dfrac{\cos\theta_1}{\cos\theta_0}$)

• bottom stress ($\langle \tau_b \rangle_y$)

$\tau_b = c_f \rho |u| u$ ， $u = \hat{u} + (0, v)$

$$u_m = \frac{\gamma}{2}\sqrt{gh}$$

$$\langle \tau_b \rangle_y = \frac{2}{\pi} c_f \rho v u_m (1+\sin^2\theta)$$

$$\underset{\underset{(2)}{\uparrow}}{=} \frac{1}{\pi} c_f \rho v \sqrt{gh} \begin{cases} \gamma\left(1+\sin^2\theta_b \dfrac{h}{h_b}\right), & \text{碎波帶內} \\ \dfrac{H}{h}\left(1+\sin^2\theta_b \dfrac{h}{h_b}\right), & \text{碎波帶外} \end{cases}$$

及 u_m 之式 ……(5)

(i.e. 碎波帶外，H/h 不爲常數 γ)

$$\left.\begin{matrix}(3)\\(4)\\(5)\end{matrix}\right\} \xrightarrow[\text{代入}]{} (1) \Rightarrow \text{一般解（近似解）}$$

• General Solution

$$V = \begin{cases} \displaystyle\sum_{n=0}^{\infty} (A_n X + B_n X^p) X^n & 0 < X < 1 \\ \displaystyle\sum_{n=0}^{\infty} C_n X^{q-n} & 1 < X < \infty \end{cases},$$

此處，$V = \dfrac{v}{v_0}$ ， $X = \dfrac{x}{x_b}$

$$v_0 = \frac{5\pi}{16} \gamma \sqrt{g h_b} \frac{\tan\beta^*}{c_f} \sin\theta_b$$

$$A_n = \begin{cases} \dfrac{1}{1-\dfrac{5P}{2}} & n=0 \\ \dfrac{a_n - \sin^2\theta_b A_{n-1}}{1-(n+1)(n+\frac{5}{2})P}, & n=1,2,\cdots\cdots \end{cases}$$

$$a_n = \begin{cases} 1 & n=0 \\ -\dfrac{1}{5}\dfrac{(2n+5)(2n-3)!!}{2^n\, n!}\sin^{2n}\theta_b & n=1,2,\cdots\cdots \end{cases}$$

$$\left(\begin{array}{l} N!! = N(N-2)(N-4)\cdots\cdots \\ N!! = 1 \qquad N\text{為負} \end{array} \right)$$

$$B_n = B_0 \begin{cases} 1 & n=0 \\ \underbrace{\dfrac{\sin^2\theta_b}{(p+n)(p+n+\frac{3}{2})p-1}\beta_{n-1},\ (\beta_0=1)}_{\beta_n} & n=1,2,\cdots \end{cases}$$

$$C_n = C_0 \begin{cases} 1 & n=0 \\ \underbrace{\dfrac{\sin^2\theta_b}{(q-n)(q-n+\frac{1}{4})Q-1}\delta_{n-1},\ (\delta_0=1)}_{\delta_n} & n=1,2,\cdots \end{cases}$$

$$B_0 = (SS_q' - S'S_q)/(S_p'S_q - S_pS_q')$$

$$C_0 = (SS_p' - S'S_p)/(S_p'S_q - S_pS_q')$$

$$S = \sum_{n=0}^{\infty} A_n, \quad S_p = \sum_{n=0}^{\infty} \beta_n, \quad S_q = \sum_{n=0}^{\infty} \delta_n$$

$$S' = \sum_{n=0}^{\infty}(n+1)A_n, \quad S_p' = \sum_{n=0}^{\infty}(p+n)\beta_n$$

$$S_q' = \sum_{n=0}^{\infty}(q-n)\delta_n$$

$$P = \frac{\pi}{2}\Gamma\frac{\tan\beta^*}{c_f} \qquad p = -\frac{3}{4} + \sqrt{\frac{9}{16} + \frac{1}{P}}$$

$$Q = \frac{\pi}{2}\Gamma\frac{\tan\beta}{c_f} \qquad q = -\frac{1}{8} - \sqrt{\frac{1}{64} + \frac{1}{Q}}$$

note ： $\theta \ll 1$ ， lie $\sin^2\theta_b \to 0$ ，則

$$\left.\begin{aligned} B_0 &= A_0\frac{(q-1)}{(p-q)} \\ C_0 &= A_0\frac{(p-1)}{(p-q)} \end{aligned}\right\}$$ 即為 Longuet-Higgins 之結果

8. DYNAMICS OF RIP CURRENTS

8－1 The Arthur model

$$D = h + \overline{\eta} \quad , \quad \xi = \frac{\partial v}{\partial x} - \frac{\partial u}{\partial y}$$

$$\underbrace{\frac{\partial\psi}{\partial y}\frac{\partial}{\partial x}\left(\frac{\xi}{D}\right) - \frac{\partial\psi}{\partial x}\frac{\partial}{\partial y}\left(\frac{\xi}{D}\right)}_{\text{nonlinear term}} = \underbrace{\frac{\partial}{\partial y}\left(\frac{R_x}{\rho D}\right) - \frac{\partial}{\partial x}\left(\frac{R_y}{\rho D}\right)}_{\text{frictional term}}$$

$$\underbrace{-\frac{\partial}{\partial y}\left\{\frac{1}{\rho D}\left(\frac{\partial S_{xx}}{\partial x} + \frac{\partial S_{xy}}{\partial y}\right)\right\} + \frac{\partial}{\partial x}\left\{\frac{1}{\rho D}\left(\frac{\partial S_{xy}}{\partial x} + \frac{\partial S_{yy}}{\partial y}\right)\right\}}_{\text{forcing term}}$$

Arthur, R.S. (1962) : " A note on the dynamics of rip currents" , J. Geophys. Res., Vol. 67 , No.7, pp.2777～2779.

Arthur 假設只有非線性項發生作用，而略去 frictional term & forcing term，則

$$\underbrace{\frac{\partial \psi}{\partial y}}_{-Du}\frac{\partial}{\partial x}\left(\frac{\xi}{D}\right)-\underbrace{\frac{\partial \psi}{\partial x}}_{Dv}\frac{\partial}{\partial y}\left(\frac{\xi}{D}\right)=0 \qquad \cdots\cdots(1)$$

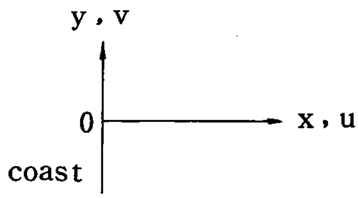

$$\therefore \quad \frac{D}{Dt}\left[\frac{\xi}{h+\bar{\eta}}\right]=0$$

$$\frac{D}{Dt}=u\frac{\partial}{\partial x}+v\frac{\partial}{\partial y} \quad , \quad \therefore \quad \frac{\xi}{h+\bar{\eta}}=F(\psi) \qquad \cdots\cdots(2)$$

$\therefore \quad \left(\frac{\xi}{h+\eta}\right)$ is conserved along a constant transport streamline

$\Rightarrow \xi$ (vertical component of vorticity) 隨水深之增加而增加

$$令 \quad \bar{\eta} \ll h \quad 則 \quad \left.\begin{aligned} u &= -\frac{1}{h}\frac{\partial \psi}{\partial y} \\ v &= \frac{1}{h}\frac{\partial \psi}{\partial x} \end{aligned}\right\} \qquad \cdots\cdots(3)$$

$$(2) \Rightarrow \frac{1}{h}\left[\frac{\partial}{\partial x}\left(\frac{1}{h}\frac{\partial \psi}{\partial x}\right)+\frac{\partial}{\partial y}\left(\frac{1}{h}\frac{\partial \psi}{\partial y}\right)\right]=F(\psi) \qquad \cdots\cdots(4)$$

設沿 x 軸之一界面，水流自淺海流向外海

則則在此界面附近。(圖(a))

$$\left|\frac{\partial v}{\partial x}\right| \ll \left|\frac{\partial u}{\partial y}\right|$$

$$\therefore \quad (4) \Rightarrow \frac{1}{h}\frac{\partial}{\partial y}\left(\frac{1}{h}\frac{\partial \psi}{\partial y}\right)=F(\psi)$$

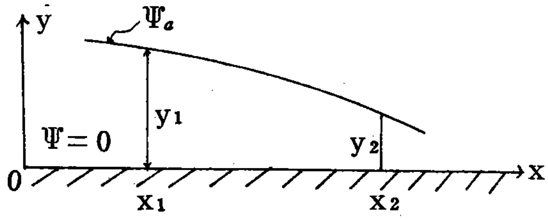

圖 (a)

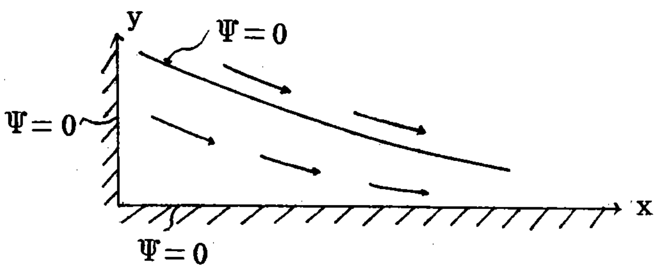

圖 (b)

⇓ mirror image

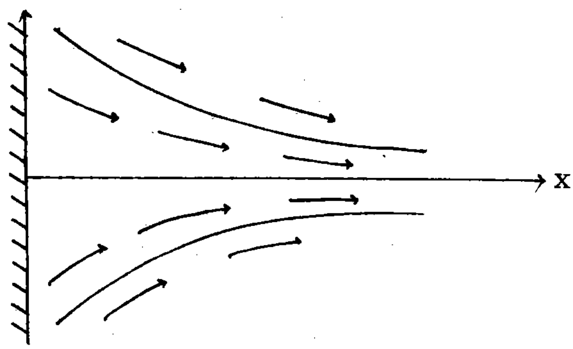

圖 (c)

令 $h\,dy = dy'$ 則得

$$\frac{d^2\psi}{dy'^2} = F(\psi)$$

積分：

$$\frac{d\psi}{dy'} = -u = f_1(\psi)$$

再積分 $y' = f_2(\psi)$

故沿流線 $\psi = \text{const}$ 上，u，y′ 均為一定

$$\text{i.e.}\quad y' = \int dy' = \int h\,dy = \text{const}$$

$$\therefore \int_0^{y_1} h(x_1, y)\,dy = \int_0^{y_2} h(x_2, y)\,dy$$

如以 $\overline{h}$ 表積分區間之平均水深，則

$$y_1\overline{h(x_1, y)} = y_2\overline{h(x_2, y)}$$

故界面與流線（ $\psi_a = \text{const}$ ）間之距離隨水深之增加面減少。
同理，圖(b)、(c)亦同。

8－2 The Tam model — the jet model

Tam, C.K.W. (1973)：" Dynamics of rip currents". J. Geophysical Research, Vol.78, No.12, pp.1937～1943.

- boundary layer analysis.
- laminar jet flow — similarity solution

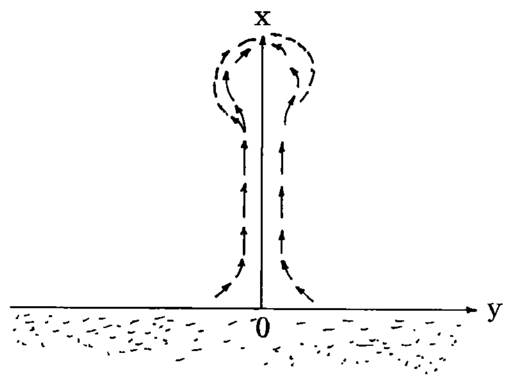

$$\begin{cases} \text{steady.} \\ \text{horizontal eddy viscosity only for mixing.} \end{cases}$$

$$\frac{\partial}{\partial x}(Du)+\frac{\partial}{\partial y}(Dv)=0 \qquad \frac{1}{\rho D}\left(\frac{\partial S_{xx}}{\partial x}+\frac{\partial S_{xy}}{\partial y}\right)$$

$$u\frac{\partial u}{\partial x}+v\frac{\partial u}{\partial y}=-g\frac{\partial \overline{\eta}}{\partial x}+\cancel{\tau_x}+A_H\left(\frac{\partial^2 u}{\partial x^2}+\frac{\partial^2 u}{\partial y^2}\right)$$

$$u\frac{\partial v}{\partial x}+v\frac{\partial v}{\partial y}=-g\frac{\partial \overline{\eta}}{\partial y}+\cancel{\tau_y}+A_H\left(\frac{\partial^2 v}{\partial x^2}+\frac{\partial^2 v}{\partial y^2}\right)$$

$$D=\overline{\eta}+h(x) \qquad \frac{1}{\rho D}\left(\frac{\partial S_{xy}}{\partial x}+\frac{\partial S_{yy}}{\partial y}\right)$$

Assume that the radiation stresses ($S_{\alpha\beta}$) have little effect on the dynamics of a rip current.

boundary layer approximation, $\begin{cases} u \gg v \\ \dfrac{\partial}{\partial x} \ll \dfrac{\partial}{\partial y} \end{cases}$

故，以上諸式成爲

$$
\begin{cases}
\dfrac{\partial}{\partial x}(Du) + \dfrac{\partial}{\partial y}(Dv) = 0 & \cdots\cdots(1) \\
u\dfrac{\partial u}{\partial x} + v\dfrac{\partial u}{\partial y} = A_H \dfrac{\partial^2 u}{\partial y^2} & \cdots\cdots(2) \\
\text{B.C. a} & \\
\left.\begin{array}{lll} \text{at} \quad y \to \pm\infty, & u \to 0 \ \left(\dfrac{\partial u}{\partial y} = 0\right) \\ \quad\quad\ y \to 0, & v \to 0,\ \dfrac{\partial u}{\partial y} = 0 \end{array}\right\} & \cdots\cdots(3)
\end{cases}
$$

conservation of x-momentum flux : $\int_{-\infty}^{\infty} \rho D(2)\,dy \Rightarrow$

$$\int_{-\infty}^{\infty} \rho D u^2 dy = M \ (\text{與 x - 無關}) \quad \cdots\cdots(4)$$

M : total momentum flux of rip current

$$\text{令} \quad \left.\begin{array}{l} uD = \dfrac{\partial \psi}{\partial y} \\ vD = -\dfrac{\partial \psi}{\partial x} \end{array}\right\} \quad \cdots\cdots(5)$$

$$\xi = D(x)\,y \quad , \quad \zeta = \int_0^x D^2(x)\,A_H\,dx \quad \cdots\cdots(6)$$

(i.e. $(x, y) \to (\xi, \zeta)$)

(1)～(4)⇒
$$\frac{\partial \psi}{\partial \xi}\frac{\partial^2 \psi}{\partial \xi \partial \zeta} - \frac{\partial \psi}{\partial \zeta}\frac{\partial^2 \psi}{\partial \xi^2} = \frac{\partial^3 \psi}{\partial \xi^3} \quad \cdots\cdots(7)$$

$$\frac{\partial \phi_{k-1/2}}{\partial t}+\frac{\partial}{\partial x}\int_{z_k}^{z_{k-1}} Su\,dz+\frac{\partial}{\partial y}\int_{z_k}^{z_{k-1}} Sv\,dz+$$

$$\left[S\left(w-u\frac{\partial Z}{\partial x}-v\frac{\partial Z}{\partial y}-\frac{\partial Z}{\partial t}\right)\right]_{k-1}-\left[S\left(w-u\frac{\partial Z}{\partial x}-v\frac{\partial Z}{\partial y}-\frac{\partial Z}{\partial t}\right)\right]_{k}$$

$$=\frac{1}{\rho_o}\left[\frac{\partial}{\partial x}\int_{z_k}^{z_{k-1}}\left(A_h^{(s)}\frac{\partial S}{\partial x}\right)dz+\frac{\partial}{\partial y}\int_{z_k}^{z_{k-1}}\left(A_h^{(s)}\frac{\partial S}{\partial y}\right)dz\right]$$

$$-\frac{1}{\rho_o}\left[\left(A_h^{(s)}\frac{\partial S}{\partial x}\right)\frac{\partial Z}{\partial x}+\left(A_h^{(s)}\frac{\partial S}{\partial y}\right)\frac{\partial Z}{\partial y}-A_v^{(s)}\frac{\partial S}{\partial z}\right]_{k-1}$$

$$+\frac{1}{\rho_o}\left[\left(A_h^{(s)}\frac{\partial S}{\partial x}\right)\frac{\partial Z}{\partial x}+\left(A_h^{(s)}\frac{\partial Z}{\partial y}\right)\frac{\partial Z}{\partial y}-A_v^{(s)}\frac{\partial S}{\partial z}\right]_{k} \quad \cdots\cdots(31)$$

各項下註數是整數減$\frac{1}{2}$者，表示它是屬於那個層次之值；而其數是整數者，表示它是在交界面之值。同時令

$$U_{k-1/2}=\int_{z_k}^{z_{k-1}} u\,dz \quad , \quad V_{k-1/2}=\int_{z_k}^{z_{k-1}} v\,dz \quad ,$$

$$\cdots\cdots(32)$$

$$\theta_{k-1/2}=\int_{z_k}^{z_{k-1}} T\,dz \quad , \quad \phi_{k-1/2}=\int_{z_k}^{z_{k-1}} S\,dz$$

一般而言，海洋內部各層的交界面，我們可以把它們分成二類，即

物質界面（流體不能穿過）$Z_k(t,x,y)$：$w_k-u_k\frac{\partial Z_k}{\partial x}-v_k\frac{\partial Z_k}{\partial y}-\frac{\partial Z_k}{\partial t}=0$

固定界面（流體能通過）$Z_k(x,y)$：$\frac{\partial Z_k}{\partial t}=0$

9. THEORETICAL MODELS FOR NEARSHORE CIRCULATIONS

9－1 The Bowen model

Bowen, A.J. : " Rip Currents, 1. Theoretical investigation" , J. Geophysical Res., Vol. 74, No.23, pp.5467 ～ 5478, 1969.

$$u\,(h+\overline{\eta})=\frac{\partial\psi}{\partial y}$$

$$v\,(h+\overline{\eta})=-\frac{\partial\psi}{\partial x}$$

$$\xi=\frac{\partial v}{\partial x}-\frac{\partial u}{\partial y}\quad,\quad D=h+\overline{\eta}$$

$$\frac{\partial\psi}{\partial y}\frac{\partial}{\partial x}\left(\frac{\xi}{D}\right)-\frac{\partial\psi}{\partial x}\frac{\partial}{\partial y}\left(\frac{\xi}{D}\right)=\frac{\partial}{\partial x}\left(\frac{\tau_y}{\rho D}\right)-\frac{\partial}{\partial y}\left(\frac{\tau_x}{\rho D}\right)$$
$$+\frac{\partial}{\partial x}\left\{\frac{1}{\rho D}\left(\frac{\partial S_{yy}}{\partial y}+\frac{\partial S_{xy}}{\partial x}\right)\right\}-\frac{\partial}{\partial y}\left\{\frac{1}{\rho D}\left(\frac{\partial S_{xx}}{\partial x}+\frac{\partial S_{xy}}{\partial y}\right)\right\}$$

(lateral diffusion is neglected)

$$H=\gamma\tan\beta'\,x\,(1+\varepsilon\cos\lambda y)$$

$$\tau_x=\rho c_b u\quad,\quad\tau_y=\rho c_b v$$

$$\Rightarrow\frac{\partial\psi}{\partial y}\frac{\partial}{\partial x}\left(\frac{\xi}{D}\right)-\frac{\partial\psi}{\partial x}\frac{\partial}{\partial y}\left(\frac{\xi}{D}\right)=\frac{c_b}{D}\left\{\xi-\frac{1}{D^2}\left(\frac{\partial\psi}{\partial x}\frac{\partial D}{\partial x}+\frac{\partial\psi}{\partial y}\frac{\partial D}{\partial y}\right)\right\}$$
$$+\frac{1}{4}g\gamma^2\tan\beta'\,\varepsilon\lambda$$

省略非線性項以及$\dfrac{\partial\psi}{\partial y}\dfrac{\partial D}{\partial y}$之微小項，則

$$\frac{1}{D^2}\left(\frac{\partial^2\psi}{\partial x^2}+\frac{\partial^2\psi}{\partial y^2}\right)-\frac{2}{D^3}\tan\beta'\,\frac{\partial\psi}{\partial x}=\frac{B}{c_b}\sin\lambda y$$

$$B=\begin{cases}-\dfrac{1}{4}g\gamma^2\tan\beta'\,\varepsilon\lambda & \text{碎波帶內}\\[2ex] 0 & \text{碎波帶外}\end{cases}$$

B.C. $x=0\ ,\ \psi=0$

$x\rightarrow\infty\ ,\ \psi=\text{finite}$

$$\psi(x,y)=\begin{cases}\sin\lambda y\ \{A_1,(\lambda x\cosh\lambda x-\sinh\lambda x)\\ \quad+\dfrac{B(\tan\beta')^2}{c_b\lambda^4}[2-(\lambda x)^2+2\lambda x\sinh\lambda x-2\cosh\lambda x]\}\\ \quad\text{，碎波帶內}\\ A_2(\lambda x+1)e^{-\lambda x}\sin\lambda y\ \text{，碎波帶外}\end{cases}$$

$$x=x_b\ ,\ \psi\ ,\ \frac{\partial\psi}{\partial x}\text{：連續}\Rightarrow\text{決定}A_1\ ,\ A_2$$

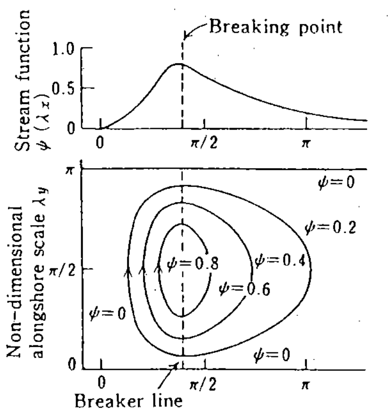

Figure 9.1 Linear solution of nearshore circulation pattern including bottom friction(Bowen,1969).

9−2 *The wave-current interaction model*

Dalrymple, R. A. and C. J. Lozano (1978) : " wave-current intaraction models for rip currents ", J. Geophysical Research, Vol.83, No. C12, pp.6063 ~ 6071.

Steady state :

$$\frac{\partial}{\partial \hat{x}}\left[\hat{U}(\hat{h}+\hat{\eta})\right]+\frac{\partial}{\partial y}\left[\hat{V}(\hat{h}+\hat{\eta})\right]=0 \qquad \cdots\cdots(1)$$

$$\hat{U}\frac{\partial \hat{U}}{\partial \hat{x}}+\hat{V}\frac{\partial \hat{U}}{\partial \hat{y}}=-\hat{g}\frac{\partial \hat{\eta}}{\partial \hat{x}}-\frac{1}{\hat{\rho}(\hat{h}+\hat{\eta})}\left(\frac{\partial \hat{S}_{\hat{x}\hat{x}}}{\partial \hat{x}}+\frac{\partial \hat{S}_{\hat{x}\hat{y}}}{\partial \hat{y}}+\hat{R}_x\right) \qquad \cdots\cdots(2)\ a$$

$$\hat{U}\frac{\partial \hat{V}}{\partial \hat{x}}+\hat{V}\frac{\partial \hat{V}}{\partial \hat{y}}=-\hat{g}\frac{\partial \hat{\eta}}{\partial \hat{y}}-\frac{1}{\hat{\rho}(\hat{h}+\hat{\eta})}\left(\frac{\partial \hat{S}_{\hat{y}\hat{x}}}{\partial \hat{x}}+\frac{\partial \hat{S}_{\hat{y}\hat{y}}}{\partial \hat{y}}+\hat{R}_y\right) \qquad \cdots\cdots(2)\ b$$

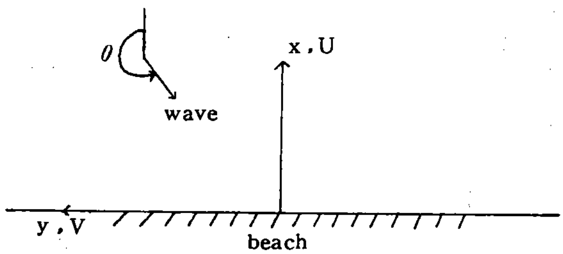

$$\hat{R}_x=\hat{\rho}F\gamma\left[\hat{g}(\hat{h}+\hat{\eta})\right]^{\frac{1}{2}}\pi^{-1}\left[(1+\cos^2\theta)\hat{U}+\left(\frac{1}{2}\sin 2\theta\right)\hat{V}\right] \qquad \cdots\cdots(3)\ a$$

$$\hat{R}_y=\hat{\rho}F\gamma\left[\hat{g}(\hat{h}+\hat{\eta})\right]^{\frac{1}{2}}\pi^{-1}\left[(1+\sin^2\theta)\hat{U}+\left(\frac{1}{2}\sin 2\theta\right)\hat{V}\right] \qquad \cdots\cdots(3)\ b$$

$$F=1.41\left[\frac{\gamma}{2\hat{k}\hat{k}_s}\right]^{-\frac{2}{3}}\approx 1.41\left[\left(\frac{\hat{g}\gamma}{\hat{H}_b}\right)^{\frac{1}{2}}/(2\hat{\sigma}\hat{k}_s)\right]^{-\frac{2}{3}} \qquad \cdots\cdots(3)\ c$$

γ : breaking index.

$\hat{k}_s$: equivalent roughness of bottom .

$(\ )_b$: value at breaking line.

$$\frac{\partial\left[\left(\hat{U}+\frac{\hat{c}_g\hat{k}_x}{\hat{k}}\right)E\right]}{\partial\hat{x}}+\frac{\partial\left[\left(\hat{V}+\frac{\hat{c}_g\hat{k}_y}{\hat{k}}\right)E\right]}{\partial\hat{y}}$$

$$=-\hat{S}_{\hat{x}\hat{x}}\frac{\partial\hat{U}}{\partial\hat{x}}-\hat{S}_{\hat{x}\hat{y}}\left[\frac{\partial\hat{U}}{\partial\hat{y}}+\frac{\partial\hat{V}}{\partial\hat{x}}\right]-\hat{S}_{\hat{y}\hat{y}}\frac{\partial\hat{V}}{\partial\hat{y}}-\hat{D} \qquad \cdots\cdots(4)$$

$\hat{D}$: energy dissipation , $\hat{k}=\hat{k}_x i+\hat{k}_y j$

$$\frac{\partial\hat{k}_x}{\partial\hat{y}}-\frac{\partial\hat{k}_y}{\partial\hat{x}}=0 \qquad \cdots\cdots(5)$$

$$\hat{\sigma}=\hat{k}\left[\hat{g}\left(\hat{h}+\hat{\eta}\right)\right]^{-\frac{1}{2}}+\hat{k}\left(\hat{U}i+\hat{V}\hat{j}\right) \qquad \cdots\cdots(6)$$

$$(1)\Rightarrow\begin{cases}\hat{U}\left(\hat{h}+\hat{\eta}\right)=-\dfrac{\partial\hat{\psi}}{\partial y}\\[2ex] \hat{V}\left(\hat{h}+\hat{\eta}\right)=\dfrac{\partial\hat{\psi}}{\partial\hat{x}}\end{cases}$$

$\hat{\lambda}=\dfrac{2\pi}{L_r}$, L_r : rip current spacing

= longshore wave number for nearshore circulation

: horizontal length scale

$\dfrac{\hat{\lambda}}{m}$ = vertical length scale , m : beach slope

let : $x=\hat{\lambda}\hat{x}$, $h=\hat{\lambda}m^{-1}\hat{h}$, $\overline{\eta}=\hat{\lambda}m^{-1}\hat{\eta}$

$k=\left(\hat{g}m\hat{\lambda}^{-1}\right)^{\frac{1}{2}}\hat{\sigma}^{-1}\hat{k}$, $a=\left(\dfrac{\gamma}{2}\right)\hat{\lambda}m^{-1}\hat{a}$

$e=\left[\dfrac{1}{8}\hat{\rho}\hat{g}\gamma^2\left(m\hat{\lambda}^{-1}\right)^2\right]^{-1}\hat{E}$, $\psi=\left(\hat{g}m\hat{\lambda}^{-1}\right)^{-\frac{1}{2}}\hat{\lambda}^2m^{-1}\hat{\psi}$

$$S=\left[\frac{1}{8}\hat{\rho}\hat{g}\gamma^2(m\hat{\lambda}^{-1})^2\right]^{-1}\hat{S},$$

$$(c_g, U, V)=(\hat{g}m\hat{\lambda}^{-1})^{-\frac{1}{2}}(\hat{c}_g, \hat{U}, \hat{V}) \qquad \cdots\cdots(7)$$

$$D=\left[\frac{1}{8}\hat{\rho}\hat{g}\gamma^2(m\hat{\lambda}^{-1})^2\right]^{-1}\left[\hat{g}m\hat{\lambda}^{-1}\right]^{-\frac{1}{2}}\hat{\lambda}^{-1}\hat{D}$$

$$(h+\overline{\eta}_0=\hat{m}x)$$

$$f=\frac{\gamma F}{m\pi}, \quad A_D=\frac{m\gamma^2}{8f}$$

上式中 $\hat{E}=\frac{1}{2}\hat{\rho}\hat{g}\hat{a}^2$

～與海底摩擦係數有關

$$\tilde{m}=\frac{1}{\left(1+\frac{3\gamma^2}{8}\right)}$$

$$\left.\begin{aligned}S_{xx}&=\frac{1}{2}e(1+2\cos^2\theta)\\S_{xy}&=S_{yx}=e\sin\theta\cos\theta\\S_{yy}&=\frac{1}{2}e(1+2\sin^2\theta)\end{aligned}\right\} \qquad \cdots\cdots(8)$$

(2)～(6)⇒

$$\begin{aligned}(h+\overline{\eta})\frac{\partial\overline{\eta}}{\partial x}=&-\frac{\gamma^2}{16}\frac{\partial}{\partial x}\left[e(1+2\cos^2\theta)\right]-\frac{\gamma^2}{8}\frac{\partial}{\partial y}(e\sin\theta\cos\theta)\\&+f(h+\overline{\eta})^{-\frac{1}{2}}\cdot\left[(1+\cos^2\theta)\frac{\partial\psi}{\partial y}-\frac{\sin^2\theta}{2}\frac{\partial\psi}{\partial x}\right]\\&-\left\{\frac{\partial\psi}{\partial y}\frac{\partial}{\partial x}\left[\frac{1}{(h+\overline{\eta})}\frac{\partial\psi}{\partial y}\right]-\frac{\partial\psi}{\partial x}\frac{\partial}{\partial y}\left[\frac{1}{(h+\overline{\eta})}\frac{\partial\psi}{\partial y}\right]\right\}\end{aligned} \qquad (9)$$

$$\begin{aligned}(h+\overline{\eta})\frac{\partial\overline{\eta}}{\partial y}=&-\frac{\gamma^2}{8}\frac{\partial}{\partial x}(e\sin\theta\cos\theta)-\frac{\gamma^2}{16}\frac{\partial}{\partial y}\left[e(1+2\sin^2\theta)\right]\\&-f(h+\overline{\eta})^{-\frac{1}{2}}\left[\frac{\partial\psi}{\partial x}(1+\sin^2\theta)-\frac{\partial\psi}{\partial y}\frac{\sin\theta}{2}\right]\end{aligned}$$

$$+\left\{\frac{\partial\psi}{\partial y}\frac{\partial}{\partial x}\left[\frac{1}{(h+\overline{\eta})}\frac{\partial\psi}{\partial x}\right]-\frac{\partial\psi}{\partial x}\frac{\partial}{\partial y}\left[\frac{1}{(h+\overline{\eta})}\frac{\partial\psi}{\partial x}\right]\right\} \tag{10}$$

$$\frac{\partial}{\partial x}\left\{e\left[-\frac{1}{(h+\overline{\eta})}\frac{\partial\psi}{\partial y}+\cos\theta(h+\overline{\eta})^{\frac{1}{2}}\right]\right\}$$

$$+\frac{\partial}{\partial y}\left\{e\left[\frac{1}{(h+\overline{\eta})}\frac{\partial\psi}{\partial y}+\sin\theta(h+\eta)^{\frac{1}{2}}\right]\right\}$$

$$=\left(\frac{1+2\cos^2\theta}{2}\right)e\frac{\partial}{\partial x}\left[(h+\overline{\eta})^{-1}\frac{\partial\psi}{\partial y}\right]$$

$$+(\sin\theta\cos\theta)e\left\{\frac{\partial}{\partial y}\left[(h+\overline{\eta})^{-1}\frac{\partial\psi}{\partial y}\right]-\frac{\partial}{\partial x}\left[(h+\overline{\eta})^{-1}\frac{\partial\psi}{\partial x}\right]\right\}$$

$$-\left(\frac{1+2\sin^2\theta}{2}\right)e\frac{\partial}{\partial y}\left[(h+\overline{\eta})^{-1}\frac{\partial\psi}{\partial x}\right]-D \quad \cdots\cdots(11)$$

$$\frac{\partial k_y}{\partial x}-\frac{\partial k_x}{\partial y}=0 \quad \cdots\cdots(12)$$

$$1=k(h+\overline{\eta})^{\frac{1}{2}}+\frac{k}{(h+\overline{\eta})}\cdot\left(-\frac{\partial\psi}{\partial y}i+\frac{\partial\psi}{\partial x}j\right) \quad \cdots\cdots(13)$$

offshore，(9)～(13)，但式(11)中，$D=0$

未知數：$\overline{\eta}$，e，ψ，θ，k，5 個

inside surf zone，(11)⇒ $e=(h+\overline{\eta})^2$ ……(14)

∴ (9)、(10)，(12)～(14)

令 basic state / perturbation

$$\begin{matrix} e = \\ \overline{\eta} = \\ \psi = \\ \theta = \\ k = \\ D = \end{matrix} \left\{ \begin{matrix} e_0 \\ \overline{\eta}_0 \\ (\psi_0 = 0) \\ \theta_0 = \pi \\ -k_0\, i \\ D_0 \end{matrix} \right\} + \left\{ \begin{matrix} \varepsilon\, e_1 \\ \varepsilon\, \overline{\eta}_1 \\ \varepsilon\, \psi_1 \\ \varepsilon\, \theta_1 \\ \varepsilon\,(-k_1\, i - k_0\, \theta_1\, j) \\ \varepsilon\, D_1 \end{matrix} \right\} \qquad \cdots\cdots(15)$$

$$0(\varepsilon^{\circ}):\ (h+\overline{\eta}_0)\frac{\partial \overline{\eta}_0}{\partial x} = -\frac{3}{16}\gamma^2 \frac{\partial e_0}{\partial x} \qquad \cdots\cdots(16a)$$

$$(h+\overline{\eta}_0)\frac{\partial \overline{\eta}_0}{\partial y} = -\frac{1}{16}\gamma^2 \frac{\partial e_0}{\partial y} \qquad \cdots\cdots(16b)$$

$$\frac{\partial}{\partial x}\left[e_0 (h+\overline{\eta}_0)^{\frac{1}{2}} \right] = D_0 \qquad \cdots\cdots(16c)$$

$$\frac{\partial k_0}{\partial y} = 0 \qquad \cdots\cdots(16d)$$

$$k_0 (h+\overline{\eta}_0)^{\frac{1}{2}} = 1 \qquad \cdots\cdots(16e)$$

$$\left.\begin{matrix} \text{offshore} & D_0 = 0\ ,\ e_0 = e_\infty\ ,\ \overline{\eta}_0 = \overline{\eta}(x_b) \\ \text{(flat bottom)} & k_0 = (h+\overline{\eta}_0)^{-\frac{1}{2}} \end{matrix}\right\} \qquad \cdots\cdots(17)$$

inside surf zone：($x=0$ 爲 $h+\overline{\eta}_0=0$ 之處)

$$\overline{\eta}_0 = -\frac{\frac{3}{8}\gamma^2 x}{1+\frac{3}{8}\gamma^2} = -\frac{3}{8}\overline{m}\,\gamma^2 x \qquad \cdots\cdots(18a)$$

$$\overline{m} = 1/(1+\frac{3}{8}\gamma^2)$$

$$D_0 = \overline{m}\,(h + \overline{\eta}_0)^{\frac{3}{2}} \qquad \cdots\cdots (18b)$$

$$e_0 = (h + \overline{\eta}_0)^2 \qquad \cdots\cdots (18c)$$

$$k_0 = (h + \overline{\eta}_0)^{-\frac{1}{2}} \qquad \cdots\cdots (18d)$$

$0(\varepsilon)$: let. $d = h + \eta_0$

$$\underbrace{d\frac{\partial \overline{\eta}_1}{\partial x} + \overline{\eta}_1 \frac{\partial \overline{\eta}_0}{\partial x}}_{①} = -\frac{3\gamma^2}{16}\frac{\partial e_1}{\partial x} - \frac{\gamma^2}{8}\frac{\partial}{\partial y}(e_0\theta_1) + 2fd^{-\frac{1}{2}}\frac{\partial \psi_1}{\partial y} \cdots\cdots (19a)$$

$$d\frac{\partial \eta_1}{\partial y} = -\frac{\gamma^2}{8}\frac{\partial}{\partial x}(e_0\theta_1) - \frac{\gamma^2}{16}\frac{\partial e_1}{\partial y} - fd^{-\frac{1}{2}}\frac{\partial \psi_1}{\partial x} \qquad \cdots\cdots (19b)$$

$$-\frac{\partial}{\partial x}\left[e_0 d^{-1}\frac{\partial \psi_1}{\partial y}\right] + \frac{\partial}{\partial y}\left[e_0 d^{-1}\frac{\partial \psi_1}{\partial x}\right] - \underbrace{\frac{\partial}{\partial x}\left[d^{\frac{1}{2}}e_1 + \frac{1}{2}d^{-\frac{1}{2}}e_0\overline{\eta}_1\right]}_{②}$$

$$-\frac{\partial}{\partial y}\left[e_0 d^{\frac{1}{2}}\theta_1\right] = \frac{3}{2}e_0\frac{\partial}{\partial x}\left[d^{-1}\frac{\partial \psi_1}{\partial y}\right] - \frac{1}{2}e_0\frac{\partial}{\partial y}\left[d^{-1}\frac{\partial \psi_1}{\partial x}\right] - D_1 \qquad \cdots\cdots (19c)$$

$$-d^{\frac{1}{2}}\frac{\partial}{\partial x}\left[d^{-\frac{1}{2}}\theta_1\right] = \frac{\partial}{\partial y}\left[\frac{1}{2}d^{-1}\overline{\eta}_1 + d^{-\frac{3}{2}}\frac{\partial \psi_1}{\partial y}\right] \qquad \cdots\cdots (19d)$$

碎波帶內時，(19c) $\rightarrow$ $\underbrace{e_1 = 2h\overline{\eta}_1}_{\uparrow\ (14)\text{、}(15)}$ $\qquad \cdots\cdots (19e)$

B.C. $\quad x \rightarrow 0\ ,\ \infty \qquad \psi_1, \theta_1, e_1, \overline{\eta}_1 \rightarrow 0$

$\qquad x = x_b\ , \qquad \psi_1, \theta_1, e_1, \overline{\eta}_1$: continuous note ：①項及②項在以前之研究中均未考慮。

A. model I-extremely small refraction angle

assume $\theta_1 = 0(\varepsilon)$. 1.e. negligible angle of incidence.

$$(19d) \Rightarrow \ \overline{\eta}_1 = -2\,d^{-\frac{1}{2}} \frac{\partial \psi_1}{\partial y} \qquad \cdots\cdots(20)$$

Let periodic functions.

$$\psi_1 = \overline{\psi}(x)\ \sin y$$

$$(e_1, \overline{\eta}_1) = [\,\overline{e}(x),\ \overline{\eta}(x)\,]\ \cos y$$

cross differentiate (19a) & (19b) ⇒

$$\overline{\psi}'' + \overline{\psi}' \left[\frac{4d}{3f} - \frac{d'}{2d'}\right] + \overline{\psi}\left[\frac{4d'}{3f} - \frac{2}{3f}\eta'_0 - \frac{2}{3}\right] = 0 \qquad \cdots\cdots(21)$$

$x=0$ ： regular singularity. (∵ $d=0$, at $x=0$)

indicial egn. → root = 0 , 2/2

↓

$\overline{e}$ unbounded at $x=0$ （由式(19e)及(20)）

$$\psi \sim \wedge x^{\frac{3}{2}} \qquad \text{as} \quad x \to 0$$

其次 continuity condition at $x = x_b$ ：

$$\lim_{\substack{x \to x_b \\ x > x_b}} \frac{\overline{\psi}'(x)}{\overline{\psi}(x)} = \lim_{\substack{x \to x_b \\ x < x_b}} \frac{\overline{\psi}'(x)}{\overline{\psi}(x)} \qquad \cdots\cdots(22)$$

$x=0$, $x=\infty$) Ψ 有限

式(22)

⇒式(21)有解

$(18a) \xrightarrow[\text{代入}]{} (21) \Rightarrow$

$$\overline{\phi}'' + (Mx - \frac{1}{2x})\overline{\phi}' + [M(1+\frac{3k^2}{16}) - \frac{2}{3}]\overline{\phi} = 0$$

$M = 4\overline{m}/3f$ (eigenparameter)

numerical experiments $\Rightarrow$ for $0 < M < 100$ and all x_b

no non-trival sol.

$\Rightarrow$ For arbitrary monotonic decreasing bottom beach profiles h(x), the present model will not yield a steady current circulation cell.

note. Mizuguchi (1976) 亦應用類似于 LeBlond·Tang 之方法，而得與此相同之結論。

B. Model II - First-order wave-current interaction

let. $(\phi_1, \theta_1) = [\overline{\phi}(x), \overline{\theta}(x)] \sin y$

$(\overline{\eta}_1, e_1) = [\overline{\eta}(x), \overline{e}(x)] \cos y$

$(19a) \sim (19e) \Rightarrow$

$$d\overline{\eta}' + \eta_0'\overline{\eta} = -\frac{3\gamma^2}{16}\overline{e}' - \frac{\gamma^2}{8}e_0\overline{\theta} + 2fd^{-\frac{1}{2}}\overline{\phi} \qquad \cdots\cdots\cdots (23a)$$

$$-d\overline{\eta} = -\frac{\gamma^2}{8}(e_0\overline{\theta})' + \frac{\gamma^2}{16}\overline{e} - fd^{-\frac{1}{2}}\overline{\phi}' \qquad \cdots\cdots\cdots (23b)$$

$$d^{\frac{1}{2}}(d^{-\frac{1}{2}}\overline{\theta})' = \frac{1}{2}d^{-1}\overline{\eta} + d^{-\frac{3}{2}}\overline{\phi} \qquad \cdots\cdots\cdots (23c)$$

$$-(e_0 d^{-1})'\overline{\phi} - e_0 d'^2\overline{\phi}' + \frac{3}{2}e_0 d' e^{-2}\overline{\phi}$$

$$= (d^{\frac{1}{2}}\overline{e} + \frac{1}{2}d^{-\frac{1}{2}} e_0 \overline{\eta})' + d^{\frac{1}{2}} (e_0 \overline{\theta}) \qquad \cdots\cdots (23d)$$

$$\overline{e} = 2 d \overline{\eta} \quad (\text{inside surf zone}) \qquad \cdots\cdots (23e)$$

(outside surf zone, flat bottom)

offshore zone : (23a) ～ (23d) , or

$$q_{11}' = M_{11} q_{11} \qquad \cdots\cdots (24)$$

$$q_{11} = (\overline{\eta} , \overline{\psi} , \overline{\theta} , \overline{e}) , \quad M_{11} = 4 \times 4 \text{ matrix}$$

inside surf zone : (23e) $\xrightarrow[\text{代入}]{}$ (23a) ～ (23c)

$$q_1' = \mathbf{M}_1 q \qquad \cdots\cdots (25)$$

$$q_1 = (\overline{\eta} , \overline{\psi} , \overline{\theta}) , \quad M_1 = 3 \times 3 \text{ Matrix}$$

- numerical sol.

A_D 大→L_r 大　　$A_D = 1.0$ 時 , $\hat{L}_r \approx 1.6 \hat{x}_b$

小→　小

9－3 *The hydrodynamic instability model*

Hino (1974) ：首先提出不穩定理論。$L_r \approx 4 x_b$

Miller, C. and A. Barcilon (1978) : " Hydrodynamic instability in the surf zone as a mechanism for the formation of horizontal gyres" , J. Geophysical Research, Vol.83, No. C 8 . pp.4107 ～ 4116.

- mildly sloping beach, parallel bottom contours.
- lateral friction effect neglected.
- steady, linear stability analysis.

基本原理：The energy for the circulation cell is derived from the potential energy stored in the wave-induced sea surface set-up (uniform, longshore independent) .

→The infinitesimal perturbation of the proper (longshore) wave length will extract the energy associated with this set-up and convert into the circulation velocities of cell.

$$\frac{\partial}{\partial x_\alpha}\widetilde{M}_\alpha = 0 \qquad \cdots\cdots(1)$$

$$\frac{\partial S_{\alpha\beta}}{\partial x_\beta} = -\rho g(h+\overline{\eta})\frac{\partial\overline{\eta}}{\partial x_\alpha} + \underbrace{\frac{2\rho S a g^{\frac{1}{2}}}{\pi(h+\overline{\eta})^{\frac{1}{2}}}(2U_1, U_2)}_{\text{bottom frictional stress}} \qquad \cdots\cdots(2)$$

$\alpha, \beta = 1, 2$ bottom frictional stress

$$\frac{\partial}{\partial x_\alpha}\{U_\alpha E + \ell_1 c_g E\} = -\underbrace{\frac{2ga^2\beta^2 E}{c(h+\overline{\eta})^3}}_{\text{energy dissipation due to wave breaking}} - \underbrace{\frac{4}{3\pi}\rho c_D g^{\frac{3}{2}} a^2 (h+\overline{\eta})^{-\frac{3}{2}}}_{\text{energy dissipation due to bottom friction}} \qquad \cdots\cdots(3)$$

$$S_{\alpha\beta} = \frac{E}{c}\ \ell_\alpha \ell_\beta + \frac{E}{2}\left(\frac{2c_g}{c} - 1\right)\delta_{\alpha\beta}$$

ℓ_1 , ℓ_2 : directional unit vectors normal and parallel to the shore.

β : a measure of vertical extent of foam region. (<1)

introduce Ψ :

$$\Psi_y = \widetilde{M}_1 \quad , \quad \Psi_x = -\widetilde{M}_2 \qquad \cdots\cdots(4)$$

ϵ : small dimensionless parameter

$D = h + \overline{\eta}$

令

$$\left.\begin{aligned} \Psi &= \Psi^{(0)}(x) + \varepsilon\Psi^{(1)}(x)\sin\lambda y + \cdots\cdots \\ \overline{\eta} &= \overline{\eta}^{(0)}(x) + \varepsilon\,\overline{\eta}^{(1)}(x)\cos\lambda y + \cdots\cdots \\ D &= D^{(0)}(x) + \epsilon D^{(1)}(x)\cos\lambda y + \cdots\cdots \\ E &= \underbrace{E^{(0)}(x)} + \varepsilon E^{(1)}(x)\cos\lambda y + \cdots\cdots \end{aligned}\right\} \qquad \cdots\cdots(5)$$

basic state
(y-independent)

($\overline{\eta}$ 求出後，即可求D，故未知數其實爲 3 個)

則 <u>in the seaward zone</u>

momentum

$$\frac{3}{2}\frac{\partial E^{(1)}}{\partial x} + 2D^{(0)}\frac{\partial \overline{\eta}^{(1)}}{\partial x} = -2Q\left\{\lambda D^{(0)^{-\frac{7}{4}}}\Psi^{(1)} - \frac{3}{2}D^{(0)^{-\frac{9}{4}}}E^{(1)}\right\} \qquad \cdots\cdots(6)$$

$$\frac{1}{2}E^{(1)} + 2D^{(0)}\overline{\eta}^{(1)} = -\frac{Q}{\lambda}D^{(0)^{-\frac{7}{4}}}\frac{\partial\Psi^{(1)}}{\partial x} \qquad \cdots\cdots(7)$$

energy $\quad \dfrac{\partial}{\partial x}\left(D^{(0)^{-\frac{1}{2}}} E^{(1)} \right) = -2QE^{(1)} D^{(0)^{-\frac{7}{4}}}$ ……(8)

<u>in the surf zone</u>

momentum $\quad \dfrac{3}{2}\dfrac{\partial E^{(1)}}{\partial x} + 2D^{(0)} \dfrac{\partial \overline{\eta}^{(1)}}{\partial x} = -2Q\left\{ \lambda D^{(0)^{m-\frac{3}{2}}} \Psi^{(1)} - \dfrac{3}{2} D^{(0)m-2} E^{(1)} \right\}$ ……(9)

$$\frac{1}{2} E^{(1)} + 2D^{(0)} \overline{\eta}^{(1)} = -\frac{Q}{\lambda} D^{(0)m-\frac{3}{2}} \frac{\partial \Psi^{(1)}}{\partial x} \quad \text{……(10)}$$

energy $\quad \dfrac{\partial}{\partial x}\left(D^{(0)\frac{1}{2}} E^{(1)} \right) = -\dfrac{5\beta^3\gamma^3}{\sigma} D^{(0)m-\frac{7}{2}} E^{(1)} - 2QD^{(0)m-\frac{3}{2}} E^{(1)} + \dfrac{7\beta^3\gamma^5}{\sigma} D^{(0)5m-\frac{9}{2}} \eta^{(1)}$ ……(11)

此處 $Q = 2\gamma c_D / \pi\sigma$

$\sigma = L_B / D_B$ = modified beach slope

L_B = distance from the shoreline to the breaker line in the presence of waves.

在討論式(6)～式(11)之解前，先討論一下 basic state

$\Psi^{(0)} \; (= \widetilde{M}_1^{(0)}) = 0$

$D^{(0)} = h(x) + \gamma^2 \overline{\eta}^{(0)}(x)$, $h(x) = 1 - x$

↑

已無因次化 $\quad (x = 0$ ： brenker line)

$E^{(0)} = (1-\alpha) D^{(0)m} + \alpha$, ($\alpha \equiv 0.1$)

$\overline{\eta}^{(0)}$ = 沿岸方向無變化時之wave set-up or set-down

Solution :

Seaward region :

$$E^{(1)} = A_0 D^{(0)-\frac{1}{2}} \exp\{-\frac{8}{5}Q(D^{(0)-\frac{5}{4}}-1)\}$$

$$\Psi^{(1)} = \frac{5A_0}{2\lambda D^{(0)}}\exp\{-\frac{8}{5}Q(D^{(0)-\frac{5}{4}}-1)\}$$

$$\overline{\eta}^{(1)} = -\frac{A_0}{4D^{(0)\frac{3}{2}}}\exp\{-\frac{8}{5}Q(D^{(0)-\frac{5}{4}}-1)\}$$

surf zone : (m = 3/2)

$$E^{(1)} = \frac{A_1}{D^{(0)\frac{1}{2}}}\exp\{\frac{2B}{3}(D^{(0)\frac{3}{2}}-1)-\frac{B\alpha^3}{3}(D^{(0)-3}-1)\}$$

$$\Psi^{(1)} = A_1\lambda\Psi + A_2 D^{(0)} I_1(\sqrt{2}\lambda D^{(0)})$$

$$\overline{\eta}^{(1)} = \frac{1}{\sqrt{2}}\{\lambda A_1 Q[I_0(\sqrt{2}\lambda D^{(0)})K + K_0(\sqrt{2}\lambda D^{(0)})J]$$
$$+ QA_2 I_0(\sqrt{2}\lambda D^{(0)}) - (E^{(1)}/(2\sqrt{2}D^{(0)}))\}$$

$$B = 5\beta^3\gamma^3/\sigma$$

$$\Psi = D^{(0)} I_1(\sqrt{2}\lambda D^{(0)})K(D^{(0)}) - D^{(0)}K_,(\sqrt{2}\lambda D^{(0)})J(D^{(0)})$$

$$K(D^{(0)}) = \int_0^{D^{(0)}} xG(x)K_1(\sqrt{2}\lambda x)dx$$

$$J(D^{(0)}) = \int_0^{D^{(0)}} xG(x)I_1(\sqrt{2}\lambda x)dx$$

$I_1(x)$, $K_1(x)$ = modified Bessel funcfions of the 2nd kind.

$\alpha = 0.1$

A_0, A_1, A_2：任意常數，由碎波點之連續條件決定之。

結果：$L_r \approx 8.8 x_b$

10. NEARSHORE CURRENTS ON A NON-STRAIGHT COAST

Lin, M.C. & J.Y. Liou (1986)："Analytical study of wave induced nearshore currents", J. of the Chinese Institute of Engineers, Vol.9, No.5, pp.437 ~ 449.

Lin, M.C. & S.Y. Hwang (1988)："Nearshore circulations on a wavy coast". Proc. 21st. International Conf. on Coastal Eng., pp.2603 ~ 2614.

- orthogonal curvillinear coordinate system.
- conformal mapping.

第三屆基礎港灣數值（數學）模式研習會論文集　　Jan. 17～18，1990　Page 173～220

有限元素法
在計算流體力學上之應用

楊德良

國立台灣大學土木工程學系教授
暨水工所所長

摘　要

本論文主要探討藉著原始變數以三種有限元素法解答不可壓縮之黏性流體，此三種方法分別是償罰函數法，壓力速度修正法及壓力速度聯立法。本文並以內流場及外流場分別說明方法之可行性，並應用到庫頁流、渠流、圓形穴流、方形穴流、循流、及流經圓柱之流場。文中並特別強調高雷諾數對於流場不穩定性及旋渦形成之影響。本文更推廣到水力學上之有趣問題，諸如層變水庫動力學、水熱模擬、自由液面流、及沉澱池，亦涉及簡易三維流場。由文中的結果顯示有限元素法不失為流體力學上一具有潛力且非常有效的計算方法。

FINITE ELEMENT ANALYSIS OF COMPUTATIONAL FLUID DYNAMICS

Der-Liang Young

Professor of Civil Engineering and
Director of Hydraulic Research Laboratory
National Taiwan University, Taipei, Taiwan, R.O.C.

ABSTRACT

Solutions of incompressible viscous flows using the primitive variables by the three finite element solution algorithms, namely the penalty function method, the pressure-velocity correction method, and the pressure-velocity coupling method are briefly reviewed. Applications to both the internal and external flow regimes are illustrated. Typical examples cover the simulations of Couette flows, channel flows, circular eddy flows, square cavity flows, recirculating flows, and flows past a circular cylinder. The effects of the high Reynolds numbers to flow instabilities and vortex eddy formations are emphasized in particular. Practical applications of these methodologies to hydraulics are also delineated. Typical examples cover the treatment of the simulation of stratified reservoir dynamics, hydrothermal modeling, free surface flows and sediment basins. Extension to simple three-dimensional flow is also undertaken. The results reveal that the finite element analysis is a very powerful approach in the realm of computational fluid mechanics.

Keywords: finite element analysis, computational fluid dynamics, internal flows, external flows, Navier-Stokes equations, free surface flows.

* This paper will be published in the Proceedings of the National Science Council, the Republic of China, Part A : Physical Science and Engineering.

1. *INTRODUCTION*

In the realm of computational fluid dynamics (CFD) especially for the solutions of the Navier-Stokes equations, the finite difference method (Roache,1972) is more popular, as comparing to the other numerical schemes, such as finite element method (FEM) (Baker,1983), or the boundary element method (Brebbia et al,1984). The reasons lie in the methodology underdevelopment and users unfamiliarity of the latter. To many fluid dynamicists, finite element approach was resisted by the misconcepts that the finite element method was considered less efficient and more difficult to use in solving flow problems, as to solve the (linear) structral mechanics fields. It is fair to say that the most vexing problems of FEM are the big computer storages and longer CPU times are needed, in particular to the three-dimensional viscous flow regimes. However, the beauty of handling irregular boundaries of field domain and the inhomogeneous properties of flow characteristics are by no means no comparison to the finite difference method, as far as finite element scheme is concerned. By the advance of supercomputers, it is confident that the drawbacks of the large storage and longer CPU will be overcome by and by in the near future.

The main purposes of this paper intend to elucidate the summary report of the writer and its collaborators past & current researches for solving the two-dimensional as well as three-dimensional incompressible viscous flows using the primitive parameters as the field variables by the finite element formulatins. There are three solution algorithms to be covered, namely, (1) the penalty function method, (2) the pressure-velocity correction method, and (3) the pressure-velocity coupling method. Comparisons for results obtained from these three approaches will be made if they permit us to do so. Furthermore, comparisons will be extended to the other formulation, such as streamfunction approach if possible. Besides, for some typical flows, analytic solutions and existing literature are used to check the accuracy of the numerical simulations.

2. GOVERNING EQUATIONS

The fundamental equations for unsteady viscous incompressible flows by neglecting effects of density stratification and free surfaces are governed by the continuity equation and the so-called Navier-Stokes equations. They can be represented by the Cartesian coordinate system in a dimensionless form as follows:

$$\frac{\partial u_i}{\partial x_i} = 0 \qquad (2.1)$$

$$\frac{\partial u_i}{\partial t} + u_j \frac{\partial u_i}{\partial x_j} = - \frac{\partial \bar{p}}{\partial x_i} + \frac{n_i}{Fr^2} + \frac{1}{Re} \frac{\partial^2 u_i}{\partial x_j \partial x_j} \qquad (2.2)$$

with boundary conditions:

$$u_i = u_i b \qquad \text{on} \quad \Gamma_\nu \qquad (2.3)$$

$$\frac{1}{Re} \frac{\partial u_i}{\partial n} - p n_i = f_{ib} \qquad \text{on} \quad \Gamma_f \qquad (2.4)$$

and initial conditions:

$$u_i = u_{io} , \quad p = p_o , \quad \frac{\partial u_{io}}{\partial x_i} = 0 \qquad \text{at} \quad t = 0 \qquad (2.5)$$

where u_i is the velocity component in the x_i-direction, p is the pressure force which may include the energy of any scalar potential field, for example $p = \bar{p} + n_i x_i / F_r^2$, $\bar{p}$ is the ordinary pressure, n_i is the direction cosine of the normal n in the x_i-directions, n is the normal at the boundary oriented towards the exterior, f_{ib} is the surface force in the x_i-direction, x_i are the Cartesian coordinates, t is the time, Γ_ν is the specified velocity boundaries, Γ_f is the specified force boundaries, Re is the Reynolds number and is defined by $Re = (VL/\nu)$, F_r is the Froude number and is defined by $F_r = V/(gL)^{1/2}$, u_{ib} and u_{io} are the specified boundary conditions and initial conditions of u_i respectively, p_o is the specified initial condition of p. Re is defined with characteristic length L, characteristic velocity V and kinematic viscosity of fluid ν. For two-dimensional flows, i = 1, 2, with x, y directions of u, v velocity components. For three-dimensional flows, i =1, 2, 3, with x, y, z directions of u, v, w velocity components.

For reason of brief, only the two-dimensional formulation will be undertaken. Extension to the three-dimensional flows will be found no difficulty at all. Thus, for the two-dimensional viscous flows, the governing equations are as follows, when the gravitatinal force is absorbed into the pressure force.

$$F_1 = \frac{\partial u}{\partial x} + \frac{\partial v}{\partial y} = 0 \qquad (2.6)$$

$$F_2 = \frac{\partial u}{\partial t} + u\frac{\partial u}{\partial x} + v\frac{\partial u}{\partial y} + \frac{\partial p}{\partial x} - \frac{1}{Re}\nabla^2 u = 0 \qquad (2.7)$$

$$F_3 = \frac{\partial v}{\partial t} + u\frac{\partial v}{\partial x} + v\frac{\partial v}{\partial y} + \frac{\partial p}{\partial y} - \frac{1}{Re}\nabla^2 v = 0 \qquad (2.8)$$

With boundary conditions:

$$u = u_b \;;\quad v = v_b \;; \qquad \text{on } \Gamma_\nu \qquad (2.9)$$

$$\frac{1}{Re}\frac{\partial u}{\partial n} - pn_x = f_{xb} \;;\quad \frac{1}{Re}\frac{\partial v}{\partial n} - pn_y = f_{yb} \qquad \text{on } \Gamma_f \quad (2.10)$$

and initial conditions:

$$u = u_o \;,\; v = v_o \;,\; p = p_o \;,\; \frac{\partial u_o}{\partial x} + \frac{\partial v_o}{\partial y} = 0 \qquad \text{at } t=0 \quad (2.11)$$

After the primitive variables, u, v, and p are found, the vorticity, Ω, and stream functions, φ, are obtained from the following definitions:

$$\Omega = \frac{\partial v}{\partial x} - \frac{\partial u}{\partial y} \tag{2.12}$$

$$\nabla^2 \varphi = - \Omega \tag{2.13}$$

Sometimes, the steady total pressure, $\hat{p}$, as defined by $\hat{p} = p + (u^2+v^2)/2$ is introduced for special purposes. It can be easily shown that the Navier-Stokes equations (steady state only from Eq. (2.7) & (2.8)) are reduced to the following equations:

for $Re \neq 0$

$$Re \frac{\partial \hat{p}}{\partial x} = - Re\, \Omega \frac{\partial \varphi}{\partial x} - \frac{\partial \Omega}{\partial y} \tag{2.14}$$

$$Re \frac{\partial \hat{p}}{\partial y} = - Re\, \Omega \frac{\partial \varphi}{\partial y} + \frac{\partial \Omega}{\partial x} \tag{2.15}$$

When $Re \to 0$, p and Ω satisfy the Cauchy-Riemann differential equations, and it is concluded that in steady flows pressure and vorticity are orthogonal when the Stokes regime prevails. On the other hand, as Re becomes larger, from Eq.(2.14) and (2.15), the total pressure is proportional to the stream function. Therefore, in this case, the total pressure contours are similar to the stream-lines. This phenomenon will be reiterated by the case studies in the following sections.

3. *FINITE ELEMENT FORMULATION*

Pressure plays a very tricky role in the solution of incompressible viscous flow problems, as observed from the continuity and Navier-Stokes equations. It is seen that the pressure does not appear in the continuity equation for the incompressible flows. In the meantime , the order of the velocity field is one-order higher than that of the pressure in the Navier-Stokes equations. This peculiar behavior makes the finite element analysis three ways to choose, according to the decoupling, iteration, and coupling of velocity and pressure fields. They are called the penalty function method, the pressure-velocity correction method, and pressure-velocity coupling method respectively. The conventional Galerkin finite element method (GFEM) is used to discretize the continuity and the Navier-Stokes equations for all three methods.

3.1 Penalty Function Method

In incompressible flows, the continuity equation can be treated either as a governing equation, as will be illustrated in the pressure-velocity correction method, and pressure-velocity coupling method, or as a constraint condition, as in the formulation of penalty function method. Therefore, penalty function method is cast as one of the optimization techniques.

The penalty function method suggests that the pressure field is eliminated by the relationship

$$p = - \alpha \left(\frac{\partial u}{\partial x} + \frac{\partial v}{\partial y} \right) \tag{3.1}$$

where α is a very big pre-assigned positive number, called the penalty parameter. It is noticed that the constraint of incompressibility condition will be automatically satisfied so long as the pressure remains finite as the penalty parameter goes to a very large number. In this way, pressure and velocity are"decoupled" each other from the systems,therefore tremendous unknowns may be reduced. Furthermore, the pressure field is obtained by a postprocess after the velocity field is obtained.

With the elimination of pressure from the momentum equations and by the procedures of the Galerkin criterion of the method of weighted residuals, the following systems are obtained:

$$
\begin{bmatrix} [M] & [0] \\ [0] & [M] \end{bmatrix} \begin{Bmatrix} \{\dot{u}\} \\ \{\dot{v}\} \end{Bmatrix} + \begin{bmatrix} [C_{11}(u)] & [C_{12}(u)] \\ [C_{21}(v)] & [C_{22}(v)] \end{bmatrix} \begin{Bmatrix} \{u\} \\ \{v\} \end{Bmatrix}
$$

$$
+ \frac{1}{Re} \begin{bmatrix} [D] & [0] \\ [0] & [D] \end{bmatrix} \begin{Bmatrix} \{u\} \\ \{v\} \end{Bmatrix} + \alpha \begin{bmatrix} [P_{11}] & [P_{12}] \\ [P_{21}] & [P_{22}] \end{bmatrix} \begin{Bmatrix} \{u\} \\ \{v\} \end{Bmatrix} = \begin{Bmatrix} \{R_u\} \\ \{R_v\} \end{Bmatrix} \tag{3.2}
$$

where [M] is the mass matrix, $[C_{11}]$, ... , $[C_{22}]$ are the momentum advection matrix, [D] is momentum diffusion matrix, $[P_{11}]$, ... , $[P_{22}]$ are the pressure force matrices, and $\{R_u\}$, $\{R_v\}$ are pressure and shear force vectors.

After the velocity are obtained, the pressure can be calculated as follows:

$$
[A]\ \{P\} = -\ \alpha\ ([\ S1\ ]\{\ u\ \} + [\ S2\ ]\{\ v\ \}) \tag{3.3}
$$

As far as the penalty function method is concerned, adoption of admissible elements and the selective reduced integration rule are the two most intricate tasks to obtain good results. T3, T3M, and T6 of triangular elements as well as Q4, Q4M, Q8, and Q9 of quadrilateral elements were all examined in this investigation. Of particular interest is the introduction of two non-conforming elements T3M and Q4M [Young and N_i, 1989] into the formulation where the degree-of-freedom lies in the middle points of the element instead of at the vertices. The intention is attributed to the concept of control volume of conservation of mass, momentum, energy, etc. For illustration, the shape (interpolation) functions of T3M, Q4M, and Q4 are listed in the following:

T3M:

$$
\begin{aligned} N_1 &= 1 - 2L_1 \\ N_2 &= 1 - 2L_2 \\ N_3 &= 1 - 2L_3 \end{aligned} \tag{3.4}
$$

$$\text{Q4M:} \quad \begin{aligned} N_1 &= (1/4)\,(1-\xi-\eta)(1+\xi-\eta) \\ N_2 &= (1/4)\,(1+\xi-\eta)(1+\xi+\eta) \\ N_3 &= (1/4)\,(1+\xi+\eta)(1-\xi+\eta) \\ N_4 &= (1/4)\,(1-\xi+\eta)(1-\xi-\eta) \end{aligned} \tag{3.5}$$

$$\text{Q4:} \quad \begin{aligned} N_1 &= (1/4)(1-\xi)(1-\eta) \\ N_2 &= (1/4)(1+\xi)(1-\eta) \\ N_3 &= (1/4)(1+\xi)(1+\eta) \\ N_4 &= (1/4)(1-\xi)(1+\eta) \end{aligned} \tag{3.6}$$

where L_i are the area coordinates for triangular elements, and ξ, η are the natural coordinates for quadrilateral elements. Q4, T6, Q8, and Q9 are C°, while T3M and Q4M are semi-C° elements, as far as continuity in element boundaries is concerned. Some of the properties of penalty elements are detailed in Young and Ni (1989).

Different orders of Gaussian quadrature rules are performed to examine the corresponding convergence. Generally speaking, the quadrilateral elements of the Lagrange family associated with the selective reduced integration rule, in particular the Q4 element, are found much superior, such as the Q8 serendipity or triangular elements. This unique feature is quite analogous to the selection of mixed type elements in the pressure-velocity coupling and pressure-velocity correction formulations.

The advantages of penalty function method is conspicuous from the fact that the velocity and pressure fields are decoupled so that much saving can be obtained from the view points of computer storage and programming. On the other hand, for very high Reynolds number, when the flow field is expecting a higher resolution of incompressible constraint, "wiggle" phenomenon of velocity distribution may be found, when the mesh size is too coarse to give accurate computation.

3.2 Pressure-Velocity Correction Method

One of the drawbacks of pressure-velocity coupling method is the large number of degrees of freedoms and nonpositive definiteness of matrix system. To overcome such shortcoming, it is proposed that velocity and pressure fields are solved separatively by the iterative procedures. The process is described as follows:

Firstly, a pressure field is assumed to be known at a priori, then the momentum equations can be disretized by the Galerkin weighted residues method;

$$\begin{bmatrix} [M] & [0] \\ [0] & [M] \end{bmatrix} \begin{bmatrix} \{\dot{u}\} \\ \{\dot{v}\} \end{bmatrix} + \begin{bmatrix} [C & (u)] & [C & (u)] \\ [C & (v)] & [C & (v)] \end{bmatrix} \begin{bmatrix} \{u\} \\ \{v\} \end{bmatrix}$$

$$+ \frac{1}{Re} \begin{bmatrix} [D][0] \\ [0][D] \end{bmatrix} \begin{bmatrix} \{u\} \\ \{v\} \end{bmatrix} = \begin{bmatrix} \{R_u\} \\ \{R_v\} \end{bmatrix} - \begin{bmatrix} [B_1]\{p\} \\ [B_2]\{p\} \end{bmatrix} = \begin{bmatrix} \{R_u(p)\} \\ \{R_v(p)\} \end{bmatrix} \tag{3.7}$$

where $[B_1]$, $[B_2]$ are the pressure force matrices. The right-hand-side of Eq. (3.7) becomes the modified pressure and shear force vectors, which are $\{R_u(p)\}$ and $\{R_v(p)\}$ respectively.

Secondarily, the continuity equation is also discretized as follows :

$$\begin{bmatrix} [B_1]^T & [0] \\ [0] & [B_2]^T \end{bmatrix} \begin{bmatrix} \{u\} \\ \{v\} \end{bmatrix} = \begin{bmatrix} \{0\} \\ \{0\} \end{bmatrix} \tag{3.8}$$

If the velocity field satisfies the continuity equation Eq.(3.8), then we have found the desirable velocity and pressure distribution. However, a pressure correction process is now necessary to be performed, and the computational cycle is repeated until the criteria of convergence of both the pressure and velocity solutions are reached.

There are various alternatives in the pressure correction process. In this study, the correction of pressure is achieved by the following four methodologies: namely (1) method of limited compressibility, (2) method of weighting values, (3) modified method of mark and cell (MAC), and (4) semi-implicit method for pressure-linked equation (such as SIMPLE, SIMPLER, SIMPLEC). Most of them are motivated from the concepts of the finite difference methods[Roache, 1972]. They will be briefly described as follows, for more details, refer to Young and Lin [1986], and Patankar [1980].

3.2.1 Method of Limited Compressibility

In this method, the incompressibility of continuity equation is perturbed by the introduction of compressibility as in the field of aerodynamics. That is, the continuity equation of Eq.(2.6) is substituted by

$$M^2 \frac{\partial p}{\partial t} + \frac{\partial u}{\partial x} + \frac{\partial v}{\partial y} = 0 \tag{3.9}$$

where M is the Mach number as defined by $M = V/C$, C is the speed of sound in the fluid. The correction of pressure $\{\Delta p\}$, as defined by

$$\{p\}_k^{n+1} = \{p\}_{k-1}^{n+1} + \{\Delta p\}_k^{n+1} \tag{3.10}$$

where n+1 is the time step at the time $(n+1)\Delta t$, and k represents the iterative times. It can be easily shown that $\{\Delta p\}$ is obtained by the known pressure and velocity fields as

$$\{K_1\}\{\Delta p\}_k^{n+1} = \{F(u_{k-1}^{n+1}, v_{k-1}^{n+1}, p_{k-1}^{n+1}, p^n)\} \tag{3.11}$$

3.2.2 Method of Weighting Values

From the penalty function method, Eq.(3.1), or from the definition of thermodynamic pressure and mechanical pressure, we can argue that the correction of pressure $\{\Delta p\}$ can also be found such that

$$[I]\ \{\Delta p\}_{k}^{n+1} = \{ F(u_{k-1}^{n+1}, v_{k-1}^{n+1})\} \tag{3.12}$$

3.2.3 Modified Method of Mark and Cell

After using the explicit method in the momentum equation and substituting into continuity equation, the $\{\Delta p\}$ can be obtained by solving the following equation

$$[K_2]\ \{\Delta p\}_{k}^{n+1} = \{ F(u_{k-1}^{n+1}, v_{k-1}^{n+1})\} \tag{3.13}$$

3.2.4 Semi-implicit Method for Pressure-linked Equation

The method was originated by Patankar and his collaborators [Patankar, 1980], and was used very popularly in the finite difference method in computational fluid mechanics and heat transfer. Several refinements or improvements were made since it first introduction as SIMPLE [Patankar & Spalding, 1972]. The remedies include SIMPLER [Patankar,1980],SIMPLEC [Van Doormaal & Raithby,1984]. It is modified to fit the finite element formulation in this investigation. In general, an expression similar to Eq.(3.13) is obtained as follows:

$$[K_3]\ \{\Delta p\}_{k}^{n+1} = \{ F(u_{k-1}^{n+1}, v_{k-1}^{n+1})\} \tag{3.14}$$

It is very interesting to notice that the correction of pressure, $\{\Delta p\}$,in general is very similar as far as the above-mentioned methods are concerned. They all depend upon the known velocity and pressure fields. However, the iteration is also heavily dependent on the multiple of the matrix to $\{\Delta p\}$. The efficiency of the iteration is determined by the inversion of the matrix. It is found that the semi-implicit method for pressure-linked equation in general yields the best results in this study, since it provides the best physical linkage between pressure and velocity fields.

As will be obvious later, the solution of the velocity matrix system in the pressure-velocity correction method is the most regular and easiest one among the three methods. The difficulty encountered in the penalty function method is the annoyance with the admissible elements and the rule of selective reduced integration. On the other hand, for the pressure-velocity coupling method, a good algorithm to handle the pivoting process in the matrix inversion is imperative.

3.3 *Pressure-Velocity Coupling Method*

In this method, mixed shape functions of velocity and pressure are introduced as follows:

$$u = \sum_{i=1}^{n} N_i u_i \ , \quad v = \sum_{i=1}^{n} N_i v_i \ , \quad p = \sum_{i=1}^{m} M_i p_i \qquad (3.15)$$

After the Galerkin finite element formulation, the continuity and the Navier-Stokes equations are reduced to the following

$$\begin{bmatrix} [M] & [0] & [0] \\ [0] & [M] & [0] \\ [0] & [0] & [0] \end{bmatrix} \begin{Bmatrix} \{\dot{u}\} \\ \{\dot{v}\} \\ \{\dot{p}\} \end{Bmatrix} + \begin{bmatrix} [C_{11}(u)] & [C_{12}(u)] & [B_1] \\ [C_{21}(v)] & [C_{22}(v)] & [B_2] \\ [A_1] & [A_2] & [0] \end{bmatrix} \begin{Bmatrix} \{u\} \\ \{v\} \\ \{p\} \end{Bmatrix}$$

$$+ \frac{1}{Re} \begin{bmatrix} [D] & [0] & [0] \\ [0] & [D] & [0] \\ [0] & [0] & [0] \end{bmatrix} \begin{Bmatrix} \{u\} \\ \{v\} \\ \{p\} \end{Bmatrix} = \begin{Bmatrix} \{R_u\} \\ \{R_v\} \\ \{0\} \end{Bmatrix} \qquad (3.16)$$

where $[A_1]$,$[A_2]$ are continuity matrices, which can be reduced to the transpose of the pressure force matrix $[B_1]$ & $[B_2]$ by an appropriate choice of shape functions and integration by parts.

It is noted that in general the mixed shape functions with velocity higher order than pressure must be used, so that no over-constraint of the systems occurs. If this rule is violated, it may induce the undesirable "checkerboard" syndrome of spurious oscillation in pressure [Carey and Oden, 1986]. Selection of admissible elements [Young and Sun, 1988] and integration by parts for the pressure term are the two most vexing issues in this formulation. Typical elements are classified into two groups: the Taylor-Hood family of elements with continuous pressure and the Crouzeix-Raviart family of elements with discontinuous pressure [Cuvelier et al,1986]. The occurence of pressure "checkerboard" syndrome is believed to be the difficulty of the imposition of the boundary conditions of the pressure, which in general is not known a priori in complicated flow fields. It is demonstrated in this study that the rule of integration by parts plays a vital role in the specification of boundary conditions of pressure. Unless the boundary conditions of pressure is definitely sure, the pressure gradient is recommended to be used directly,so that there is no additional pressure boundary conditions appear. Furthermore, in this case, the constant pressure mode can not be adopted.

Common mixed interpolation functions used are Q8-Q4 elements, it is verified that whether the integration by parts is taken or not will yield the same results, if the boundary conditions of pressure are well imposed in both cases.

From Eq.(3.16) it is observed that the coupling or interaction with velocity makes the matrix system nonpossitively definite. Obviously it is imperative that a partial pivoting equation solver is needed to circumvent this handicap. The frontal solution program [Irons, 1970] was introduced in this study.

As far as three-dimensional admissible elements are concerned, there are not many at this moment. According to Cuvelier et al

[1986] and Fortin [1981], the simplest elements are H14 for velocity and H1 for pressure for hexahedronal elements or H27 for velocity and H8 for pressure. However, in this investigation,H20 for velocity and H8 for pressure are adopted [Young and Sun, 1988]. It is further noticed that for H1 element the pressure is constant, while for the H8 element the pressure is trilinear.

From Eq. (3.2), (3.7), and (3.16), the primitive variable formulation reduced the whole systems to the systems of nonlinear ordinary differential equations, no matter whether the penalty function method, or the pressure-velocity correction method, or the pressure-velocity coupling method is used. To solve these transient, highly nonlinear matrix equations, efficiently iterative equation solvers are inevitable. Semidiscrete approximation of time integration scheme with a weighting factor is used to cope with the transient problems. As far as nonlinearity is concerned, the linear schemes of the Picard, and modified Newton-Raphson as well as the quadratic scheme of the Newton-Raphson iterative approaches are exploited.

4. *MODEL APPLICATIONS*

To test the feasibility of the present mathematical models, some steady and unsteady two-dimensional, internal and external flow problems will be illustrated. Typical examples will cover both the analytic (exact) as well as approximate solutions obtained by other alternatives, such as Couette flows, channel flows, circular eddy flows, square cavity flows, recirculating flows, and flows past a circular cylinder. This paper will emphasize on two benchmark flow problems, the effect of the Reynolds number on flow instabilities of square cavity flows and the vortex shedding of a Karman vortex street of flow past a circular cylinder.

4.1 Couette Flow

This is the most simple flow field for a steady-state two-dimensional flow. Due to the simplicity and linearity of flow characteristics, an analytic solution was found to be [Schlichting, 1968]

$$u = - y^2 + 2.75 y - 0.5 \qquad (4.1)$$

Fig.1 shows the comparison between the analytic and finite element solutions. It is conspicously seen that the two results are almost identical. Furthermore, the three options of primitive variable formulations all yield the same results. Since there is a reverse flow, it is reasoned that the pressure gradient is adverse, i.e. $\partial p/\partial x < 0$.

4.2 Channel Flow

The developing channel flow (or the entry channel flow) is another typical steady-state two-dimensional flow problem which also attracted previous numberical modellers. Yamada et al [1975] have found the solutions from the variational finite element approach. Fig.2 shows the comparison between the Yamada et al [1975] results with present solutions. It is very clear that there is very little deviation from each other except the pressure distribution in the entry zone where the gradient is very big. Also shown in Fig.3 are the distributions of pressure, velocity, streamline, and vorticity. The pressure near the entry corner is singular,so that the variation of pressure near those regions behaves very drastically. This physical characteristic is also reflected from the vorticity and velocity fields.

4.3 Circular Eddy Flow

The circular eddy flow is a very interesting problem to be introduced, since it provides exact solution in the Stokes regime, namely for Re = 0. For the Stokes flow, the exact solution is given by [Hu, 1987] from the Green's function approach :

$$
\varphi = \begin{cases} -\dfrac{(1-r^2)}{2\pi}\left[\tan^{-1}\dfrac{(1-r)\tan\frac{\theta}{2}}{(1+r)} + \tan^{-1}\dfrac{(1-r)\cot\frac{\theta}{2}}{(1+r)}\right], & -\pi<\theta<0 \\ \dfrac{(1-r^2)}{2\pi}\left[\tan^{-1}\dfrac{(1+r)\tan\frac{\theta}{2}}{(1-r)} + \tan^{-1}\dfrac{(1+r)\cot\frac{\theta}{2}}{(1-r)}\right], & 0<\theta<\pi \end{cases} \qquad \text{.......... (4.2)}
$$

or given by Burggraf [1966] from the method of separation of variables.

Comparison between the two exact solutions with the present study revealed that the three results are not readily distiguishable .Fig.4 depicts the distribution of velocity, streamline, pressure, and vorticity for Re $\approx$ 0. It is also clear for the Stokes flows the inertia force is completely negligible. In this situation, the pressure and vorticity fields satisfy the Cauchy-Riemann equations, and consequently the two families of lines are orthogonal. Flow fields are symmetric with respect to the line through the geometric center. As Re increases, the down flows enhance since the inertia becomes dominant.

Fig.5 is the flow characteristics for Re = 400. As Re increases the vorticity center will move downward and downstream and then back again to the geometric center wherein an inviscid core developed. At this moment,the viscosity effect is confined to a very thin boundary layer near solid boundaries. However, there exists an inviscid core in most portion of the circular eddy,which behaves like a rigid-body rotation or a forced vortex. This founding was also obtained by other approach, such as the boundary element method [Camp and Gipson ,1987].

4.4 Square Cavity Flow

Due to the simplicity of geometry and intrinsic features of a physical nature, the square cavity flow has attracted so many numerical or analytic investigators. This is the most fascinating example of internal flows in the realm of computational fluid mechanics, since the nonlinear instabilities will be revealed when Re increases from small to large numbers.

In the Stokes flow ($Re \rightarrow 0$) which corresponds to a very low Reynolds number, the circulating gyre was dominated by the viscous force, and the flow fields are symmetric along the center line ($x = 1/2$) of the cavity, as shown in Fig.6, which illustrates the distribution of velocity, streamline, vorticity contours, and pressure contours. As in the circular eddy flow, the pressure and vorticity contours are orthogonal to each other, as is evident from Fig.6.

When Re is increased, the inertia begins to play an important role. As a consequence, the vortex center has shifted downstream, pressure and vorticity distribution get more complex, and corner eddies start to appear. As Re increases to 400, the above-mentioned physical characteristics become more conspicous. The transient state of the set-up of the circulation of the cavity is depicted in Fig.7. In particular, the vortex center first moves downstream, and penetrates deeply into the cavity, and finally moves back to the geometric center of the cavity. This illustrates the fact that the viscous force is confined only to the boundary layer, and most of the region away from the boundaries behaves like an inviscid core of a vortex, as mentioned by Burggraf [1966].

The formation of corner eddies, as pointed out by Moffatt[1964] is another very strange phenomenon in the square cavity simulation. It is seen that the nonlinearity (high Re) and corner separation are the two major mechanisms to form the secondary currents. Comparison of the circular eddy flow and square cavity flow demonstrates that at Re = 400, there are a big lower right-hand secondary eddy and a small lower left-hand secondary eddy appear. However, no secondary eddies are observed for the circular cavity even for Re = 400 on the other hand. This illustrates the conjecture that for lower Re the corner effect is the dominant force as far as formation of secondary eddies or currents is concerned.

In the recirculating flows, it will be shown that the topography effects will play the same role in the circulating patterns and number of circulating gyres. As Re increases further, the number of secondary eddies will increase. It is observed that as many as seven secondary eddies will be formed in the upper left, lower right, and lower left corners when Re approaches 20,000 or higher for a square cavity. This also reflects that the inertia force is another trigger factor in the formation of secondary eddies. Unfortunately there is no direct comparison of the number and location of the secondary eddies for both the circular cavity and square cavity for higher Re. It is further interesting to mention that the strength of circulating gyres for primary cell and other secondary cells are several orders magnitude different.

Table 1 provides the summary of the preliminary results of the highest Re ever accomplished with respect to each scheme. Besides, some authoritative literature in this effort is also included for comparison. It is recapitulated that all three FEM schemes have the capabilities to simulate the flow characteristics of lower Re regimes. Nevertheless, the deviation among them is aattributed to different schemes and mesh sizes. However, only the pressure-velocity coupling method is able to perform the much higher Re flows .Fig.8 illustrates the distribution of streamline, total pressure, vorticity contour, and velocity for Re = 10,000.

4.5 Recirculating Flows

So far we have concentrated on simple geometries except with case of the circular eddy flow. As envisaging before, the most powerful capability of the finite element analysis is to handle irregular boundaries. To demonstrate this, a recirculating water basin is introduced. Fig.9 shows the distribution of streamlines of a recirculating flow with irregular topography at Re = 400. As compared to the circulating gyres of circular eddy flow and square cavity flow at the same Re, it is evident that there is only one major circulating gyre in the circular eddy flow, one primary circulating gyre and two minor corner secondary eddies in square cavity flow. However, in the irregular topography, as realized in a natural lake or reservoir, there are three equivalent circulating vortices which coexist in the enclosed water basin. The formation of the horizontal gyres is attributed to the shallow water environment of the recirculating basin.

This illustrates that the effect of topography plays a vital role in the circulating patterns and number of circulating gyres. It is further demonstrated that for Re = 200, only two circulating cells are formed. These characteristics are the most controversial arguments in the literature of lake circulation research. Different circulating gyres will induce the opposite currents, and thereby cause errors in the transport of the parameters of water qualities, such as pollutants, etc.

4.6 Flow Past A Circular Cylinder

After several internal flow problems are considered, the only external example to be explored is the uniform flow over a circular cylinder. The Reynolds numbers of Re = 10, 20, 30, 40, and 100 were simulated. If the Re is too small, singular solutions may appear due to the Stokes' paradox. It is concluded that the computed physical properties, such as the drag coefficient, separation angle, and length of standing eddy, are all in good agreement with existing numerical or experimental results for steady-state solution covering the range of Re = 10, 20, 30, and 40.

The simulation also demonstrates that when Re increases angle of minimum pressure decreases, and pressure increases. It is also found that the higher the Re, the angle of the separation point (where vorticity is zero) is smaller, and the variation of vorticity is larger. For detailed discussion of these salient characteristics, see Young and Ni [1989].

For transient and higher Re cases, say Re = 100, the vortex shedding behind the circular cylinder, a well known phenomenon of the Karman vortex street, emerges as shown in Fig.10. An oscillating frequency of Strouhal number S = 0.163 was obtained. This number is found to be very comparable to other studies, as shown in Table 2 of Young [1988]. The formation, growth, separation, and downstream transport of the vortex eddies are best illustrated by Fig.11. From the characteristics of vortex shedding, the coefficients of drag are found equal when the alternating eddy is either in the upper or lower portion of the cylinder. The vortex shedding of the Karman vortex streets is a conspicous characteristic of the bifurcation of the hydrodynamic instability of the Navier-Stokes equations.

5. *FURTHER EXTENSIONS*

With the assumptions of neglect of density stratification and free surfaces, the model has been applied to the above homogeneous fluids and rigid-lid surfaces. In practical applications of this methodology to the hydraulic engineering problems, such as treatment of the simulation of stratified reservoir dynamics, hydrothermal modeling, free surface flows, and hydraulics of sediment transport, three-dimensional flow simulation, etc, the above-mentioned schemes must be further extended to cover those special features. Due to the lack of space, only very brief statements will be made, and for more details, appropriate references will be cited.

5.1 Three-dimensional Cavity Flow [Young and Sun,1988]

Extension of the two-dimensional cavity flow is simple in concept, however, the numerical implementation from two-dimensions to three-dimensions was found not trivial. The major difficulties lie in the drastic increase of the degrees-of-freedom in flow field and therefore the solution algorithm becomes more and more difficult. Furthermore, the boundary integration and the associated boundary conditions become more sophisticated and it is not obvious how they should be imposed.Fig.12 shows the flow field of a three-dimensional

Stokes flow($Re \to 0$)problem. The velocity profile along the symmetric surface ($Z = 0.5$) reflects the two-dimensional characteristics of Fig. 6, as obtained from section 4.4. The three-dimensional nature is very crucial to the simulation of hydrodynamic instability as well as turbulent flows, since any vortex dynamics can only be visualized by three-dimensional consideration, such as vortex stretching and vortex eddies. Nevertheless, the simulation of three-dimensional high Re flows is still very limited and therefore more attention and effort are needed.

5.2 Sediment Basin Simulation [Young and Chu,1987]

The simulation of sediment basin is another typical extension of the model, since after the flow field is obtained, the concentration of the sediment is governed by the following sediment transport equation :

$$\frac{\partial c}{\partial t} + u\frac{\partial c}{\partial x} + (v - v_s)\frac{\partial c}{\partial y} = \frac{1}{ReSe}\nabla^2 c \qquad (5.1)$$

where c is the concentration, Se is the Schmidt number, and v_s is the settling velocity of the particle of the sediment.

Using the arrangement of baffle partitions, the design of settling tanks in the sedimentary basins has been successfully accomplished to satisfy the engineering standards in the fields of hydraulic or sanitary engineering works. Fig.13 shows the velocity and concentratioin distribution of a three baffles in a typical sediment basin. By appropriate partition, the path of the sediment particles can be elongated so that the trap efficiency of the sediment particles will be enhanced. The potential of using finite element technique to design the sediment tanks is very high, since it is shown that the size, location, number of the baffles will influence the flow field and its associated concentration distribution. The versatilities of FEM are the most suitable tools to do the sensitivity analysis of engineering layout, so that a most efficient sediment basin can be realized.

5.3 Stratified Reservoir Dynamics [Young and Lin,1987]

The dynamics of homogenous reservoir (or lake) circulation is easily handled by the extension of the previous examples, such as recirculating flow, where the effect of topography is vividly described. When the reservoir is stratified, either by the temperature, or by the concentration of the sediment, as in the case of a density current, the circulating patterns and the circulating gyres become very complicated. For illustration, if the density stratification is due to the thermal mechanism, then the governing equations are augmented to include the heat equation and equation of state as follows:

$$\frac{\partial T}{\partial t} + u\frac{\partial T}{\partial x} + v\frac{\partial T}{\partial y} = \frac{1}{RePr}\nabla^2 T \tag{5.2}$$

$$\rho = \rho_0 [1 - \beta (T - T_0)^2] \tag{5.3}$$

where T is the temperature, Pr is the Prandtl number, ρ and ρ_0 are the ambient and reference density respectively, T and T_0 are the ambient and reference temperature respectively, and β is the coefficient of volumetric expansion.

A transient two-dimensional hypothetical stratified reservoir with irregular topography is simulated for different wind and thermal loadings. The results reveled that by the primitive-variable finite element formulation, the characteristics of circulating gyres and the thermal structures, such as the salient features of the formation, maintenance, and erosion of the thermocline of the reservoir dynamics can be well predicted. Fig.14 illustrates the formation of multiple thermocline in the epilimnion and hypolimnion of a stratified reservoir.

It is concluded that a reservoir will go through the seasonal heating and cooling cycles, and become stratified or homogeneous circulation, when the wind shear stress is imposed, or when the reservoir is under operation. By adjusting the approximate loading conditions, it is demonstrated that the major characteristics of the reservoir dynamics can be simulated by this model.

5.4 Hydrothermal Modeling [Young and Cheng,1988]

Hydrothermal model is very important to the control of thermal pollution in a body of water. Theoretically, the governing equations are the same as those of the stratified reservoir dynamics of sec. 5.3. However, due to the weakly stratified interaction, the flow and thermal fields can be decomposed each other and become uncoupled. Therefore, the velocity field is first computed, and then the calculated velocity solutions are used to solve the advection-diffusion equation for the temperature. The process is very similar to that of the Sec. 5.2 sediment basin simulation. In addition, if there are observed data available,such as in the temperature monitoring system of waste heat dissipation of power plant through cooling ponds, the Kalman filter algorithm can be incorporated to identify the physical parameters, such as the parameters controling the heat transfer of air-water interface, as well as the eddy diffusivities. The details appear in Young and Cheng [1988].

Fig. 15 is the temperature distribution of a cooling lake simulated by the finite element analysis, with and without taking the Kalman filter algorithm into consideration. The improvement of the result with using the Kalman filter is very conspicuous. The reason lies in the consideration of the uncertainties of model structures, parameters,and measurements in the extended Kalman filter algorithms . Advantages of application of combination of the Kalman filter and the finite method element to the hydrothermal modeling is demonstrated.

5.5 *Free Surface Flows [Young and Liu,1988; Young and Lin, 1988]*

The inclusion of the effect of a free surface into the flow regime is a very annoying task in the computational hydraulics. There are two ways to treat free surface flows in general, the first one is to treat the free surface through the unknown boundary conditions, and the other is to take the free surface from the viewpoint of governing equations, such as in shallow water theory [Stoker, 1957],or the concept of volume of fraction (SOLA-VOF)[Nichols et al, 1980]. In the former,the free surface boundary is a moving boundary, and is constrainted by the kinematic and dynamic boundary conditions. In the latter, the free surface is reformulated as the field variable, therefore relieves the difficulty of unknown moving boundary condition, and also transform the original governing equations.

In his study, for the first case, a free surface boundary is mapped into a fixed domain by a coordinate system transformation technique. After the transformation the governing equations of the two-dimensional viscous incompressible free surface flows are discretized by the finite element analysis, since now the free surface boundaries become fixed. The model was used to test some two-dimensional viscous incompressible free surface flow fields, such as propagation of a moving bore due to impulse force;wind-driven circulation of a cavity with the consideration of free surface effects;as well as the viscous effects on the damping of the free oscillation of a sloshing tank. Fig. 16 depicts the velocity distribution of a square cavity, the effect of the free surface to the flow field is vividly visualized from the picture. In general, the free surface might play an important role in the lake or reservoir circulation, just as the topography does.

In the second case, one-dimensional and two-dimensional shallow water equations, or the so called de Saint Venant equations are used for the governing equations. The free surfaces will become the unknow variables, thereby will be solved by the standard finite element method. Fig.17 illustrates the wave propagation of a triangular flood hydrograph through an open channel. The flood wave transports from the upstream to the downstream by the appropriate wave speed, and in the meantime, attenuates gradually the flood peak along the downstream reach. The free surfaces of the water profile are also obtained accurately. Comparison of the existing literature reveals that the results obtained from the finite element approach is very close.

6. *CONCLUSION AND RECOMMENDATION*

Formulation of incompressible viscous flows using the primitive parameters as the field variables by the three finite element solution algorithms, namely the penalty function method, the pressure-velocity correction method, and the pressure-velocity coupling method are briefly reviewed. The applications to both internal and external flow regimes, which represent the typical computational fluid dynamics problems since they are governed by the continuity and the Navier-Stokes equations, are well demonstrated in this study.

In the penalty function method, the pressure is eliminated from the momentum equation by introducing a preassigned large penalty parameter. Seven different elements, T3, T3M, T6, Q4, Q4M, Q8 and Q9 were employed to study the convergence and stability of the element behaviors in coping with the reduced integration rules. It was found that the elements make little difference in the lower Reynolds-number regime. However,the Q4 dominates the accuracy among the seven elements as long as higher Reynolds-number flows are considered. It is evident that the admissible elements play a vital role in the penalty function method in high Reynolds-number flows.

For the pressure-velocity correction method, the velocity fields are solved iteratively from the momentum equation by the preguessed pressure, the pressure is then corrected successively by the continuity equation. Several pressure correction schemes, such as limited compressibility, weighting value method, modified method of mark and cell, and semi-implicit method for pressure-linked equation are briefly discussed. Due to the nonlinear nature of equations themselves, two iterative methods, the Newton-Raphson and modified Newton-Raphson schemes are also addressed and compared to each other.

So far as the pressure-velocity coupling method is concerned, the traditional finite element velocity-pressure algorithm is used. Special treatment of the equation solvers for the velocity and pressure fields is mentioned. However, due to the non-positively definite matrix system, a partial pivoting equation solver is indespensable, thus makes the algorithm very tedious to cope with. In addition, the mixed shape functions with velocity higher order than pressure are recommended.

This paper has solved some steady and unsteady two-dimensional internal and external flow problems. Typical examples cover the illustrations of Couette flows, channel flows, square cavity flows, circular eddy flows, recirculating flows, and flows past a circular cylinder. The effect of the high Reynolds number to flow instabilities and vortex formations is emphasized in particular. The advantages and disadvantages for these three primitive-variable formulations for solving the high Reynolds-number flows are elucidated by the explanation of case studies.

Practical applications of this methodology to hydraulic engineering problems are also delineated. Typical examples cover the the treatment of the simulation of the stratified reservoir dynamics, hydrothermal modeling, free surface flows and sediment basins, etc. Extention to three-dimensional flow is also undertaken, although only in very simple flow field due to the limitations of computer capacity.

The applications of finite element analysis to computational fluid dynamics problems have made positive contribution, as visualized from the present review. It is by no menas that this methodology is near complete. On the other hand, it is fair to say that finite element computational fluid mechanics is still in its infancy and needs much efforts and attention. The potential of research is still very high, and needs more researchers to devote to. The following are some suggestions for the further works as far as applications of finite element methods to computational fluid dynamics problems are concerned:

1. Search for the new "admissible elements" and small "discretization systems" from the viewpoint of fluid mechanics. The drawback of the conventional finite element is to deal with the very large matrix systems, in particular for three-dimensional flows. Much works are needed to concentrate on the transform of large system to the small system so that personal computers (PC) or mini computers are able to do the solution instead of supercomputers. This may cover the mass lumping technique, multiple level discretization, multiple layer discretization, adaptive grid system, and the associated new admissible elements, etc.

2. Success in the high Reynolds-number computation by the finite element formulation is in progress. However, very high Reynolds number flows will become turbulent. The hydrodynamic transition of course is due to the nonlinear bifurcation of the hydrodynamic instability. To take care of such phenomena, a very comprehensive finite element algorithm is indespensable. In particular, the nonlinear term of advection always yields numerical instability and convergence problems. Therefore, a search for new algorithms to guarantee the global convergence or large radius of convergence is very desirable. A very promising way is to introduce the operator splitting scheme to separate the advective and diffusive dominated flows so that the physical characteristics of hyperbolic and parabolic partial differential equations can be incorporated into the numerical integrations.

ACKNOWLEDGEMENTS

Work described in this paper was partially supported by the National Science Council of the Republic of China under the Research Grants NSC-76-0410-E002-08, NSC-77-0410-E002-12, and NSC-77-0410-E002-32. It is greatly appreciated. The writer would like to express his sincere gratitude and appreciation for the excellent computer works from Messrs. C.M. Hunag, Q.H. Lin, C.H. Wang, W.B.Ni, C.M. Chu, C.C. Sun, Y.S. Liu, Y.K. Lin, and K.S. Cheng.

REFERENCES

1. Baker, A.J.,1983, "Finite Element Computational Fluid Mechanics", McGraw-Hill, N.Y.

2. Brebbia, C. A., J.C.F. Telles, and L. C. Wrobel, 1984, "Boundary Element Techniques", springer-Verlag, Berlin, Heidelberg.

3. Burggraf, O.R.1966, "Analytic and Numerical Studies of Structure of Steady Separated Flows", J. Fluid Mech. 24, 131-151.

4. Camp, C.V., and G.S. Gipson, 1987 "A boundary element method for viscous flows at low Reynolds number", in Bouondary Elements IX, Vol. 3 : Fluid Flow and Potential Applications, Editored by, Brebbia, C.A., W.L.Wendland, and G.Kuhn, Springer-Verlag, Berlin, Heidelberg, 420-431.

5. Carey, G.F.,& J.T. Oden, 1986,"Finite Elements : Fluid Mechanics, Vol VI, Prentice-Hall, N.J.

6. Cuvelier, C., A. Segal, and A.A. Van Steenhoven, 1986, Finite Element Methods and Navier-Stokes Equations, Reidel Publishing Co., Dordrecht, Holland.

7. Fortin, M. 1981, "Old and new finite elements for incompressible flows", Int. J. Numer. Methods Fluids, 1, 347-364.

8. Hu, T.Y. 1987,"Analytic solutions of some two-dimensional viscous incompressible flow problems", MS Thesis, National Taiwan University, Taipei.

9. Irons, B.M. 1970, "A frontal solution program for finite element analysis", Int. J. Numer. Methods Eng. 2, 5-32.

10. Moffatt, H. K., 1964, "Viscous and resistive eddies near a sharp corner", J. Fluid Mech., 18, 1-18.

11. Nichols, B.D., C.W. Hirt, and R.S.Hotchkiss, 1980, "SOLA-VOF : A solution algorithm for transient fluid flow with multiple free boundaries", Los Alamos Scientific Laboratory, Report, LA-8355.

12. Patankar, S.V., 1980, "Numerical Heat Transfer and Fluid Flow", McGraw-Hill, N.Y.

13. Patankar, S.V., and D.B. Spalding, 1972 "A calculation procedure for heat, mass and momentum transfer in three-dimensional parabolic flows", Int. J. Heat Mass Transfer, 15, 1787-1806.

14. Roache, P. J. 1972, "Computational fluid Dynamics", Hermosa Publishers, Albuquerque, N.M.

15. Schlichting, H. 1968, "Boundary Layer Theory", 6th ed., McGraw-Hill, N.Y.

16. Stoker, J.J. 1957, "Water Waves", Wiley-interscience, N.Y.

17. Van Doormaal, J.P. and G.D. Raithby, 1984,"Enhancements of SIMPLE method for predicting incompressible fluid flows", Numer. Heat Transfer, 7, 147-163.

18.Yamada, K., Y.Ito, T. Yokouchi, T. Tamano, and T. Ohtsubo, 1975, "Finite element analysis of steady fluid and metal flow", in Finite Element in Fluids", Vol.1, Wiley, N.Y., 73-94.

19.Young, D.L. 1988, "Primitive variable solutions of incompressible viscous flows", Proceedings of the International Conference on Computational Methods in Flow Analysis, Okayama, Japan, 422-429.

20.Young, D.L. and K.S. Cheng, 1988, "Application of kalman filter and finite element to hydrothermal modeling", proceedings of the Third International symposium on Refined Flow Modeling and Turbulence Measurements, Tokyo, Japan, 345-352.

21.Young, D.L. and C.M. Chu, 1987, "Finite element simulation of rectangular sedimentation basins", Proceedings of the First Conference on the Application of Computers to Civil and Hydraulic Engineering, Chungli, Taiwan, 161-167.

22.Young, D.L., and Q.H. Lin, 1986, "Application of finite element method to 2-D flows",Proceedings of the Third Naitonal Conference on Hydraulic Engineering, Taipei, 223-242.

23.Young, D.L. and Q.H. Lin, 1987, "Finite element modeling of reservoir dynamics", Proceedings of 22th IAHR Biennial Congress, Lausanne, Switzerland, Technical Session C1, 76-80.

24.Young, D.L., and Y.K. Lin, 1988, "Application of finite element method to channel network flows",Proceedings of the 12th National Conference of Theoretical and Applied Mechanics, Taipei, 1-8.

25.Young, D.L., and Y.S. Liu, 1988, "Finite element calculation of free surface flows", Proceedings of 10th Conference on Ocean Engineering in the Republic of China, Taipei, 629-636.

26.Young, D.L., and W.B. Ni, 1989, "Penalty finite element applications to flow problems", in Recent Advances in Computational

Fluid Dynamics, Lecture Notes in Engineering, Springer-Verlag, Berlin, 484-507.

27. Young, D.L., and C.C. Sun, 1988, "Study of primitive variable finite element analysis of 2D, 3D viscous flows", Proceedings of the 12th National Conference of Theoretical and Applied Mechanics Taipei, 45-54.

28. Young, D.L., C.M. Huang, and Q.H. Lin, 1986, "Application of finite element method to 2-D circulating flows", Proceedings of Symposium on Circulating Water Channel in the Republic of China, Taipei, 45-56.

Table 1 Comparison of $_c$, Ω_c and p_c Parameters with others for Square Cavity Flow

Re	Methods	$-{}_c$	$-\Omega_c$	$-p_c$
0	(1)18x18 Q	0.0994	3.20	0
	(2)12x12 T	0.0971	2.877	0
	(3)21x21 Q	0.0973		0
	(4)40x40 D	0.100	3.20	0
100	(1)18x18 Q	0.1007	3.20	0.0927
	(2)16x16 T	0.1015	3.0887	0.0901
	(3)24x24 T	0.0989		0.084
	(4)40x40 D	0.1015	3.14	0.0905
	(6)129x129 D	0.1034	3.1665	
	(7)121x121 D	0.1033	3.182	
400	(2)16x16T	0.1073	2.1894	0.0974
	(3)34x40 Q	0.11	2.26	0.1004
	(4)40x40 D	0.1017	2.142	0.0896
	(6)257x257 D	0.1139	2.29	
	(7)141x141 D	0.1297	2.281	
1000	(1)18x18 Q	0.107	2.0	0.0928
	(2)16x16 T	0.1038	1.6605	0.0851
	(6)129x129 D	0.1179	2.049	
	(7)141x141 D	0.11603	2.026	
5000	(1)40x40 Q	0.119	1.90	0.11
	(3)40x50 Q	0.122	1.94	0.1175
	(5)50x50 D	0.0861	1.29	
	(6)257x257 D	0.119	1.8602	0.11
10000	(1)40x40 Q	0.1184	1.90	0.11
	(5)50x50 D	0.0873	1.21	
	(6)257x257 D	0.119731	1.88082	
	(7)180x180 D	0.10284	1.622	
	(8)50x50 Q	0.101		0.064
15000	(1)50x50 Q	0.12	1.88	0.11
17500	(1)50x50 Q	0.12	1.88	0.11
20000	(1)50x50 Q	0.12	1.87	0.11
	(5)50x50 D	0.0982	1.35	

Remarks:

Methods:
(1)Pressure-Velocity Coupling Method
(2)Pressure-Velocity Correction Method
(3)Penalty Function Method
(4)Finite Difference Method [Burggraf, 1966]
(5)Finite Difference Method [Nallasamy and Krishna Prasad,1977]
(6)Finite Difference Method [Ghia et al, 1982]
(7)Finite Difference Method [Schreiber and Keller, 1983]
(8)Modified Finite Element Method [Gresho et al, 1984]
T: Triangular Element
Q: Quadrilateral Element
D: Finite Difference Method
18x18: Mesh Grid Size
p_c: Pressure at Vortex Center

Table 2 Comparison of C_D , C_L and S Parameters with Others of Re=100 for Flow over Circular Cylinder

	Jordan and Fromm	Patel	Smith and Brebbia	Gresho et al	Young
C	1.28	1.29	1.43	1.27	1.42
			Mean		
C	±0.5	±0.5	±0.5	±0.6	±0.5
S	0.160	0.133	0.166	0.161	0.163

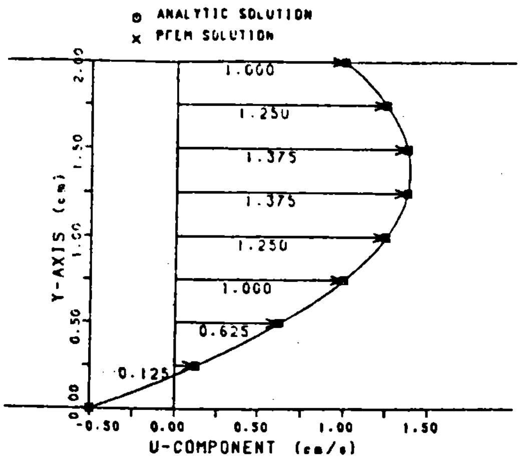

Fig. 1 : Couette flow simulation.

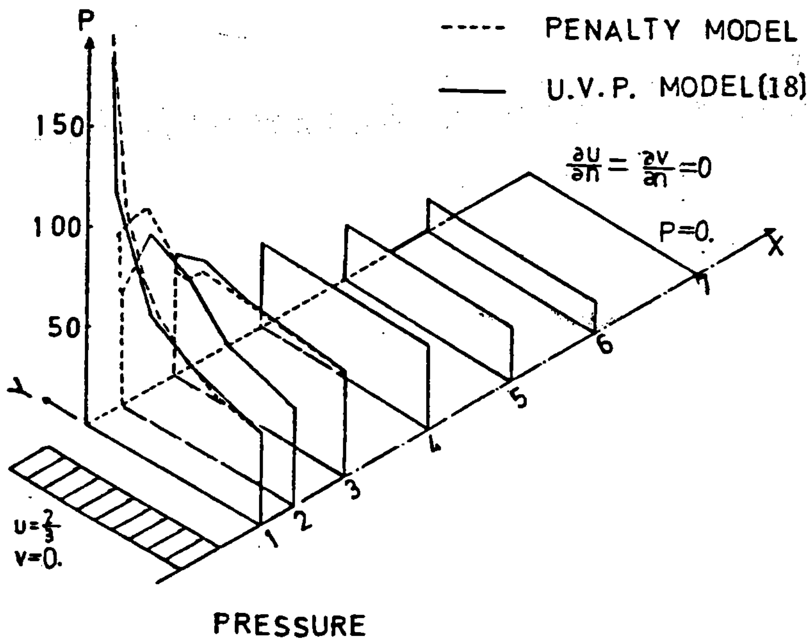

Fig. 2 : Comparison of pressure distributionof Yamada et al & Present study.

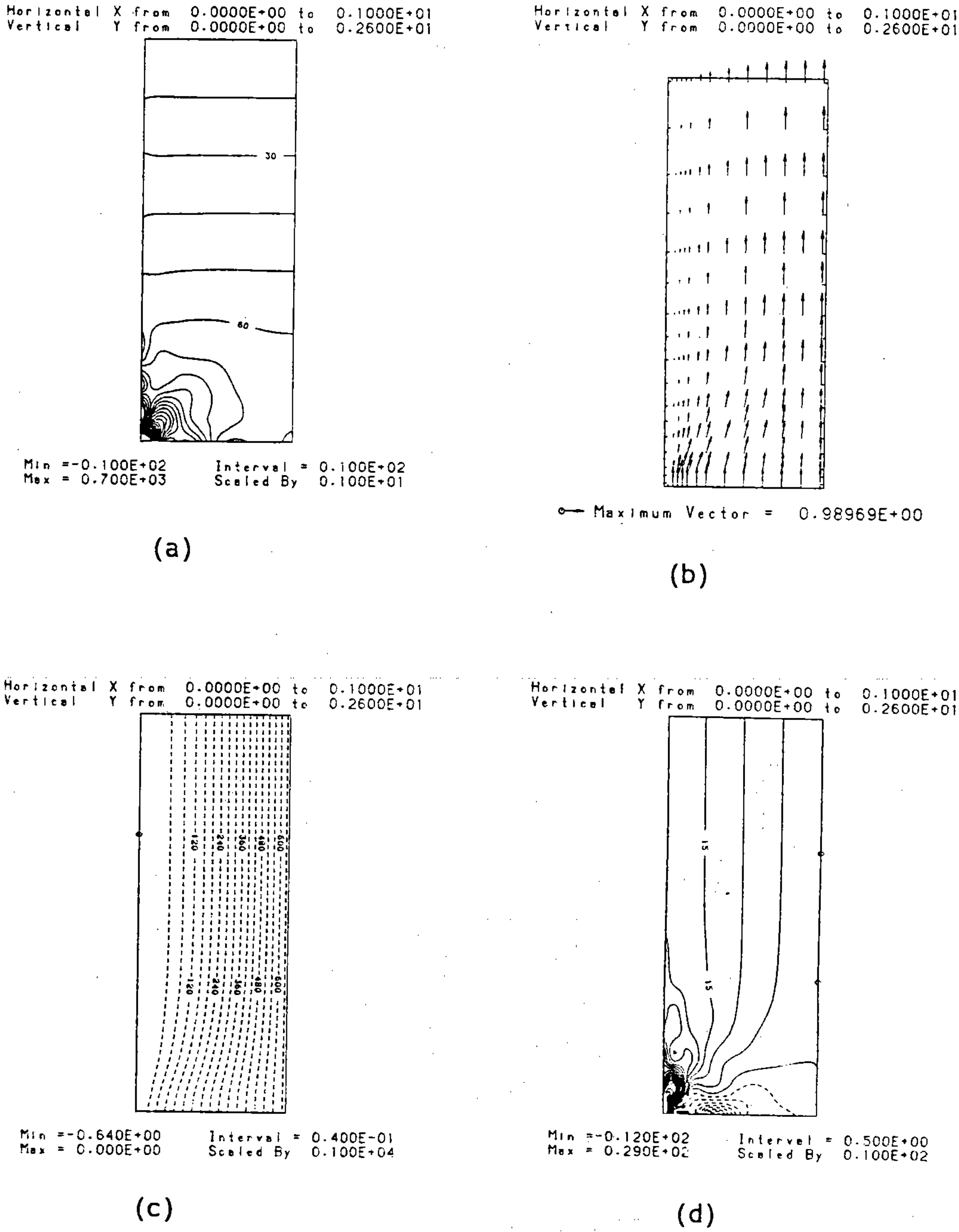

Fig. 3 : Distribution of pressure, velocity, streamline, and vorticity of an entry channel flow.

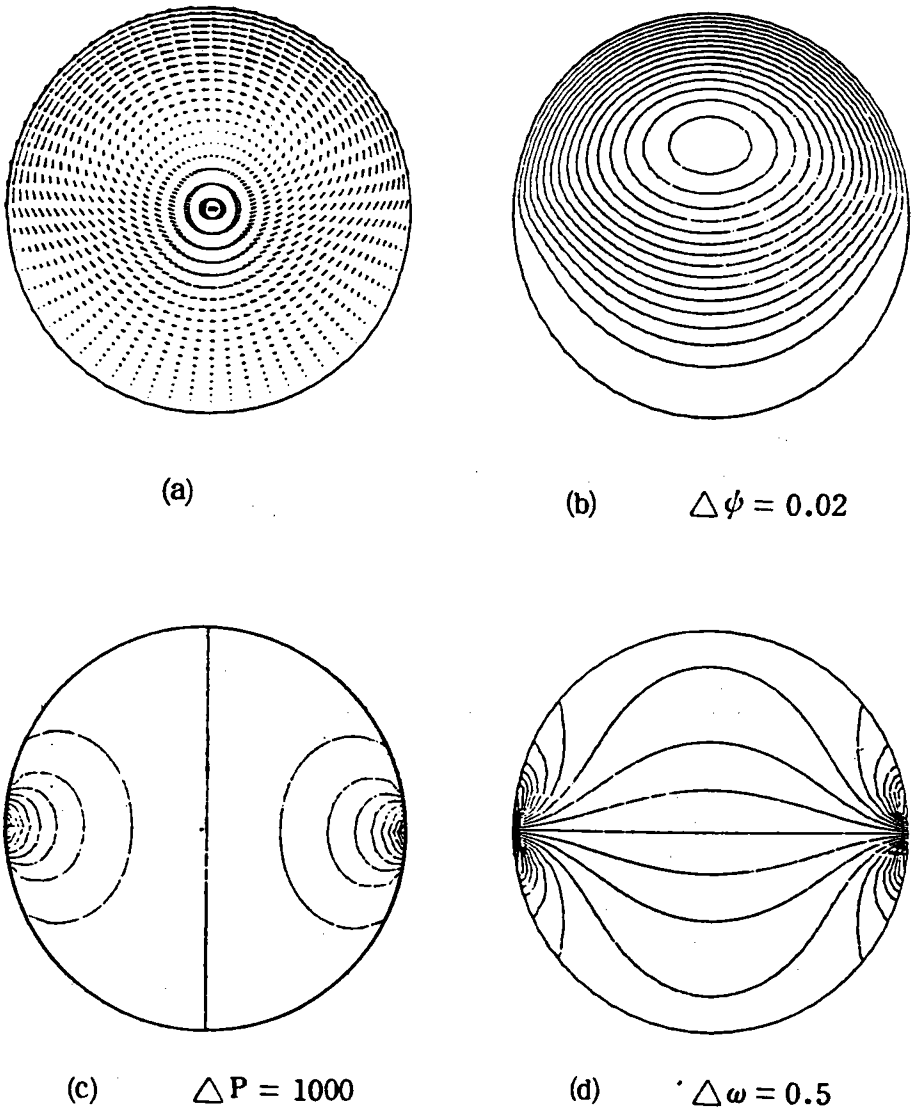

Fig. 4 : Distribution of velocity, streamline, pressure, and vorticity in a ciraular eddy of Re = 0.001 [after Young and Ni (1989)].

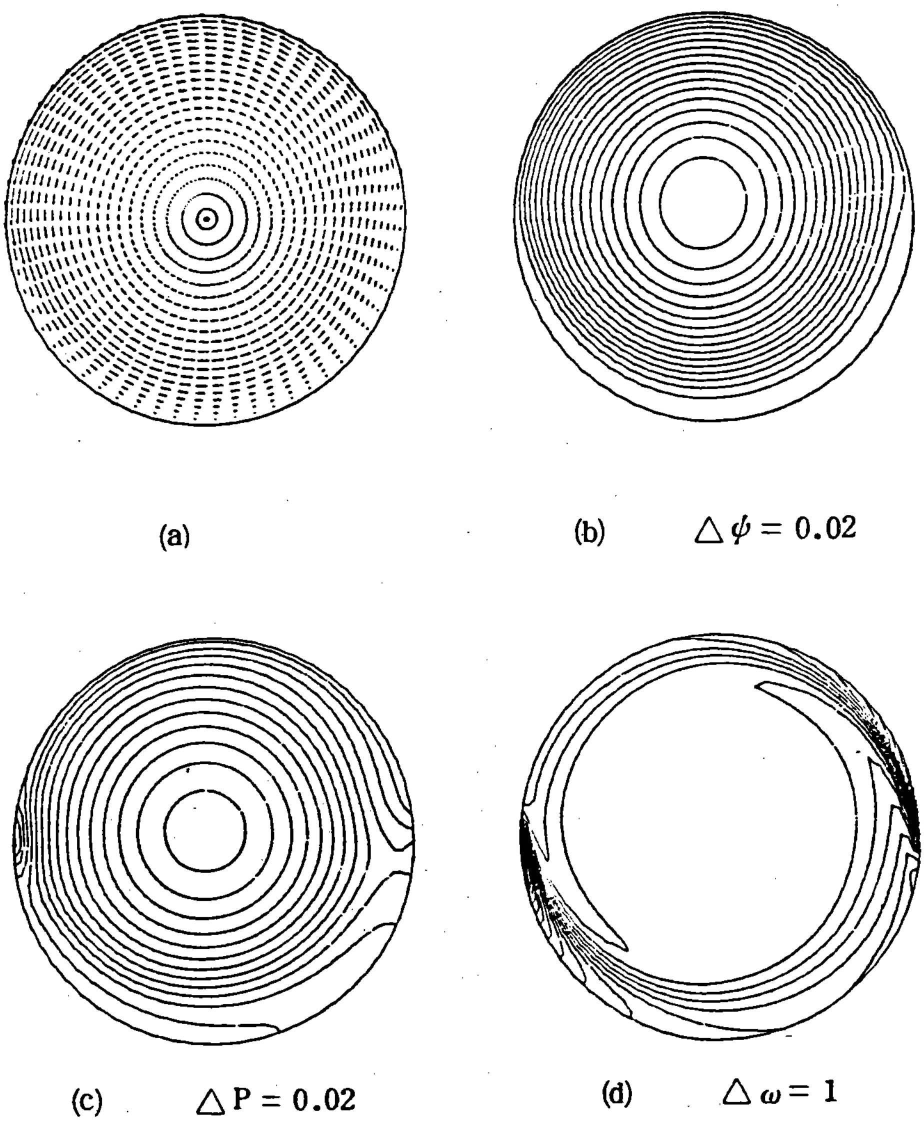

Fig. 5 : Distribution of velocity, streamline, pressure, and vorticity in a ciraular eddy of Re=400 [after Young and Ni (1989)].

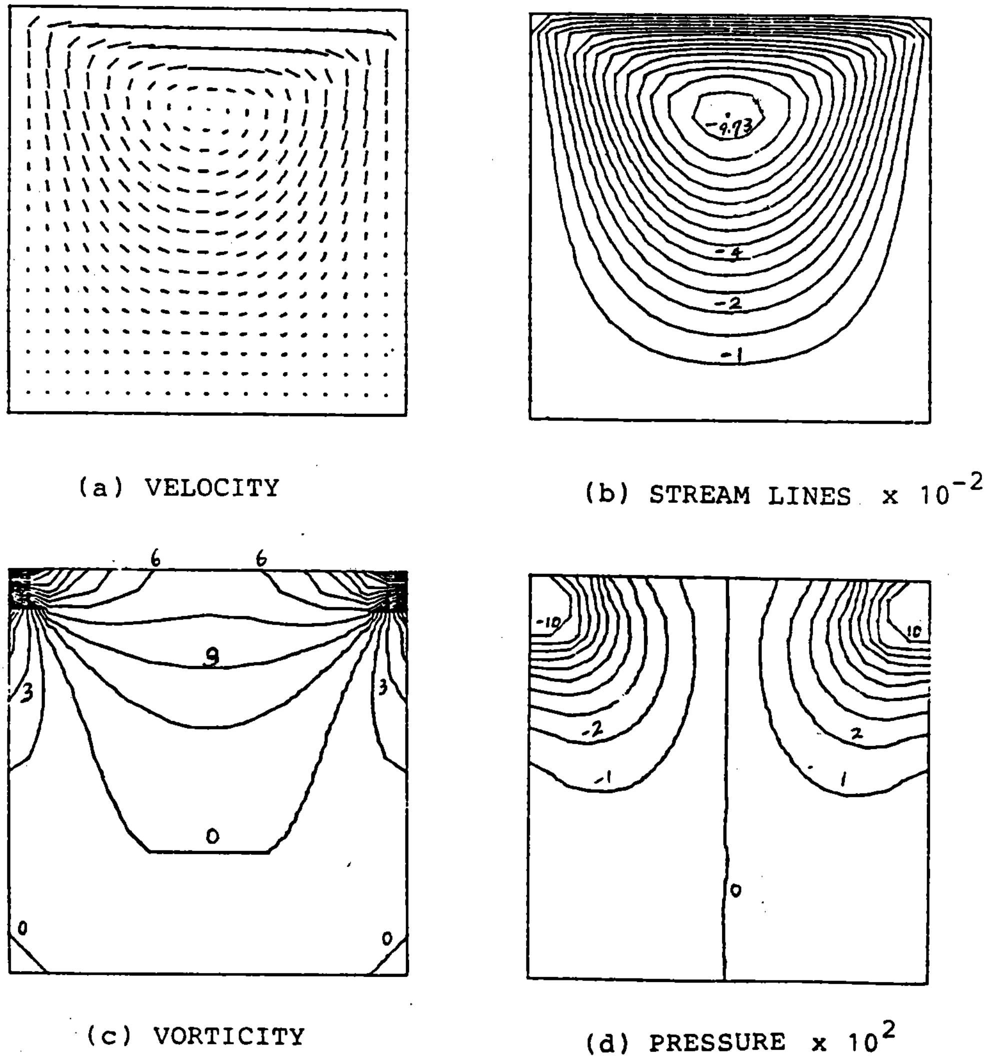

Fig. 6 : Distribution of velocity, streamline, vorticity, and pressure in a square cavity of Re=0.01 [after Young et al (1986)].

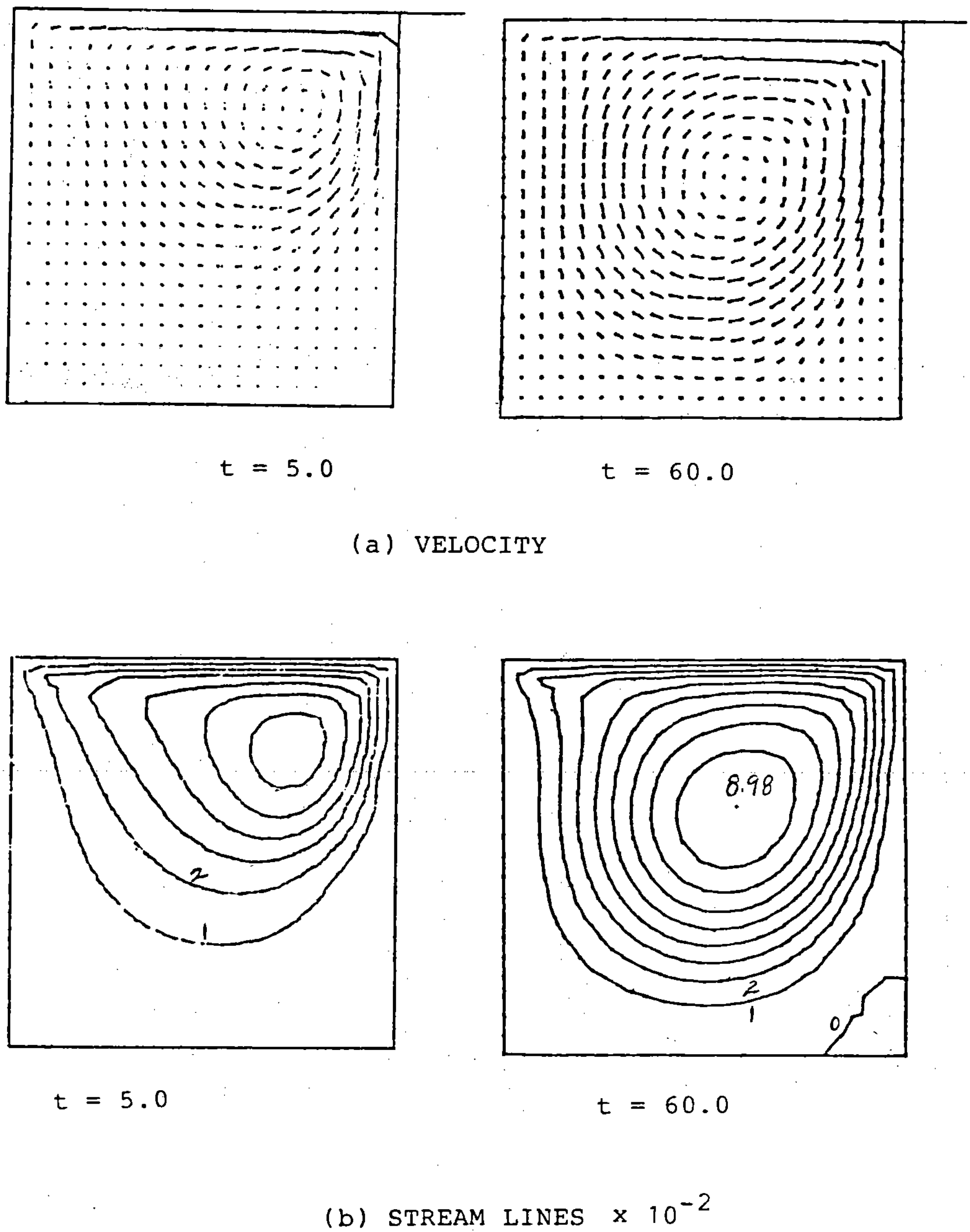

Fig. 7 : Distribution of velocity, streamline, pressure, and vorticity in a square cavity of Re=400 [after Young et al (1986)].

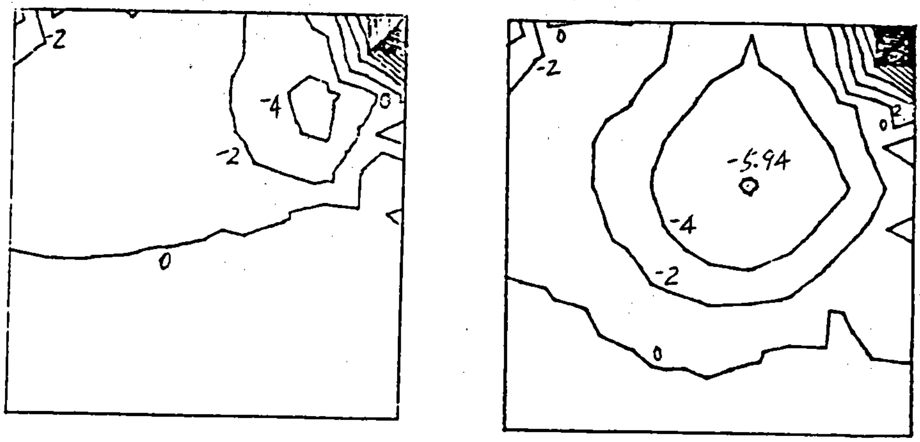

t = 5.0

t = 60.0

(c) PRESSURE x 10^{-2}

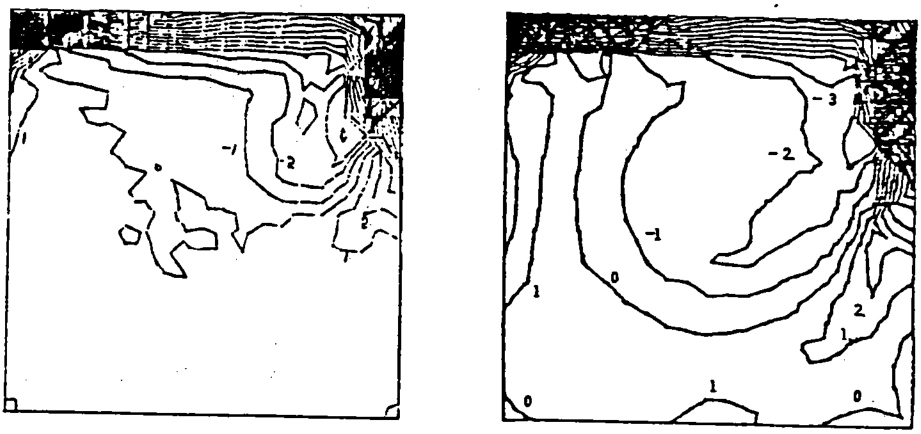

t = 5.0

t = 60.0

(d) VORTICITY

Fig. 7 : Distribution of velocity, streamline, pressure, and vorticity in a square cavity of Re=400 [after Young et al (1986)].

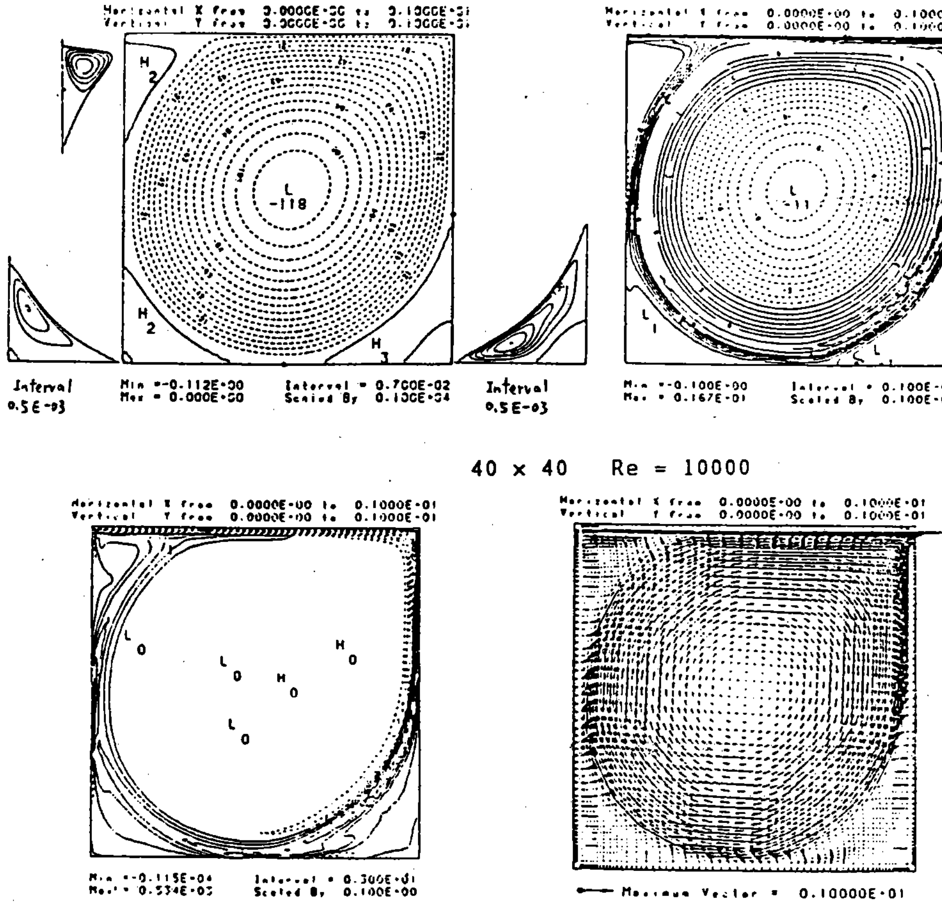

40 x 40 Re = 10000

Fig. 8 : Distribution of streamline, total pressure, vorticity, and velocity in a square cavity of Re = 10000 [after Young and Sun (1988)].

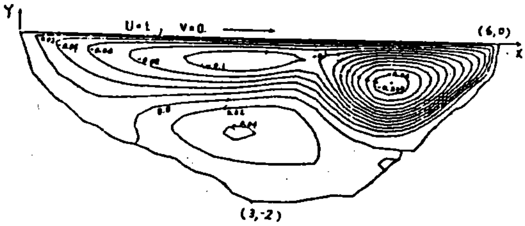

Fig. 9 : Boundary conditions and distribution of streamlines for irregular topography of a recirculating flow at Re=400.

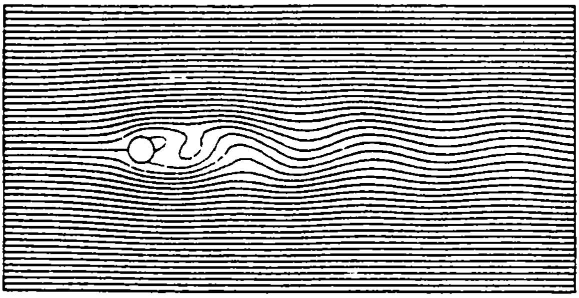

(a) t = 28.04 , $\triangle\psi = 0.25$

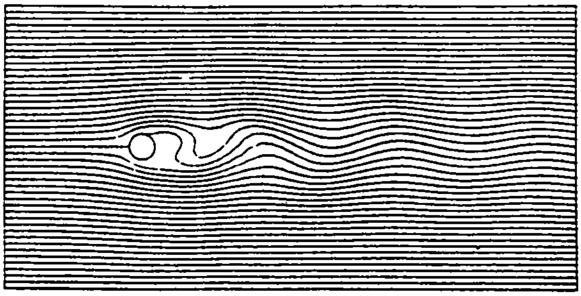

(b) t = 29.20 , $\triangle\psi = 0.25$

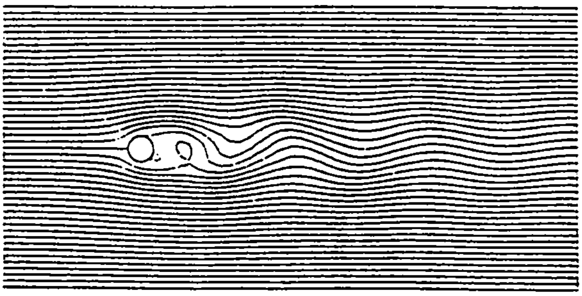

(c) t = 30.70 , $\triangle\psi = 0.25$

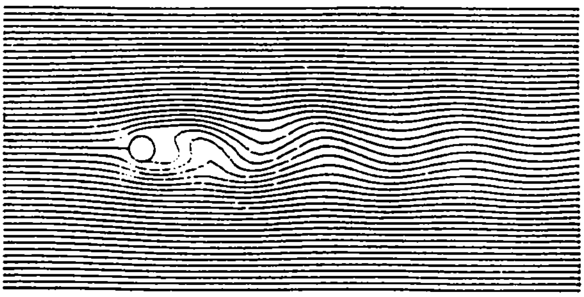

(d) t = 32.20 , $\triangle\psi = 0.25$

Fig.10 : Streamlines as a function of time for uniform flow past a circular cylinder [after Young and Ni (1989)].

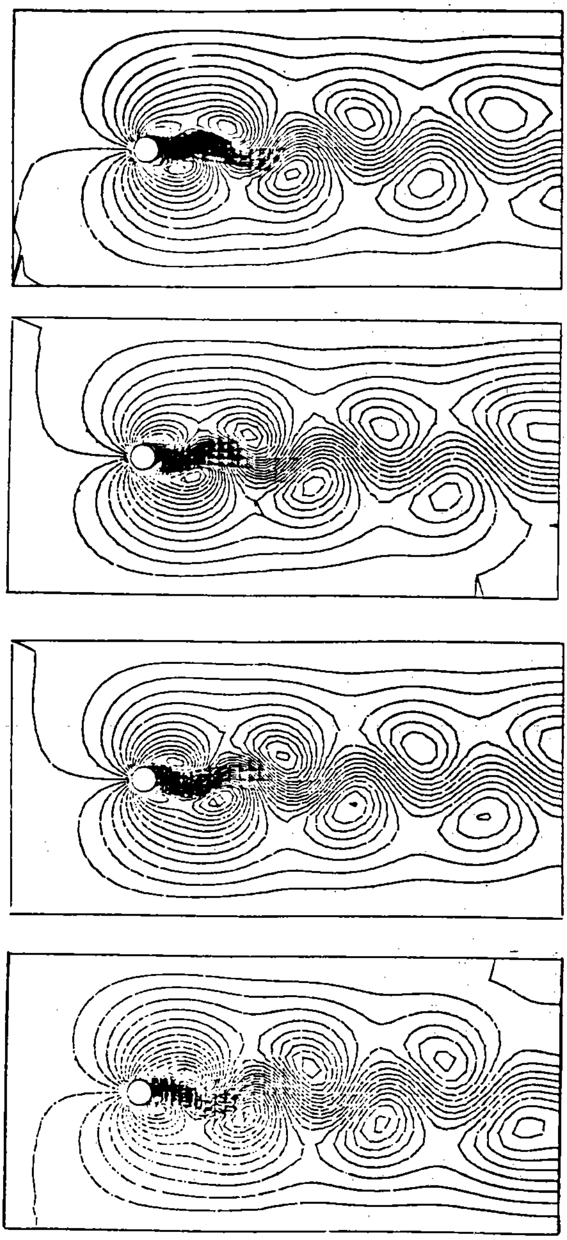

(a) $t = 28.04$, $\triangle\psi_{re} = 0.05$

(b) $t = 29.20$, $\triangle\psi_{re} = 0.05$

(c) $t = 30.70$, $\triangle\psi_{re} = 0.05$

(d) $t = 32.20$, $\triangle\psi_{re} = 0.05$

Fig.11 : Relative streamlines as a function of time for Karman vortex streets [after Young and Ni (1989)].

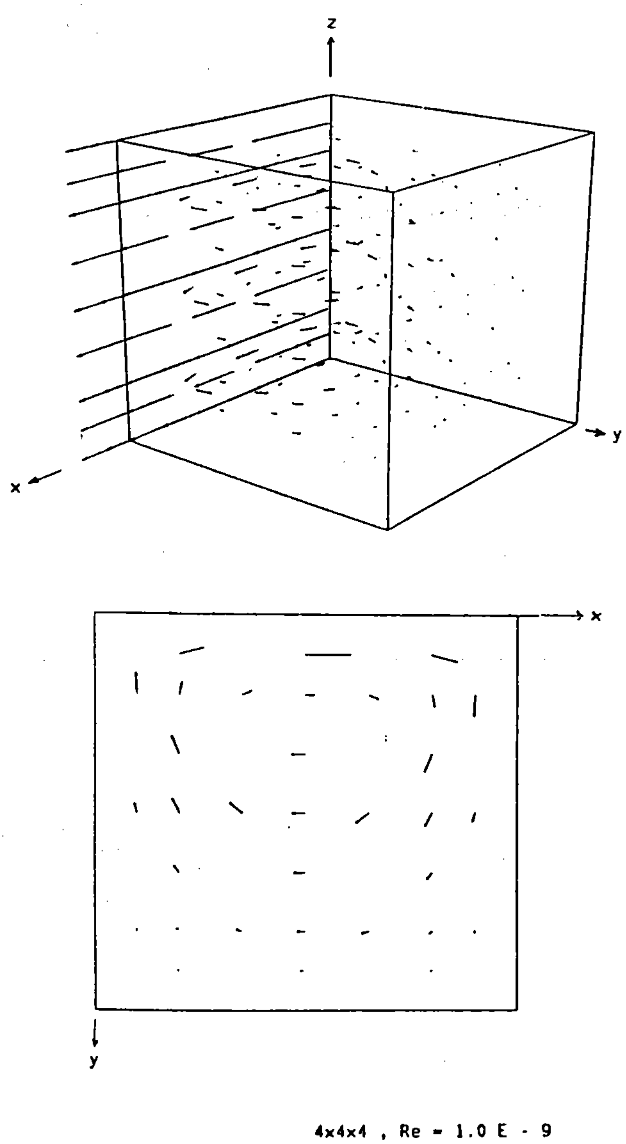

Fig.12 : Velocity distribution of a three-dimensional cubic cavity of Re -> 0 [after Young and Sun (1988)].

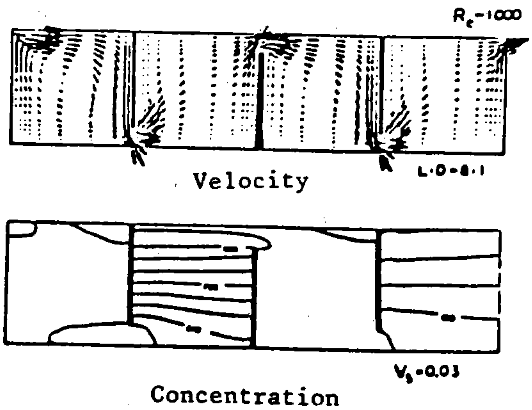

Fig.13 : Velocity and concentration distribution of a rectangular sediment basin.

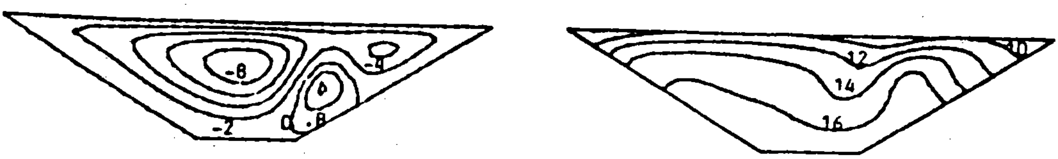

Streamlines ($x10^2$) (Left) and Isotherms (Right), t=7,500 s

Fig.14 : Distribution of streamlines and isotherms of a stratified reservoir.

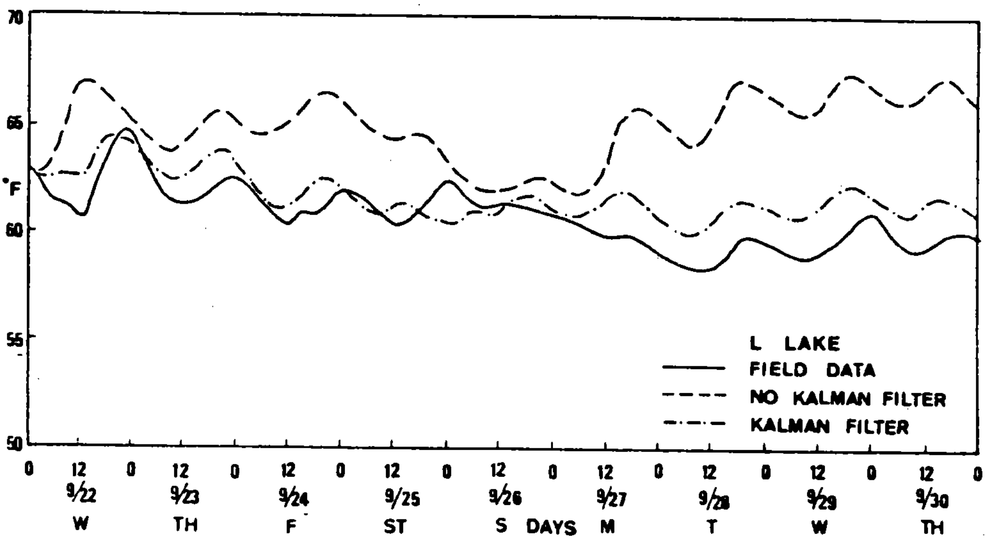

Fig.15 : Simulation of thermal hydraulics for a cooling system.

VELOCITY

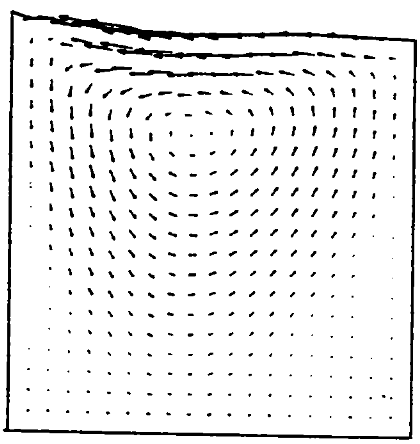

Fig.16 : Simulation of square cavity with free surface.

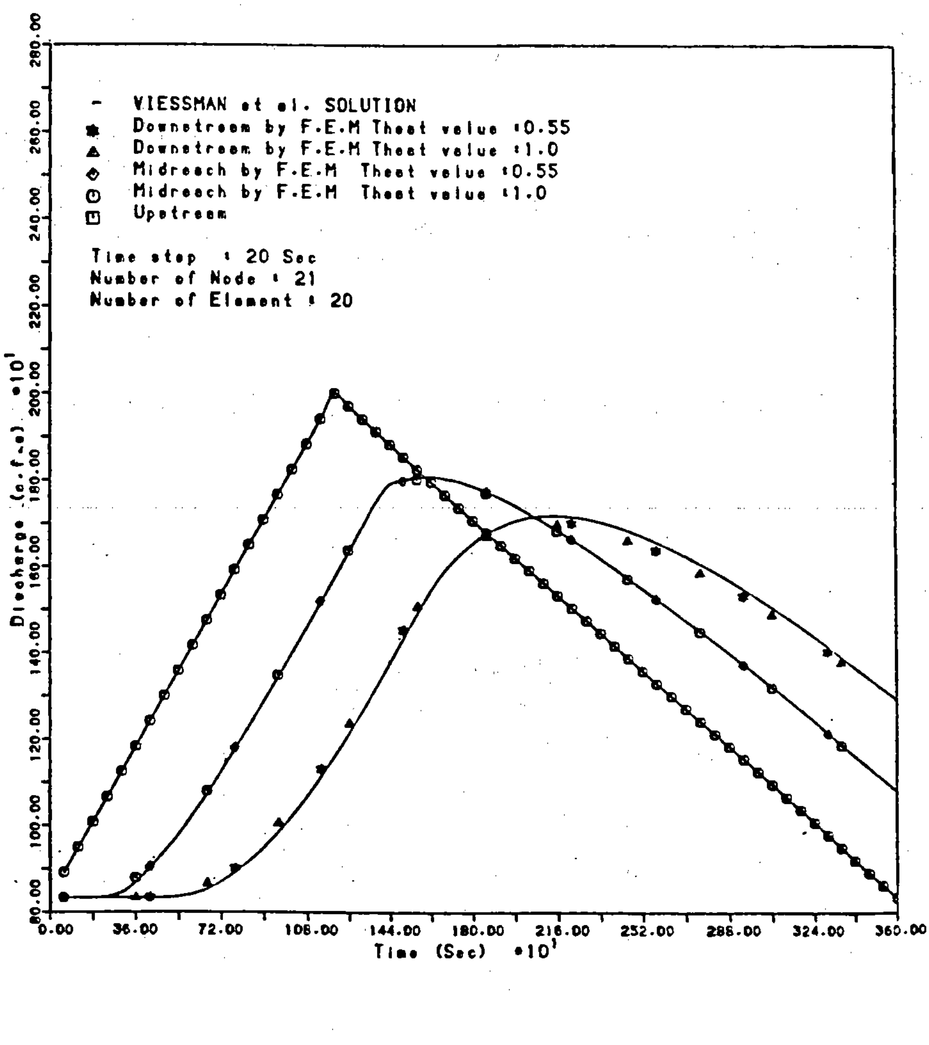

Fig.17 : Simulation of a flood wave propagation in open channel [after Young and Lin (1988)].

第三屆基礎港灣數值（數學）模式研習會論文集 Jan. 17～18，1990 Page 221～250

三度空間海洋數值模式

李賢文

國立台灣海洋大學海洋學系

一、引 言

三度空間海洋數值模式的發展已有二十餘年的歷史，此方面之發展以美國普林斯頓大學（Princeton University）的地球物理流體動力實驗室（Geophical Fluid Dynamics Laboratory）的Bryan和Cox二位先生的貢獻最多，他們發表一系列海洋數值模式之論文（Bryan and Cox, 1967, 1968; Bryan, 1969,1979; Cox, 1970, 1975, 1979）。

一般而言，三度空間海洋數值模式之發展，大都是考慮多層次的模式；上述Bryan和Cox之模式，也都以多層次模式爲主。Simons(1973) 依多層次模式之概念，發展了一個湖泊的三度空間數值模式。

另一方面，三度空間海洋數值模式之垂直座標，並不分別層次，而採取Galerkin method來處理，但水平方面仍採用定差方式，此方面之研究，可參考Davies and Owen (1979), Davies (1979,1980), Owen (1980)。

本文要依據Simons (1973) 的多層次模式架構，來探討三度空間海洋數值模式之發展。

二、基本數理方程式

我們描述海水運動的方程式如下：

$$\frac{\partial u}{\partial t} + u\frac{\partial u}{\partial x} + v\frac{\partial u}{\partial y} + w\frac{\partial u}{\partial z}$$

$$= fv - \frac{1}{\rho}\frac{\partial p}{\partial x} + \frac{1}{\rho}\left[\frac{\partial}{\partial x}\left(A_h\frac{\partial u}{\partial x}\right) + \frac{\partial}{\partial y}\left(A_h\frac{\partial u}{\partial y}\right) + \frac{\partial}{\partial z}\left(A_v\frac{\partial u}{\partial z}\right)\right] \quad \cdots\cdots\cdots(1)$$

$$\frac{\partial v}{\partial t} + u\frac{\partial v}{\partial x} + v\frac{\partial v}{\partial y} + w\frac{\partial v}{\partial z}$$

$$= -fu - \frac{1}{\rho}\frac{\partial p}{\partial y} + \frac{1}{\rho}\left[\frac{\partial}{\partial x}\left(A_h\frac{\partial v}{\partial x}\right) + \frac{\partial}{\partial y}\left(A_h\frac{\partial v}{\partial y}\right) + \frac{\partial}{\partial z}\left(A_v\frac{\partial v}{\partial z}\right)\right] \quad \cdots\cdots(2)$$

$$\frac{\partial u}{\partial x} + \frac{\partial v}{\partial y} + \frac{\partial w}{\partial z} = 0 \quad \cdots\cdots(3)$$

$$\frac{\partial p}{\partial z} = -\rho g \quad \cdots\cdots(4)$$

$$\frac{\partial T}{\partial t} + u\frac{\partial T}{\partial x} + v\frac{\partial T}{\partial y} + w\frac{\partial T}{\partial z}$$

$$= \frac{1}{\rho}\left[\frac{\partial}{\partial x}\left(A_h^{(T)}\frac{\partial T}{\partial x}\right) + \frac{\partial}{\partial y}\left(A_h^{(T)}\frac{\partial T}{\partial y}\right) + \frac{\partial}{\partial z}\left(A_v^{(T)}\frac{\partial T}{\partial z}\right)\right] \quad \cdots\cdots(5)$$

$$\frac{\partial S}{\partial t} + u\frac{\partial S}{\partial x} + v\frac{\partial S}{\partial y} + w\frac{\partial S}{\partial z}$$

$$= \frac{1}{\rho}\left[\frac{\partial}{\partial x}\left(A_h^{(S)}\frac{\partial S}{\partial x}\right) + \frac{\partial}{\partial y}\left(A_h^{(S)}\frac{\partial S}{\partial y}\right) + \frac{\partial}{\partial z}\left(A_v^{(S)}\frac{\partial S}{\partial z}\right)\right] \quad \cdots\cdots(6)$$

(1)式和(2)式分別代表運動方程式之 x 向和 y 向分量；(3)式爲流體靜力方程式；(4)式爲不可壓縮流體的連續方程式，而海水一般可以視爲不可壓縮；(5)式爲熱傳方程式；(6)式爲塩度擴散方程式。在此我們採用右手直角座標系統； x

軸、y軸和z軸分別指向東方、北方和上方。上述方程式中，所使用符號之意義如下：

u、v、w：分別爲x，y和z方向之速度分量。

p：海水壓力。

ρ：海水密度。

g：重力加速度。

f：柯氏參數$= 2\Omega \sin\phi$。

（Ω＝地轉角速度，ϕ＝緯度）

T：海水溫度。

S：海水塩度。

A_h：動量的水平交換係數。

A_v：動量的垂直交換係數。

$A_h^{(T)}$：熱量的水平交換係數。

$A_v^{(T)}$：熱量的垂直交換係數。

$A_h^{(S)}$：塩分的水平交換係數。

$A_v^{(S)}$：塩分的垂直交換係數。

另外我們還需要一個狀態方程式，以描述海水密度、溫度、塩度、壓力間的關係，即其形式如下，

$$\rho = \rho(T, S, p) \qquad \cdots\cdots\cdots(7)$$

最近由聯合國教科文組織（UNESCO）之海洋學表格及標準聯合審查委員會（Joint Panel on Oceanographic Tables and Standards）在1981年定義出一個狀態方程式適合於海洋學之用。在這個方程式中，密度（ρ）之單位爲Kg/m^3（$= 10^{-3} g/cm^3$），壓力（p）之單位爲巴（bar），溫度爲℃，塩度是實用塩度單位（practical salinity unit）。實用塩度單位與常用塩度單位（‰，即千分之幾）所表示之塩度數值，相差無幾。

利用此種狀態方程式，以求出海水密度，需要一連串的步驟。首先利用下式決定純水之密度（ρ_w）：

$$\rho_w = 999.842594 + 6.793952 \times 10^{-2}\,T - 9.095290 \times 10^{-3}\,T^2 + 1.001685 \times 10^{-4}\,T^3 - 1.120083 \times 10^{-6}\,T^4 + 6.536332 \times 10^{-9}\,T^5 \quad \cdots\cdots(8)$$

其次，用下式決定在一大氣壓（即海水壓力 $p=0$ ）之海水密度：

$$\rho(S,T,0) = \rho_w + S\,(0.824493 - 4.0899 \times 10^{-3}\,T + 7.6438 \times 10^{-5}\,T^2 - 8.2467 \times 10^{-7}\,T^3 + 5.3875 \times 10^{-9}\,T^4) + S^{\frac{3}{2}}(-5.72466 \times 10^{-3} + 1.0227 \times 10^{-4}\,T - 1.6546 \times 10^{-6}\,T^2) + 4.8314 \times 10^{-4}\,S^2 \quad \cdots\cdots(9)$$

最後再由下式決定在海水壓力爲 p 時之密度：

$$\rho(S,T,p) = \frac{\rho(S,T,0)}{1 - \dfrac{p}{K(S,T,p)}} \quad \cdots\cdots(10)$$

其中K爲正割全容係數（ secant bulk modulus ）。這個K值也是由三個步驟得來。純水之K值爲：

$$K_w = 19652.21 + 148.4206\,T - 2.327105\,T^2 + 1.360477 \times 10^{-2}\,T^3 - 5.155288 \times 10^{-5}\,T^4 \quad \cdots\cdots(11)$$

在一大氣壓（海水壓力 $p=0$ ）之K值爲：

$$K(S,T,0) = K_w + S\,(54.6746 - 0.603459\,T + 1.09987 \times 10^{-2}\,T^2 - 6.1670 \times 10^{-5}\,T^3) + S^{\frac{3}{2}}(7.944 \times 10^{-2} + 1.6483 \times 10^{-2}\,T - 5.3009 \times 10^{-4}\,T^2) \quad \cdots\cdots(12)$$

最後在海水壓力爲 p 時之K值爲：

$$K(S,T,p) = K(S,T,0) + p\,(3.239908 + 1.43713 \times 10^{-3}\,T + 1.16092 \times 10^{-4}\,T^2 - 5.77905 \times 10^{-7}\,T^3) + pS\,(2.2838 \times 10^{-3} - 1.0981 \times 10^{-5}\,T - 1.6078 \times 10^{-6}\,T^2) + 1.91075 \times 10^{-4}\,pS^{\frac{3}{2}}$$

$$+ p^2 (8.50935 \times 10^{-5} - 6.12293 \times 10^{-6} T$$
$$+ 5.2787 \times 10^{-8} T^2)$$
$$+ p^2 S (-9.9348 \times 10^{-7} + 2.0816 \times 10^{-8} T$$
$$+ 9.1697 \times 10^{-10} T^2)$$

當我們將(1)，(2)，(5)，(6)分別與(3)式合併，則可得下列方程式：

$$\frac{\partial u}{\partial t} + \frac{\partial}{\partial x}(uu) + \frac{\partial}{\partial y}(uv) + \frac{\partial}{\partial z}(uw)$$
$$= fv - \frac{1}{\rho}\frac{\partial p}{\partial x} + \frac{1}{\rho_o}\left[\frac{\partial}{\partial x}\left(A_h \frac{\partial u}{\partial x}\right) + \frac{\partial}{\partial y}\left(A_h \frac{\partial u}{\partial y}\right)\right.$$
$$\left. + \frac{\partial}{\partial z}\left(A_v \frac{\partial u}{\partial z}\right)\right] \qquad \cdots\cdots (13)$$

$$\frac{\partial v}{\partial t} + \frac{\partial}{\partial x}(vu) + \frac{\partial}{\partial y}(vv) + \frac{\partial}{\partial z}(vw)$$
$$= - fu - \frac{1}{\rho_o}\frac{\partial p}{\partial y} + \frac{1}{\rho_o}\left[\frac{\partial}{\partial x}\left(A_h \frac{\partial v}{\partial x}\right) + \frac{\partial}{\partial y}\left(A_h \frac{\partial v}{\partial y}\right)\right.$$
$$\left. + \frac{\partial}{\partial z}\left(A_v \frac{\partial v}{\partial z}\right)\right] \qquad \cdots\cdots (14)$$

$$\frac{\partial T}{\partial t} + \frac{\partial}{\partial x}(Tu) + \frac{\partial}{\partial y}(Tv) + \frac{\partial}{\partial z}(Tw)$$
$$= \frac{1}{\rho_o}\left[\frac{\partial}{\partial x}\left(A_h^{(T)} \frac{\partial T}{\partial x}\right) + \frac{\partial}{\partial y}\left(A_h^{(T)} \frac{\partial T}{\partial y}\right) + \frac{\partial}{\partial z}\left(A_v^{(T)} \frac{\partial T}{\partial z}\right)\right] \quad (15)$$

$$\frac{\partial S}{\partial t} + \frac{\partial}{\partial x}(Su) + \frac{\partial}{\partial y}(Sv) + \frac{\partial}{\partial z}(Sw)$$

$$=\frac{1}{\rho_o}\left[\frac{\partial}{\partial x}\left(A_h^{(s)}\frac{\partial S}{\partial x}\right)+\frac{\partial}{\partial y}\left(A_h^{(s)}\frac{\partial S}{\partial y}\right)+\frac{\partial}{\partial z}\left(A_v^{(s)}\frac{\partial S}{\partial z}\right)\right] \cdots (16)$$

在此我們採用 Boussinesque 近似，即上述方程式中密度之變異被忽略，其中 ρ_o 爲海水的平均密度，爲了方便起見，通常我們可以取 $\rho_o = 1\ g\ cm^{-3}$。

在海洋深度爲 z 之壓力，我們可以利用流體靜力方程式來決定，即

$$p = p_a + \rho_o g(\zeta - z) + \int_z^\zeta \rho' g dz$$

$$= p_a + \rho_o g(\zeta - z) + \int_z^\zeta \sigma dz \qquad \cdots\cdots (17)$$

其中 $\rho' = \rho - \rho_o$ ， $\sigma = \rho' g$ 。而密度 ρ 可由⑽式得知。
上式中 p_a 代表海面的大氣壓力，ζ 代表實際海面與靜止的平均海平面之差值。

如此⒀和⒁二式中之壓力梯度可改寫如下：

$$\frac{\partial p}{\partial x} = \frac{\partial p_a}{\partial x} + \rho_o g \frac{\partial \zeta}{\partial x} + \frac{\partial}{\partial x}\left(\int_z^\zeta \sigma dz\right)$$

$$\cdots\cdots (18)$$

$$\frac{\partial p}{\partial y} = \frac{\partial p_a}{\partial y} + \rho_o g \frac{\partial \zeta}{\partial y} + \frac{\partial}{\partial y}\left(\int_z^\zeta \sigma dz\right)$$

此處我們引進兩個代表壓力的符號，即

$$P = p_a + \rho_o g \zeta \quad , \qquad P' = \int_z^\zeta \sigma dz$$

P 代表正壓的（ barotropic ）壓力部分，
P′ 代表斜壓的（ baroclinic ）壓力部分。

因此(18)式變成

$$\frac{\partial p}{\partial x} = P_x + P'_x \quad , \quad \frac{\partial p}{\partial y} = P_y + P'_y \qquad \cdots\cdots (19)$$

其中

$$P_x = \frac{\partial P}{\partial x} = \frac{\partial p_a}{\partial x} + \rho_o g \frac{\partial \zeta}{\partial x}$$

$$P'_x = \frac{\partial P'}{\partial x} = \frac{\partial}{\partial x}\int_z^{\zeta} \sigma \, dz$$

而 P_y 與 P'_y 的形式類似，它們分別正壓的壓力部分與斜壓的壓力部分對 y 之偏微分。

描述海水流動及溫度與塩度的擴散過程，除了上述的數理方程式之外，我們還需要邊界條件。此即，

(一)運動邊界條件：

$$w = u\frac{\partial \zeta}{\partial x} + v\frac{\partial \zeta}{\partial y} + \frac{\partial \zeta}{\partial t} \quad \text{，在海面} \quad z = \zeta\,(x, y, t)$$

$$\cdots\cdots (20)$$

$$w = -u\frac{\partial H}{\partial x} - v\frac{\partial H}{\partial y} \quad \text{，在海底} \quad z = -H\,(x, y)$$

(二)動力邊界條件：

$$A_v\frac{\partial u}{\partial z} - \left(A_h\frac{\partial u}{\partial x}\right)\frac{\partial \zeta}{\partial x} - \left(A_h\frac{\partial u}{\partial y}\right)\frac{\partial \zeta}{\partial y} = \tau_{sx}$$

$$\text{在海面} \quad z = \zeta(x, y, t) \qquad (21)$$

$$A_v\frac{\partial v}{\partial z} - \left(A_h\frac{\partial v}{\partial x}\right)\frac{\partial \zeta}{\partial x} - \left(A_h\frac{\partial v}{\partial y}\right)\frac{\partial \zeta}{\partial y} = \tau_{sy}$$

此處 τ_{sx} 和 τ_{sy} 分別代表 x 和 y 方向海面的風剪力。

$$A_v \frac{\partial u}{\partial z} + (A_h \frac{\partial u}{\partial x}) \frac{\partial H}{\partial x} + (A_h \frac{\partial u}{\partial y}) \frac{\partial H}{\partial y} = \tau_{bx}$$

在海底　$z = -H(x, y)$ (22)

$$A_v \frac{\partial v}{\partial z} + (A_h \frac{\partial v}{\partial x}) \frac{\partial H}{\partial x} + (A_h \frac{\partial v}{\partial y}) \frac{\partial H}{\partial y} = \tau_{by}$$

此處 τ_{bx} 和 τ_{by} 分別代表 x 和 y 方向的海底摩擦剪力。

㈢溫度之邊界條件

$$A_v^{(T)} \frac{\partial T}{\partial z} - (A_h^{(T)} \frac{\partial T}{\partial x}) \frac{\partial \zeta}{\partial x} - (A_h^{(T)} \frac{\partial T}{\partial y}) \frac{\partial \zeta}{\partial y} = q_T ,$$

在海面　$z = \zeta(x, y, t)$　…… (23)

$$A_v^{(T)} \frac{\partial T}{\partial z} + (A_h^{(T)} \frac{\partial T}{\partial x}) \frac{\partial H}{\partial x} + (A_h^{(T)} \frac{\partial T}{\partial y}) \frac{\partial H}{\partial y} = 0 ,$$

在海底　$z = -H(x, y)$　…… (24)

此處 q_T 代表海面上垂直向下的熱通量（heat flux）。

㈣塩度的邊界條件：

$$A_v^{(S)} \frac{\partial S}{\partial z} - (A_h^{(S)} \frac{\partial S}{\partial x}) \frac{\partial \zeta}{\partial x} - (A_h^{(S)} \frac{\partial S}{\partial y}) \frac{\partial \zeta}{\partial y} = q_s ,$$

在海面　$z = \zeta(x, y, t)$　…… (25)

$$A_v^{(S)} \frac{\partial S}{\partial z} + (A_h^{(S)} \frac{\partial S}{\partial x}) \frac{\partial H}{\partial x} + (A_h^{(S)} \frac{\partial S}{\partial y}) \frac{\partial H}{\partial y} = 0 ,$$

在海底　$z = -H(x, y)$　…… (26)

此處 q_s 代表海面上垂直向下的塩分通量，它是（蒸發量一降水量）的函數。

上述的邊界條件僅適用於海面和海底。對於側面海岸，則垂直於海岸無

水量輸送；同時利用不滑動條件，即海岸處之切線速度為零。

對於封閉的海域，上述邊界條件，已足夠可用。但對於開放的海域，則需另定開口的邊界條件。

三、多層次模式

為了建立三度空間的數值模式，此處我們以多層次模式為基礎，其構造如圖1所示。

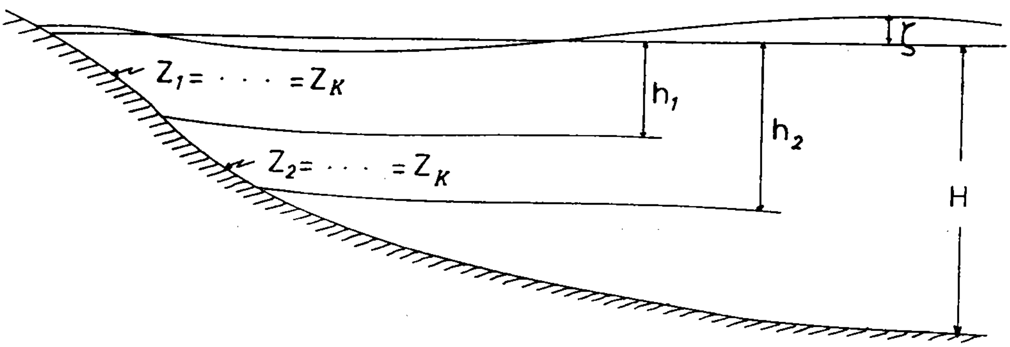

圖1　多層次模式之模式

在圖中K表示層次之數目；h_k（$k=1,2,\cdots\cdots,K-1$）表示第k個交界面與平靜海面（$z=0$）之距離

令　$z=z_k(x,y,t)$，　　$k=0,1,\cdots\cdots,K$，

則可得

$z_0=\zeta(x,y,t)$，　　在海面；

$z_k=-h_k(x,y,t)$，$k=1,2,\cdots\cdots,K-1$，在內部交界面；

$z_K=-H(x,y)$；　　在海底。

如果我們將(3)，(13)，(14)，(15)，(16)對任意一層由 Z_k 到 Z_{k-1} 積分，並且使用積分與微分順序交換原則，可以得到下列方程式，

$$\frac{\partial U_{k-1/2}}{\partial t}+\frac{\partial V_{k-1/2}}{\partial t}+\left[w-u\frac{\partial Z}{\partial x}-v\frac{\partial Z}{\partial y}\right]_{k-1}$$

$$-\left[w-u\frac{\partial Z}{\partial x}-v\frac{\partial Z}{\partial y}\right]_{k}=0 \qquad \cdots\cdots(27)$$

$$\frac{\partial U_{k-1/2}}{\partial t}+\frac{\partial}{\partial x}\int_{z_k}^{z_{k-1}} uu\,dz+\frac{\partial}{\partial y}\int_{z_k}^{z_{k-1}} uv\,dz+$$

$$\left[u\left(w-u\frac{\partial Z}{\partial x}-v\frac{\partial Z}{\partial y}-\frac{\partial Z}{\partial t}\right)\right]_{k-1}-$$

$$\left[u\left(w-u\frac{\partial Z}{\partial x}-v\frac{\partial Z}{\partial y}-\frac{\partial Z}{\partial t}\right)\right]_{k}$$

$$=fV_{k-1/2}-\frac{P_x}{\rho_o}\left(Z_{k-1}-Z_k\right)-\frac{1}{\rho_o}\int_{z_k}^{z_{k-1}} P_x'\,dz+$$

$$\frac{1}{\rho_o}\left[\frac{\partial}{\partial x}\int_{z_k}^{z_{k-1}}\left(A_h\frac{\partial u}{\partial x}\right)dz+\frac{\partial}{\partial y}\int_{z_k}^{z_{k-1}}\left(A_h\frac{\partial u}{\partial y}\right)dz\right]$$

$$-\frac{1}{\rho_o}\left[\left(A_h\frac{\partial u}{\partial x}\right)\frac{\partial Z}{\partial x}+\left(A_h\frac{\partial u}{\partial y}\right)\frac{\partial Z}{\partial y}-\left(A_v\frac{\partial u}{\partial z}\right)\right]_{k-1}$$

$$+\frac{1}{\rho_o}\left[\left(A_h\frac{\partial u}{\partial x}\right)\frac{\partial Z}{\partial x}+\left(A_h\frac{\partial u}{\partial y}\right)\frac{\partial Z}{\partial y}-\left(A_v\frac{\partial u}{\partial z}\right)\right]_{k} \qquad \cdots\cdots(28)$$

$$\frac{\partial V_{k-1/2}}{\partial t}+\frac{\partial}{\partial x}\int_{z_k}^{z_{k-1}} vu\,dz+\frac{\partial}{\partial y}\int_{z_k}^{z_{k-1}} vv\,dz+$$

$$\left[v\left(w-u\frac{\partial Z}{\partial x}-v\frac{\partial Z}{\partial y}-\frac{\partial Z}{\partial t}\right)\right]_{k-1}-\left[v\left(w-u\frac{\partial Z}{\partial x}-v\frac{\partial Z}{\partial y}-\frac{\partial Z}{\partial t}\right)\right]_{k}$$

$$=-fU_{k-1/2}-\frac{P_y}{\rho_o}(Z_{k-1}-Z_k)-\frac{1}{\rho_o}\int_{z_k}^{z_{k-1}}P'_y\,dz$$

$$+\frac{1}{\rho_o}\left[\frac{\partial}{\partial x}\int_{z_k}^{z_{k-1}}\left(A_h\frac{\partial v}{\partial x}\right)dz+\frac{\partial}{\partial y}\int_{z_k}^{z_{k-1}}\left(A_h\frac{\partial v}{\partial y}\right)dz\right]$$

$$-\frac{1}{\rho_o}\left[\left(A_h\frac{\partial v}{\partial x}\right)\frac{\partial Z}{\partial x}+\left(A_h\frac{\partial V}{\partial y}\right)\frac{\partial Z}{\partial y}-\left(A_v\frac{\partial v}{\partial z}\right)\right]_{k-1}$$

$$+\frac{1}{\rho_o}\left[\left(A_h\frac{\partial v}{\partial x}\right)\frac{\partial Z}{\partial x}+\left(A_h\frac{\partial v}{\partial y}\right)\frac{\partial Z}{\partial y}-\left(A_v\frac{\partial v}{\partial z}\right)\right]_{k} \quad \cdots\cdots(29)$$

$$\frac{\partial\theta_{k-1/2}}{\partial t}+\frac{\partial}{\partial x}\int_{z_k}^{z_{k-1}}Tu\,dz+\frac{\partial}{\partial y}\int_{z_k}^{z_{k-1}}Tv\,dz+$$

$$\left[T\left(w-u\frac{\partial Z}{\partial x}-v\frac{\partial Z}{\partial y}-\frac{\partial Z}{\partial t}\right)\right]_{k-1}-\left[T\left(w-u\frac{\partial Z}{\partial x}-v\frac{\partial Z}{\partial y}-\frac{\partial Z}{\partial t}\right)\right]_{k}$$

$$=\frac{1}{\rho_o}\left[\frac{\partial}{\partial x}\int_{z_k}^{z_{k-1}}\left(A_h^{(T)}\frac{\partial T}{\partial x}\right)dz+\frac{\partial}{\partial y}\int_{z_k}^{z_{k-1}}\left(A_h^{(T)}\frac{\partial T}{\partial y}\right)dz\right]$$

$$-\frac{1}{\rho_0}\left[\left(A_h^{(T)}\frac{\partial T}{\partial x}\right)\frac{\partial Z}{\partial x}+\left(A_h^{(T)}\frac{\partial T}{\partial y}\right)\frac{\partial Z}{\partial y}-A_v^{(T)}\frac{\partial T}{\partial z}\right]_{k-1}$$

$$+\frac{1}{\rho_o}\left[\left(A_h^{(T)}\frac{\partial T}{\partial x}\right)\frac{\partial Z}{\partial x}+\left(A_h^{(T)}\frac{\partial T}{\partial y}\right)\frac{\partial Z}{\partial y}-A_v^{(T)}\frac{\partial T}{\partial z}\right]_{k} \quad \cdots\cdots(30)$$

$$\frac{\partial \phi_{k-1/2}}{\partial t}+\frac{\partial}{\partial x}\int_{z_k}^{z_{k-1}} Su\,dz+\frac{\partial}{\partial y}\int_{z_k}^{z_{k-1}} Sv\,dz+$$

$$\left[S\left(w-u\frac{\partial Z}{\partial x}-v\frac{\partial Z}{\partial y}-\frac{\partial Z}{\partial t}\right)\right]_{k-1}-\left[S\left(w-u\frac{\partial Z}{\partial x}-v\frac{\partial Z}{\partial y}-\frac{\partial Z}{\partial t}\right)\right]_{k}$$

$$=\frac{1}{\rho_o}\left[\frac{\partial}{\partial x}\int_{z_k}^{z_{k-1}}\left(A_h^{(s)}\frac{\partial S}{\partial x}\right)dz+\frac{\partial}{\partial y}\int_{z_k}^{z_{k-1}}\left(A_h^{(s)}\frac{\partial S}{\partial y}\right)dz\right]$$

$$-\frac{1}{\rho_o}\left[\left(A_h^{(s)}\frac{\partial S}{\partial x}\right)\frac{\partial Z}{\partial x}+\left(A_h^{(s)}\frac{\partial S}{\partial y}\right)\frac{\partial Z}{\partial y}-A_v^{(s)}\frac{\partial S}{\partial z}\right]_{k-1}$$

$$+\frac{1}{\rho_o}\left[\left(A_h^{(s)}\frac{\partial S}{\partial x}\right)\frac{\partial Z}{\partial x}+\left(A_h^{(s)}\frac{\partial Z}{\partial y}\right)\frac{\partial Z}{\partial y}-A_v^{(s)}\frac{\partial S}{\partial z}\right]_{k} \quad \cdots\cdots(31)$$

各項下註數是整數減$\frac{1}{2}$者，表示它是屬於那個層次之值；而其數是整數者，表示它是在交界面之值。同時令

$$U_{k-1/2}=\int_{z_k}^{z_{k-1}} u\,dz \quad , \quad V_{k-1/2}=\int_{z_k}^{z_{k-1}} v\,dz \quad ,$$

$$\cdots\cdots(32)$$

$$\theta_{k-1/2}=\int_{z_k}^{z_{k-1}} T\,dz \quad , \quad \phi_{k-1/2}=\int_{z_k}^{z_{k-1}} S\,dz$$

一般而言，海洋內部各層的交界面，我們可以把它們分成二類，即

物質界面（流體不能穿過）$Z_k(t,x,y)$：$w_k-u_k\frac{\partial Z_k}{\partial x}-v_k\frac{\partial Z_k}{\partial y}-\frac{\partial Z_k}{\partial t}=0$

固定界面（流體能通過）$Z_k(x,y)$：$\frac{\partial Z_k}{\partial t}=0$

海洋內部如採用物質界面，則可討論水內波(internal wave)之情形。但如僅研究不同層次的流況，則採用固定界面較方便。因此在多層次模式中，除了(32)式所列的 4 個應變數之外，各層的厚度

$$D_{k-1/2} \equiv Z_{k-1} - Z_k$$

也是變數。但如採用固定的水平界面，即

$$h_k = \text{const.} \qquad k = 1, 2, \cdots\cdots, K-1 .$$

則除了第一層因海面波動而不定外，其餘各層都是定值。

由於海面上自由波動的存在，使得時間差分間隔受到嚴格的限制。爲了減少運算的時間，我們計算內部各層的流動時，我們將過濾掉自由表面波；如此計算內部各層的流動時，其時間差分間隔，可略爲擴大。也就是說，我們可以將上述(27) ~(29)的層次方程式，轉換成專門計算自由表面波動的外模式(external mode)，和專門計算內部流動的內模式(internal mode)。

當我們將(27), (28), (29)等表示各層次的運動方程式，由第 1 層加到最底層，則得到外模式如下

$$\frac{\partial \zeta}{\partial t} = -\left(\frac{\partial U}{\partial x} + \frac{\partial V}{\partial y}\right) \qquad \cdots\cdots (33)$$

$$\frac{\partial U}{\partial t} = fV - (\zeta + H)\frac{P_x}{\rho_o} - \sum_{k=1}^{K}\left(\frac{1}{\rho_o}\int_{Z_k}^{Z_{k-1}} P_x' \, dz\right) + \nabla\cdot\int_{-H}^{\zeta}\left(\frac{A_h}{\rho_o}\nabla u - u\vec{u}\right)dz$$

$$+ \frac{\tau_{sx} - \tau_{bx}}{\rho_o} \qquad \cdots\cdots (34)$$

$$\frac{\partial V}{\partial t} = -fU - (\zeta + H)\frac{P_y}{\rho_o} - \sum_{k=1}^{K}\left(\frac{1}{\rho_o}\int_{Z_k}^{Z_{k-1}} P_y' \, dz\right) + \nabla\cdot\int_{-H}^{\zeta}\left(\frac{A_h}{\rho_o}\nabla v - v\vec{u}\right)dz$$

$$+ \frac{\tau_{sy} - \tau_{by}}{\rho_o} \qquad \cdots\cdots\cdots (35)$$

其中

$$U = U_{1/2} + \cdots\cdots + U_{K-1/2} \text{，} V = V_{1/2} + \cdots\cdots + V_{K-1/2} \qquad \cdots\cdots(36)$$

而 ∇ 代表水平梯度運算器，$\vec{u} = (u, v)$ 爲水平速度向量。

(33)，(34)，(35) 就是可用來計算暴潮的方程式，而且通常計算暴潮時往往將海水視爲均勻的流體，即 $P'_x = P'_y = 0$。(33)～(35) 式中，我們已經運用了海面及海底的邊界條件。

當我們將上下相鄰之平均速度相減，即可得內模式之方程式：

$$\frac{\partial}{\partial t}(\bar{u}_{k-1/2} - \bar{u}_{k+1/2}) = f(\bar{v}_{k-1/2} - \bar{v}_{k+1/2})$$

$$-\frac{1}{\rho_o}\left(\frac{1}{D_{k-1/2}}\int_{z_k}^{z_{k-1}} P'_x\,dz - \frac{1}{D_{k+1/2}}\int_{z_{k+1}}^{z_k} P'_x\,dz\right)$$

$$+\frac{1}{\rho_o}\frac{1}{D_{k-1/2}}\left\{\left[A_v\frac{\partial u}{\partial z} - \left(A_h\frac{\partial u}{\partial x}\right)\frac{\partial Z}{\partial x} - \left(A_h\frac{\partial u}{\partial y}\right)\frac{\partial Z}{\partial y}\right]_{k-1}\right.$$

$$\left.-\left[A_v\frac{\partial u}{\partial z} - \left(A_h\frac{\partial u}{\partial x}\right)\frac{\partial Z}{\partial x} - \left(A_h\frac{\partial u}{\partial y}\right)\frac{\partial Z}{\partial y}\right]_k\right\}$$

$$-\frac{1}{\rho_o D_{k+1/2}}\left\{\left[A_v\frac{\partial u}{\partial z} - \left(A_h\frac{\partial u}{\partial x}\right)\frac{\partial Z}{\partial x} - \left(A_h\frac{\partial u}{\partial y}\right)\frac{\partial Z}{\partial y}\right]_k\right.$$

$$\left.-\left[A_v\frac{\partial u}{\partial z} - \left(A_h\frac{\partial u}{\partial x}\right)\frac{\partial Z}{\partial x} - \left(A_h\frac{\partial u}{\partial y}\right)\frac{\partial Z}{\partial y}\right]_{k+1}\right\}$$

$$+\frac{1}{D_{k-1/2}}\nabla\cdot\int_{z_k}^{z_{k-1}}\left(\frac{A_h}{\rho_o}\nabla u - u\vec{u}\right)dz - \frac{1}{D_{k+1/2}}\nabla\cdot\int_{z_{k+1}}^{z_k}\left(\frac{A_h}{\rho_o}\nabla u - u\vec{u}\right)dz$$

$$-\frac{1}{D_{k-1/2}}\left\{\left[u\left(w - u\frac{\partial Z}{\partial x} - v\frac{\partial Z}{\partial y} - \frac{\partial Z}{\partial t}\right)\right]_{k-1} - \left[u\left(w - u\frac{\partial Z}{\partial x} - v\frac{\partial Z}{\partial y} - \frac{\partial Z}{\partial t}\right)\right]_k\right\}$$

$$+\frac{1}{D_{k+1/2}}\{[u(w-u\frac{\partial Z}{\partial x}-v\frac{\partial Z}{\partial y}-\frac{\partial Z}{\partial t})]_k-[u(w-u\frac{\partial Z}{\partial x}-v\frac{\partial Z}{\partial y}-\frac{\partial Z}{\partial t})]_{k+1}\}$$

$$\cdots\cdots(37)$$

$$\frac{\partial}{\partial t}(\bar{v}_{k-1/2}-\bar{v}_{k\,1/2})=-f(\bar{u}_{k-1/2}-\bar{u}_{k+1/2})$$

$$-\frac{1}{\rho_0}(\frac{1}{D_{k-1/2}}\int_{z_k}^{z_{k-1}}P_y'\,dz-\frac{1}{D_{k+1/2}}\int_{z_{k+1}}^{z_k}P_y'\,dz)$$

$$+\frac{1}{\rho_o}\frac{1}{D_{k-1/2}}\{[A_v\frac{\partial v}{\partial z}-(A_h\frac{\partial v}{\partial x})\frac{\partial Z}{\partial x}-(A_h\frac{\partial v}{\partial y})\frac{\partial Z}{\partial y}]_{k-1}$$

$$-[A_v\frac{\partial v}{\partial z}-(A_h\frac{\partial v}{\partial x})\frac{\partial Z}{\partial x}-(A_h\frac{\partial v}{\partial y})\frac{\partial Z}{\partial y}]_k\}$$

$$-\frac{1}{\rho_o}\frac{1}{D_{k+1/2}}\{[A_v\frac{\partial v}{\partial z}-(A_h\frac{\partial v}{\partial x})\frac{\partial Z}{\partial x}-(A_h\frac{\partial v}{\partial y})\frac{\partial Z}{\partial y}]_k$$

$$-[A_v\frac{\partial v}{\partial z}-(A_h\frac{\partial v}{\partial x})\frac{\partial Z}{\partial x}-(A_h\frac{\partial v}{\partial y})\frac{\partial Z}{\partial y}]_{k+1}\}$$

$$+\frac{1}{D_{k-1/2}}\nabla\cdot\int_{z_k}^{z_{k-1}}(\frac{A_h}{\rho_o}\nabla v-v\vec{u})dz-\frac{1}{D_{k+1/2}}\nabla\cdot\int_{z_{k+1}}^{z_k}(\frac{A_h}{\rho_o}\nabla v-v\vec{u})dz$$

$$-\frac{1}{D_{k-1/2}}\{[v(w-u\frac{\partial Z}{\partial x}-v\frac{\partial Z}{\partial y}-\frac{\partial Z}{\partial t})]_{k-1}-[v(w-u\frac{\partial Z}{\partial x}-v\frac{\partial Z}{\partial y}-\frac{\partial Z}{\partial t})]_k\}$$

$$+\frac{1}{D_{k+1/2}}\{[v(w-u\frac{\partial Z}{\partial x}-v\frac{\partial Z}{\partial y}-\frac{\partial Z}{\partial t})]_k-[v(w-u\frac{\partial Z}{\partial x}-v\frac{\partial Z}{\partial y}-\frac{\partial Z}{\partial t})]_{k+1}\}$$

$$\cdots\cdots(38)$$

(37) 式和 (38)式中，我們已經將自由海面波動過濾掉。
而且

$$\bar{u}_{k-1/2}=\frac{U_{k-1/2}}{D_{k-1/2}} \quad , \quad \bar{v}_{k-1/2}=\frac{V_{k-1/2}}{D_{k-1/2}}$$

代表任意一層的平均流速。

上述的外模式與內模式的方程式都很複雜。爲了方便起見，我們將海洋內部各層次的界面取爲不動的水平面。則內部界面上的摩擦剪力爲

$$\left[A_v\frac{\partial u}{\partial z}-\left(A_h\frac{\partial u}{\partial x}\right)\frac{\partial Z}{\partial x}-\left(A_h\frac{\partial u}{\partial y}\right)\frac{\partial Z}{\partial y}\right]_k=\left[A_v\frac{\partial u}{\partial z}\right]_k$$

$$\left[A_v\frac{\partial v}{\partial z}-\left(A_h\frac{\partial v}{\partial x}\right)\frac{\partial Z}{\partial x}-\left(A_h\frac{\partial v}{\partial y}\right)\frac{\partial Z}{\partial y}\right]_k=\left[A_v\frac{\partial v}{\partial z}\right]_k \qquad \cdots\cdots(39)$$

$k=1$, …… , $K-1$ 。

在海面 $z=z_o=\zeta(x,y,t)$，則使用邊界條件 (21)式，在海底 $z=z_K=-H(x,y)$，則應用邊界條件 (22) 式。

如此在內部界面，動量的垂直擴散可以下式求其近似值；

$$\left[A_v\frac{\partial u}{\partial z}\right]_k=A_v\frac{\bar{u}_{k-1/2}-\bar{u}_{k+1/2}}{Z_{k-1/2}-Z_{k+1/2}}=2A_v\frac{\bar{u}_{k-1/2}-\bar{u}_{k+1/2}}{D_{k-1/2}+D_{k+1/2}}$$

$$\left[A_v\frac{\partial v}{\partial z}\right]_k=A_v\frac{\bar{v}_{k-1/2}-\bar{v}_{k+1/2}}{Z_{k-1/2}-Z_{k+1/2}}=2A_v\frac{\bar{v}_{k-1/2}-\bar{v}_{k+1/2}}{D_{k-1/2}+D_{k+1/2}} \qquad \cdots\cdots(40)$$

其中 $\quad Z_{k-1/2}=\frac{1}{2}\left(Z_{k-1}+Z_k\right)$。

對於溫度與塩度在內部界面的垂直擴散，同樣地也利用 (40)式的近似關係得之。

如果我們對整層的水平動量交換係數視爲常數，即 $A_h=$ const.，則

$$\nabla\cdot\int_{z_k}^{z_{k-1}} A_h \nabla u\, dz = \frac{\partial}{\partial x}\int_{z_k}^{z_{k-1}} (A_h \frac{\partial u}{\partial x}) dz + \frac{\partial}{\partial y}\int_{z_k}^{z_{k-1}} (A_h \frac{\partial u}{\partial y})\ dz$$

$$= A_h\ (\frac{\partial^2 U_{k-1/2}}{\partial x^2} + \frac{\partial^2 U_{k-1/2}}{\partial y^2})$$

$$\nabla\cdot\int_{z_k}^{z_{k-1}} A_h \nabla v\, dz = \frac{\partial}{\partial x}\int_{z_k}^{z_{k-1}} (A_h \frac{\partial v}{\partial x})\ dz + \frac{\partial}{\partial y}\int_{z_k}^{z_{k-1}} (A_h \frac{\partial v}{\partial y})\ dz$$

$$= A_h\ (\frac{\partial^2 V_{k-1/2}}{\partial x^2} + \frac{\partial^2 V_{k-1/2}}{\partial y^2}) \qquad \cdots\cdots (41)$$

$k = 1$,……, $K-1$ 。

對於表面第一層水平擴散之計算，我們忽略自由水面之波動。

因此

$$\frac{1}{D_{k-1/2}}\nabla\cdot\int_{z_k}^{z_{k-1}} \frac{A_h}{\rho_o}\nabla u\, dz - \frac{1}{D_{k+1/2}}\nabla\cdot\int_{z_{k+1}}^{z_k} \frac{A_h}{\rho_o}\nabla u\ dz$$

$$= \frac{A_h}{\rho_o}\left[\frac{\partial^2}{\partial x^2}(\bar{u}_{k-1/2} - \bar{u}_{k+1/2}) + \frac{\partial^2}{\partial y^2}(\bar{u}_{k-1/2} - \bar{u}_{k+1/2})\right] \quad \cdots (42)$$

$$\frac{1}{D_{k-1/2}}\nabla\cdot\int_{z_k}^{z_{k-1}} \frac{A_h}{\rho_o}\nabla v\, dz - \frac{1}{D_{k+1/2}}\nabla\cdot\int_{z_{k+1}}^{z_k} \frac{A_h}{\rho_o}\nabla v\ dz$$

$$= \frac{A_h}{\rho_o}\left[\frac{\partial^2}{\partial x^2}(\bar{v}_{k-1/2} - \bar{v}_{k+1/2}) + \frac{\partial^2}{\partial y^2}(\bar{v}_{k-1/2} - \bar{v}_{k+1/2})\right] \quad \cdots (43)$$

$k = 1$,……, $K-2$ 。

最底下一層的水平動量擴散，則由下列近似關係求得

$$\int_{z_K}^{z_{K-1}} A_h \nabla(u, v)\, dz = \left[A_h D \nabla\left(\frac{U}{D}, \frac{V}{D}\right)\right]_{K-1/2}$$

$$= \left[A_h D \nabla(\bar{u}, \bar{v})\right]_{K-1/2}$$

上式括弧中的應變數，皆爲最低層（K－1／2）之平均値。

對於非線性項的計算，則採用下列近似關係，

$$\int_{z_k}^{z_{k-1}} \Psi u\, dz = \left[\frac{\Psi U}{D}\right]_{k-1/2} \quad , \quad \int_{z_k}^{z_{k-1}} \Psi v\, dz = \left[\frac{\Psi V}{D}\right]_{k-1/2} \qquad \cdots\cdots (44)$$

其中Ψ代表u，v，T，S中的任一個應變數，而$\Psi_{k-1/2}$則代表$U_{k-1/2}$，$V_{k-1/2}$，$\theta_{k-1/2}$，$\phi_{k-1/2}$中之任一個。

如果在任一層內，其密度變化不大，則斜壓的壓力部分可以下列近似關係表示，

$$\int_{z_k}^{z_{k-1}} P'_x\, dz \equiv \int_{z_k}^{z_{k-1}} \frac{\partial P'}{\partial x}\, dz = D_{k-1/2} \frac{\partial P'_{k-1/2}}{\partial x}$$

$$\cdots\cdots (45)$$

$$\int_{z_k}^{z_{k-1}} P'_y\, dz \equiv \int_{z_k}^{z_{k-1}} \frac{\partial P'}{\partial y}\, dz = D_{k-1/2} \frac{\partial P'_{k-1/2}}{\partial y}$$

（其中 $P'_{k-1/2} = \int_{z_{k-1/2}}^{\zeta} \sigma\, dz$ ）

因此(37)式中斜壓的壓力差値，可以寫成

$$\frac{1}{D_{k-1/2}}\int_{z_k}^{z_{k-1}} P'_x\, dz - \frac{1}{D_{k+1/2}}\int_{z_{k+1}}^{z_k} P'_x\, dz = \frac{\partial}{\partial x}\left(P'_{k-1/2} - P'_{k+1/2}\right) = -\frac{\partial}{\partial x}\int_{z_{k+1/2}}^{z_{k-1/2}} \sigma\, dz \quad (46)$$

我們繼續取下列近似關係，

$$\frac{\partial}{\partial x}\int_{z_{k+1/2}}^{z_{k-1/2}}\sigma\, dz=(Z_{k-1/2}-Z_{k+1/2})\frac{\partial\bar{\sigma}_k}{\partial x} \quad \cdots\cdots(47)$$

如此可得

$$\frac{1}{D_{k-1/2}}\int_{z_k}^{z_{k-1}}P'_x\, dz-\frac{1}{D_{k+1/2}}\int_{z_{k+1}}^{z_k}P'_x\, dz=\frac{D_{k-1/2}+D_{k+1/2}}{2}\frac{\partial\bar{\sigma}_x}{\partial x} \quad \cdots\cdots(48)$$

對於 y 方向，其方法完全相同。

上式中

$$\bar{\sigma}_k=g\,\rho'_k=g\,(\bar{\rho}_k-\rho_o) \quad \cdots\cdots(49)$$

而 $\bar{\rho}_k=\rho(\bar{S}_k, \bar{T}_k, \bar{p}_k)$ 可由（10）式求得，其中壓力可利用那一層（即第 k 層）的平均深度換算之，而溫度與塩度則爲

$$\bar{S}_k=\frac{1}{2}(\bar{S}_{k-1/2}+\bar{S}_{k+1/2})=\frac{1}{2}\left(\frac{\phi_{k-1/2}}{D_{k-1/2}}+\frac{\phi_{k+1/2}}{D_{k+1/2}}\right) \quad \cdots\cdots(50)$$

$$\bar{T}_k=\frac{1}{2}(\bar{T}_{k-1/2}+\bar{T}_{k+1/2})=\frac{1}{2}\left(\frac{\theta_{k-1/2}}{D_{k-1/2}}+\frac{\theta_{k+1/2}}{D_{k+1/2}}\right) \quad \cdots\cdots(51)$$

對於 (34)式中整個水柱的斜壓力，則如下可得，

$$\sum_{k=1}^{K}\int_{z_k}^{z_{k-1}}P'_x\, dz=\sum_{k=1}^{K}D_{k-1/2}\frac{\partial P'_{k-1/2}}{\partial x}$$

$$=H\frac{\partial P'_{1/2}}{\partial x}+\left(\sum_{k=2}^{K}D_{k-1/2}\right)\left(\frac{\partial P'_{3/2}}{\partial x}-\frac{\partial P'_{1/2}}{\partial x}\right)+\cdots\cdots$$

$$+D_{K-1/2}\left(\frac{\partial P'_{K-1/2}}{\partial x}-\frac{\partial P'_{K-3/2}}{\partial x}\right) \quad \cdots\cdots(52)$$

(52) 式的右邊，除了第 1 項之外，可利用 (46) ～ (51) 求得。第 1 項則由下列近似關係求出，

$$\frac{\partial P'_{1/2}}{\partial x}=\frac{\partial}{\partial x}\int_{z_{1/2}}^{\zeta}\sigma\,dz=(\zeta-Z_{1/2})\frac{\partial\bar{\sigma}_{1/2}}{\partial x}=\left[\zeta-\frac{1}{2}(\zeta+Z_1)\right]\frac{\partial\bar{\sigma}_{1/2}}{\partial x}$$

$$=-\frac{Z_1}{2}\frac{\partial\bar{\sigma}_{1/2}}{\partial x} \qquad\cdots\cdots(53)$$

而 $\bar{\sigma}_{1/2}$ 爲第 1 層之值，其大小爲

$$\bar{\sigma}_{1/2}=g\,\rho'_{1/2}=\rho(\bar{\rho}_{1/2}-\rho_o)$$

一般而言，在表層海水壓力對密度影響甚小，故可由表層的平均塩度與溫度決定，

$$\bar{\rho}_{1/2}=\rho(\bar{S}_{1/2},\ \bar{T}_{1/2})$$

(30) 和 (31) 中的水平擴散，利用下式求之，

$$\int_{z_k}^{z_{k-1}}\left(A_h^{(T)}\frac{\partial T}{\partial x}\right)dz=\left[A_h^{(T)}D\frac{\partial}{\partial x}\left(\frac{\theta}{D}\right)\right]_{k-1/2} \qquad\cdots\cdots(54)$$

上式爲 x 分量的形式；對於 y 分量，其形式也類同。

(54)式是以溫度水平擴散爲例；塩度的擴散項，其計算亦同。

最後在內部界面處的溫度、塩度及水平速度可以下式得之；在此我們以溫度爲例，

$$T_k=\frac{1}{2}\left(\frac{\theta}{D}\right)_{k-1/2}+\frac{1}{2}\left(\frac{\theta}{D}\right)_{k+1/2} \qquad\cdots\cdots(55)$$

內部界面處的垂直速度，則直接利用 (37)式解之。實際的解法將在下節討論。

當我們解出內模式的速度垂直切變，即 ($\bar{u}_{k-1/2}-\bar{u}_{k+1/2}$) 和 ($v_{k-1/2}$

$-\bar{v}_{k+1/2}$ ），則可以由下列方式推算出各層的平均流速，我們以 x 向的流速來說明；利用下式疊代計算卽可，

$$\bar{u}_{k+1/2}=\bar{u}_{k-1/2}-(\bar{u}_{k-1/2}-\bar{u}_{k+1/2}) \qquad \cdots\cdots(56)$$

在（56）式的疊代關係中，只要將第 1 層的平均流速 $\bar{u}_{1/2}$ 當做初值，就可疊代求出其他各層的平均流速。$\bar{u}_{1/2}$ 的求法如下。

依據定義可知

$$\bar{u}_{1/2}\cdot D_{1/2}=U_{1/2}=U-\sum_{k=2}^{K}U_{k-1/2}$$

或

$$\bar{u}_{1/2}\cdot D_{1/2}+\bar{u}_{1/2}\left(\sum_{k=2}^{K}D_{k-1/2}\right)=U+\bar{u}_{1/2}\left(\sum_{k=2}^{K}D_{k-1/2}\right)$$

$$-\sum_{k=2}^{K}\bar{u}_{k-1/2}\cdot D_{k-1/2}$$

如此，我們可再改寫爲

$$\bar{u}_{1/2}\cdot H=U+\sum_{k=2}^{K}(\bar{u}_{1/2}-\bar{u}_{k-1/2})D_{k-1/2}$$

卽

$$\bar{u}_{1/2}\cdot H=U+\sum_{k=1}^{K}(H-h_k)(\bar{u}_{k-1/2}-\bar{u}_{k+1/2}) \qquad \cdots\cdots(57)$$

如此，由（57）式可得 $\bar{u}_{1/2}$ 。

外模式（34）與（35）中，非線性項的近似關係如同（44）式；而動量水平擴散項的近似關係如同（54）式 。

我們已經將所有的控制方程式解析過了，但是整個系統的外力，卻是由邊界條件而來。爲了求海面風剪力，我們採用下列的參數化關係，

$$\tau_{sx}=\rho_a C_D W_x\,|\vec{W}| \quad , \quad \tau_{sy}=\rho_a C_D W_y\,|\vec{W}|$$

其中 W_x 和 W_y 分別是風速 $\vec{W}$ 的 x 和 y 分量；而 ρ_a 爲空氣的密度（$=1.25\times10^{-3}$

$g\ cm^{-3}$ ），C_D 為拉力係數（ drag coefficient ），是無因次常數，其值隨風速大小而有不同。計算暴潮時，由於是強風的關係，我們常取

$$C_D = 2.6 \times 10^{-3}$$

但在一般風速下，根據最近的觀測結果，

$$C_D = 1.2 \times 10^{-3}$$

海底的摩擦剪力，亦是利用參數化關係表示，即

$$\tau_{bx} = \rho K_D \bar{u}_{K-1/2} \,|\, \underset{\sim}{\bar{u}}_{K-1/2} \,| \quad , \quad \tau_{by} = \rho K_D \bar{v}_{K-1/2} \,|\, \underset{\sim}{\bar{u}}_{K-1/2} \,|$$

其中 $\bar{u}_{K-1/2}$ 為最底下一層的平均流速向量，而 K_D 為海底摩擦係數，通常我們可取

$$K_D = 2.5 \times 10^{-3}$$

當我們不考慮季節性的海況變動時；則短時間內，海面上的熱通量 q_T 與塩分通量 q_S ，對我們所考慮的海水流動與溫度及塩度的擴散影響不大，因此往往可以忽略。

最後我們需要代入模式運算的參數為動量、熱量、塩分的交換係數，它們的值都和運動規模有關，而在定差模式中它們也和網格點距離有關，其大小範圍如下：

$$10^5 < A_h < 10^9 \quad g\ cm^{-1} sec^{-1}$$

$$0 < A_h < 10^3 \quad g\ cm^{-1} sec^{-1}$$

$$10^5 < A_h^{(T)} < 10^9 \quad g\ cm^{-1} sec^{-1}$$

$$0 < A_v^{(T)} < 3 \times 10^2 \quad g\ cm^{-1} sec^{-1}$$

$$10^5 < A_h^{(S)} < 10^8 \quad g\ cm^{-1} sec^{-1}$$

$$0 < A_v^{(S)} < 10^2 \quad g\ cm^{-2} sec^{-1}$$

四、數值方法

上述的多層次模式方程式（27）～（31），及由此演化出來的外模式方程式（33）～（35）與內模式方程式（37），（38）等。我們將利用定差方法解之。我們所用的網格點如圖 2 所示。各應變數的空間微分及時間微分，將以下列差分形式計算；令F（ x ， y ， t ）代表任意應變數，則

$$\frac{\partial F(x,y,t)}{\partial x}=\frac{F(x+\frac{1}{2}\Delta x,y,t)-F(x-\frac{1}{2}\Delta x,y,t)}{\Delta x}=\frac{\delta_x F}{\Delta x}$$

$$\frac{\partial F(x,y,t)}{\partial y}=\frac{F(x,y+\frac{1}{2}\Delta y,t)-F(x,y-\frac{1}{2}\Delta y,t)}{\Delta y}=\frac{\delta_y F}{\Delta y} \qquad (58)$$

$$\frac{\partial F(x,y,t)}{\partial t}=\frac{F(x,y,t+\frac{1}{2}\Delta t)-F(x,y,t-\frac{1}{2}\Delta t)}{\Delta t}=\frac{\delta_t F}{\Delta t} \qquad (59)$$

其中ζ點的時間與U點、V點、W點的時間相差半個間隔Δ t 。而W，T和S等點的位置則與ζ點相同。

為了避免不同的網格點會出現相異的結果，我們在這裡使用二組共軛的網格點。由於擴散具有 Laplacian 的運算形式，因此當我們取所欲求值之點與其周圍 4 點，以計算 Laplacian 運算結果，如此這二組網格點自然產生共軛關係。亦即 Laplacian 之運算格點如下：

$$\frac{\partial^2 U}{\partial x^2}+\frac{\partial^2 U}{\partial y^2}=\frac{1}{(\Delta S')^2}\Big[U(x'+\Delta x',y',t-\frac{1}{2}\Delta t)+U(x'-\Delta x',y',t-\frac{1}{2}\Delta t)$$
$$+U(x',y'+\Delta y',t-\frac{1}{2}\Delta t)+U(x',y'-\Delta y',t-\frac{1}{2}\Delta t)-4U(x',y',t-\frac{1}{2}\Delta t)\Big]$$

$$\cdots\cdots (60)$$

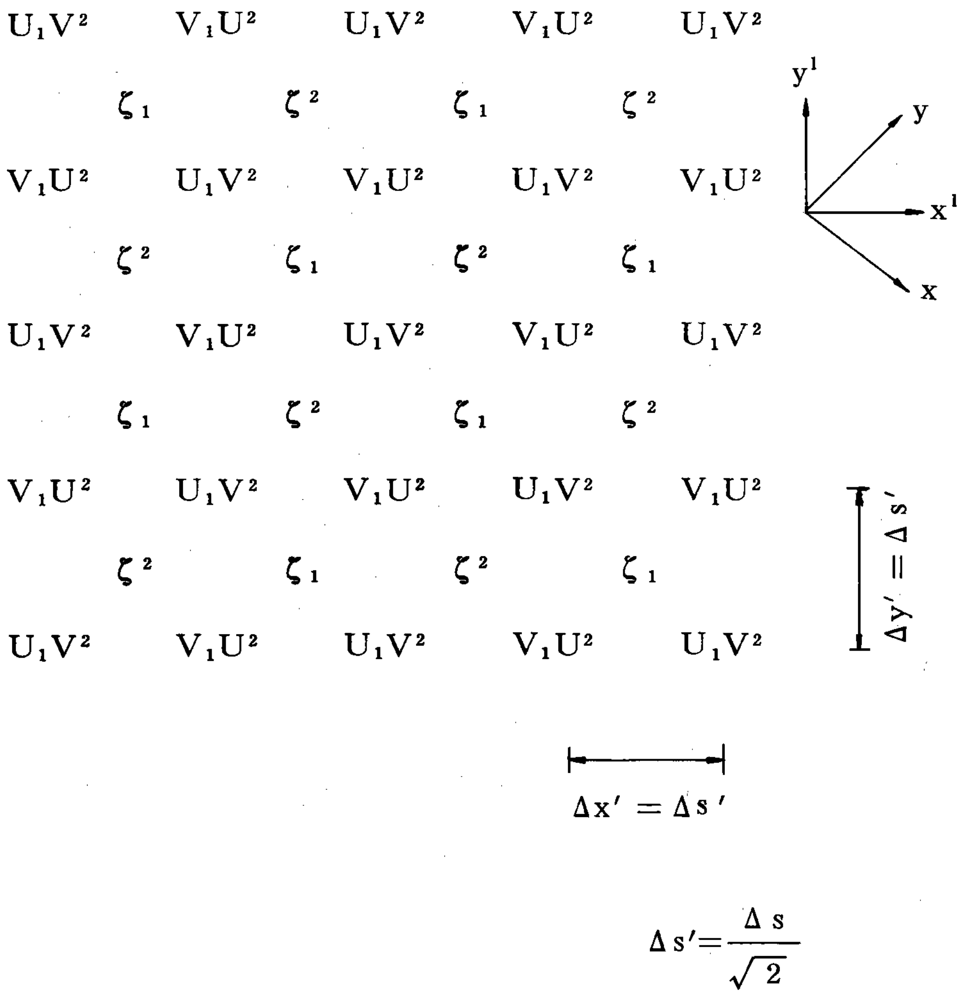

圖2　Richardson 共軛網格點結構。第一組網格點以下註 1 表示，第二組網格點以上註 2 表示。W，T和 S的計算點與 ζ 點具同樣的位置。

$$\frac{\partial^2 V}{\partial x^2}+\frac{\partial^2 V}{\partial y^2}=\frac{1}{(\Delta S')^2}\left[V(x'+\Delta x',y',t-\frac{1}{2}\Delta t)+V(x'-\Delta x',y',t-\frac{1}{2}\Delta t)\right.$$

$$\left.+V(x',y'+\Delta y',t-\frac{1}{2}\Delta t)+V(x',y'-\Delta y',t-\frac{1}{2}\Delta t)-4V(x',y',t-\frac{1}{2}\Delta t)\right]$$

其中點（x，y）與點（x′，y′）是同一點，卽

$$U(x,y)\equiv U(x',y') \quad , \quad V(x,y)\equiv V(x',y').$$

利用共軛網格點結構，對於柯氏力項與非線性項的計算也比較方便。爲了求柯氏力項，我們需要時間內插，卽

$$fV(x,y,t)\cong\frac{1}{2}f\left[V(x,y,t-\frac{1}{2}\Delta t)+V(x,y,t+\frac{1}{2}\Delta t)\right]$$

$$fU(x,y,t)\cong\frac{1}{2}f\left[U(x,y,t-\frac{1}{2}\Delta t)+U(x,y,t+\frac{1}{2}\Delta t)\right] \qquad (61)$$

如此外模式之差分方程式爲

$$\frac{\zeta(x,y,t)-\zeta(x,y,t-\Delta t)}{\Delta t}=\frac{-1}{\Delta S}\left[U(x+\frac{1}{2}\Delta x,y,t-\frac{1}{2}\Delta t)\right.$$

$$-U(x-\frac{1}{2}\Delta x,y,t-\frac{1}{2}\Delta t)+V(x,y+\frac{1}{2}\Delta y,t-\frac{1}{2}\Delta t)$$

$$\left.-V(x,y-\frac{1}{2}\Delta y,t-\frac{1}{2}\Delta t)\right] \qquad \cdots\cdots(62)$$

$$\frac{U(x,y,t+\frac{1}{2}\Delta t)-U(x,y,t-\frac{1}{2}\Delta t)}{\Delta t}=\frac{1}{2}f\left[V(x,y,t-\frac{1}{2}\Delta t)\right.$$

$$\left.+V(x,y,t+\frac{1}{2}\Delta t)\right]-gH\frac{\zeta(x+\frac{1}{2}\Delta x,y,t)-\zeta(x-\frac{1}{2}\Delta x,y,t)}{\Delta S}$$

$$-\sum_{k=1}^{K}\left(\frac{1}{\rho_o}\int_{Z_k}^{Z_{k-1}} P_x' \, dz\right)+\frac{\tau_{sx}-\tau_{bx}}{\rho_o}+\frac{A_h}{\rho_o}\left(\frac{\partial^2 U}{\partial x^2}+\frac{\partial^2 U}{\partial y^2}\right) \quad \cdots\cdots (63)$$

$$\frac{V(x,y,t+\frac{1}{2}\Delta t)-V(x,y,t-\frac{1}{2}\Delta t)}{\Delta t}=\frac{1}{2}f\left[U(x,y,t-\frac{1}{2}\Delta t)\right.$$

$$\left.+U(x,y,t+\frac{1}{2}\Delta t)\right]-gH\frac{\zeta(x,y+\frac{1}{2}\Delta y,t)-\zeta(x,y-\frac{1}{2}\Delta y,t)}{\Delta S}$$

$$-\sum_{k=1}^{K}\left(\frac{1}{\rho_o}\int_{Z_k}^{Z_{k-1}} P_y' \, dz\right)+\frac{\tau_{sy}-\tau_{by}}{\rho_o}+\frac{A_h}{\rho_o}\left(\frac{\partial^2 V}{\partial x^2}+\frac{\partial^2 V}{\partial y^2}\right) \quad \cdots\cdots (64)$$

(63) 與 (64) 式中的水平擴散項之差分形式，已在前述 (60) 式中顯現出來。

當我們使用上述的網格點結構時，我們所需要的穩定條件爲 Courant－Friedrichs－Lewy 的定規，即

$$\frac{\Delta t}{\Delta S}<\frac{1}{\sqrt{2\,gH_{max}}}$$

(65) 式的準繩適用外模式。而內模式因不受自由水面波之影響，其計算時間的間隔可放大爲外模式的 3 ～ 5 倍。

海洋內部界面處的垂直速度，可由 (27) 式轉化成定差方程式而解出，

$$W_{k-1}(x,y,t-\frac{1}{2}\Delta t)-W_k(x,y,t-\frac{1}{2}\Delta t)$$

$$=-\frac{1}{\Delta S}\left[U_{k-1/2}(x+\frac{1}{2}\Delta x,y,t-\frac{1}{2}\Delta t)-U_{k-1/2}(x-\frac{1}{2}\Delta x,y,t-\frac{1}{2}\Delta t)\right.$$

$$\left.+V_{k-1/2}(x,y+\frac{1}{2}\Delta y,t-\frac{1}{2}\Delta t)-V_{k-1/2}(x,y-\frac{1}{2}\Delta y,t-\frac{1}{2}\Delta t)\right] \qquad (66)$$

其中　$k=2,\cdots\cdots,K-1$.

如我們從最低下一層開始運算，配合邊界條件(20)式，而當各層的水平流速都已應用(56)式算出，則由(66)式就可算出各界面之垂直流速。

任一層的溫度擴散方程式，即(30)式，其定差形式如下，

$$\frac{\partial \theta}{\partial t}+\frac{1}{\Delta x'}(\overline{U}^1\overline{T}^1-\overline{U}^2\overline{T}^2)+\frac{1}{\Delta y'}(\overline{V}^1\overline{T}^3-\overline{V}^2\overline{T}^4)$$

$$+W_{k-1}(x',y')\frac{\overline{T}(x',y')+\overline{T}_{k-3/2}(x',y')}{2}-W_k(x',y')\frac{\overline{T}(x',y')+\overline{T}_{k+1/2}(x',y')}{2}$$

$$=\frac{A_k^{(T)}}{\rho_o}\{\frac{1}{\Delta x'}[\overline{D}^1\frac{\overline{T}(x'+\Delta x',y')-\overline{T}(x',y')}{\Delta x'}-\overline{D}^2\frac{\overline{T}(x',y')-\overline{T}(x'-\Delta x',y')}{\Delta x'}]$$

$$+\frac{1}{\Delta y'}[\overline{D}^3\frac{\overline{T}(x',y'+\Delta y')-\overline{T}(x',y')}{\Delta y'}-\overline{D}^4\frac{\overline{T}(x',y')-\overline{T}(x',y'-\Delta y')}{\Delta y'}]\}$$

$$+\frac{2A_v^{(T)}}{\rho_o}\cdot\frac{\overline{T}_{k-3/2}-\overline{T}}{D_{k-3/2}-D}-\frac{2A_v^{(T)}}{\rho_o}\cdot\frac{\overline{T}-\overline{T}_{k+1/2}}{D-D_{k+1/2}} \qquad \cdots\cdots(67)$$

其中表示第 k−1/2 層的下註及時間變數(t)都已省略。而其中一些符號的意義如下，

$$\overline{T}_{k-1/2}=\frac{\theta_{k-1/2}}{D_{k-1/2}}\ (=\overline{T})$$

$$\overline{U}^1=\frac{1}{2}[U(x'+\frac{1}{2}\Delta x',y'+\frac{1}{2}\Delta y')+U(x'+\frac{1}{2}\Delta x',y'-\frac{1}{2}\Delta y')]$$

$$\overline{U}^2=\frac{1}{2}[U(x'-\frac{1}{2}\Delta x',y'+\frac{1}{2}\Delta y')+U(x'-\frac{1}{2}\Delta x',y'-\frac{1}{2}\Delta y')]$$

$$\overline{V}^1=\frac{1}{2}[V(x'+\frac{1}{2}\Delta x',y'+\frac{1}{2}\Delta y')+V(x'-\frac{1}{2}\Delta x',y'+\frac{1}{2}\Delta y')]$$

$$\overline{V}^2=\frac{1}{2}[V(x'+\frac{1}{2}\Delta x',y'-\frac{1}{2}\Delta y')+V(x'-\frac{1}{2}\Delta x',y'-\frac{1}{2}\Delta y')]$$

$$\overline{T}^1 = \frac{1}{2}\left[\overline{T}(x',y') + \overline{T}(x'+\Delta x',y')\right]$$

$$\overline{T}^2 = \frac{1}{2}\left[\overline{T}(x',y') + \overline{T}(x'-\Delta x',y')\right]$$

$$\overline{T}^3 = \frac{1}{2}\left[\overline{T}(x',y') + \overline{T}(x',y'+\Delta y')\right]$$

$$\overline{T}^4 = \frac{1}{2}\left[\overline{T}(x',y') + \overline{T}(x',y'-\Delta y')\right]$$

$$\overline{D}^1 = \frac{1}{2}\left[D(x'+\frac{1}{2}\Delta x',y'+\frac{1}{2}\Delta y')+D(x'+\frac{1}{2}\Delta x',y'-\frac{1}{2}\Delta y')\right]$$

$$\overline{D}^2 = \frac{1}{2}\left[D(x'-\frac{1}{2}\Delta x',y'+\frac{1}{2}\Delta y')+D(x'-\frac{1}{2}\Delta x',y'-\frac{1}{2}\Delta y')\right]$$

$$\overline{D}^3 = \frac{1}{2}\left[D(x'+\frac{1}{2}\Delta x',y'+\frac{1}{2}\Delta y')+D(x'-\frac{1}{2}\Delta x',y'+\frac{1}{2}\Delta y')\right]$$

$$\overline{D}^4 = \frac{1}{2}\left[D(x'+\frac{1}{2}\Delta x',y'-\frac{1}{2}\Delta y')+D(x'-\frac{1}{2}\Delta x',y'-\frac{1}{2}\Delta y')\right]$$

如同前述，點 $(x,y)\equiv(x',y')$ 表示正求某一應變數之值時所處之位置。

塩度擴散方程式，(31)式，其定差形式完全同(67)式。

五、討論與結論

我們在上節所發展出來的數值模式，基本上僅適用於封閉的海域。對於開放的海域，則需要開口邊界條件。一般而言，開口邊界愈長，則我們所考慮的海域與外界交流就愈頻繁，開口的邊界條件就愈複雜。對於近似封閉的港灣，則所需的開口邊界條件就較簡單。

開口邊界條件之設立，與我們所研究的現象有關。如我們僅考慮潮汐運動

，則我們可以在開口邊界上代入潮汐的預測值，以計算所研究海域的潮流變化。此種潮汐模式，通常不考慮風剪力。

如我們所研究的現象是颱風暴潮，則我們的開口邊界條件，可以利用顛倒氣壓計數效應所形成之海面波動代入，即

$$\Delta \zeta = -\frac{\Delta p_a}{\rho_o g}$$

其中 Δp_a 代表開口邊界上水位點之氣壓與遠處參考氣壓之差。

另外，處理風吹流的數值模式，亦可使用輻射條件（radiation condition），詳細的討論，請參考 Chapman（1985）。

但是上述的開口邊界條件，僅適用於均質流體。對於非均質流體，則除了流況或水位的開口邊界條件，還需要溫度及鹽度的開口邊界條件。這些溫度與鹽度的邊界條件，幾乎沒有任何理論可以推導出來，因此往往需要視所研究之海域環境情況而有特別的假設條件。

我們在上節所探討的多層次模式，也可用來探討污染擴散情況。例如熱污染的數值模式，我們可以不需考慮鹽度變化，狀態方程式也可簡化。而其他區域性的污染物擴散情況，其控制方程式也完全類似鹽度擴散方程式；如此上述多層次模式，也可適用於三度空間污染擴散情形。

參考文獻

Bryan, K. and M. D. Cox (1967) A numerical investigation of the oceanic general circulation. Tellus 19, pp.54-80.

Bryan, K, and M. D. Cox (1968) A nonlinear model of an ocean driven by wind and differential heating : part I and II. J. Atmos. Sci. 25, pp.945-978.

Bryan, K. (1969) A numerical method for the study of ocean circulation. J. Computat. Phys. 4, pp.347-376.

Bryan, K. (1979) Models of the world Ocean. Dyn. Atmos. oceans 3, pp.327-338.

Chapman, D. C. (1985) Numerical treament of cross-shelf open boundaries in a barotropic coastal ocean model. J. Phys. Oceanogr. 15, pp.1060-1075.

Cox, M. D. (1970) A mathematical model of the Indian Dcean. Deep-Sea Res. 17, pp. 47-75.

Cox, M. D. (1975) A baroclinic model of the world ocean : Preliminary results. In "Numerical Models of Ocean Circulation", pp.107-120. Natl. Acad. Sci., Washington, D. C.

Cox, M. D. (1979) A numerical study of Somali current eddies. J. Phys. Oceanogr. 9, pp.311-326.

Davies, A. M. and A. Owen (1979) Three dimensional numerical sea model using the Galerkin method with a polynomial basis set. Appl. Math Modelling 3, pp. 421-428.

Davies, A. M. (1979) Application of the Galerkin method to the formulation of a three-dimensional nonlinear hydrodynamic numerical sea model. Appl. Math. Modelling 4, pp.245-256.

Davies, A. M. (1980) Three dimensional hydrodynamic numerical models: part 1 and 2. In "Proceedings of the Norwegian Coastal Current Symposium", Geilo, Nerway, Bergen University. pp.370-426.

Owen, A. (1980) A three-dimensional model of the Bristol Channel, J. Phys. Oceanogr. 10, pp.1290-1302.

Simons, T. J. (1973) Development of three-dimensional numerical models of the Great Lakes. Scientic Series No.12, Inland waters Directorate, Canada Centre for Inland Waters.

第三屆基礎港灣數值(數學)模式研習會論文集 Jan. 17～18，1990 Page 251～258

颱風湧浪預報數值模式

梁乃匡

台灣大學海洋研究所教授

一、引 言

民國 76 年 10 月 24 日 聯合報第五版的頭條標題：颱風遠在天邊？災難近在眼前！國小師生郊遊，變生貓鼻頭。滔天巨浪拍岸，吞噬九學童。

這是一件最近最鮮明的颱風湧浪造成的災難，而事實上，在過去不乏進行中海岸工程，因無發佈陸上颱風警報而未作預防措施，以致該工程遭湧浪破壞的例子。此外，在東海岸，即使連海上颱風警報都未發佈，因颱風湧浪的干擾而使海上施工白做或做得不理想，也是經常發生的事。

何謂湧浪？就是遠處的風在該處吹出風浪，然後傳遞到本地的浪。這種浪通常為長週期長峯型，週期大約在 10 秒到 20 秒之間。因為浪跑的速度與週期成正比，以波能的速度而言，湧浪傳遞速度大約在 28 公里／小時～ 56 公里／小時之間。一般颱風移動速度大多在 10 公里／小時～ 20 公里之間，因此颱風湧浪必定比颱風先到，況且颱風不一定經過本地，而湧浪是自颱風暴風圈向四面八方傳出的。就是這個緣故，民國 76 年 10 月在貓鼻頭造成 9 名學童喪生事件的禍首是前一天中度颱風琳恩所吹出來的湧浪。因此預報颱風湧浪的颱風資料可能是過去的實際資料而非預測資料，使得颱風湧浪的預測準確度大為提高。作者曾在民國 71年提出颱風湧浪的預報方法（梁， 1982 ），並在往後陸續提出修改(Liang & Chien ， 1985 ；梁， 1987 ；Liang ， 1989)，但似乎並未被廣泛利用，究其原因，可能是沒有提供實用程式，一般以為很麻煩所致。本文將提供一份用BASIC 語言寫的電腦程式，可在任何個人電腦上使用。本程式未考慮遮蔽效應，所以只適合無遮蔽的情況。由於遮蔽效應只會使波高減小，站在安全的立場，並無影響。

二、模式介紹

本模式乃是利用 Bretschneider（ Bretschneicher & Tamage ， 1976 ）推算颱風波浪的方法，估計不移動颱風中心最大風速半徑R處的代表波高H_R（呎）及週期T_R（秒），以作爲颱風風場內的代表波浪條件。湧浪波高先以作者的元素波模式的觀念（ Liang ， 1973 ），將颱風視爲不移動的點波源，則湧浪波高與H_R・R 成正比與颱風中心與測站間的距離開方成反比，比例常數爲經驗常數。進而考慮因颱風移動而造成之波高增加或減少的堆積與消退效應，本效應乃根據能量守恒原則。週期乃是先選出相關較高的無因次參數對，再以實測資料迴歸經驗公式，湧浪實測週期採用波譜之最大能量頻率之倒數T_P。

估算颱風湧浪的步驟如下：

(一)求颱風中心最大風速U_R

$$U_R = K\sqrt{P_N - P_O} - 0.5fR \quad （節） \qquad \cdots\cdots\cdots(1)$$

其中P_N爲正常氣壓，等於 29.92 吋汞柱高，P_O爲颱風中心氣壓單位亦爲吋汞柱高，R爲颱風最大風速半徑，單位爲浬，理論上可以由氣壓分佈曲線求得，但事實上氣壓分佈曲線很不容易獲得，因此以七級風暴風半徑R7 的十分之一來近似。

k爲係數， f 爲科氏力係數，二者與緯度的關係如表一。

表一　k及 f 值與緯度之關係

緯度 ϕ	20	22.5	25	27.5	30	32.5	35	37.5	40.0
f	0.18	0.20	0.22	0.24	0.26	0.28	0.30	0.32	0.34
k	67	67	67	66	66	66	66	65	64

(二)將 U_R 換算成 10 公尺高 10 分鐘平均風速為

$$U_{RS} = 0.865\,U_R \qquad \cdots\cdots\cdots (2)$$

(三)以美國 51 個颶風實測資料得出波高推算公式為

$$H_R = k'\sqrt{R\triangle P} \qquad \cdots\cdots\cdots (3)$$

其中 $\triangle P = P_N - P_O$，H_R 為距中心 R 處波高，單位呎。

k' 為 $\frac{fR}{U_R}$ 之函數，如表二所示。

表二　k′ 與 fR／U_R 之關係

fR／U_R	k′	fR／U_R	k′	fR／U_R	k′
0	7.50	.085	5.20	0.24	3.85
.005	7.25	.090	5.13	0.25	3.80
.010	7.05	.095	5.06	0.26	3.75
.015	6.85	.100	5.00	0.27	3.70
.020	6.70	.110	4.88	0.28	3.65
.025	6.55	.120	4.76	0.29	3.60
.030	6.40	.130	4.66	0.30	3.55
.035	6.25	.140	4.57	0.31	3.50
.040	6.10	.150	4.50	0.32	3.45
.045	5.95	.160	4.42	0.33	3.40
.050	5.80	.170	4.34	0.34	3.35
.055	5.70	.180	4.28	0.35	3.30
.060	5.60	.190	4.18	0.36	3.26
.065	5.49	.200	4.10	0.37	3.23
.070	5.42	.210	4.03	0.38	3.20
.075	5.34	.220	3.97	0.39	3.17
.080	5.27	.230	3.91	0.40	3.15

(四)颱風中心R處週期可由波高H_R及海面風速求出，如下：

$$T_R = 0.378 U_{RS} \tanh \left[\ell n \left\{ \left(1+\frac{40H_R}{U_{RS}^2} \right) \Big/ \left(1-\frac{40H_R}{U_{RS}^2} \right) \right\}^{0.5} \right]^{0.6} \quad \cdots\cdots\cdots (4)$$

(五)用下式求出湧浪週期

$$T_P = (0.003 DD \cdot R7 / T_R^4 + 0.22) U_{RS} \quad \cdots\cdots\cdots (5)$$

其中DD是颱風中心與推算點的距離，單位海浬，R7是颱風七級風暴風半徑，單位公里。

(六)用下式求出湧浪波高

$$H_{1/3} = 0.006 R7 \cdot H_R / (DD)^{1/2} \quad \cdots\cdots\cdots (6)$$

$H_{1/3}$單位爲公尺。

(七)因爲颱風在移動，湧浪將產生堆積與消退的現象，當颱風與推算點的距離變小，則波高將增大，稱爲堆積；當颱風與推算點的距離變大，則波高將減小，稱爲消退。(6)式求出的湧浪波高應乘以一修正係數λ，

$$\lambda = \left(\frac{T_D}{T_D'}\right)^{1/2} \quad \cdots\cdots\cdots (7)$$

其中　$T_D = T_2 - T_1$ $\cdots\cdots\cdots (8)$

T_1，T_2爲相鄰兩次出現颱風的時刻，一般爲6小時。

$$T_D' = T_2 + T lag\, 2 - (T_1 + T lag\, 1) \quad \cdots\cdots\cdots (9)$$

$$T lag = \frac{DD}{1.56 T_P} \quad (\text{小時}) \quad \cdots\cdots\cdots (10)$$

T_D'爲相鄰兩次出現颱風之湧浪在測站出現之時間差，T lag爲湧浪自颱風中心傳抵測站所需的時間。

(八)修正後的湧浪波高爲

$$H_{1/3}' = \lambda H_{1/3} \quad (\text{公尺}) \qquad \cdots\cdots\cdots (11)$$

三、實用電腦程式及實例

用BASIC語言寫成的颱風湧浪預報程式乙種如下：

```
10  REM TYPHOON SWELL PREDICTION
20  INPUT "LATO=",LATO
30  INPUT "LONO=",LONO
40  INPUT "DATE=",DATE
50  INPUT "TIME=",TIME
60  INPUT "LAT= ",LAT
70  INPUT "LON=",LON
80  INPUT "PC=",PC
90  INPUT "R7=",R7
100 DD=60*SQR(LAT-LATO)^2+(LON-LONO)^2)
110 DEF FNH(M)=-2*EXP(-M)/(EXP(M)+EXP(-M))+1
120 R=.1*R7/1.852
130 K=-LAT/7.5+70
140 DP=(1000+(1000-PC)/10-PC)/33.87
150 UR=K*SQR(DP)-.55*R
160 US=.865*UR
170 F=.5236*SIN(LAT*3.14159/180)
180 KP=7.59-41.21*(F*R/UR)+160.51*(F*R/UR)^2-219.32*(F*R/UR)^3
190 HR=KP*SQR(R*DP)
200 D=((1+(10*HR)/(US)^2)/(1-(40*HR)/(US)^2))
```

```
210 IF D=<1 THEN LET D=1
220 Z=(LOG(D^.5))^.6
230 TR=.3785*US*FNH(Z)
240 HS=.006*R7*HR/SQR(DD)
250 TP=US*(.003*DD*R7/TR^4+.22)
260 LAG=DD/1.56/TP
270 TORIG=DATE*24+TIME
280 TARIV=TORIG+LAG
290 DATUM=INT(TARIV/24)
300 ZEIT=TARIV-24*DATUM
310 IF TARIVO=0 THEN GOTO 330 ELSE
320 NANDA=SQR((TORIG-TORIGO)/(TARIV-TARIVO))
330 H13=NANDA*HS
340 PRINT "DAY" ;TAB(10); "TIME"; TAB(20); "HS"; TAB(30);"H13
    "; TAB(40); "TP"; TAB(50);"NANDA"
350 PRINT DATUM; TAB(5); ZEIT; TAB(16); HS; TAB(30); H13;TAB
    (35);TP;TAB(50);NANDA
360 TARIVO=TARIV
370 TORIGO=TORIG
380 INPUT "X=",X
390 IF X=0 THEN GOTO 40 ELSE
400 END
```

使用時先鍵入RUN然後按RETURN，則出現LAT0 ＝ _ 鍵入測站緯度後按RETURN，則出現LON0 ＝ _ ，以下爲一實例：

```
RUN
LATO= [21.9]        測站緯度（方格內爲鍵入數字）
LONO= [120.8]       測站經度
DATE= [8]           日　期
```

TIME= $\boxed{14}$ 時 間

LAT= $\boxed{18.4}$ 颱風中心緯度

LON= $\boxed{128.3}$ 颱風中心經度

PC= $\boxed{985}$ 颱風中心氣壓

R7= $\boxed{150}$ 七級風暴風半徑（公里）

DAY（日期）	TIME（時間）	HS（波高）	H13（修正波高）
9	12.50156	.5173534	0

TP（週期）	NANDA（修正係數）
14.14684	0

（因係第一筆資料，無法算波高修正係數 λ，所以 $\lambda=0$，H13 = 0）

X= $\boxed{0}$ 鍵入 0 則程式由陳述 40 繼續

DATE= $\boxed{8}$

TIME= $\boxed{20}$

LAT= $\boxed{18.8}$

LON= $\boxed{127.0}$

PC= $\boxed{983}$

R7= $\boxed{150}$

DAY	TIME	HS	H13	TP	NANDA
9	15.65231	.6061421	.8364551	13.56624	1.379965

X= $\boxed{1}$ 鍵入非 0，則程式終止

OK

本程式未考慮月，如跨月時，將日期繼續加上去，例如由 9 月到 10 月，10 月 1 日取 31 日即可，餘類推。

四、討論與結論

應用本程式時，先撥電話 166，可得知颱風時間、中心位置、中心氣壓及

七級風暴風半徑，陸續記下，輸入個人電腦（先輸入測站經緯度）便可求出湧浪波高週期及抵達時間。因求出之波高為代表波高或示性波高，可能出現的最大波高為上述的兩倍。由於本法中的經驗常數從少數的資料迴歸而來，將來有更多資料時，應該再修改，無論如何現在的方法已經可以用了。

五、參考文獻

1.梁乃匡（1982）颱風湧浪的預報方法，第六屆海洋工程研討會論文集，民國71年9月台中市，P.5－1～5－19。

2.LIANG, N.K. and C.C. Chien(1985) A Typhoon Swell Hindcasting Technique Modified by Land Sheltering Effect, Proceedings, Air-Sea Interaction Workshop, Dec. 7-16, 1985, Taipei, pp.279-312.

3.梁乃匡（1987）颱風湧浪週期推算法之探討，第九屆海洋工程研討會論文集，民國76年11月台南 pp.371～382。

4.LIANG, N.K. (1989) A Revised Typhoon Swell Prediction Method, Journal of Harbour Technology, Vol.4, pp.1-10.

5.Bretschneider, C.L. and E.E. Tamage(1976) Hurricane Wind and Wave Forecasting Techniques, Proceedings 15th International Coastal Engineering Conference, pp.202-237.

第三屆基礎港灣數值(數學)模式研習會論文集 Jan. 17～18 , 1990 Pnge 259～279

SHOALING OF A SMALL AMPLITUDE WAVE ON IMPERMEABLE SLOPES

Lee, Chung-Pan, Herng-Wen Jang** and Hwung-Hweng Hwung****

ABSTRACT

Wave shoaling and reflection of a small amplitude wave train travelling on a slope have been studied analytically. The slope is first partitioned and approximated by a zigzag line and the flow field is correspondingly divided and approximated by a group of rectangular sub-domains. In each sub-domain, the induced flow is represented by a series of velocity potentials. The velocity potentials in each domain satisfy the Laplace equation. Both kinematic and dynamic boundary conditions are matched on the free surface and the boundary between any two sub-domains. Only the kinematic boundary condition is applied on an impermeable boundary. Furthermore, Sommerfeld's radiation condition is applied at the infinity.

Analytical results show that wave height decreases as water depth decreases for incident waves with larger deep water wave steepness, but decreases first and then increases as water depth decreases for those with smaller steepness. Analytical results also give envelopes with distinguishable loops and nodes. The ratio of wave height to water depth increases as water becomes shallower, with higher velues corresponding to those incident waves with larger steepness. Furthermore, local wave steepness increases as water depth decreases and as deep water steepness increases.

---

* Associate Professor, Institute of Marine Geology, National Sun Yat-Sen University, Kaoshiung, Taiwan, R.O.C.

** Master of Engineering,Hydraulic and Ocean Engineering Department National Cheng-Kung University, Tainan, Taiwan, R.O.C.

*** Professor, Hydraulic and Ocean Engineering Department, National Cheng-Kung University, Tainan, Taiwan, R.O.C.

1. INTRODUCTION

Waves deform as they propagate toward shallow water. The deformation process is denoted as shoaling. Reflection also occurs on a nature beach and is usually considered separatively. Related studies about shoaling often assumed a gradually varying slope due to the use of a perturbation parameter involved the bottom slope. Reflection was then not considered in these cases. However, shoaling and reflection occur simultaneously and may couple to each other, especially for nonlinear waves.

Potential theory is applied in this study under the assumption that the flow is irrotational. Assumptions on the fluid are inviscid and incompressible. Furthermore, a slope is approximated by a zigzag line and no hypothesis about the slope is assumed. Theoretically, the zigzag line will approach the original line as the steps of the zigzag line approaches to zero. Thus, the successful use of the approximation depends on whether the steps of the zigzag line are sufficiently small. A trial and error process is then used to test the convergence of the solution depending on the approximation. Small amplitude assumption is still made in this study and can be released for nonlinear waves. In this case, another mathematical technique may be needed to treat the nonlinear boundary conditions on the free surface.

For a linearized boundary value problem with rectangular domains as in this study, the method of separation of variables can be applied successfully. The solution in the flow field is represented by an infinite series of eigen-functions. When the series is truncated to finite terms, the convergence of the finite series is also confirmed.

Analytical solutions show that reflection is as important as shoaling in the potential flow where inviscid fluid consumes no energy. The effects of slopes have been illustrated for linear waves on typical slopes.

2. *THEORETICAL DERIVATION*

Consider a small amplitude incident wave train travelling toward an impermeable slope, Fig. 1. Assume that the fluid is inviscid and incompressible and the flow field is irrotational. A single-valued velocity potential can then be defined as :

$$\vec{V} = -\nabla\Phi \qquad (1)$$

From the definition of the velocity potential, the continuity equation of the incompressible fluid results in the Laplace equation

$$\nabla^2\Phi = 0 \qquad (2)$$

The linearized Bernoulli's equation of the velocity potential can be written as

$$-\frac{\partial\Phi}{\partial t} + \frac{p}{\rho} + gz = 0 \qquad (3)$$

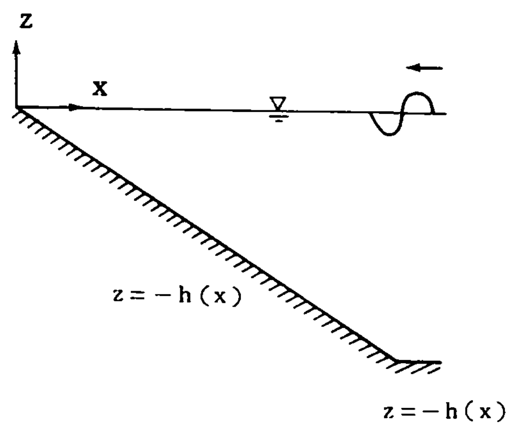

Fig. 1 Definition sketch of the flow field.

Physical constraints impose the requirement that the velocity potential of the flow field matches dynamic and kinematic boundary conditions on the boundaries. For potential flow, a dynamic boundary condition (DBC) requires that the pressure is continuous across a boundary. This can be derived from Newton's second law. For a boundary separating two immiscible fluids, such as a free surface, surface tension may be important and needs to be included. However, surface tension is not considered in this study. In addition, a kinematic boundary condition (KBC) requires that the velocity normal to a boundary is continuous across the boundary. This is the consequence of the conservation of mass. These conditions in potential flows are different from those in real fluids where stress and velocity rather than pressure (normal stress) and normal velocity are required to be continuous across a boundary. The difference in the dynamic boundary conditions is obvious because shear stresses as well as normal stresses exist in real fluids. However,the difference in the kinematic boundary conditions is caused by the fact that real flows are observed to not slip when they contact rigid boundaries. Consequently, even though conservation of mass has been satesfied if the normal velocities are continuous across a boundary, the continuity of tangential velocities across the boundary is further required to insure the no-slip boundary condition in real fluids.

The linearized boundary value problem of the velocity potential in the flow field, Fig. 1, can be decribed by Fig.2, where both KBC and DBC are matched at the free surface and only KBC is specified at the impermeable sea bed. The DBC at the sea bed will be satisfied automatically and therefore is not shown in the figure. In addition, Sommerfeld's radiation condition is satisfied by the reflected waves to insure a unique solution.

As shown in Fig.2, the dependence of the bottom slope on x-axis raises a mathematical difficulty to apply one of the mathematical techniques, the method of separation of variables, to solve the Laplace equation even though all equations are linear. In a two dimensional problem, a rectangular domain is one in which a rectragular coordinate system can be set such that every boundary of the domain is parallel to one of the axes. In this system, a linear equation on the boundaries is also variable independent and separable. This suggests a procedure to solve the current problem by partitioning the original flow domain into a gourp of rectangular sub-domains as shown in Fig. 3. Theoretically, the approximation approaches perfection when the number of the partitions approaches infinity.

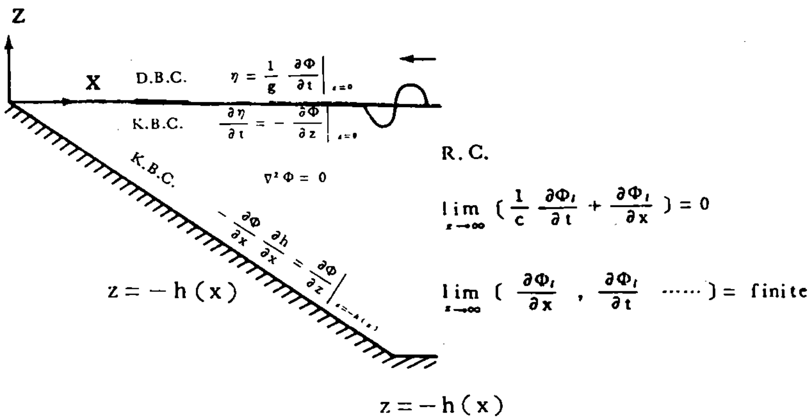

Fig. 2 The linearized boundary value problem of the original flow field.

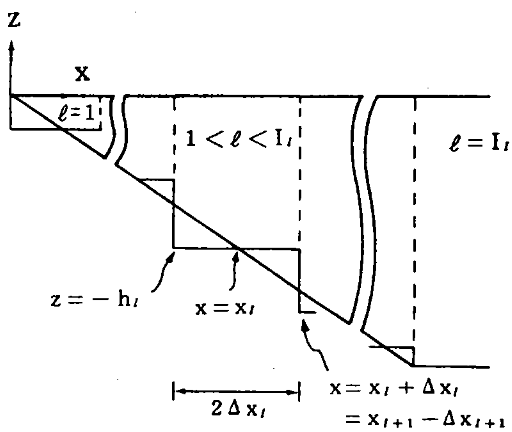

Fig. 3 Rectangular partitions of the original domain.

There are three different types of sub-domains given in Fig. 3. The first domain, denoted by $\ell = 1$, has an impermeable vertical wall and a transmissive vertical boundary separating this domain and the next domain. The last domain, denoted by $\ell = I_{\ell}$, has a boundary at infinity and a vertical boundary containing a transmissive portion and an impermeable portion. Other domains have a transmissive boundary and a boundary with both transmissive and impermeable portions. The differential equation and boundary conditions of each type of sub-domains are given in Fig.4, 5, and 6, respectively.

In each sub-domain there is a series of velocity potentials which satisfy the Laplace equation. The velocity potentials match both kinematic and dynamic boundary conditions on the free surface and on the boundaries separating two sub-domains. However, only the kinematic boundary condition is matched on a fixed impermeable boundary. In this case, the dynamic boundary condition provides the pressure distribution on the boundary. In addition, the induced velocity potentials in the domain containing incident waves satisfy Sommerfeld's radiation condition.

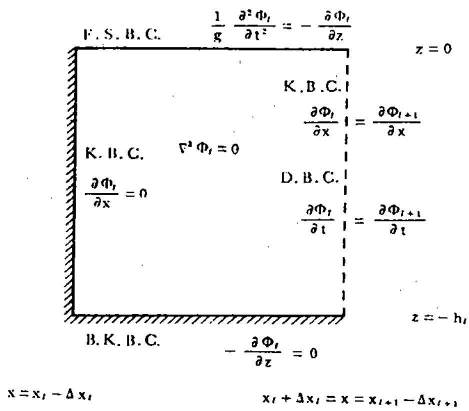

Fig. 4 The differential equation and boundary conditions of the sub-domain $\ell = 1$.

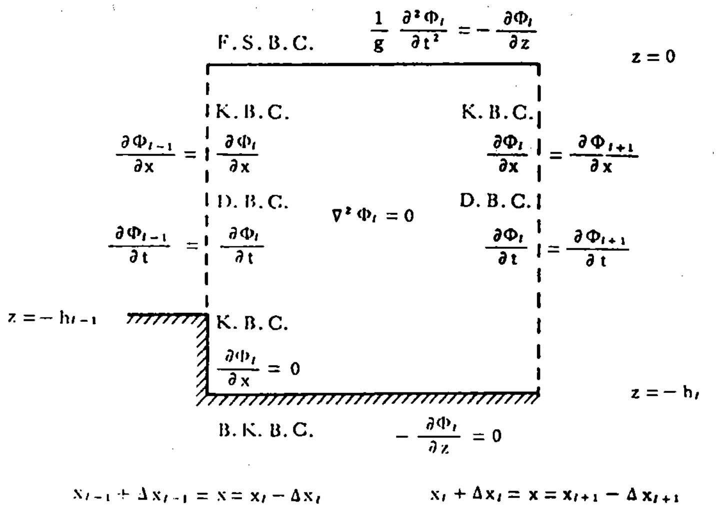

Fig. 5 The differential equation and boundary conditions of the sub-domain $1 < \ell < I_\ell$.

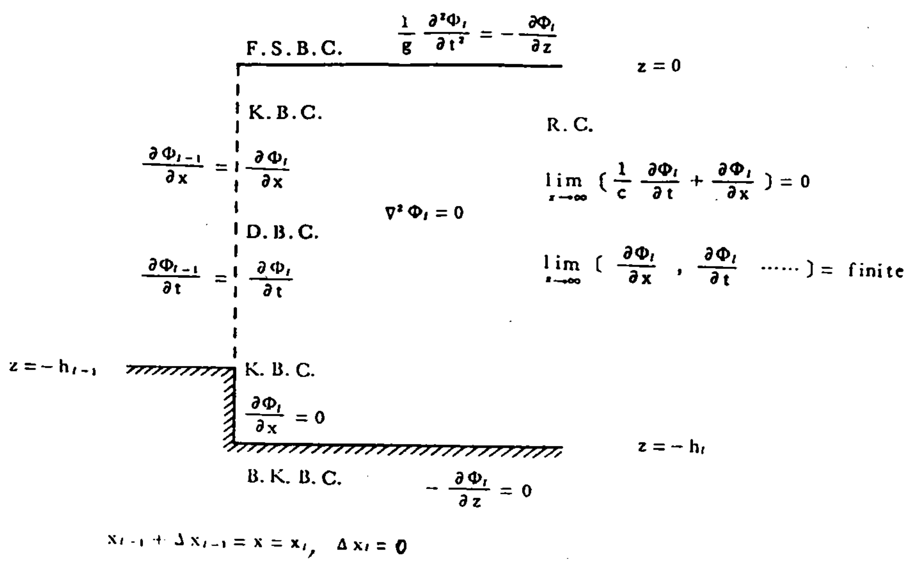

Fig. 6 The differential equation and boundary conditions of the sub-domain $\ell = I_\ell$.

consider an incident wave train with a wave profile given as

$$\eta_I = a_I e^{-i(k_I x + \sigma t - \frac{\pi}{2})} \qquad \cdots\cdots\cdots (4)$$

and the corresponding velocity potential as

$$\phi_I = A_I \cosh k_I (h_{II} + z) e^{-i[k_I(x - x_{jI}) + \sigma t]} \qquad \cdots\cdots\cdots (5)$$

$$= \frac{-a_I g e^{-ik_I x_{II}}}{\sigma \cosh k_I h_{II}} \qquad \cdots\cdots\cdots (6)$$

where σ is the angular frequency, k_I is the angular number, and a_I is its amplitude. The angular frequency and number satisfy the dispersion equation.

$$\frac{\sigma^2}{g} = k_I \tanh k_I h_{II} \qquad \cdots\cdots\cdots (7)$$

Applying the method of separation of variables and matching the boundary conditions, the velocity potentials in each sub-domain have been solved and given as

$$\Phi_I = \sum_{n=1}^{\infty} \phi_{In} = \sum_{n=1}^{w} X_{In}(x) Z_{In}(z) e^{-i\sigma t}$$

$$= \sum_{n=1}^{\infty} [A_{In} e^{K_{In}(x - x_I)} + B_{In} e^{-K_{In}(x - x_I)}]$$

$$\cos [K_{In}(h_I + z)] e^{-i\sigma t} \qquad \cdots\cdots\cdots (8)$$

where

$$A_I = A_{I1} \qquad \cdots\cdots\cdots (9)$$

and the eigenvalues can be determined by the dispersion equation

$$-\frac{\sigma^2}{g} = K_{In} \tan K_{In} h_I \qquad \cdots\cdots\cdots (10)$$

with

$$n = 1 \quad K_{ln} = -i k_{ln}$$

$$n \geq 2 \quad K_{ln} = k_{ln} \qquad (n - \frac{3}{2})\pi < k_{ln} h_l < (n - 1)\pi \quad \cdots\cdots (11)$$

The unknown coefficients in eq.(8) are the solutions of a matrix equation whose coefficient matrix is established by the following equations, for finite modes of waves,

$$A_{lm} = B_{lm} e^{2K_{lm}\Delta x_l} \qquad \ell = 1 \quad \cdots\cdots\cdots (12)$$

$$\sum_{n=1}^{\infty} [A_{ln} e^{-K_{ln}\Delta x_l} + B_{ln} e^{K_{ln}\Delta x_l}] < Z_{l-1m} Z_{ln} >$$

$$= [A_{l-1m} e^{K_{l-1m}\Delta x_{l-1}} + B_{l-1m} e^{-K_{l-1m}\Delta x_{l-1}}]$$

$$< Z_{l-1m} Z_{l-1m} > \qquad 1 < \ell \leq I_l \quad \cdots\cdots\cdots (13)$$

$$K_{lm} [A_{lm} e^{-K_{lm}\Delta x_l} - B_{lm} e^{K_{lm}\Delta x_l}] < Z_{lm} Z_{lm} >$$

$$= \sum_{n=1}^{\infty} K_{l-1n} [A_{l-1n} e^{K_{l-1n}\Delta x_{l-1}} - B_{l-1n} e^{-K_{l-1n}\Delta x_{l-1}}] \times$$

$$< Z_{lm} Z_{l-1n} > \qquad 1 < \ell \leq I_l \quad \cdots\cdots\cdots (14)$$

where $< Z_{\ell n} Z_{\alpha\beta} >$ is defined as

$$< Z_{ln} Z_{\alpha\beta} > = \int_{-h_l}^{0} Z_{ln}(z) Z_{\alpha\beta}(z) dz \quad \cdots\cdots\cdots (15)$$

It is understood that eqs. (12), (13) and (14) were obtained from integrating the KBC and/or DBC at the vertical boundaries.

In terms of the velocity potential given by eq. (8), the flow field in each sub-domain can be completely determined with fluid particle velocities computed from eq.(1), pressure distribution from Bernoulli's equation given by eq.(3), and the wave profile from the free surface dynamic boundary condition given by

$$\eta = \frac{1}{g} \left. \frac{\partial \Phi}{\partial t} \right|_{z=0} \quad \cdots\cdots\cdots (16)$$

3. *ANALYTICAL SOLUTION ILLUSTRATION*

For a given bottom slope and a set of wave conditions, to find the flow properties involves how many partitions of the slope and how many modes of waves should be taken in eq.(8). Thus the convergence of the infinite series should be tested first. However, to provide a rigorous mathematical proof is out of our knowledge. Instead, a trial and error scheme is presented here. In the trial, the original slope is first approximated by a partition with $I\ell$ steps. Then a computation criterion of flow properties (H/Ho in the domain containing incident waves and the KBC at some arbitrary vertical boundaries are chosen in the study, where H is the local wave height and Ho is the deep water wave height) is tested while increasing the number of wave modes. The number of the partition may need to increase if it is difficulty to reach the criterion and another trial is required. Results of an illustrating trial with $I\ell$ = 14 are shown in Fig.7 (plotted for H/Ho at five positions) and Fig.8 (plotted for the relative flux, or the KBC, on the both sides of five arbitrary boundaries) for four wave conditions (Ho/Lo are 0.0087, 0.0097, 0.0377 and 0.0415, respectively, where Lo is the deep water wave length) on two slopes (1/10 and 1/70). In all cases shown in Fig.7 and 8, there is a consistent trend to converge as the number of wave modes reaches over 5. Results also show that waves with small steepness converge fast than those with large steepness do. This implies that more wave modes should be considered for steep waves to converge.

On the other hand, the convergence of wave properties w.r.t. the number of partitions is tested separatively. Results for the number of wave modes taken as 5 are shown in Fig. 9. A consistent trend of convergence is found for all wave conditions on the two tested slopes as the number of partitions is over 14. As shown in Fig. 9, it is also found that the milder slope (1/70) converges slower than the steeper slope (1/10) does. This means that more partitions may be needed for a mild slope to converge.

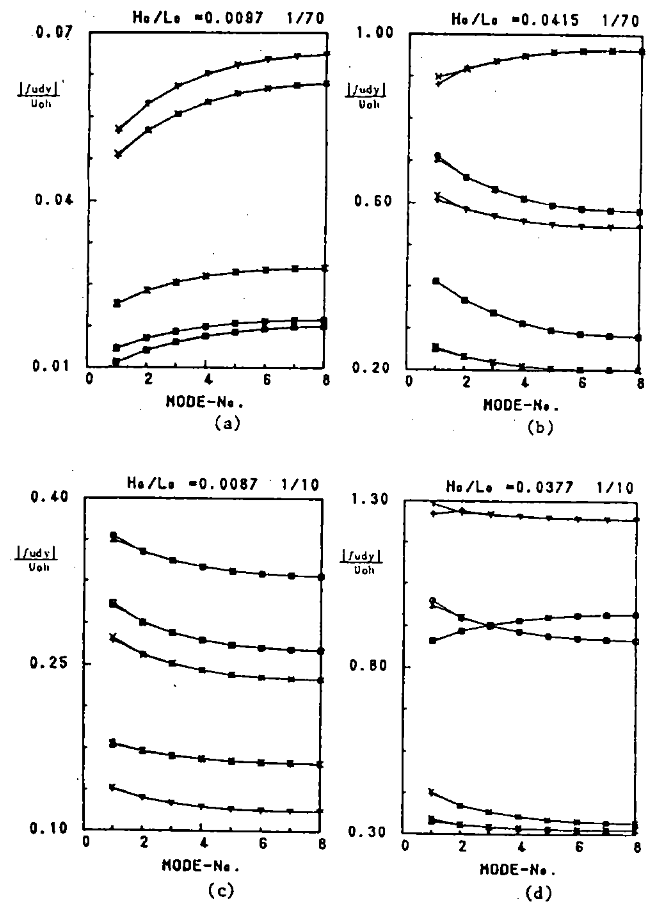

Fig. 7 Convergence of H/Ho w.r.t. the number of wave modes.

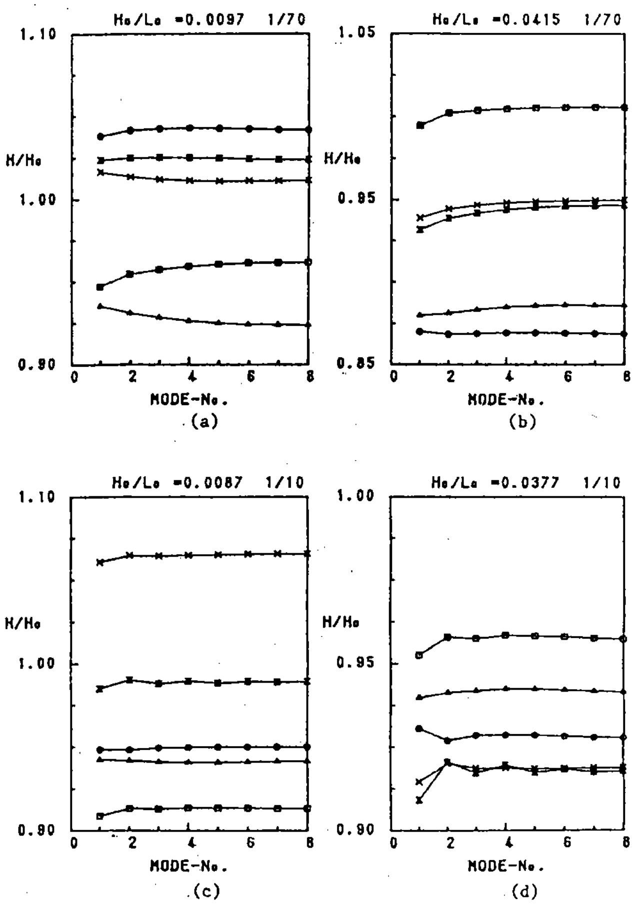

Fig. 8 Convergence of KBC at vertical boundaries w.r.t. the number of wave modes.

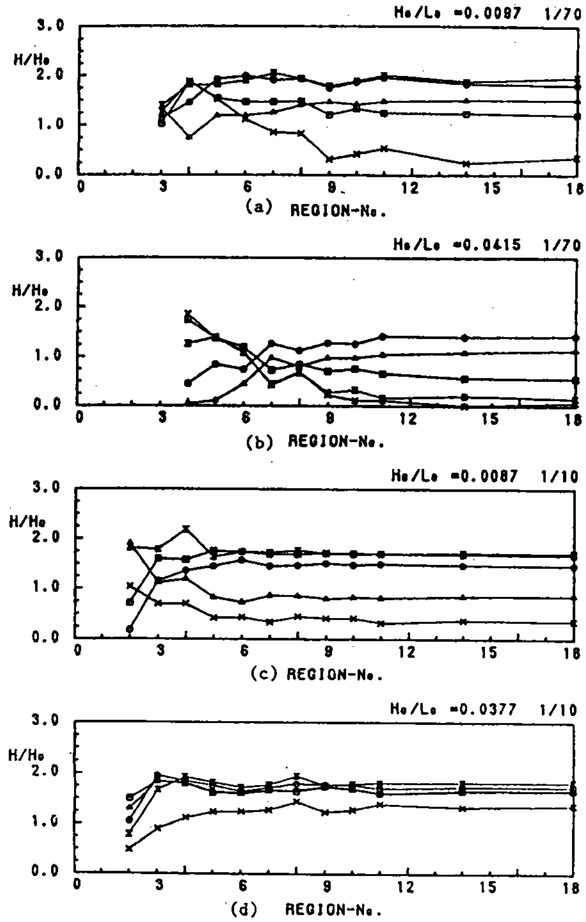

Fig. 9 Convergence of H/Ho w.r.t. the number of partitions.

The following results demonstrate the effects of deep water wave steepness and bottom slope on shoaling coefficient H/Ho, H/h, and local wave steepness H/L where h is the local water depth and L is the local wave length. For the purpose of simplicity, the number of wave modes is taken as 5 and the number of partitions as 14.

The dependence of H/Ho on the slope and Ho/Lo is illustrated in Fig.10. three slopes (1/10, 1/30 and 1/50) and two deep water wave steepnesses (0.0053 and 0.0602) are studied. In Fig.10, the shoaling coefficient H/Ho is graphed as a function of h/Lo. Local shoaling coefficients of waves with small Ho/Lo (0.0053) tend to decrease first and then increase again as water becomes shallower. However, for waves with large Ho/Lo (0.0602), local shoaling coefficients tend to decrease monochromatically, especially for the case with mild slope (1/50). The existence of wave envelopes with distinguishable nodes and loops implies a perfect reflection. This is because no energy loss is considered in inviscid fluid.

The dependence of H/Ho on Ho/Lo can be seen in another way. That is, for a fixed slope, H/Ho for different Ho/Lo can be plotted in one graph. This is shown in Fig.11 for four slopes, respectively. The value of H/Ho shown in Fig.11 was the ratio of the wave height at the loops to Ho. As shown in the figure,the shoaling coefficients of different Ho/Lo decrease first from a constant value of 2 as waves start to shoal and then increase again as water decreases further. Shoaling effects are enlarged by milder slopes because of a longer slope.

The dependence of H/h and H/L on the slope and Ho/Lo is illustrated in Fig. 12 and 13, respectively. As water depth decreases, both H/h and H/L increase monochromatically,with emphasizing effects from larger Ho/Lo, and stronger shoaling effects caused by milder slopes as expected.

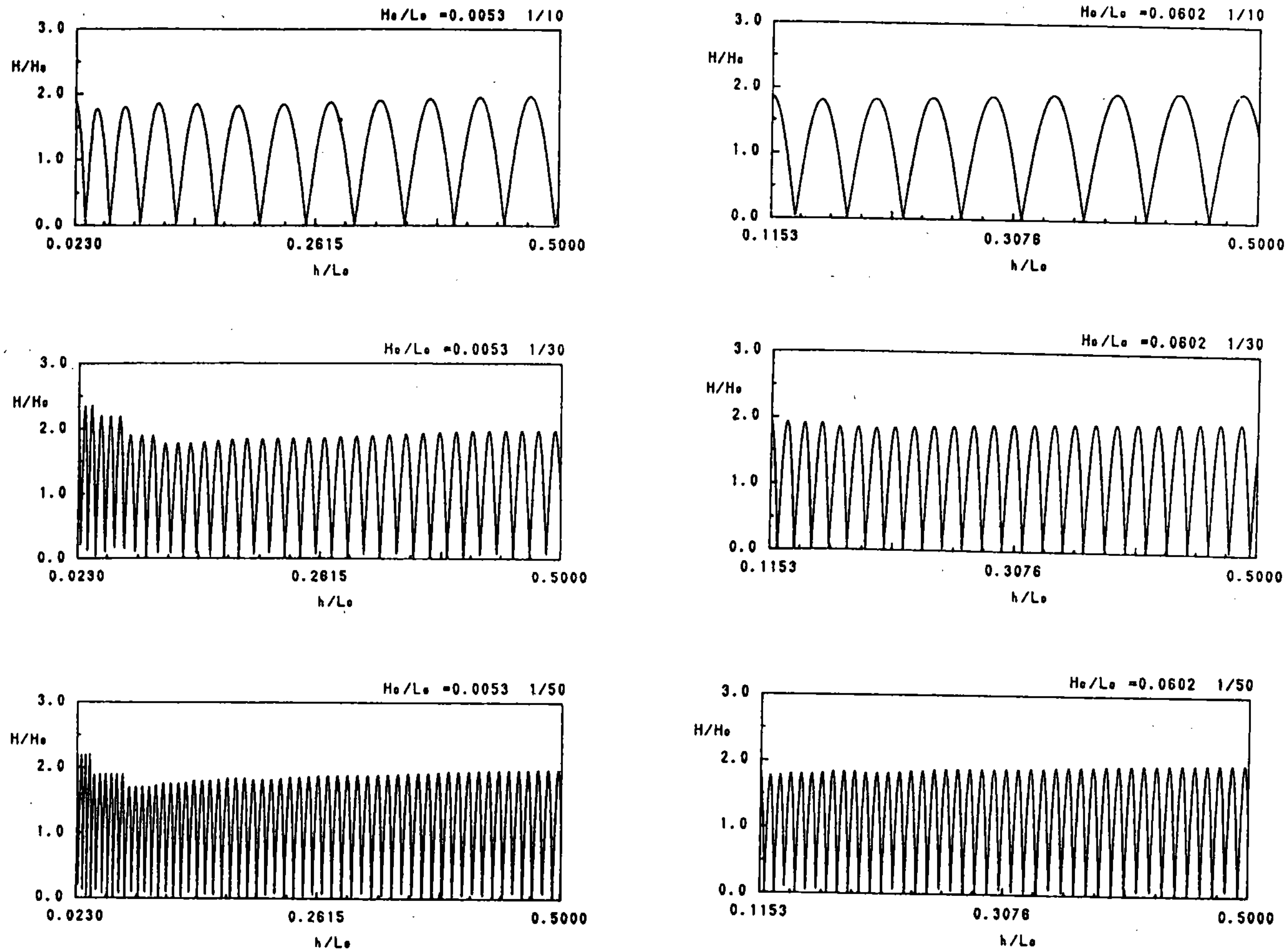

Fig. 10 The dependence of H/Ho on slopes and Ho/Lo.

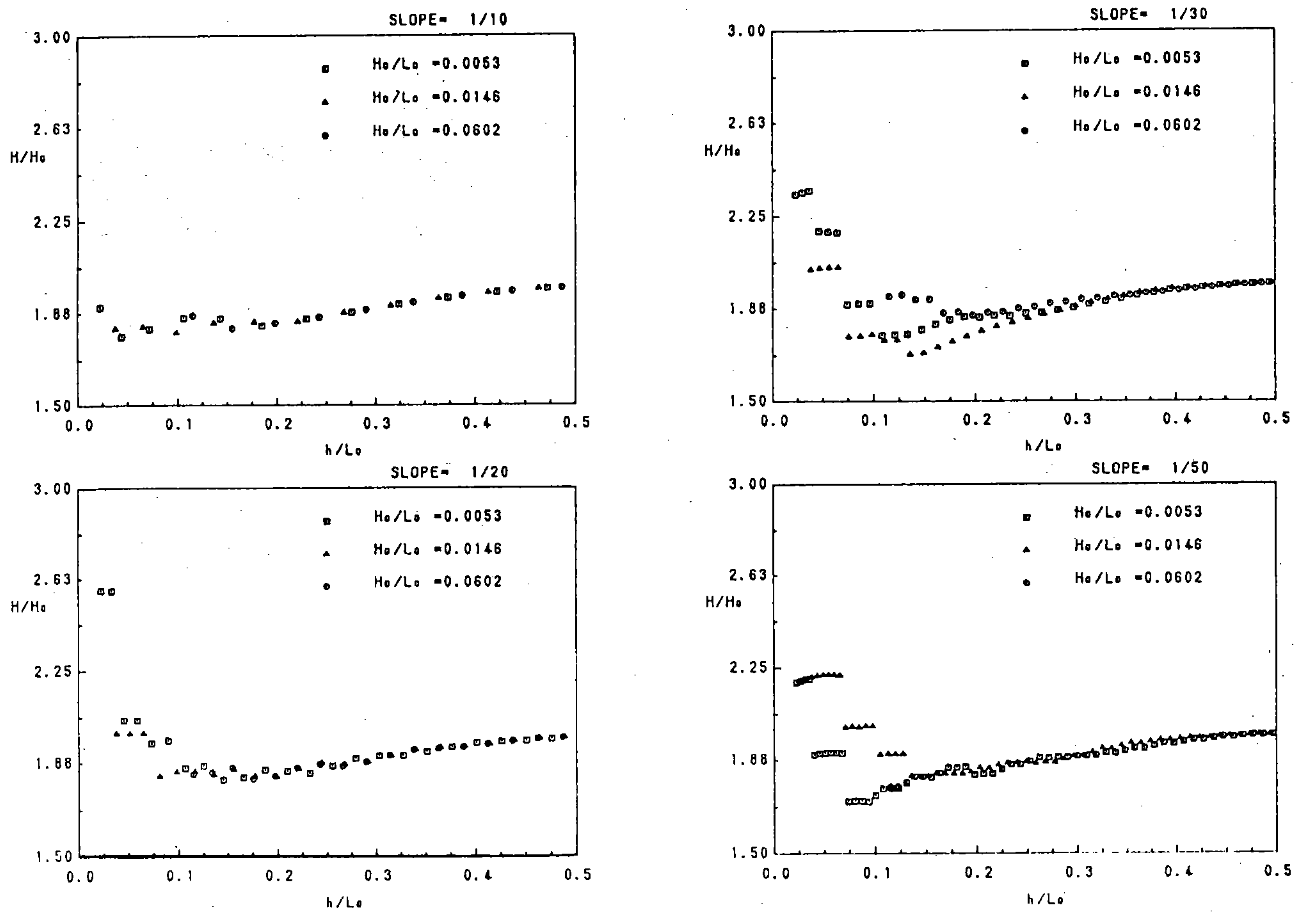

Fig. 11 The dependence of H/Ho on Ho/Lo, for specific slopes.

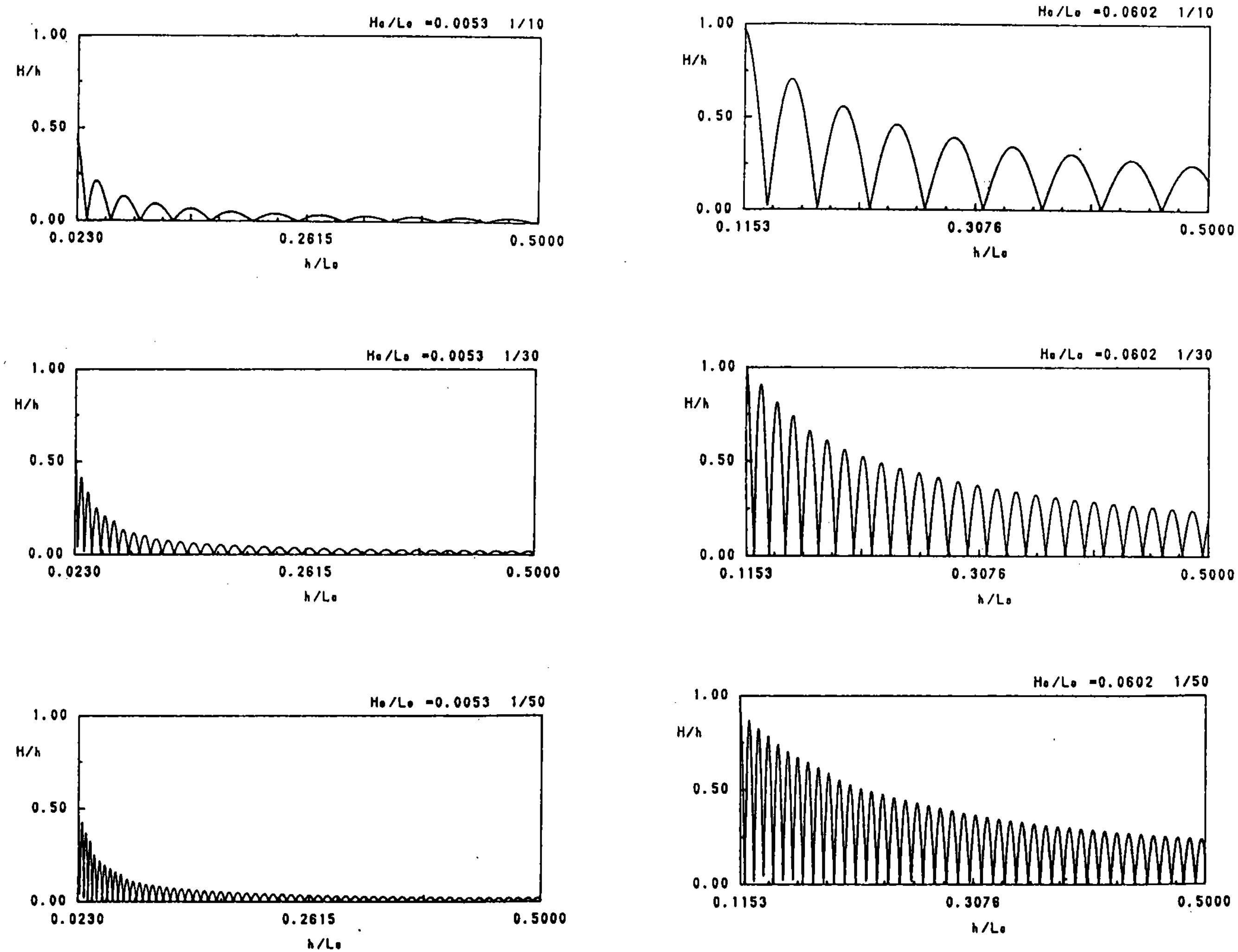

Fig. 12 The dependence of H/h on slopes and Ho/Lo.

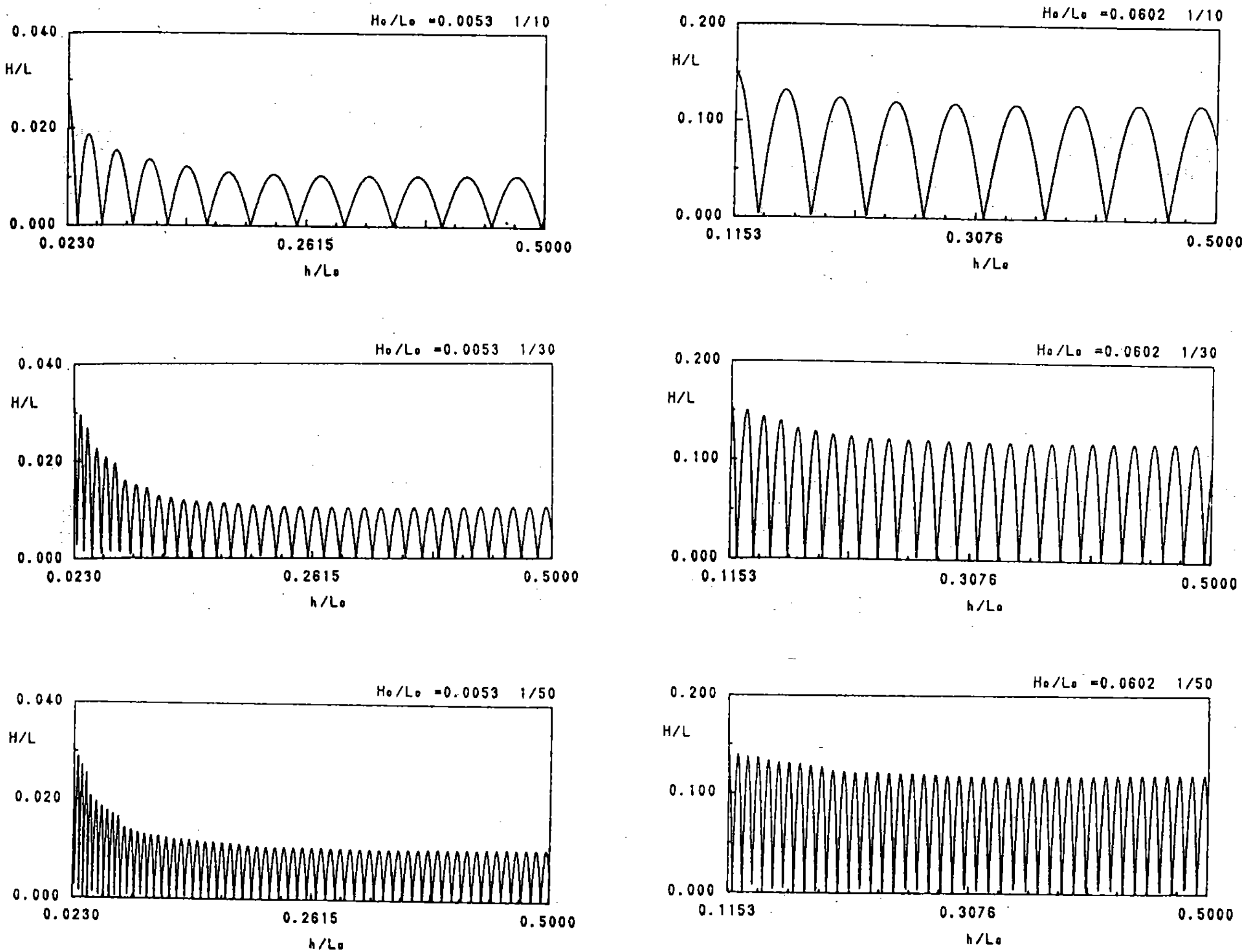

Fig. 13 The dependence of H/L on slopes and Ho/Lo.

4. *CONCLUSION AND DISCUSSION*

A solution scheme has been developed and the shoaling effects have been studied analytically. The scheme involved to approximate a slope by a zigzag line and to partition the original flow field into a group of rectangular sub-domains. In each sub-domain all equations become variable independent and separable and therefore the method of separation of variables can be applied. The velocity potential in each sub-domain is represented by a series of eigen-functions. The convergence of the infinite series and the partition have been domonstrated by a trial and error procedure.

Analytical results show that for waves with larger Ho/Lo wave height decreases as water depth decreases,but for waves with smaller Ho/Lo wave height decreases first as water depth decreases and then increases as water depth becomes shallower. Furthermore, both H/h and H/L increase as water depth decreases.

Nonlinear effects of waves have not been considered in the study. However, nonlinear conditions are usually developed in the process of shoaling and may cause the breaking of waves. Future study will try to include the weak nonlinear effects on the free surface, and then develop to include stronger nonlinear effects. Furthermore, wave energy is usually dissipated due to the seepage flow throught a permeable sand bed. Studies on the effects due to a permeable slope will also be very valuable.

5. *BIBLIOGRAPHY*

1. Biesel, F. 1952. "Study of Wave Propagation in Water of Gradually Varying Depth", U.S. National Bureau of Standards, Gravity waves, NBS circular 521, pp.243-253.

2. Carrier, G. F. and H. P. Greenspan. 1958. "Water Waves of Finite Amplitude in a Sloping Beach", J.F.M., Vol.4, pp.97-109.

3. Carrier, G. F. 1966. "Gravity Waves on Water of Variable Depth", J.F.M., Vol.24, part 4, pp.641-659.

4. Chen, Y. Y. and H. H. Hwung. 1982. "Water Waves Propagating on Beaches of Arbitrary Slope", 18th Coastal Eng. Conf. ASCE pp.811-822.

5. Iwagaki, Y., T. Sakai, J. Kainuma, and T. Kawashima. 1971. "Experiments on Horizontal Water Particle Vellocity at Water Surface of Near Breaking Waves", Coastal Eng. in Japan, Vol.14, pp.17-24.

6. Iwagaki, Y. 1972. "On the Vertical Distribution of Water Particle Velocity Induced by Waves on Beach", Coastal Eng. in Japan, Vol. 15, pp.35-41.

7. Iwagaki, Y. and T. Sakai.1972. "Shoaling of Finite Amplitude Long Waves on a Beach of Constant Slope", Coastal Eng., pp.347-364.

8. Lee, C.P.1987. "Wave Interaction with Permeable Structure", Ph.D. dissertation, Oregon State University, Corvallis, Oregon, USA.

9. LeM'ehaut'e, B. and L.M. Webb. 1964. "Periodic Gravity Waves over a Gentle Slope at a Third Order of Approximation", Coastal Eng., pp.23-40.

10. Miles, J.W. 1967. "Surface Wave Scattering Matrix for a Shelf",

J.F.M., Vol.28, part 4, pp.755-767.

11.Newman, J.N. 1965. "Propagation of Water over an Infinite Step", J.F.M., Vol.34, part 2, pp.399-415.

12.Shuto, N. 1962, "A Solution of Waves of Finite Height", Coastal Eng. in Japan, Vol.5, pp.2-8.

13.Shuto, N. 1972, "Standing Waves in Front of a Sloping Dike", Coastal Eng. in Japan, Vol.15, pp.13-23.

14.Svendsen, I.A. and J.B. Hansen. 1977. "The Wave Height Variation for Regular Waves in Shoaling Water", Coastal Eng., Vol.1, pp.261-284.

第三屆基礎港灣數值（數學）模式研習會論文集　　Jan. 17～18，1990 Pnge 281～309

在時間領域上之波浪與結構物互相作用之有限元素法模擬

李兆芳

國立成功大學水利及海洋工程系副教授

摘　要

本文之主要目的在說明利用有限元素法在時間領域上模擬波浪與結構物互相作用之問題時必須要處理的一些問題，而重點則在說明一種分析波浪與結構物互制作用之動力分析方法。文中首先分別建立含自由水面邊界之流體運動以及結構物運動之有限元素法方程式，對於流體運動而言，主要考慮爲利用勢能流理論配合Galerkin之加權殘差法、Green定理以及有限元素觀念建立流體運動之數值模式；而結構物運動方程式中則考慮可含多個剛性結構物、結構物錨碇以及結構物間互相連接互制影響。在流體與結構物互制之動力分析模式中，流體運動之動力分析乃就水面波動之特性將流體方程式分割爲顯式以及隱式方程式；結構物之動力分析則使用Newmark 隱式模式，而流體與結構物之互制則建立一個含顯式－隱式分割流體模式與隱式結構物模式互相作用之一種交替疊代的動力分析方法。文中最後以一具瞬變特性之含流體與結構物互制作用之圓柱浮體自由振盪爲計算例，說明所提流體與結構物互制之動力分析的正確性，同時藉以說明利用數值模式求解物理問題並輔助對於物理現象瞭解所具有之重要性。

一、前　言

探討海洋波浪與結構物互相作用問題，其主要目的在分析波浪受到結構物影響引起波浪流場之變化，波力作用結構物上之大小，以及結構物之動力與穩定性計算。作用結構物上之波力分析將提供結構物設計之參考，而結構物動力及穩定性分析則決定結構物完成後實際操作使用之可行性及安全性。分析波力作用在結構物上之大小，首先要考慮的爲波浪和結構物彼此間互相影響之關係（Sarpkaya and Issacson，1981）。當結構物特性長度（D）與波浪特性長度（L）之比值D／L小於 0.2 時，流體運動作用於結構物上之拖曳(drag)效應相對重要，波力之計算一般使用Morison公式，此種結構物相對的稱爲小結構物（small body）；當D／L大於 0.2 時，流體運動作用於結構物上之慣性（inertia）效應相對重要，波力之計算一般則使用勢能流(potential flow）理論，此種結構物則相對的稱爲大結構物（large body）。對於波浪與結構物互相作用所引致作用在結構物上之波力分析，基本上可分成在頻率領域（frequency domain）與時間領域（time domain）上兩種分析（Lee，1986)。在頻率領域分析方法中，所考慮之波浪以及結構物之運動均假設已達穩定之週期性運動，而分析結果所求得的則爲波浪以及結構物運動相關函數之振幅與相位角。在時間領域上之分析方法則大都使用在瞬變(transient）分析上，即從起始條件（initial condition)開始求得波浪以及結構物運動相關函數之時間變化。本文所考慮之問題則爲波浪與大結構物間互相作用在時間領域上之分析。

對於波浪與大結構物互相作用之問題在時間領域上之分析，由於整個問題包括求解波浪運動、結構物動力分析以及波浪與結構物間之互制效應，因此，完全以理論解析之方式求解整個問題僅線性問題才較有可能。利用理論解析之方式求解含波浪與結構物互相作用之問題，可以Ursell 所解一浮式結構在水面自由振盪之問題爲代表（Ursell，1964）。Ursell所解之問題爲給定圓柱浮體一已知吃水深度，待浮體四週之水面恢復平靜後放開浮體讓其自由振動

，探討浮體之運動情形以及浮體四週水波之生成、傳播與衰減之情形。在Ursell 提出之理論解中，由於數學式過於複雜，在該篇文章中僅討論理論解之極限（asymptotic）特性。對於Ursell 之理論解，Maskell and Ursell (1970)特別加以討論才提出一足供計算之表示式。僅管如此，Maskell and Ursell 之解析解亦僅解出浮體之運動，至於浮體四週水面波浪之運動情形則由於問題過大而被迫作罷。

對於波浪與大結構物互相作用之問題在時間領域上之分析，由於在理論解析上數學過於複雜，因此在問題之求解過程只好訴諸於使用數值模式。使用數值模擬方法求解一物理上之問題，最大之好處在於避開求解問題過程中繁雜的數學問題，取而代之的則以一系統化的、程式化的方式求解問題。利用數值方法在時間領域上模擬波浪與大結構物互相作用之問題，在數值方法處理上可能遭遇之困難分以下三點說明：

(1)非線性變動之自由水面邊界：描述自由水面運動之邊界條件爲一非線性方程式，以數值方法求解須訴諸求解非線性方程式特殊方法；自由水面爲一自由變動之邊界，涵蓋問題領域之數值格網須隨自由水面邊界之運動而調整且需保持數值計算之精確。在處理非線性水面波浪問題中，Multer (1973)使用Lagrange 方法描述自由水面運動以簡化該邊界條件。Nakayama (1983)應用加權殘差之觀念處理自由水面非線性動力邊界條件，配合邊界元素法求解非線性波浪問題。Jagannathan (1986)使用Vinje and Brevig 方法，利用複變函數之流速勢能函數求解具週期性空間變化之非線性波問題。有關變動邊界問題，基本上乃調整數值領域以因應邊界之變動。O' Brien (1983)在其使用之方法中，則僅於變動邊界附近之數值領域隨著調整以因應邊界之變動。Lai (1986)使用元素轉換（mapping）之方法把變動之問題領域轉換到規則之數值領域以方便數值之計算。

(2)無反射之數值邊界：有限領域之數值模式計算具有無限領域之問題時，在數值模式中必須設定足以模擬無限領域之邊界條件——無反射邊界條件，此一邊界條件之恰當與否將影響到數值模式之正確性。有關水波浪之瞬變分析的無反射邊界條件，Orlanski (1976)首先運用Sommerfeld 輻射

(radiation)邊界條件計算水流中熱對流及擴散問題。 Jagannathan (1986)及Lee(1986)則把Sommerfeld 輻射邊界條件利用到計算瞬變水波浪之分析，對於該邊界條件中之波速則視爲隨時間改變而以數值方法計算出來。

(3)流體與結構物互制之動力分析：分析含流體與結構物互相作用之問題時，由於作用給結構物之流體作用力爲未知，且結構物之運動引致流場變化亦爲所要求解的，因此，欲求解此種問題必須同時求解流場與結構物之運動。然而，利用數值方法作流體和結構物之動力分析其特性差異頗大。流體性質較柔，容易隨著邊界運動而變形，在動力分析上常使用顯式法(explicit method);結構物其性較剛，因此在動力分析上常使用隱式法(implicit method)。合併使用顯式法以及隱式法運用在流體與結構物互制分析上則爲相當關鍵性，且將影響對整個問題模擬之成功或失敗。對於含流體與結構物互制之動力分析，常用之方法有field elimination 方法，如Geers (1975) ; simultaneous solution 方法，如 Bathe and Sonnad (1980) ; partitioned (or staggered) solution方法，如Park and Felippa (1983)。其中，field elimination方法乃設法消去以減少互相作用之物理量，然此舉會增高問題中控制方程式之微分階數而增加數值處理上之困難。Simultaneous solution方法則同時求解互制分析中所有互相作用之物理量，然由於同時求解之物理量變數過多，以致於最後求解之矩陣過大而於實際計算上可行性不高。介於前述兩種方法之間的則爲分割(partitioned)方法，此法最大優點在於儘量利用互制問題中各個物理量之特性作動力分析而互制特性則經由互制邊界條件以外差或內差方式互傳於各物理量間。由於互制各物理量之特性的不同，partitioned solution方法可分爲implicit- implicit分割方法，如Park , Felippa and DeRuntz (1977)和implicit-explicit 分割方法，如Belytschko and Mullen (1977)。關於 partitioned solution方法之穩定性及精度分析可見Park and Felippa (1983)。

本文爲描述波浪與大結構物互相作用在時間領域上之分析，數值模擬所用之方法爲有限元素法，重點放在流體與結構物互制之動力分析上。所考慮之問題將限於線性之流體與結構物互制分析上，因此，上述所提非線性變動之自由水面邊界條件將可簡化，然而所提分析方法則可以應用到非線性問題上。

二、波浪與結構物互制之有限元素方程式

所考慮波浪和結構物互制作用問題定義如圖 1 所示，對問題所選用之參考座標爲固定卡氏座標 x_i ， $i = 1 , 2 , 3$ 。

2.1 波浪運動之有限元素方程式

描述波浪運動常假設所考慮流體爲無粘滯性且爲不可壓縮而流體運動爲非旋流，則對於流體運動之描述可使用一流速勢能函數 $\Phi_T(x_1, x_2, x_3, t)$ ，而流體速度可定義爲

$$\vec{V}_T(x_1, x_2, x_3, t) = -\vec{\nabla}\Phi_T(x_1, x_2, x_3, t) \qquad \cdots\cdots(1)$$

對於波浪流場若有一入射波浪進入流場，則可將整個流場流速勢能函數分成入射波流速勢能函數 Φ_I 與擾動波流速勢能函數 Φ

$$\Phi_T = \Phi_I + \Phi \qquad \cdots\cdots(2)$$

擾動波浪流場之控制方程式可寫爲

$$\nabla^2\Phi(x_1, x_2, x_3, t) = 0 \quad , \quad \text{in } D \quad , \quad 0 \leq t < \infty \qquad \cdots\cdots(3)$$

式中 ∇^2 爲 Laplacian 運算子；D爲波浪流場之領域。

波浪流場之邊界條件爲：自由水面邊界， B_1 ，其上之動力及運動條件合寫爲

$$\frac{\partial\Phi}{\partial n_f} + \frac{1}{g}\frac{\partial^2\Phi}{\partial t^2} = 0 \quad , \quad \text{on } B_1 \qquad \cdots\cdots(4)$$

式中，g 爲重力常數，$\vec{n}_f$ 爲自由水面之單位法線向量即在正 x_2 方向。底床邊界，B_2，其上之運動條件可寫爲

$$\frac{\partial \Phi}{\partial n_b} = 0 \ , \quad \text{on} \quad B_2 \ ; \qquad x_2 = -h(x_1, x_3) \qquad \cdots\cdots(5)$$

式中，$\vec{n}_b$ 爲底床邊界之外向（ outward ）單位法線向量；h 爲水深。數值模式之無反射邊界，B_3，其上之邊界條件可表出爲

$$\frac{\partial \Phi}{\partial n_r} + \frac{1}{C}\frac{\partial \Phi}{\partial t} = 0 \quad , \text{ on } B_3 \ ; \quad C = C(t) \qquad \cdots\cdots(6)$$

式中，$\vec{n}_r$ 爲無反射邊界之外向單位法線向量；C(t)爲通過無反射邊界之波速，其值可以下式計算

$$C = -\frac{\partial \Phi / \partial t}{\partial \Phi / \partial n_r} \quad , \quad \text{on } B_3 \qquad \cdots\cdots(7)$$

有關C（ t ）值之討論可參考Lee and Leonard (1987)。在結構物與流體交界面，S_m，其上之運動條件可寫爲

$$\frac{\partial \Phi}{\partial n_m} + \frac{\partial \Phi_I}{\partial n_m} + \vec{v}_m \cdot \vec{n}_m = 0 \ , \ \text{on } S_m \ ; \ m = 1, \cdots, N \qquad \cdots\cdots(8)$$

式中，下標m表第m個結構物；N表總共結構物之個數；$\vec{n}_m$ 爲流體邊界 S_m 上之外向單位法線向量；$\vec{v}_m$ 爲結構物邊界之運動速度。

利用Galerkin 加權殘差法配合Green定理，對於上述流體運動之邊界值問題的積分方程式可表出爲

$$\iiint_D \vec{\nabla}\Phi \cdot \vec{\nabla}\delta\Phi \ dD + \iint_{B_1} \frac{1}{g}\frac{\partial^2 \Phi}{\partial t^2} \delta\Phi \ dB + \frac{1}{C}\iint_{B_3} \frac{\partial \Phi}{\partial t} \delta\Phi \ dB$$
$$+ \sum_{m=1}^{N} \iint_{S_m} \left(\frac{\partial \Phi_I}{\partial n_m} + \vec{v}_m \cdot \vec{n}_m \right) \delta\Phi \ dB = 0 \qquad \cdots\cdots(9)$$

對於(9)式之積分方程式可以利用數值方法，如有限元素法，化成代數式然後再加以求解。有關有限元素法之詳細介紹可參考有關書籍，如Zienkiewicz (1977)。利用同參數元素(isoparametric element)之觀念，有限元素上之空間座標以及流場函數可用同一函數來表示

$$x_i(\tau_1,\tau_2,\tau_3)=\widetilde{H}^j(\tau_1,\tau_2,\tau_3)x_i^j\,,\quad i=1,2,3 \qquad \cdots\cdots(10)$$

$$\Phi(\tau_1,\tau_2,\tau_3,t)=\widetilde{H}^j(\tau_1,\tau_2,\tau_3)\phi^j(t) \qquad \cdots\cdots(11)$$

式中，重覆出現指標代表累加，$j=1,\cdots,N_e$，N_e 表一元素上所取節點(node)總數；$\widetilde{H}^j$ 爲元素第 j 個節點上之形狀函數(shape function)，τ_i，$i=1,2,3$，表有限元素上之自然座標；x_i^j 爲元素上第 j 個節點上之 x_i 座標，而 ϕ^j 則爲第 j 個節點上之 ϕ 值。將(10),(11)式代入(9)式可得

$$\Big\{\sum_{B_1}L_1^{jq}\ddot{\phi}^j+\sum_{B_3}L_2^{jq}\dot{\phi}^j+\sum_{D}L_3^{jq}\phi^j + \sum_{m=1}^{N}\sum_{S_m}L_4^q+\sum_{m=1}^{N}\sum_{S_m}L_5^{\ell iq}v_\ell^i\Big\}\phi^q=0 \qquad \cdots\cdots(12)$$

式中，$\sum_{B_1}$，$\sum_{B_3}$，$\sum_{D}$，$\sum_{S_m}$分別代表在B_1，B_3，D，S_m上之元素組合(assemblage)；

$$L_1^{jq}=\frac{1}{g}\int_{-1}^{1}\int_{-1}^{1}H^jH^q\,|\bar{J}|\,d\tau_1d\tau_2 \qquad \cdots\cdots(13)$$

$$L_2^{jq}=\frac{1}{C}\int_{-1}^{1}\int_{-1}^{1}H^jH^q\,|\bar{J}|\,d\tau_1d\tau_2 \qquad \cdots\cdots(14)$$

$$L_3^{jq}=\int_{-1}^{1}\int_{-1}^{1}\int_{-1}^{1}\frac{\widetilde{H}^j}{\partial x_k}\,\frac{\widetilde{H}^q}{\partial x_k}\,|\widetilde{J}|\,d\tau_1\,d\tau_2\,d\tau_3 \qquad \cdots\cdots(15)$$

$$L_4^q=\int_{-1}^{1}\int_{-1}^{1}\frac{\partial\Phi_I}{\partial x_\ell}\,\varepsilon_{\ell mn}\,\frac{\partial H^r}{\partial\tau_1}\,\frac{\partial H^j}{\partial\tau_2}\,H^q\,d\tau_1\,d\tau_2\;x_m^r\,x_n^j \qquad \cdots\cdots(16)$$

$$L_5^{\ell iq}=\int_{-1}^{1}\int_{-1}^{1}H^i\,\varepsilon_{\ell mn}\,\frac{\partial H^r}{\partial\tau_1}\,\frac{\partial H^j}{\partial\tau_2}\,H^q\,d\tau_1\,d\tau_2\,x_m^r\,x_n^j \qquad \cdots\cdots(17)$$

其中，$\varepsilon_{\ell mn}$為一組合符號，其值為1 當 ℓ ，m，n 為偶組合，其值為－1 當 ℓ ，m，n 為奇組合，其值為0 當 ℓ ，m，n 中有任兩者相同； H^j 為元素之形狀函數 $\widetilde{H}^j$ 計算在邊界上者。｜$\widetilde{J}$｜及｜$\bar{J}$｜則分別為 $\widetilde{H}^j$及H^j之 Jacobian 轉換的行列值。(13)－(17)式之積分可用數值積分方法如Gauss quadrature 方法計算。(12)式則為流體作動力分析所要用之方程式。

2.2 剛性結構物運動方程式

若考慮之結構物為剛性，則其運動方程式通式可寫為

$$\sum_{i=1}^{6}\{M_{jmim}\ddot{U}_{im}+(k_{jmim}+\widetilde{k}_{jmim}+Q_{jmim})U_{im}-\sum_{\substack{\ell=1\\ \ell\neq m}}^{N}\widetilde{Q}_{jmi\ell})U_{i\ell}\}$$

$$=F_{jm}\quad;\quad j=1,2,3,4,5,6$$
$$m=1,\cdots\cdots,N \qquad \cdots\cdots(18)$$

式中，M_{jmim}，k_{jmim}，Q_{jmim}，$\widetilde{k}_{jmim}$ 分別為第m個結構物受到第 i 個自由度運動而在第 j 個自由度上之質量，錨碇回復力(restoring force)常數，結構物與結構物間連接互動本身對本身之回復力常數，以及靜壓回復力常數；$\widetilde{Q}_{jmi\ell}$ 為第m個與第 ℓ 個結構物間連接互動之回復力常數；$\ddot{U}_{im}$ 與 U_{im} 則分別為第m個結構物在轉動中心之第 i 個自由度之加速度與位移。

(18)式等號右邊之水動壓總力可由流體動壓力就流體與結構物之交界面積分求得

$$F_{jm}=\rho\int\int_{S_m}\left(\frac{\partial\Phi_I}{\partial t}+\frac{\partial\Phi}{\partial t}\right)n_{jm}\,dB \qquad \cdots\cdots(19)$$

式中，ρ 為流體密度；n_{jm}為第m個結構物六個單位法線向量中第 j 個分量。

三、波浪與結構物互制之動力分析

上述(12)及(18)式分別為波浪與結構物之運動方程式，由式中可看出波浪與結構物之互制作用係經由流體與結構物之交界面上之運動邊界條件，(8)式，以及動力邊界條件，(19)式。在以下波浪與結構物互制動力分析之討論中，流體運動方程式將依流體之動力特性使用以顯式積分法為主之顯式－隱式分割方法，而結構物運動方程式則依其特性使用隱式積分法。

3.1 顯示 — 隱式分割流體運動方程式

將(12)式流體運動有限元素法方程式之總體(global)矩陣方程式寫出並計算在時間($t+\Delta t$)以及第 r 個疊代(iteration)步驟，

$$
\left[{}^{t+\Delta t}_{r}M_f\right]\left\{{}^{t+\Delta t}_{r}\ddot{\phi}\right\}+\left[{}^{t+\Delta t}_{r}C_f\right]\left\{{}^{t+\Delta t}_{r}\dot{\phi}\right\}+\left[{}^{t+\Delta t}_{r}K_f\right]\left\{{}^{t+\Delta t}_{r}\phi\right\}
= \left\{{}^{t+\Delta t}_{r}F_f\right\} \qquad \cdots\cdots(20)
$$

式中，

$$
\left[{}^{t+\Delta t}_{r}M_f\right] = \text{流體質量矩陣} = \Big[\sum_{{}^{t+\Delta t}_{r}B_1} {}^{t+\Delta t}_{r}L_1^{jq}\Big] \qquad \cdots\cdots(21)
$$

$$
\left[{}^{t+\Delta t}_{r}C_f\right] = \text{流體阻尼矩陣} = \Big[\sum_{{}^{t+\Delta t}_{r}B_3} {}^{t+\Delta t}_{r}L_2^{jq}\Big] \qquad \cdots\cdots(22)
$$

$$
\left[{}^{t+\Delta t}_{r}K_f\right] = \text{流體剛度矩陣} = \Big[\sum_{{}^{t+\Delta t}_{r}D} {}^{t+\Delta t}_{r}L_3^{jq}\Big] \qquad \cdots\cdots(23)
$$

$$
\left\{{}^{t+\Delta t}_{r}F_f\right\} = \text{流體載重矩陣} \qquad \cdots\cdots(24)
$$

$$
= -\Big\{\sum_{m=1}^{N}\sum_{{}^{t+\Delta t}_{r}S_m} {}^{t+\Delta t}_{r}L_4^{q}\Big\} - \Big\{\sum_{m=1}^{N}\sum_{{}^{t+\Delta t}_{r}S_m} {}^{t+\Delta t}_{r}L_5^{\ell iq}\ {}^{t+\Delta t}_{r}v_{\ell}^{i}\Big\}
$$

$$\{ {}^{t+\Delta t}_{r}\phi \} = \text{擾動流速勢能函數矩陣} \qquad \cdots\cdots(25)$$

若將（20）式之矩陣詳細表示出來則可寫爲

$$
{}^{t+\Delta t}_{r}\left[\begin{array}{c|r}
\quad & \\
\quad & \\
\quad & \\
\quad & \\
\quad & \\
\quad & \\
\quad & \\
\hline
 & M_f M_f \\
 & M_f M_f M_f \\
 & M_f M_f
\end{array}\right]
{}^{t+\Delta t}_{r}\left[\begin{array}{c}
\ddot{\phi}_s \\
\ddot{\phi}_s \\
\ddot{\phi}_d \\
\ddot{\phi}_d \\
\ddot{\phi}_d \\
\ddot{\phi}_{rd} \\
\ddot{\phi}_r \\
\ddot{\phi}_r \\
\hline
\ddot{\phi}_{fr} \\
\ddot{\phi}_{fs} \\
\ddot{\phi}_f
\end{array}\right]
$$

$$
+\;{}^{t+\Delta t}_{r}\left[\begin{array}{c}
\quad \\
\quad \\
\quad \\
\quad \\
\quad \\
C_f C_f \\
C_f C_f C_f \\
C_f C_f \;\; C_f \\
\hline
C_f \;\; C_f \\
\quad \\
\quad
\end{array}\right]
{}^{t+\Delta t}_{r}\left[\begin{array}{c}
\dot{\phi}_s \\
\dot{\phi}_s \\
\dot{\phi}_d \\
\dot{\phi}_d \\
\dot{\phi}_d \\
\dot{\phi}_{rd} \\
\dot{\phi}_r \\
\dot{\phi}_r \\
\hline
\dot{\phi}_{fr} \\
\dot{\phi}_{fs} \\
\dot{\phi}_f
\end{array}\right]
$$

$$
+\ {}^{t+\Delta t}\left[\begin{array}{l|l}
K_fK_fK_f & \\
K_fK_f & \\
K_f\quad K_fK_f\quad K_f & \\
\qquad K_fK_fK_f & K_f \\
\qquad\quad K_fK_f & \\
\qquad K_f\qquad K_fK_f & \\
\qquad\qquad\quad K_fK_fK_f & \\
\qquad\qquad\qquad K_fK_f & \\
\hline
\qquad\quad K_f & K_fK_f \\
 & K_fK_fK_f \\
 & \qquad K_fK_f
\end{array}\right]
\ {}^{t+\Delta t}_{\quad r}\left[\begin{array}{c}
\phi_s \\ \phi_s \\ \phi_d \\ \phi_d \\ \phi_d \\ \phi_{rd} \\ \phi_r \\ \phi_r \\ \hline \phi_{fr} \\ \phi_{fs} \\ \phi_f
\end{array}\right]
=
\ {}^{t+\Delta t}_{\quad r}\left[\begin{array}{c}
F_f \\ F_f \\ 0 \\ 0 \\ 0 \\ 0 \\ 0 \\ 0 \\ \hline 0 \\ F_f \\ 0
\end{array}\right]
\tag{26}
$$

式中，ϕ_s，ϕ_d，ϕ_{rd}，ϕ_r，ϕ_{fr}，ϕ_{fs}，ϕ_f分別代表在結構物邊界上S，領域中D，底床 B_2 與無反射邊界 B_3 交界處，無反射邊界 B_3 上，自由水面邊界 B_1 與無反射邊界 B_3 交界處，自由水面邊界 B_1 與結構物邊界S交界處，自由水面邊界 B_1 上之流速勢能函數，如圖 2 所示。

由 (26) 式可明顯看出流體運動方程式之慣性力 (inertia) 項僅產生在自由水面邊界，阻尼 (damping) 項僅產生在無反射邊界，而剛度 (stiffness) 項則貫連所有的邊界。依此，若欲維持使用顯式積分法對流體運動方程式作動力分析，則僅可能實施於自由表面邊界與無反射邊界上，而其他邊界以及領域內部份則必須使用隱式積分法分析，這一點即爲本文使用顯式－隱式分割法的動機所在。在本文中爲配合使用無反射邊界條件的數值計算，無反射邊界將使用隱式方法。利用顯式－隱式分割法對於流體運動之流速勢能函數 { ϕ } 可定義顯式群 { ϕ^e } 以及隱式群 { ϕ^i }，而 (26) 式可表爲簡明之分割方程式

$$
\left[\begin{array}{c|c} 0 & 0 \\ \hline 0 & {}^{t+\Delta t}_{r}M_f \end{array}\right]
\left[\begin{array}{c} {}^{t+\Delta t}_{r}\ddot{\phi}^{i} \\ \hline {}^{t+\Delta t}_{r}\ddot{\phi}^{e} \end{array}\right]
$$

$$
+\left[\begin{array}{c|c} {}^{t+\Delta t}_{r}C_f^{i} & {}^{t+\Delta t}_{r}C_f^{ie} \\ \hline {}^{t+\Delta t}_{r}C_f^{ie} & {}^{t+\Delta t}_{r}C_f^{e} \end{array}\right]
\left[\begin{array}{c} {}^{t+\Delta t}_{r}\dot{\phi}^{i} \\ \hline {}^{t+\Delta t}_{r}\dot{\phi}^{e} \end{array}\right]
$$

$$
+\left[\begin{array}{c|c} {}^{t+\Delta t}_{r}K_f^{i} & {}^{t+\Delta t}_{r}K_f^{ie} \\ \hline {}^{t+\Delta t}_{r}K_f^{ie} & {}^{t+\Delta t}_{r}K_f^{e} \end{array}\right]
\left[\begin{array}{c} {}^{t+\Delta t}_{r}\phi^{i} \\ \hline {}^{t+\Delta t}_{r}\phi^{e} \end{array}\right]
=\left[\begin{array}{c} {}^{t+\Delta t}_{r}F_f^{i} \\ \hline {}^{t+\Delta t}_{r}F_f^{e} \end{array}\right]
\qquad \cdots\cdots(27)
$$

式中，右上標 e 和 i 分別代表顯式和隱式，ie 則代表隱式群與顯式群互制作用的部份。由（27）式代表顯式群之流體運動方程式可寫出爲

$$
[{}^{t}M_f]\{{}^{t}\ddot{\phi}^{e}\}+[{}^{t}C_f^{e}]\{{}^{t}\dot{\phi}^{e}\}+[{}^{t}K_f^{e}]\{{}^{t}\phi^{e}\}
$$
$$
=\{{}^{t}F_f^{e}\}-[{}^{t}C_f^{ie}]\{{}^{t}\dot{\phi}^{i}\}-[{}^{t}K_f^{ie}]\{{}^{t}\phi^{i}\} \qquad \cdots\cdots(28)
$$

(28)式中 $[{}^{t}C_f^{ie}]$，$\{{}^{t}\dot{\phi}^{i}\}$，$[{}^{t}K_f^{ie}]$，$\{{}^{t}\phi^{i}\}$ 等項則由隱式群最近一次疊代之值計算。對（28）式由於其使用顯式積分法，因此左上標之時間使用 t 且左下標代表疊代次數之 r 也省略。由（27）式代表隱式群之流體運動方程式可寫出爲

$$
[{}^{t+\Delta t}_{r}C_f^{i}]\{{}^{t+\Delta t}_{r}\dot{\phi}^{i}\}+[{}^{t+\Delta t}_{r}K_f^{i}]\{{}^{t+\Delta t}_{r}\phi^{i}\}
$$
$$
=\{{}^{t+\Delta t}_{r}F_f^{i}\}-[{}^{t+\Delta t}_{r}C_f^{ie}]\{{}^{t+\Delta t}\dot{\phi}^{e}\}-[{}^{t+\Delta t}_{r}K_f^{ie}]\{{}^{t+\Delta t}\phi^{e}\} \qquad \cdots(29)
$$

(29)式中 $\{{}^{t+\Delta t}\dot{\phi}^{e}\}$，$\{{}^{t+\Delta t}\phi^{e}\}$ 等項由顯式群之值計算。

對於顯式群流體運動方程式，（28）式，之時間微分項可用中央差分表出

$$
\{{}^{t}\ddot{\phi}^{e}\}=\frac{1}{\Delta t^{2}}(\{{}^{t-\Delta t}\phi^{e}\}-2\{{}^{t}\phi^{e}\}+\{{}^{t+\Delta t}\phi^{e}\}) \qquad \cdots\cdots(30)
$$

$$\{{}^{t}\dot{\phi}^{e}\}=\frac{1}{2\Delta t}\left(-\{{}^{t-\Delta t}\phi^{e}\}+\{{}^{t+\Delta t}\phi^{e}\}\right) \qquad \cdots\cdots(31)$$

利用(30)及(31)式，(28)式可改寫整理爲

$$[{}^{t}\overline{K}_{f}^{e}]\{{}^{t+\Delta t}\phi^{e}\}=[{}^{t}\overline{F}_{f}^{e}] \qquad \cdots\cdots(32)$$

式中，

$[{}^{t}\overline{K}_{f}^{e}]$ = 流體顯式群重組(modified)剛度係數

$$=\frac{1}{\Delta t^{2}}[{}^{t}M_{f}]+\frac{1}{2\Delta t}[{}^{t}C_{f}^{e}] \qquad \cdots\cdots(33)$$

$[{}^{t}\overline{F}_{f}^{e}]$ = 流體顯式群重組載重矩陣

$$\begin{aligned}&=\{{}^{t}F_{f}^{e}\}-[{}^{t}C_{f}^{ie}]\{{}^{t}\dot{\phi}^{i}\}-[{}^{t}K_{f}^{ie}]\{{}^{t}\phi^{i}\}\\&+[{}^{t}M_{f}]\frac{1}{\Delta t^{2}}\left(-\{{}^{t-\Delta t}\phi^{e}\}+2\{{}^{t}\phi^{e}\}\right)\\&+[{}^{t}C_{f}^{e}]\frac{1}{2\Delta t}\{{}^{t-\Delta t}\phi^{e}\}-[{}^{t}K_{f}^{e}]\{{}^{t}\phi^{e}\}\end{aligned} \qquad \cdots\cdots(34)$$

對於隱式群流體運動方程式，(29)式，之時間微分項可用簡單的後向差分表出

$$\{{}^{t+\Delta t}_{\ \ \ r}\dot{\phi}^{i}\}=\frac{1}{\Delta t}\left(\{{}^{t+\Delta t}_{\ \ \ r}\phi^{i}\}-\{{}^{t}\phi^{i}\}\right) \qquad \cdots\cdots(35)$$

利用(35)式，(29)式可改寫整理爲

$$[{}^{t+\Delta t}_{\ \ \ r}\overline{K}_{f}^{i}]\{{}^{t+\Delta t}_{\ \ \ r}\phi^{i}\}=\{{}^{t+\Delta t}_{\ \ \ r}\overline{F}_{f}^{i}\} \qquad \cdots\cdots(36)$$

式中，

$[{}^{t+\Delta t}_{\ \ \ r}\overline{K}_{f}^{i}]$ = 流體隱式群重組剛度矩陣

$$=\frac{1}{\Delta t}[{}^{t+\Delta t}_{\ \ \ r}C_{f}^{i}]+[{}^{t+\Delta t}_{\ \ \ r}K_{f}^{i}] \qquad \cdots\cdots(37)$$

$$\{ {}^{t+\Delta t}_{r}\overline{F}^{i}_{f} \} = \text{流體隱式群重組載重矩陣}$$

$$= \{ {}^{t+\Delta t}_{r}F^{i}_{f} \} - [{}^{t+\Delta t}_{r}C^{ie}_{f}] \{ {}^{t+\Delta t}\dot{\phi}^{e} \}$$

$$- [{}^{t+\Delta t}_{r}K^{ie}_{f}] \{ {}^{t+\Delta t}\phi^{e} \} + \frac{1}{\Delta t} [{}^{t+\Delta t}_{r}C^{i}_{f}] \{ {}^{t}\phi^{i} \} \quad (38)$$

3．2　隱式結構物運動方程式

將結構物運動方程式（18）式以矩陣方式表出可寫爲

$$[M_s]\{ {}^{t+\Delta t}_{r+1}\ddot{U} \} + [K_s]\{ {}^{t+\Delta t}_{r+1}U \} = \{ {}^{t+\Delta t}_{r+1}F_s \} \quad \cdots\cdots (39)$$

式中，

$$[M_s] = \text{結構質量矩陣}$$

$$= [\sum_{i=1}^{6} M_{j\ mim}] \quad \cdots\cdots (40)$$

$$[K_s] = \text{結構剛度矩陣}$$

$$= [\sum_{i=1}^{6} (k_{j\ mim} + Q_{j\ mim} - \sum_{\substack{\ell=1 \\ \ell \neq m}}^{N} \widetilde{Q}_{j\ mi\ell}) + \widetilde{k}_{jm}] \quad \cdots\cdots (41)$$

$$\{ {}^{t+\Delta t}_{r+1}F_s \} = \text{結構載重矩陣} \quad \cdots\cdots (42)$$

$$\{ {}^{t+\Delta t}_{r+1}\ddot{U} \} = \text{結構加速度矩陣} \quad \cdots\cdots (43)$$

$$\{ {}^{t+\Delta t}_{r+1}U \} = \text{結構位移矩陣} \quad \cdots\cdots (44)$$

對於結構物運動方程式之動力分析可利用收斂性很好之Newmark 方法（Bathe and Wilson，1976），由 Newmark 方法結構物之位移，速度以及加速度可表出爲

$$\{ {}^{t+\Delta t}_{r}U \} = \{ {}^{t}U \} + \{ {}^{t}\dot{U} \}\Delta t + [(1/2-\beta)\{ {}^{t}\ddot{U} \} + \{ {}^{t+\Delta t}_{r+1}\ddot{U} \}]\Delta t^2 \quad \cdots\cdots (45)$$

$$\{ {}^{t+\Delta t}_{r+1}\dot{U} \} = \{ {}^{t}\dot{U} \} + [(1-\alpha)\{ {}^{t}\ddot{U} \} + \{ {}^{t+\Delta t}_{r+1}\ddot{U} \}] \Delta t \qquad \cdots\cdots (46)$$

$$\{ {}^{t+\Delta t}_{r+1}\ddot{U} \} = \frac{1}{\beta \Delta t^2} \{ {}^{t+\Delta t}_{r+1}U \} - \frac{1}{\beta \Delta t^2} \{ {}^{t}U \} - \frac{1}{\beta \Delta t} \{ {}^{t}\dot{U} \}$$

$$- (\frac{1}{2\beta} - 1) \{ {}^{t}\ddot{U} \} \qquad \cdots\cdots (47)$$

代入（ 45 ）－（ 47 ）式，結構物運動方程式（ 39 ）式重新整理爲

$$[\overline{K}_s] \{ {}^{t+\Delta t}_{r+1}U \} = \{ {}^{t+\Delta t}_{r+1}\overline{F}_s \} \qquad \cdots\cdots (48)$$

式中，

$[\overline{K}_s]$ = 結構重組剛度矩陣

$$= [K_s] + \frac{1}{\beta \Delta t^2} [M_s] \qquad \cdots\cdots (49)$$

$\{ {}^{t+\Delta t}_{r+1}\overline{F}_s \}$ = 結構重組載重矩陣

$$= [{}^{t+\Delta t}_{r+1}F_s] + [M_s] (\frac{1}{\beta \Delta t^2} \{ {}^{t}U \} + \frac{1}{\beta \Delta t} \{ {}^{t}\dot{U} \}$$

$$+ (\frac{1}{2\beta} - 1) \{ {}^{t}\ddot{U} \}) \qquad \cdots\cdots (50)$$

求解（ 48 ）式可求得結構物運動位移，接著利用（ 46 ）和（ 47 ）式可分別求出速度和加速度。對於Newmark 方法中之係數 α 和 β 分別選用 1/4 和 1/2 可得到良好之結果。

3．3　顯示 — 隱式分割流體與隱式結構物互制之動力分析

本節所要說明的爲利用前述經過分割的流體運動方程式：顯式方程式，(32)式和隱式方程式，（ 36 ）式，與隱式結構方程式，（ 48 ）式，作流體與結構物互制之動力分析。在此先說明互制分析方法於時間 $t=\Delta t$ 的起始計算，接著再說明任意時間 $t = t + \Delta t$ 之互制分析過程。

在時間 $t = \Delta t$， 由顯式流體運動方程式，(32)－(34)式，可看出 $\{{}^{\Delta t}\phi^{e}\}$之求得完全由起始條件$\{{}^{0}\phi\}$，$\{{}^{0}\dot{\phi}\}$ 計算。因此若給定問題之起始條件爲一切靜止則所求得$\{{}^{\Delta t}\phi^{e}\} = \{0\}$，此點似乎不甚合理。又如利用由此求得之值提供給隱式流體運動方程式計算則對以後時間之結果亦含有累積之誤差。爲得到更正確之起始計算數值解乃提出以下一完全隱式之計算方法。

利用Newmark 隱式積分法，配合引用(45)－(47)式，流體運動方程式，(20)式，計算在時間 $t = \Delta t$ 以及第 r 個疊代步驟可表出爲

$$[{}^{\Delta t}_{r}\overline{K}_{f}]\{{}^{\Delta t}_{r}\phi\} = \{{}^{\Delta t}_{r}F_{f}\} \qquad \cdots\cdots (51)$$

式中，

$$[{}^{\Delta t}_{r}\overline{K}_{f}] = \frac{1}{\beta\Delta t^{2}}[{}^{\Delta t}_{r}M_{f}] + \frac{\alpha}{\beta\Delta t}[{}^{\Delta t}_{r}C_{f}] + [{}^{\Delta t}_{r}K_{f}] \qquad \cdots\cdots (52)$$

$$\begin{aligned}[{}^{\Delta t}_{r}\overline{F}_{f}] = &\{{}^{\Delta t}_{r}F_{f}\} + [{}^{\Delta t}_{r}M_{f}]\Big(\frac{1}{\beta\Delta t^{2}}\{{}^{0}\phi\} + \frac{\alpha}{\beta\Delta t}\{{}^{0}\dot{\phi}\} \\ &+ \Big(\frac{1}{2\beta} - 1\Big)\{{}^{0}\ddot{\phi}\}\Big) + [{}^{\Delta t}_{r}C_{f}]\Big(\frac{1}{\beta\Delta t}\{{}^{0}\phi\} \\ &+ \Big(\frac{\alpha}{\beta} - 1\Big)\{{}^{0}\dot{\phi}\} + \Big(\frac{\alpha}{2\beta} - 1\Big)\{{}^{0}\ddot{\phi}\}\Delta t\Big)\end{aligned} \qquad \cdots\cdots (53)$$

在(53)式中之$\{{}^{0}\ddot{\phi}\}$項可如以下計算

$$\{{}^{0}\ddot{\phi}\} = [{}^{0}M_{f}]^{-1}(\{{}^{0}F_{f}\} - [{}^{0}C_{f}]\{{}^{0}\dot{\phi}\} - [{}^{0}K_{f}]\{{}^{0}\phi\}) \qquad (54)$$

對結構動力分析而言，則可從隱式結構運動方程式，(48)式，計算在時間 $t = \Delta t$，配合利用流體運動計算第 r 次疊代之結果，求解第$(r+1)$次疊代計算，其計算式可表出如下

$$[\overline{K}_{s}]\{{}^{\Delta t}_{r+1}U\} = \{{}^{\Delta t}_{r+1}\overline{F}\} \qquad \cdots\cdots (55)$$

式中，

$[\overline{K}_s] = (49)$式

$$[{}^{\Delta t}_{r+1}\overline{F}_s] = \{{}^{\Delta t}_{r+1}F_s\} + [M_s]\left(\frac{1}{\beta\Delta t^2}\{{}^{0}U\} + \frac{1}{\beta\Delta t}\{{}^{0}\dot{U}\}\right.$$

$$\left.+\left(\frac{1}{2\beta} - 1\right)\{{}^{0}\ddot{U}\}\right) \qquad \cdots\cdots(56)$$

(56)式中之$\{{}^{0}\ddot{U}\}$項可由以計算如下

$$\{{}^{0}\ddot{U}\} = [{}^{0}M_s]^{-1}(\{{}^{0}F_s\} - [{}^{0}K_s]\{{}^{0}U\}) \qquad \cdots\cdots(57)$$

利用由(55)式求解出之結構物運動第($r+1$)次疊代結果，可提供給流體運動方程式再計算，如此反覆交替疊代計算直到收斂爲止完成第一個時距之計算。

對於第二個時距以後之流體與結構物互制分析之計算則可以任意時間 $t+\Delta t$ 時之求解過程來說明。假設在時間 $t-\Delta t$ 以及 t 之流場和結構物運動皆爲已知，則首先由顯式流體運動方程式，(32)式，可求出$\{{}^{t+\Delta t}\phi^{e}\}$，再配合利用前面時間之流場以及結構物運動，則隱式流體運動方程式以及結構物運動方程式之重組剛度矩陣與重組載重矩陣，(37)－(38)式以及(49)－(50)式，均可以計算。至於隱式流體運動方程式以及隱式結構物運動方程式間互制分析之交替疊代計算則與前述第一個時距之計算過程相同。

四、計算例

對於以上所建立之波浪與結構物運動之有限元素法模式以及波浪與結構物運動互制之動力分析方法，在本節則以一計算例來說明。所考慮之問題爲給定一圓柱浮體，半徑 a 爲 0.8 公尺，一起始吃水深度 ${}^{0}U_2 = -0.05$ 公尺，待浮體四周之水面恢復平靜後再放開浮體，所考慮問題之水深爲10公尺。利用本文建立之有限元素法模式即可用來求解圓柱浮體被釋放後之自由振盪情形。

在有限元素法模式中所用之有限元素格網如圖 3 所示，由於所考慮之問題對 x_2 座標軸對稱因此只計算半個問題領域。此圓柱浮體之自然振動週期約爲 1.6 秒，計算所使用之時間間距爲 0.05秒（約週期／32）。利用本文模式計算出來圓柱浮體在垂直方向之運動位移如圖 4 所示，圓柱浮體之運動從開始釋放後便在垂直方向上下振盪且一面衰減至停止。本文計算結果並與由Ursell（1964）求得之理論解析解計算之結果比較，由圖 4 可看出數值結果與理論解相當穩合。由數值模擬結果亦可算出作用在單位寬圓柱浮體上之垂直方向之無因次水動壓力 $f_2=F_2/\rho g a\,|{}^0U_2|$ 之時間之變化如圖 5 所示，而正如所預期的，最大動壓力出現在圓柱體剛剛釋放後不久。

利用數值模式在時間領域上模擬水面波浪運動，最具功能的還是能把水面之變化眞確表達出來。對於圓柱浮體自由振盪所產生在各個時間 0.5 秒，1.0 秒，1.4 秒，2.0 秒，3.0 秒，4.0 秒，6.0 秒，8.0 秒，10.0 秒，12.0 秒，14.0 秒和 16.0秒時之水面運動分別繪如圖 6 (a)－6(ℓ)。由圖 6 可看出，水面波浪運動之形成乃相對於圓柱浮體之自由振盪運動，由於結構物之不斷運動乃造就出一面成長之波浪，而也由於浮體運動之逐漸衰減因而也使得形成之波浪無法達到完全發展而造成一種純粹瞬變之波浪，此一系列瞬變波浪則介在這種成長與衰減之能量互傳中逐漸往外傳出，終至水面恢復靜止。圖 7 (a)－7 (f)所顯示的分別爲通過固定位置 x_1 爲 0.8 公尺，4.64 公尺，8.0 公尺，12.32 公尺，17.92 公尺以及 23.68 公尺處之水位時間變化。由圖 7 可看出通過各位置之波浪皆呈波群之型態經過，愈接近結構物則此波群中之最大波愈大，愈遠離結構物則波群中各波浪間之能量傳輸情形愈明顯因而各波浪之大小愈平均。

五、結　論

本文之主要目的爲以有限元素法爲基礎，在時間領域上討論水面波浪與大型結構物互相作用之動力分析。所考慮之問題則僅爲線性互制分析。在互制作用動力分析中，對於流場之分析則根據流體運動方程式之特性將其分割成顯式群與隱式群，對於結構物之動力分析則採用隱式積分法。對於流體與結構物互

制之動力分析則使用顯式－隱式分割流體與隱式結構物運動之交替疊代分析方法。又爲改進起始時間之計算，對於流體與結構物之動力互制分析乃使用全隱式積分方法以計算第一個時間間距之結果。文中最後以一具瞬變特性之含流體與結構物互制作用之圓柱浮體自由振盪爲計算例，說明所提流體與結構物互制之動力分析的正確性，同時藉以說明利用數值模式求解物理問題並輔助對於物理現象瞭解所具有之重要性。

六、參考文獻

Bathe, K.J. and Sonnad, V., On Effective Implicit Time Integration in Analysis of Fluid-Structure Problems, Int. J. for Num. Meth. in Engrg., Vol.15, 1980, pp.943-948.

Bathe, K.J. and Wilson, E.L., Numerical Methods in Finite Element Analysis, Prentice Hall, 1976.

Belytschko, T. and Mullen, R., Mesh Partitions of Explicit-Implicit Time Integration, in Formulations of Computational Algorithms in Finite Element Analysis, Ed. by Bathe, et al, MIT Press, Cambridge, Mass., 1977.

Geers, T.L., Transient Response Analysis of Submerged Structures, Finite Element Analysis of Transient Nonlinear Structural Behavior, Ed. by Belytschko, T., et al, AMD-Vol.14, ASME, New York, N.Y., 1975.

Jagannathan, S., Simulation of Two-Dimensional Nonlinear Free Surface Flows, Ocean Structural Dynamics Symposium, 1986, pp.130-144.

Lai, C.P. Wave Interaction With Structure : Hydrodynamic Loadings on Pltforms and Docks, Ph.D. Thesis, University of Southern California, 1986.

Lee, J-F. and Leonard, J.W., A Time Dependent Radiation Condition for Transient Wave-Structure Interactions, Ocean Engineering, Vol.14, No.6, 1987, pp.469-488.

Lee, J-F., Finite Element Analysis of Wave-Structure Interactions in the Time Domain, Ph.D. Thesis, Oregon State University, USA, 1986.

Maskell, S.J. and Ursell, F., The Transient Motion of a Floating Body, Journal of Fluid Mechanics, Vol.44, pt.2, 1970, pp.303-313.

Multer, R.H., Exact Nonlinear Model of Wave Generator, Journal of the Hydraulic Division, Proc. of ASCE, 1973, pp.31-47.

Nakayama, T., Boundary Element Analysis of Nonlinear Water Wave Problems, Int. J. for Num. Meth. in Engrg., Vol.19, 1983, pp.953-970.

O'Brien, P.J., A Nonlinear Finite Element Model for the Generation of Waves in a Laboratory Wave Flume, M.S. Thesis, University College, Galway, 1983.

Orlanski, I., A Simple Boundary Condition for Unbounded Hyperbolic Flows, J. of Computational Physics, Vol.21, 1976, pp.251-269.

Park, K.C. and Felippa, C.A., Partitioned Analysis of Coupled Systems, in Computational Methods for Transient Analysis, Ed. by Belytschko, T., et al., North-Holland, 1983.

Park, K.C., Felippa, C.A. and DeRuntz, J.A., Stabilization of Staggered Solution Procedures for Fluid-Structure Interaction Analysis, in Computational Methods for Fluid-Structure Interaction Problems, AMD, Vol.26, ASME, 1977.

Sarpkaya, T. and Isaacson, M., Mechanics of Wave Forces on Offshore Structures, Van Nostrand Reihold Co., 1981.

Ursell, F., The Decay of the Free Motion of a Floating Body, Jounal of Fluid Mechanics, Vol.19, 1964, pp.305-319.

Zienkiewicz, O.C., The Finite Element Method, McGraw-Hill, London, 1977.

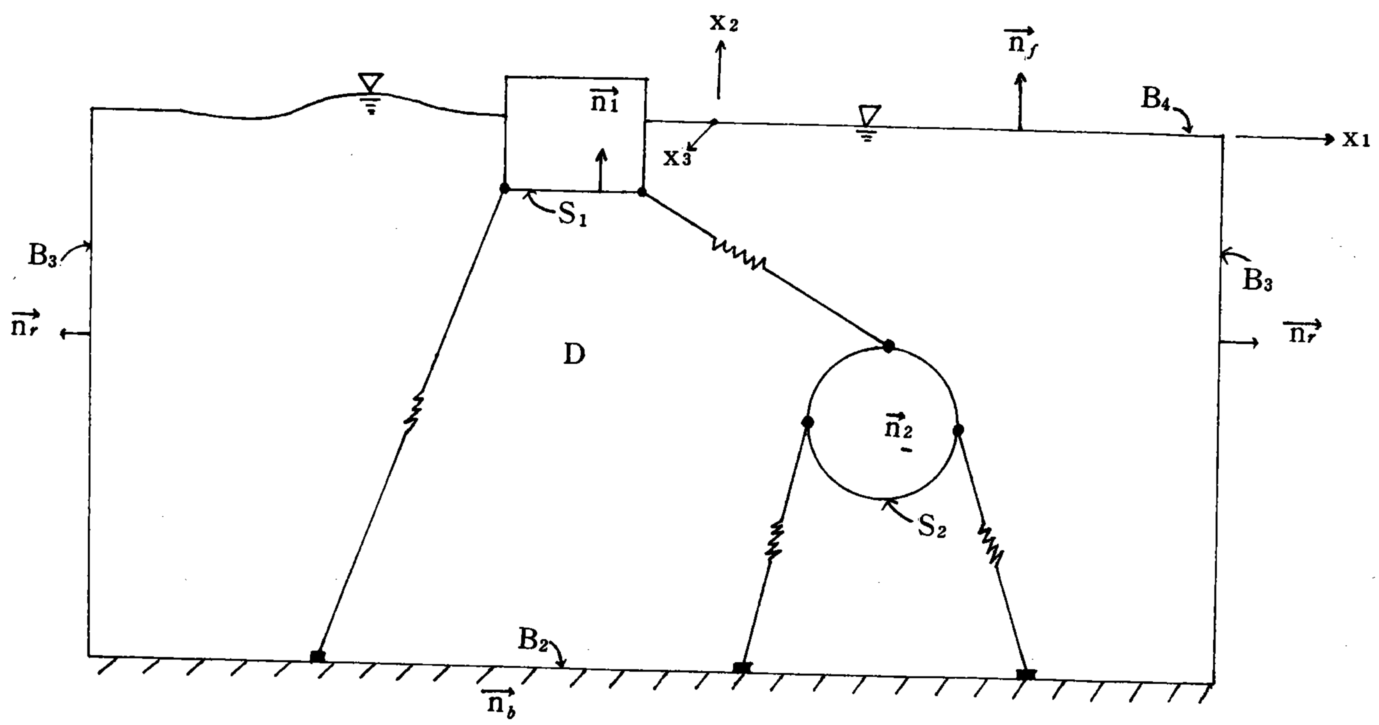

圖 1　在時間領域上波浪與結構物互制分析定義圖

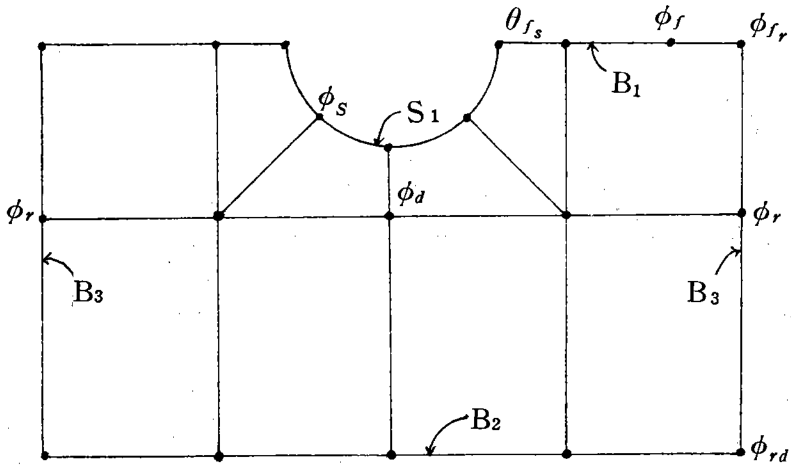

圖 2　顯式－隱式分割流體有限元素節點定義圖

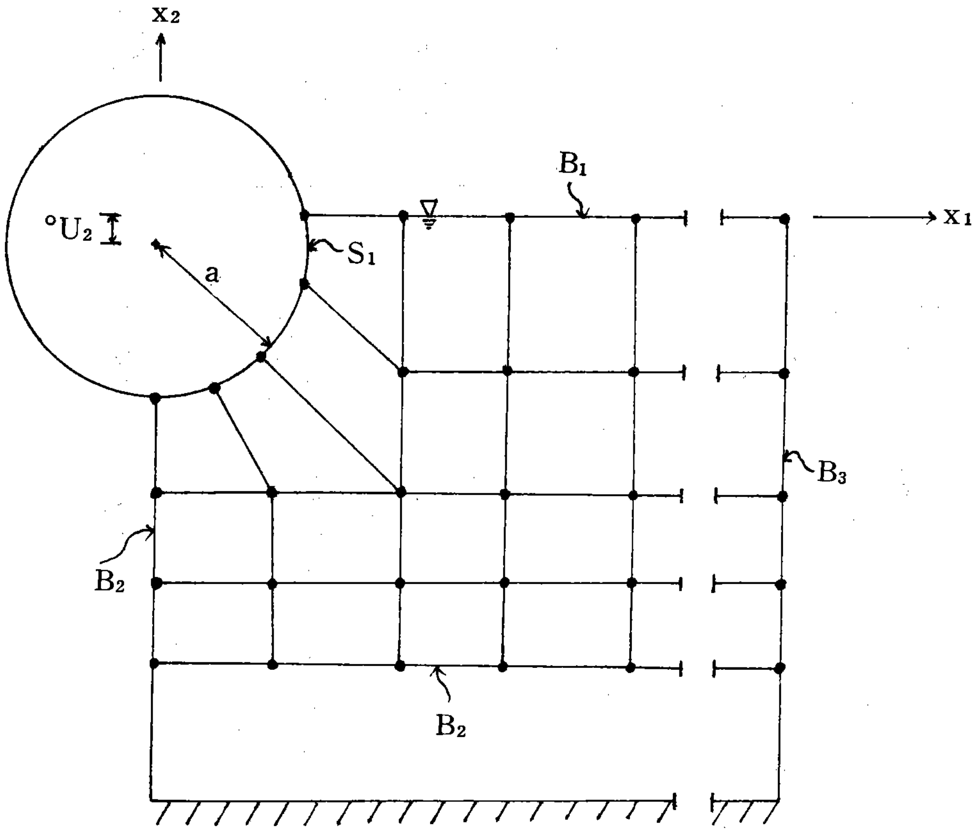

圖 3　圓柱浮體自由振盪問題有限元素格網示意圖

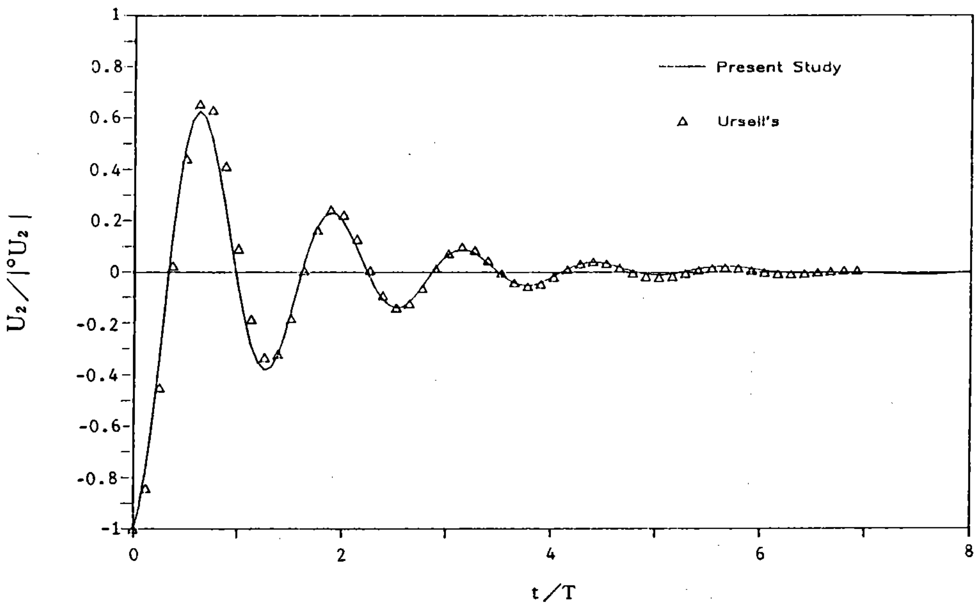

圖 4　圓柱浮體自由振盪問題結構物之位移時間關係

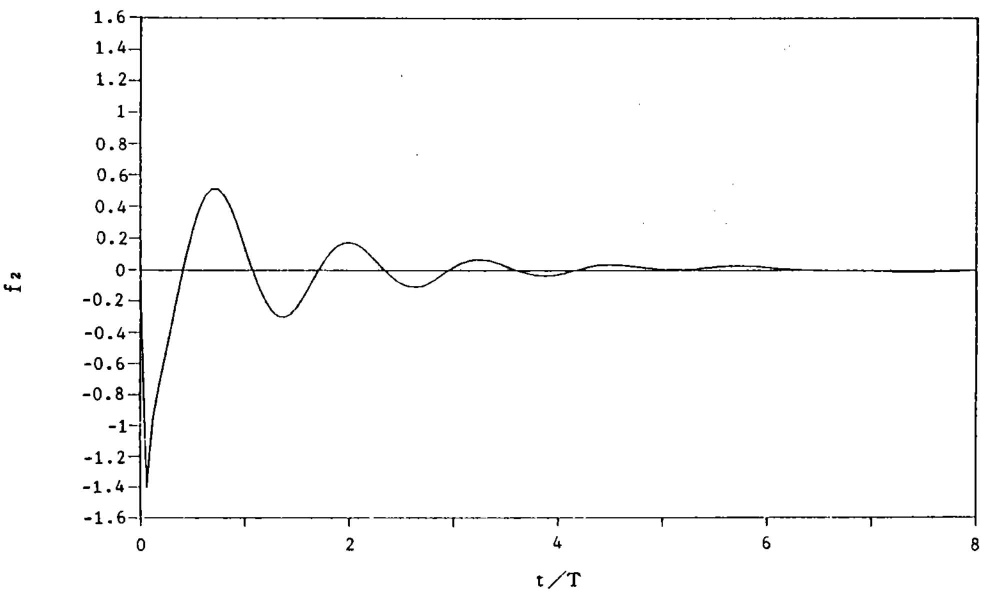

圖 5　圓柱浮體自由振盪問題作用於結構物上之無因次垂直力

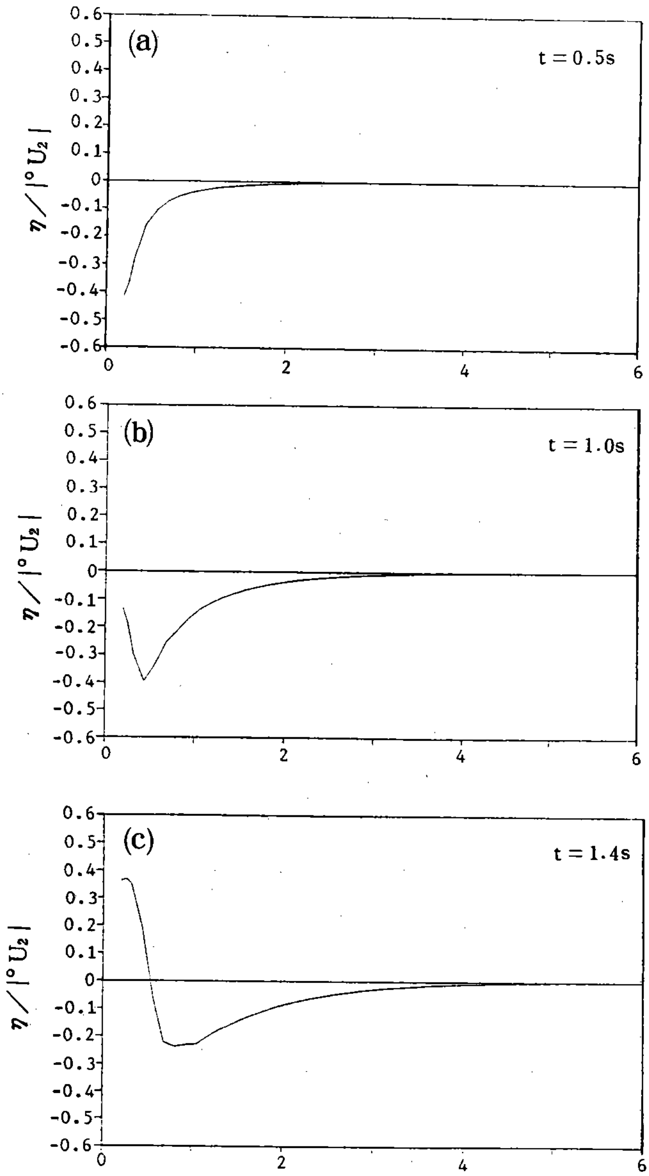

圖 6　圓柱浮體自由振盪問題各時間之水面變化

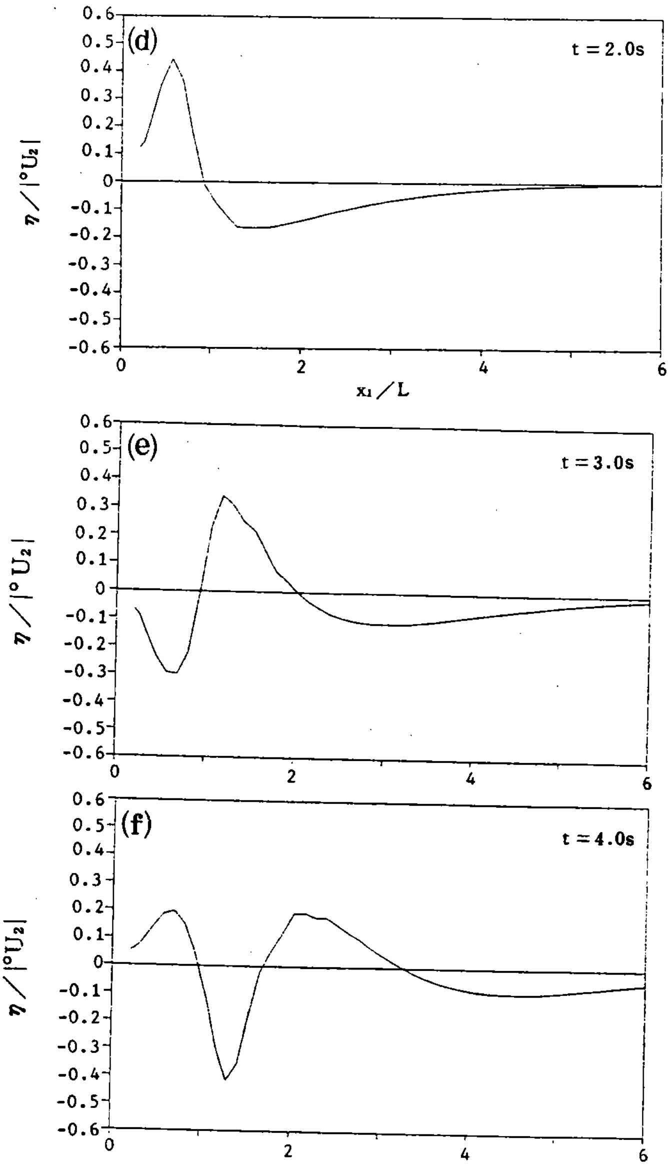

圖 6　圓柱浮體自由振盪問題各時間之水面變化（續）

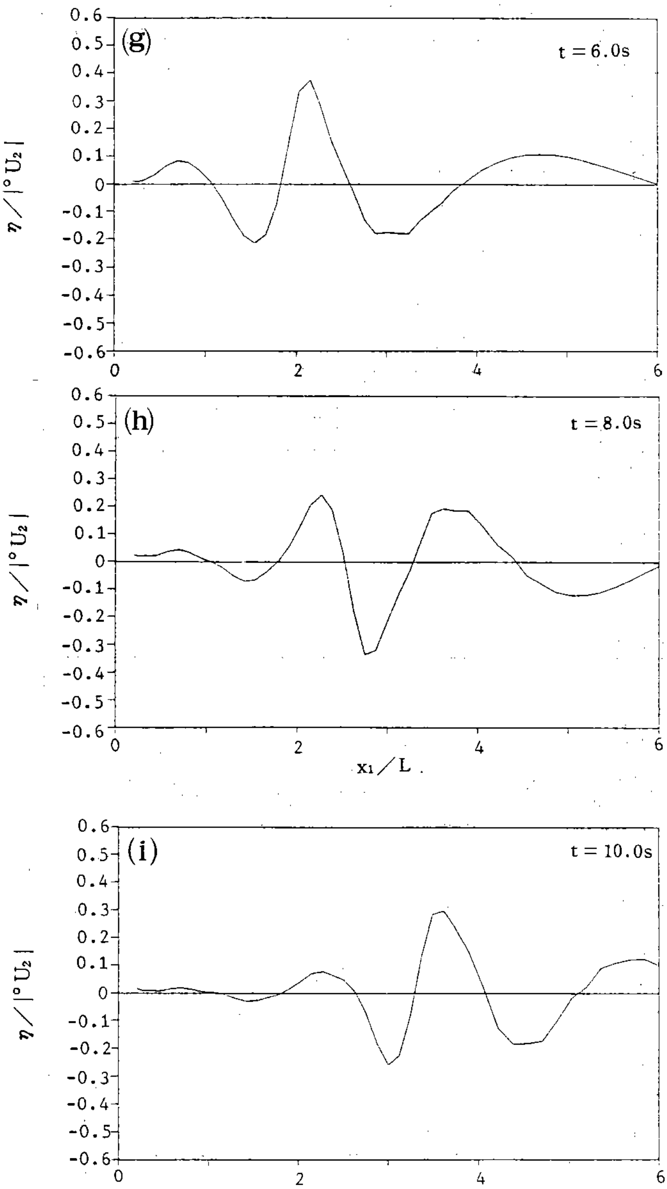

圖 6　圓柱浮體自由振盪問題各時間之水面變化（續）

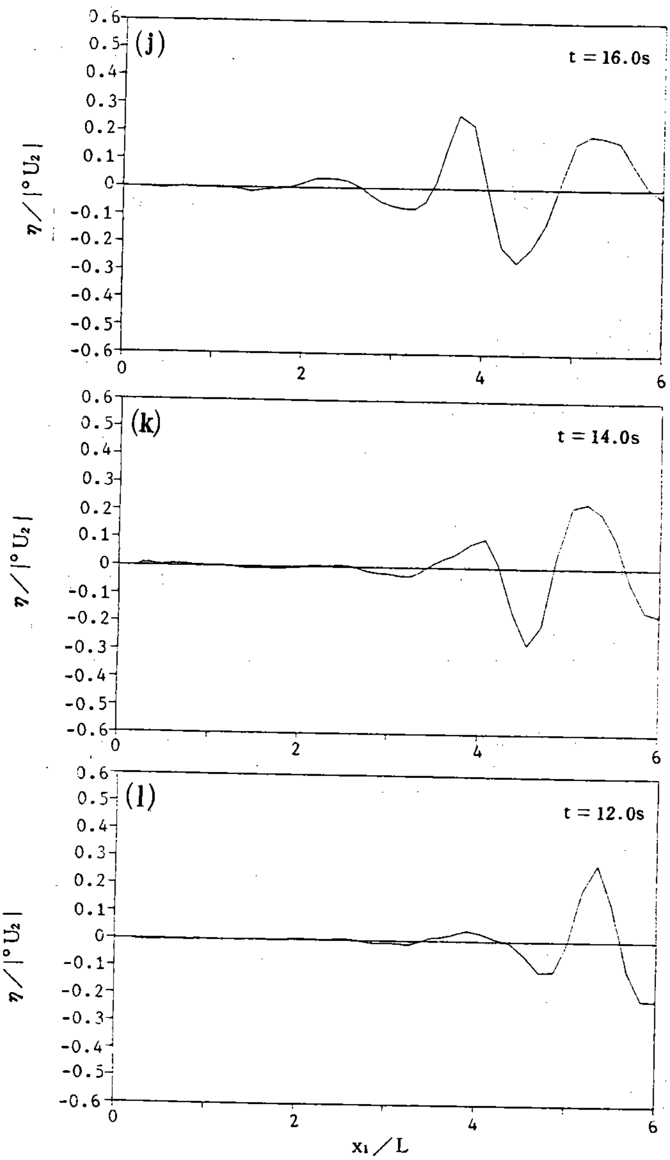

圖 6　圓柱浮體自由振盪問題各時間之水面變化（續）

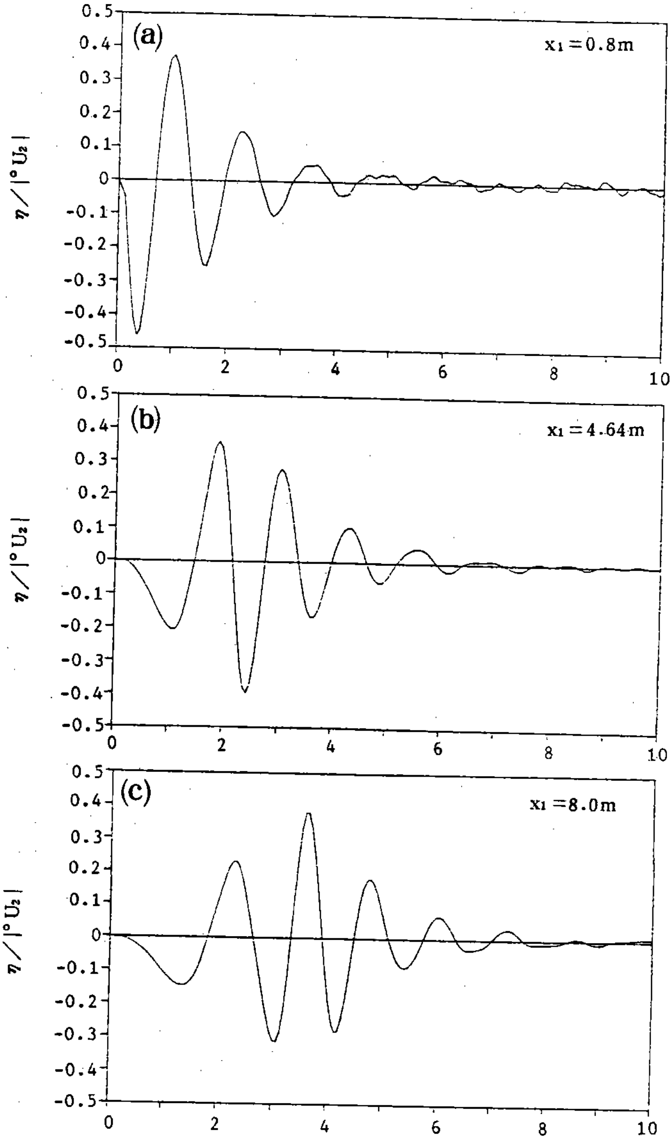

圖 7　圓柱浮體自由振盪問題各固定位置之水位時間變化

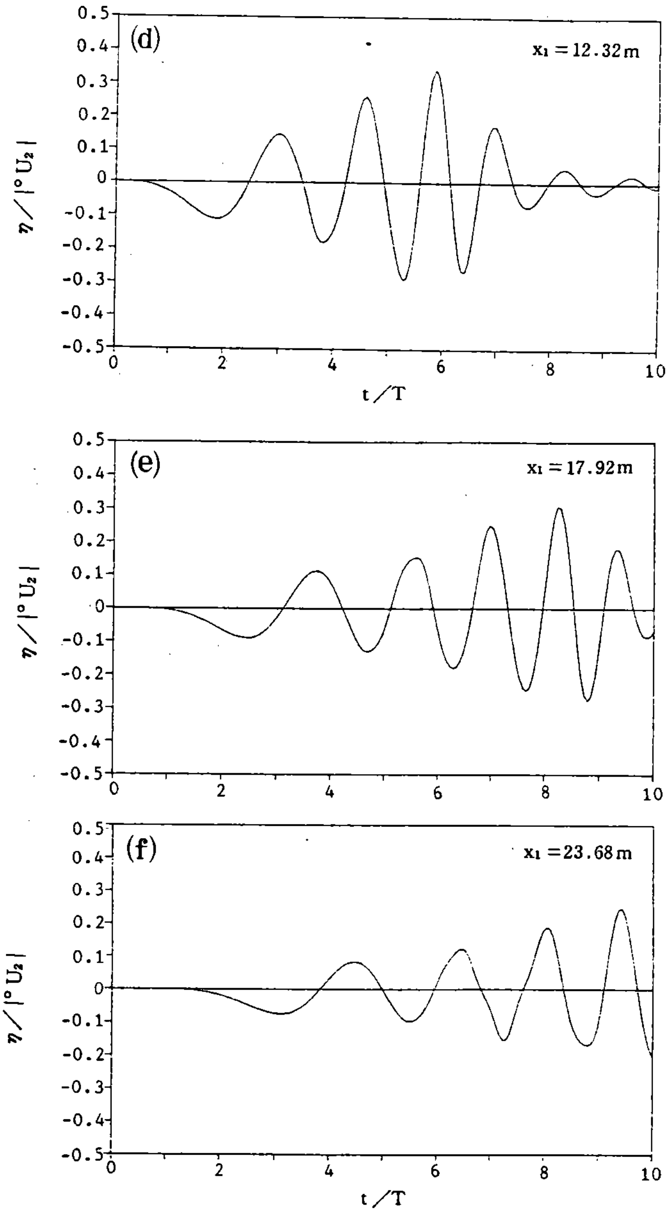

圖 7　圓柱浮體自由振盪問題各固定位置之水位時間變化（續）